DEVELOPMENT AND DEMONSTRATION OF AN ULTRA-LOW-BACKGROUND LIQUID SCINTILLATION COUNTER

A Dissertation

by

JENNIFER LYNN ERCHINGER

Submitted to the Office of Graduate and Professional Studies of
Texas A&M University
in partial fulfillment of the requirements for the degree of

DOCTOR OF PHILOSOPHY

Chair of Committee,	Craig M. Marianno
Committee Members,	John W. Poston, Sr.
	Charles M. Folden III
	Sunil S. Chirayath
Head of Department,	Yassin A. Hassan

August 2017

Major Subject: Nuclear Engineering

ABSTRACT

The Ultra-Low Background Liquid Scintillation Counter (ULB LSC) constructed at Pacific Northwest National Laboratory further expands the capabilities of LSC by utilizing background reduction techniques to achieve lower minimum detectable activities. Hence, alpha and beta detection capabilities are enhanced for samples that have previously required extended count times, large sample volumes, and/or complex separation chemistry. The three-chamber ULB LSC system design includes layers of passive shielding in conjunction with active rejection of cosmic muon interactions with the goal of reaching background rates on the order of 10 to 100 counts per day. GEANT4 Monte Carlo radiation transport simulations for the full shield showed an expected count rate of 10 counts per day from the environmental radiation backgrounds, in addition to a systematic count rate of 15 counts per day expected from initial tests with a partial build. The observed chamber background is 11 counts per day for the left chamber and 2 counts per day for the right chamber, including systematic and environmental radiation backgrounds, over an energy range of 25-2500 keV. This is an improvement in reducing background count rates by approximately 2 orders of magnitude compared to commercially available systems. Initial test results of ^{90}Sr/^{90}Y samples with the ULB LSC show promising results for spectral capabilities, though the detection efficiencies of 15% and 60% for these samples in the left and right chambers, respectively, were lower than expected. Further testing will improve characterization of the light collection efficiency, spectral capabilities, and alpha/beta separation by pulse shape analysis. The ULB LSC broadens trace level measurement capabilities that will impact applications in nuclear nonproliferation, treaty verification, and environmental and geochemical science studies.

DEDICATION

Dedicated to my loving and supportive family, in all its various forms — genetic, faith, and academic.

To my parents, your words of encouragement, wisdom, and love have kept me calm and focused. To my sister, your lively spirit and energy maintained mine. To my church families, your prayers were uplifting. To my academic circle, especially between TAMU and PNNL, your guidance and challenges have been instructive and invaluable.

ACKNOWLEDGEMENTS

To Dr. Marianno: You have my deepest gratitude for bringing me into your research group and giving me my first exposure to the field of nuclear security. I came into the Nuclear Engineering department with a limited idea of what the possibilities were for a career in Health Physics, and you broadened my vision to the vast opportunities available in the nuclear field. Thank you for guiding me to grow in independence in my graduate research and encouraging me as I began to forge my own path. You taught me the skills to think critically, judge impartially, and work my way through the unexpected, as is prone to happen in research.

To Dr. Orrell: I cannot thank you enough for taking a leap of faith in bringing me on to the ULB LSC project. You gave me incredible opportunities to take initiative, help lead a team, and participate in project management. I appreciate the time you always made for me and the freedom you gave me in exploring other opportunities at PNNL, from lectures to assisting on sister projects. As a project manager you are an exemplary role model, and as a mentor you took me from following instructions to making decisions. I am so thankful to have had the opportunity to work with you.

Many thanks and my sincerest appreciation to the rest of the ULB LSC project team. Your guidance as I came on board with the ongoing project work and your support throughout the project have made this a wonderful place to work and grow as a scientist and researcher.

To Dr. Poston, Dr. Chirayath, and Dr. Folden: Thank you for your patience as I have gone through this process and your faith in me to be a productive and contributing member of this community. I appreciate the time and thought you have given me and this project. I am a more thoughtful and critical researcher as a result.

NOMENCLATURE

BLG	Bent Light Guide
HV	High Voltage
LPCVD	Low-Pressure Chemical Vapor Deposition
LSC	Liquid Scintillation Counting
MDA	Minimum Detectable Activity
NI	National Instruments
OFHC	Oxygen-Free High Conductivity
PMT	Photomultiplier Tube
PNNL	Pacific Northwest National Laboratory
PSA	Pulse Shape Analysis
PSD	Pulse Shape Discrimination
PVT	Polyvinyl Toluene
SUL	Shallow Underground Laboratory
TAMU	Texas A&M University
ULB LSC	Ultra-Low-Background Liquid Scintillation Counter
ULBPC	Ultra-Low Background Proportional Counter

TABLE OF CONTENTS

Page

LIST OF FIGURES

LIST OF TABLES

TABLE Page

1. INTRODUCTION AND LITERATURE REVIEW

1.1 Liquid Scintillation Counting

Liquid scintillation counting (LSC) has been used as a radiometric technique since the early 1950's (Rapkin, 1971; L'Annunziata and Kessler, 2012). The high detection efficiency, automation in measurement and data processing, and spectroscopic capabilities enabling mixed sample analysis have made this one of the more popular methods of radiation detection, particularly for samples with alpha- and beta-emitters. While this methodology and the development of commercial liquid scintillation counters made great strides through the 1950's to the 1980's, improvements in detection limits by reducing background count rates have not been significantly altered since the introduction of the Wallac Quantulus^{TM} in 1984 (Kaihola, 1994). Typical background reduction methods involve passive shielding of the sample with lead from environmental gamma rays, coincidence counting of the sample, anti-coincidence with a cosmic signal, and pulse-shape analysis methods. In an effort to keep the system size and weight reasonable for commercial products, these methods of background reduction have been limited by necessity. Particularly, the weight and size are most affected by the amount of passive shielding and surface area used for anti-coincidence with cosmic signals.

The sensitivity of this technique is directly related to the background count rate. Reductions in the background count rate decrease the detection limit, increasing the sensitivity of the method. Such limitations on reducing the background count rate, while necessary for commercial products, result in a limitation on the sensitivity of the method. While the current methods are adequate for many applications of liquid scintillation counting, there are areas in which increased sensitivity would be

beneficial. A system with enhanced background reduction techniques will have a lower background count rate. This in turn would decrease the detection limits, and thereby the minimum detectable activity. This instrument could detect radioactivity at levels indistinguishable from background in current instrumentation. By creating a more sensitive instrument, the amount of time spent enriching and preparing samples for analysis could be decreased. In some cases, the overall process time to prepare the sample and to collect measurement data could be decreased as well.

The research presented here describes the application of ultra-low-background methods to liquid scintillation counting. By reducing the background to ultra-low levels (<100 counts per day), the sensitivity of the technique can be increased by a factor of 20 over those achieved with current commercial technology. In addition to increased sensitivity, the sample size and/or total process time for a sample can be decreased with low-background-detection methods. For liquid scintillation counting, the application of low-background methods can cut days off sample processing time and reduce sample sizes from tens of liters to single digits for the case of tritium water samples.

1.1.1 Fundamental Principles

Scintillation of organic compounds as a result of radiation exposure was first documented in 1948 by Lieselott Herforth (L'Annunziata and Kessler, 2012). Her thesis work included discussion on the conversion of energy from radiation to photons through the absorption of that energy by aromatic compounds. Herforth's work with Kallmann was the foundation for the development of liquid scintillation analysis for quantitative measurement of radioactivity in samples.

A variety of detection methods exist to identify and quantify the radioactive parent nuclei based on the decay processes. One such method is liquid scintillation

counting. In LSC, the energy released in radioactive decay is converted into visible photons, which are converted to an electrical signal by photomultiplier tubes or other light detection methods such as silicon photomultipliers. This is particularly useful for detecting alpha and beta particles.

1.1.1.1 Radiation Fundamentals

Energy is released by unstable atoms in the form of waves or particles in order to transition to a more stable nuclear structure. This release of energy in the decay process may result in the emission of a gamma (γ) ray, x-ray, electron ($\beta-$), positron ($\beta+$), neutron, or alpha (α) particle. Liquid scintillation is primarily used for alpha and beta detection, though it can also detect gammas, x-rays, Auger and internal conversion electrons, neutrinos, and double beta decay, among others.

Alpha decay results in the energetic production of a helium nucleus with charge of +2 (the alpha particle) and the daughter nucleus from a parent radionuclide. The helium nucleus retains most of the energy of the decay since it is generally much lighter than daughter nucleus. Alpha particles typically have an energy between 2-8 MeV, and are monoenergetic for a single decay. A unique energy is associated with the alpha decay of a radionuclide, and the alpha particles from that decay will have on average the same energy. This is represented by single peaks for the alpha decays of different radionuclides.

Beta decay of a parent radionuclide results in three products: the daughter nucleus, an electron ($\beta-$), and an anti-neutrino. For positron decay, the products are the daughter nucleus, a positron ($\beta+$), and a neutrino. Since the energy of the decay is now divided between three particles, the beta particles are not monoenergetic. The division of energy can result in beta particles with energies from zero to the maximum decay energy, all for decay from the same parent. This spread in energy is

called a continuous spectrum, with an average beta energy of ∼1/3 of the maximum decay energy. The energy of beta particles typically ranges from a few keV to a few MeV, depending on the parent radionuclide.

Alpha and beta particles present detection challenges due to their low range in a medium and high linear energy transfer. The larger mass and charge of the alpha cause it to have a high linear energy transfer (energy deposited per unit distance) with surrounding materials. The lighter and singly charged beta particles travel further between interactions and thus have a lower linear energy transfer. In air, alphas have a range of centimeters and betas have a range on the order of meters. These particles can be stopped by thin materials (a piece of paper or plastic for alphas and betas, respectively). When there is some distance between the radioactive source and the detector, alpha particles can be shielded by intervening material and lose most or all of their energy before being detected. This can lead to reduced count rates and degraded energy spectra. The tortuous paths that beta particles take as they lose energy can result in incomplete energy spectra and difficulty in characterizing the source. Any energy lost outside of the detection medium is not registered in the detector, thus resulting in an underestimate of the particle energy.

1.1.1.2 Molecular Interactions

In LSC, the full energy of the decay can be captured by putting the source (emitting) radionuclides into a surrounding detection medium - a liquid scintillation cocktail. The liquid scintillation cocktail contains both a solvent and a fluor solute. The solvent molecules are organic compounds that contain at least one aromatic ring. The aromatic ring is an essential characteristic of the solvent molecule. It is the feature necessary to absorb the energy of the radioactive decay into the pi-bonds of the aromatic ring and transfer that energy to the fluor solute molecules. The fluor

solute, or organic scintillator, molecules are also organic molecules with an aromatic ring. As organic scintillators, the fluor solute is soluble in the organic solvent and dissolved in a concentration of 2-10 g/L. Examples of organic scintillators include PPO, *p*-terphenyl, *bis*-MSB, and POPOP.

The alpha or beta particle, with its original energy from the decay, interacts with the solvent molecules in the LSC cocktail. In each interaction, the surrounding solvent molecules absorb some amount of energy from the particle. Since solvent molecules are present in higher concentration than the fluor scintillation molecules, the solvent molecules absorb the majority of the energy. The particle continues to interact with surrounding molecules until it has lost all its energy and thermalizes or binds to a molecule. These interactions result in excited solvent molecules along the particles track. These excited solvent molecules transfer the energy to the organic scintillator (fluor) molecules through interactions between the pi-bonds of the aromatic rings. The scintillator molecules are then in an excited state and release the energy through fluorescence as they return to their ground state. In fluorescence, the scintillation molecules emit photons of a known wavelength during the release of excess energy in de-excitation. The photons emitted are typically between 275-430 nm from the organic scintillators, but the exact wavelength depends on the particular scintillator. The intensity of the photon emission from a decay event is proportional to the energy of the decay, and the rate at which these photon emissions occur is related to the rate at which decays are occurring (the activity of the sample).

Alpha and beta particles transfer the excitation energy from solvent to scintillation molecules with different efficiencies. Alpha particles have a fluorescent yield of $\sim$1 photon per keV of the particle energy in scintillation cocktail, while the fluorescent yield for betas is $\sim$10 photons per keV of the particle energy. The effect of this ten-fold difference in fluorescent yield is generally an overlap of the alpha

and beta spectra. The calibrations for alpha and beta detection must performed independently performed before measurement of unknown samples in order to have confidence in the spectra of mixed samples. For example, a sample with 7 MeV-alpha particles and beta particles with an endpoint energy of 900 keV would show overlapping spectra from both particles on the same spectrum. The beta particles would result in a continuous spectrum from zero to 900 keV for the betas, with a maximum at the average around 300 keV. The monoenergetic alpha particles would have a single peak on the spectrum at 7 MeV for the alpha calibration, which would overlap at 700 keV on the beta spectrum due to the ten-fold difference in fluorescent yield described above.

Immersing the sample in essentially a 4-pi detection medium results in more accurate energy spectra and increases the detection efficiency to near 100% for alpha particles and 80-100% for most betas. Counting efficiency for beta-emitters is dependent on particle energy. For the hard-to-detect, low-energy (<50 keV) beta decays like tritium, the counting efficiency is closer to ∼30%.

The time it takes for the light pulse to decay, or decay time, is different between alpha and beta particles as well. The light decays more quickly for beta particles than for alpha particles. Alpha particles, and other high-stopping-power charged particles, cause more triplet-state excitation in the solvent molecules than beta particles. Triplet states take longer to de-excite and fluoresce than the typical singlet state excitation. As a result, the light pulses for alpha particles can be 35-40 ns longer than light pulses from beta particles (L'Annunziata and Kessler, 2012). This pulse shape characteristic can be useful when trying to separate alpha and beta pulses.

1.1.1.3 Photoelectric Conversion

The photons emitted from the sample vial are converted to electrons at the bialkali photocathode of the photomultiplier tube (PMT). Photons are converted with some quantum efficiency ($\approx$ 20-30% at peak wavelength). Essentially, this results in 1 in every 3-5 photons that hit the photocathode getting converted to an electron. The photoelectrons generated by a photon burst from a decay event are multiplied through a series of dynode stages to produce a signal current. The dynode stages are increasingly positively charged. The photoelectrons are accelerated towards the first dynode. Upon impact, they produce an avalanche of secondary electrons. The photoelectrons and secondary electrons are accelerated toward the second dynode, and create another avalanche of electrons on that dynode. This process continues along the dynode series, resulting in the amplification of a small number of photoelectrons to an electrical pulse. In some cases, very few photons are generated in or escape from the vial. In order to produce a signal from such small numbers of photons and even smaller number of photoelectrons, the amplification factor must be large. The amplification factor, or gain, for PMTs in liquid scintillation counters is typically $>10^6$. The electrical signal after amplification is proportional to the number of photons impinging on the photocathode, which in turn is proportional to the energy deposited by the beta particle, summarized in Eq. 1.1. Thus, the intensity of the pulse is proportional to the initial particle energy. The activity of the sample can be calculated from the frequency of the pulses.

$$\text{Energy}_{Decay} \propto \#\ \text{Photons}_{LSCcocktail} \propto \#\ \text{Electrons}_{Photocathode} \propto \text{Signal}_{PMT} \quad (1.1)$$

1.1.1.4 Pulse Counting and Summation

Coincidence counting involves the use of multiple PMTs to detect photon emissions. Generally, liquid scintillation counting systems with coincidence circuits use two PMTs, but there are systems that use three PMTs. Coincidence counting enables differentiation between random background events and true decay events. For a given decay event in a vial, the photon emission from the event is isotropic and rapid. The decay and scintillation processes take on the order of 2-10 ns for light decay. A decay event will then result in isotropic emission of multiple photons which are detected by the two PMTs within the light decay time. Generally, coincident events within 18 ns are considered a true decay event (L'Annunziata and Kessler, 2012). Events that are only detected or generated in one PMT are rejected. This reduces the background count rate, since the probability of random events in both PMTs during the 18 ns coincidence window is much lower than the probability of a random event in a single PMT.

Additionally, the detected photons from true decay events can be summed to generate an event signal. The summation circuit reconstructs the event signal with the summed intensity of the individual PMT signals. The summation of the PMT events optimizes the signal to noise ratio and helps to compensate for variation in light intensity due to the location of the decay within the vial. The coincidence and summation circuits are essential for the detection and characterization of low-energy beta-emitters, such as tritium. The individual signals go to an analog-to-digital converter (ADC), where the analog signal with a known pulse height is converted to a digital signal with a number representing the pulse height. The digital signal is used to increment the energy histogram in a multi-channel analyzer to produce the spectral shape of the decays in the sample. The individual signals are summed

in post-processing for the total event energy, where the energy values are calculated from the digital signals using the energy calibration of the respective detector.

Factors such as electronic noise and quenching of the scintillation light output of the sample must be accounted for in data analysis (Carles et al., 2004; Salonen et al., 2012; Bagan et al., 2008). Using two PMTs in coincidence reduces the random background noise rate, and calibrated quench curves are used to determine and correct for the extent of the sample quenching. A complete overview of quench correction methods is available in L'Annuzia's Handbook on Radioactivity Analysis (Salonen et al., 2012).

1.1.1.5 Low-Background Design Characteristics

The design for the ULB LSC is based on detection systems currently operating in the Shallow Underground Laboratory (SUL) at Pacific Northwest National Laboratory (Aalseth, 2012; Runkle et al., 2012). The basic idea of nesting layers of different shielding materials has been utilized in low-background detection systems, specifically the CASCADES array of high purity germanium detectors and an array of low background gas-proportional counters (Keillor et al., 2009; Seifert et al., 2013). Plastic scintillation panels are used on the outermost layer to discriminate against cosmic ray muons. Borated polyethylene moderates and captures the fast and thermal neutrons from cosmic ray-induced events or natural radiation background in the surrounding rocks and walls. For external gamma rays, different layers of lead are used. The layers are graded so that the background from the lead decreases the closer it is to the detector chamber. The beta decay of ^{210}Pb to ^{210}Bi adds an internal bremsstrahlung background. The low background lead is low in ^{210}Pb and can shield against the bremsstrahlung from the outer lead layer. An inner copper lining is used to attenuate any remaining bremsstrahlung background from the low-

background lead layer. The background contributions of each part of the system must be considered in the design of ultra-low background systems.

By reducing the intrinsic background contributions from the passive shielding materials, the lowest practically achievable background can be reached. By reducing the background in Currie's Equation for the minimum detectable activity (MDA) in Eq. 1.2, the MDA can be improved for more sensitive measurements (Currie, 1968). Alternatively, a smaller sample size can be used with a lower-background instrument to reach a given MDA.

$$\text{MDA} \equiv L_D = \frac{2.71 + 4.65\sqrt{C_b T_b}}{\varepsilon \times V_s \times T_s \times 60} \tag{1.2}$$

C_b is the background count rate (cpm), T_b is the background count time (min), ε is the counting efficiency, V_s is the sample mass (g), T_s is the sample count time (min), and the factor of 60 is used to express the MDA in Bq/g. The MDA for measurements of liquid samples can be expressed in units of Bq/mL if the sample mass is replaced by a volume (mL). The constant 2.71 accounts for a zero blank case, corresponding to a 5% probability of false negatives (Type II error), and 4.65 addresses a 5% probability of both false positives (Type I error) and false negatives (Type II error) in equivalent observations of blank and gross (sample plus blank) signals.

Ultra-low background count rates have been achieved with other radiation detection units in the Shallow Underground Laboratory through a combination of design principles that include both passive and active shielding, the ≈30 meters-water-equivalent overburden of the SUL, and careful incorporation of high-purity materials into the systems (Aalseth, 2012; Runkle et al., 2012; Keillor et al., 2011; Aalseth et al., 2009). Similar considerations for the ULB LSC should result in a 10-100 times

reduction in observed background count rates.

1.1.2 Applications of Liquid Scintillation Counting

Liquid scintillation counting techniques have been developed for a variety of alpha- and beta-emitting radionuclides. Chemical methods for isolating the radionuclides and converting them into the correct chemical form for liquid scintillation counting are integral to low-level (sub-Bq) detection and have been developed for a myriad of applications. Isolation methods for low-level ($<$1 Bq L^{-1}) quantities remain under investigation (Finch et al., 2016). For most of the LSC applications described below, the anticipated analysis capabilities of the ULB LSC would reduce the achievable MDA, the sample size, or total processing times to reach a given MDA.

Liquid scintillation counting has proven to be an effective method for analyzing tritium levels for environmental monitoring, age dating, and nuclear safeguards applications. Tritium concentrations in groundwater can be used to monitor hydrologic processes and perform age-dating on the groundwater (Morgenstern and Taylor, 2009; Plastino et al., 2007). The tritium content in natural water samples must be enriched for most LSC samples to obtain an adequate net count rate. Electrolytic enrichment, the most common method, is a significant contributor to the total process time for analysis by liquid scintillation counting (Morgenstern and Taylor, 2009; Vaupotic et al., 2011; Plastino et al., 2007). The total sample volume must go through a series of enrichment stages depending on the initial and required final concentrations.

Tritium concentrations in ice cores have been studied to correlate tritium spikes in sections of the ice cores with global fallout from nuclear weapons testing, and create a time-profile for the entire ice core (Kern et al., 2009). Vaupotic et al. (2011) used LSC to determine the tritium concentrations in spring water as determined by LSC as a baseline before the construction of a nuclear waste repository in Slove-

nia. Environmental monitoring around nuclear power plants also has used LSC for determining the tritium concentrations in the water near the power reactor output channel (Janovics et al., 2014). Tritium concentrations in drinking water sources, such as rain water and creek water, around a nuclear research facility in Serbia were analyzed by three preparation methods with a Quantulus^{TM} 1220 instrument (Nikolov et al., 2013).

Tritium concentration levels have been investigated in environmental samples using LSC around the Tokai reprocessing plan in Japan to monitor regulatory compliance and estimate the effective dose equivalent to the public. (Matsuura et al., 1995; Koarashi et al., 2008). Further details on the impact of the ULB LSC on these measurements and specific improvements to MDA, sample size, and process time for each example is available in the Journal of Radioanalytical and Nuclear Chemistry (Douglas, 2016). Most of these procedures require some method of enrichment of the tritium concentration. The required net count rates would be lower for an ultra-low background LSC, which would reduce or eliminate the amount of electrolytic enrichment necessary for the sample. Sample sizes and total processing time for tritium measurements would be reduced for meeting the lower net count rates needed with the ULB LSC.

The ULB LSC would improve upon previous work with ^{90}Sr by reducing MDAs and sample sizes. Strontium-90 is another radionuclide that can be used for monitoring nuclear facilities, fallout, and nuclear accidents. Strontium-90 has a high toxicity and a long residence time (radiological half-life of 28.8 years and biological half-life of 49.3 years (Courti et al., 2001)), which makes it an important radionuclide for monitoring dose assessment for humans (E.P. Hardy, 1977; Torres et al., 2000). Uptake of ^{90}Sr into food and milk after an incident would constitute an ingestion risk, especially for infants. Oikawa et al. (2013) analyzed ^{90}Sr in water off the Fukushima

coast in the aftermath of the Fukushima-Daiichi accident by counting the ^{90}Y daughter of ^{90}Sr with a low-background beta proportional counter. Takagai et al. (2014) have reported results of Inductively Coupled Plasma Mass Spectrometry (ICP-MS) analysis of ^{90}Sr in soil down-wind from the Fukushima-Daiichi nuclear power plant. Liquid scintillation methods with a 10-100 times background reduction could become a viable alternative for such analysis of ^{90}Sr, after spectral deconvolution and subtraction of the ^{90}Y ingrowth (Noakes JE, 1992; Kim et al., 2009), with smaller sample sizes. The high radiotoxicity of ^{90}Sr and daughter ^{90}Y have precipitated a volume of research on the rapid analysis of radiostrontium in milk (Kim et al., 2009; Maxwell and Culligan, 2009; Eikenberg et al., 2009). The Quantulus^{TM} 1220 has been incorporated into these methods after chemical purification (Kim et al., 2009). An instrument with a lower background would reduce the MDA or sample size requirement. Similarly, Heilgeist (2000) studied the ^{90}Sr concentrations in food samples with a Quantulus^{TM} 1220, where again an ultra-low background instrument would reduce the sample size and processing time. Commercially-available technologies are able to meet the regulatory limits for these applications. While an instrument with a lower background could still improve upon these procedures, the largest impact would come from the ability to measure samples that are only slightly elevated above background, such as following the spread of contamination in the environment.

Other applications of LSC include measurement of ^{227}Ac. This radionuclide can be used as an environmental chronometer to study ocean circulation patterns up to 100 years ago. Actinium-227 is not particle-reactive, and is released into the water column upon the decay of the parent ^{231}Pa, which is particle-reactive and remains in ocean floor sediment. Given the 21.8-year half-life of ^{227}Ac, a concentration of ^{227}Ac in seawater greater than that expected from the decay of ^{235}U present is indicative of water transport from the ocean floor (Geibert et al., 2002). The small concentration

of ^{227}Ac, however, presents measurement challenges to its use as an oceanographic tracer. Alpha spectrometry of the ^{227}Ac daughters is the current method of choice for analysis, but requires at least four months of ingrowth prior to counting (Geibert et al., 2002; Geibert and Voge, 2008; Percival and Martin, 1974). With a lower background instrument, direct counting of the ^{227}Ac could be achieved with LSC, minimizing the processing and sample preparation time required for the necessary daughter ingrowth.

Low background liquid scintillation methods have also been applied to the analysis of ^{222}Rn concentrations in groundwater for dose estimation (Lopez et al., 2004; Barnett and McKlveen, 1992). Additionally, low-background LSC has been used for determining radium and uranium concentrations in groundwater for monitoring water quality, uranium mining and ore processing, and phosphate fertilizer contamination (Sanchez-Cabeza and Pujol, 1998; Salonen, 1993; Salonen and Hukkanen, 1997). In addition to carbon dating, LSC of the ^{14}C concentration in tree rings has been useful in estimating historic occurrences of solar flares by subsequent atmospheric production and retention of ^{14}C (Suzuki et al., 1999).

1.1.3 Implications of an Ultra-Low-Background System

Advances in low-background liquid scintillation counting have extended liquid scintillation measurements to lower MDA levels, quantification, identification, and spectral analysis of alpha- and beta-emitting radionuclides. Commercial units such as the PerkinElmer Wallac Quantulus^{TM} 1220 have made this technique a consistent, viable, and available tool for researchers and for analysts (Vaupotic et al., 2011; Plastino and Kaihola, 2004). The commercial units make use of shielding with low background lead, automated sample movement, external source calibration and quench correction methods within a fairly compact unit. Units such as the Wal-

lac 1220 Quantulus^{TM} system from Perkin Elmer employ many of the background reduction techniques previously discussed. The resulting background rates are low, around 1 count per minute (cpm) in the low energy beta (tritium) window (Vaupotic et al., 2011; Plastino et al., 2007).

There are limitations to the background reduction inherent in the design of the available low-background systems that the development of an ultra-low background system can improve upon. Natural background radiation in the detection system materials and space considerations limit the background reduction in the commercial low-background systems. The design of the ultra-low background system can incorporate reductions in the background from all contributing source terms, both internal and external to the apparatus. By addressing each individual element in the system design, the background rate can be reduced by a factor of 10-100 below that of current low-background systems.

Typical commercial low-background liquid scintillation counters with backgrounds of ≈1 count per minute (cpm) can achieve detection limits on the order of 1 Bq of ^{3}H per liter with 1000-minute counting times. With a combination of a background of 10-100 counts per day and sample counting times on the order of days (to improve statistics in such a low-count-rate environment), the lower limit of detection of an ultra-low-background system could be more than an order of magnitude lower than is achievable in most commercial instruments.

Some of these applications require large volumes or sample sizes just to produce grams of detectable material. Liquid scintillation counting with very low background count rates can be a competitive process against other analysis techniques such as mass spectrometry or alpha spectrometry. In some cases, a lower achievable MDA will allow for more sensitive detection with the current techniques. In situations where the MDA is already sufficient, reduced sample size or total processing time for

the method would be a more prudent use of resources. For example, an improved MDA may allow greater reach in age-dating applications and geochronology. If tritium levels are known to be above a previously quantified level, the ULB LSC could decrease the required sample sizes and/or processing and analysis times.

The applications cited above highlight areas that a ULB LSC could have a high impact. Depending on the analysis technique, such a system would provide greater sensitivity and faster total process time. The amount of sample processing and enrichment could be reduced, particularly with regard to tritium in water samples. The reduction of necessary sample size would be the highest impact for applications in analysis of ^{90}Sr samples. For applications that currently utilize other detection methods over LSC, the ULB LSC could open liquid scintillation counting as a competitive option for immediate measurement of low concentrations of radionuclides that have previously relied on subsequent detection of in-grown daughter radionuclides, such as ^{227}Ac.

1.2 Proposed Research

The objectives for the research described in this work were to develop and characterize an Ultra-Low Background Liquid Scintillation Counter, from design aspects through testing with radioactive samples. The ULB LSC was designed to minimized background count rates using best practices of low-background system design and simulation estimates. System development included aspects of component testing, simulation validation, and system checks with a partial build. The final build was tested with LSC cocktail and radioactive samples for characterization of system performance and observed background count rates.

1.2.1 Design and Simulation

The ULB LSC shield design discussed in the next chapter is drawn from the concept of a layered shield, similar to those shields used in currently operating underground systems. Iterations of a simulation/design loop resulted in a simulation-informed shield design. Background contributions from each shield component in addition to external radiation background were investigated using GEANT4.

GEANT4 is a Monte Carlo methodology-based toolkit for particle transport developed and maintained by collaboration between scientists and software engineers across the globe. Applications can be developed for complex detector geometries for testing with any number of particles over a large energy range (from eV to TeV depending on the particle). Users can build their own application for a particular detector geometry, defining the geometry volumes, locations, and material properties. The application developer also defines the physics and particles used in the simulation by including the appropriate physics models. Particle paths and interactions can be tracked, and depending on the needs of the application, any relevant information can be written out into ROOT files for data management and analysis (Agostinelli et al., 2003; Allison et al., 2006).

Each shielding material for the ULB LSC was adjusted to achieve the lowest optimal, but reasonably achievable, background in the scintillation cocktail volume. Maintaining effective and efficient light collection in an ultra-low background environment presents another challenge. It is important that the light detection system (photomultiplier tubes) be as close as possible to the samples to ensure the highest collection efficiency achievable. However, background radiation from the naturally occurring radioactive materials (NORM) in the PMTs themselves is an unacceptably large background component for an effective ultra-low background system. Moving

the PMTs away from the sample will reduce the background interference by the inverse square of the distance between the sample and detector. However, this will also reduce the light collection efficiency.

Losses to the detection system collection efficiency can be minimized by adding a light guide between the sample and the PMTs. A unique design component for the system discussed in this research uses a bent, hollow copper light guide with a reflective coating. Using a bent light guide will allow the sample to be shielded from intrinsic radiation in the PMTs by an additional lead brick inserted between the PMT and the sample. The low-background lead brick inserted into the copper shielding between the PMT and sample chamber will attenuate any radiation in the direct path between the two. The estimated collection efficiency for a 99% specularly reflective coating is 36.9% per PMT, compared to the 34.4% per PMT from a similar, though shorter, straight orientation (Bernacki et al., 2015). From simulation, there is no loss in light collection efficiency from changing to a bent orientation, which complements the background reduction by moving the PMTs further from the vial. The final shield design incorporated nested layers of different shielding materials around hollow light guides with a highly reflective coating to obtain the most efficient light collection in the lowest achievable background environment. Using bent light guides will minimize the background contribution from the low-radioactivity PMTs, and the reflective coating will maintain light output from the sample vial to the PMT face.

A series of medium-fidelity simulations were conducted using GEANT4 to inform the shield design, estimate the total background observed in the system, and identify the largest background contributors. These simulations used geometries of blocks and cylinders to build a basic version of the shield. A high-fidelity simulation of the final shield design was created in GEANT4 to generate the most accurate background

estimation and to estimate the results of the system performance for different test cases. The system geometry was modeled as closely as possible to the finalized system design. Radionuclide levels in the construction materials were known via chemical assay or through prior research findings. Estimated neutron and gamma fluence rates were used for external sources; detailed primary modeling of cosmic ray-induced backgrounds was not a primary focus. The system performance was and can be further informed and understood through modeling, particularly to elucidate unexpected or deviating backgrounds.

1.2.2 Component Testing

The ULB LSC was constructed in the clean room environment in the Shallow Underground Laboratory (Aalseth, 2012; Runkle et al., 2012). The light collection, detection, and read-out components of the system were tested above ground before cleaning and transfer underground. From this testing, any adjustments that needed to be made could be anticipated or taken care of before construction. A quantitative assessment of the light detection system was performed above ground while the system was being built underground. Two acrylic light guides in the shape of the hollow light guide chambers were made to test for differences between straight and bent channel configurations. These guides are essentially negatives of the hollow copper light guides. Light collection with these guides was analyzed with the light guides unwrapped and then wrapped in Teflon® and electrical tape. Single-photon counting experiments were performed for a set of Hamamatsu R11410-MOD photomultiplier tubes in coincidence to mimic the detector setup and to reduce false counts from the dark current and cosmic ray backgrounds.

1.2.3 Characterization

Once the system became operational, the ULB LSC was characterized and compared to the Wallac Quantulus^{TM} 1220 in the above ground laboratory. The characterization included the performance of the rejection of cosmic events through active veto, observed background reduction, and light collection system for the ULB LSC. Events coincident between the LSC vial and external plastic scintillator panels are attributed to cosmic ray interactions. Rejection of these events from collected data for the ULB LSC is referred to as the "cosmic veto." The actual background count rate and contributions were determined. Light collection efficiencies and total detection efficiency were determined. Understanding of the light collection mechanisms and systems was aided by high-fidelity simulations of the system and the associated parameters.

1.2.4 Demonstration

The final segment of this research was a demonstration of the capabilities of the ULB LSC, relating to practical application of the system. A set of ^{90}Sr samples were prepared from dilution of readily available stock solution and counted in the ULB LSC. The spectral deconvolution capabilities were investigated by the analysis of the ^{90}Sr and ingrown daughter ^{90}Y. The activity was calculated from the counts, with corrections for mass and time normalization and background subtraction.

2. DESIGN AND SIMULATION

2.1 Simulation-Informed Design

A GEANT4 model was created from the original design concept to investigate background reduction methods through simulation. The original design was based on prior experience with low-background systems at PNNL and high-energy physics collaborations. As simulations were conducted to investigate different background mitigation methods, the model and design were modified to further reduce the overall background. The system design was intended to achieve the minimum background count rate in the sample chambers, maximize the ability to reject (or "veto") events due to cosmic muon interactions with a cosmic veto assembly, and create an effective sample changing mechanism. The goal of the simulations was to find the optimal balance between cost and effectiveness of materials in reducing the background environment inside the chamber.

2.1.1 Low Background Design Principles

Best practices of low-background shielding have been identified in high-energy physics experiments and similar low-background instrumentation in the SUL at PNNL. From lessons learned with experimental setups in the SUL, a 6-sided cosmic veto assembly of plastic scintillator panels was identified as necessary to optimally veto (>99%) LSC events coincident with signals from the cosmic veto assembly. Plastic scintillator panels of 5.08-cm thickness have been used successfully in the Ultra-Low Background Proportional Counter (ULPBC) and CASCADES germanium systems (Seifert et al., 2013; Aalseth et al., 2009; Keillor et al., 2009). A new feature in these ULB LSC panels was to use inset PMTs on the small, enclosed sides of the system. The PMTs were encased within the panel dimensions instead of in an

external housing protruding from the panels. In addition to a cosmic veto, 5.08-cm of borated polyethylene is set up around the lead cave to moderate environmental neutrons. The thermal neutron fluence rate used in simulation was measured with the ULBPC, which has 5.08-cm-thick borated polyethylene panels on each side. To achieve at least a similar thermal neutron fluence rate, the same amount and type of materials were used in the ULB LSC. Lead was used to decrease external gamma contributions to background. Three layers of lead of decreasing ^{210}Pb concentration were nested to minimize contributions to the background from the lead itself. Lead-210 decays by beta emission of 4.2 keV (84%) and 16.2 keV (16%) average energies. The bremsstrahlung radiation emitted as the beta slows down within the lead is itself an intrinsic background. By decreasing the concentration of ^{210}Pb in lead closer to the inner chamber of the system, the resulting bremsstrahlung contribution to background is decreased. The layers with lower ^{210}Pb concentrations mitigate the gamma-radiation background while contributing less bremsstrahlung to the background. Oxygen-Free High Conductivity (OFHC) copper was used inside the lead to reduce the background contributions from ^{210}Pb bremsstrahlung that escapes the lead layers. Inserting a copper liner into the CASCADES internal chamber resulted in a noticeable decrease in the low-energy background, so a copper layer was incorporated into the ULB LSC from design principles onward (Aalseth, 2012).

Creating a hollow reflective light guide out of the copper was chosen to avoid introducing another background element. The light guide was designed to be cut out of the copper quadrants which would then be coated with a metal layer to obtain a specularly reflective surface (Bernacki et al., 2015). The light guide has an upward 90° curve on either end to reduce the interactions of background emissions from the PMTs with the scintillation cocktail. Two PMTs are placed at the ends of the light guide to collect light in coincidence. The light guides were coated by Epner

Technology, Inc. (Brooklyn, NY). The reflective coating on the copper was a thin layer of silver deposited with low-pressure chemical vapor deposition (LPCVD), with no additional buffing or polishing. Silver was chosen for its 95% reflectivity at 420 nm (the emission wavelength of the Ultima Gold cocktails). Without any further polishing before coating, the light guides had a reflectance of 74%. The partial build was constructed with one of the 74% reflectance guides. This light collection efficiency was insufficient for the 1 keV threshold goal of the ULB LSC. Both guides were sent back to be polished and recoated, which resulted in an 88% reflectance.

The two PMTs at the ends of the light guide were set to trigger the data acquisition system for events coincident on both PMTs within a specified time window (1027 ns for this research). This was done to improve the signal-to-noise ratio by reducing accidental triggers or dark current noise rates. A copper cooling plate was placed below the copper light guides to stabilize the temperature around 5°C. A water/ethylene glycol mixture was chosen to be pumped through copper tubing set in the cooling plate and cycles through a heat exchanger outside the dark box. Future LSC samples will also be refrigerated before analysis to minimize chemiluminecense from the cocktail.

2.1.2 Medium Fidelity GEANT4 Model

The initial GEANT4 model consisted of an outer lead shield encompassing an ultra-low background lead shield, which housed the three chambers from the copper guides inwards. The two outer chambers were outfitted with the light guides, vials, LSC cocktail, and PMT cavities, tubes, and bases. The geometry includes a 10.16 cm thickness of lead around the opening to each PMT cavity as end caps for the background studies. The central chamber was left uninstrumented, containing a copper block, vial, and LSC cocktail. Figure 2.1 shows the model visualized using

GEANT4. The geometry files for the initial, iterative simulations (Version 3) and for the background source studies (Version 4) are attached in Appendix A.

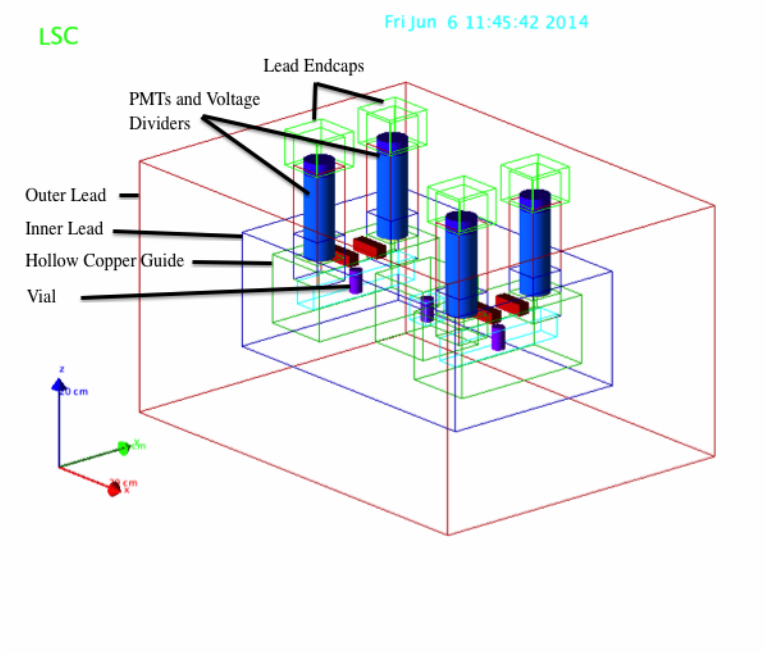

Figure 2.1: Visual representation of the medium fidelity GEANT4 model.

2.1.3 ULB LSC Shield Design

The ULB LSC has two main sections - the dark box and the sample changer mechanism. Figure 2.2 shows the dark box in the lower half of the system and sample changer in the upper half of the assembly. The dark box houses the bent-hollow copper light guide cut out of the copper, surrounding lead layers, copper cooling plate, borated polyethylene, and veto panels described in Section 2.1.1. The outer box was constructed from Bosch framing and aluminum panels, with taped edges to ensure a light-tight configuration.

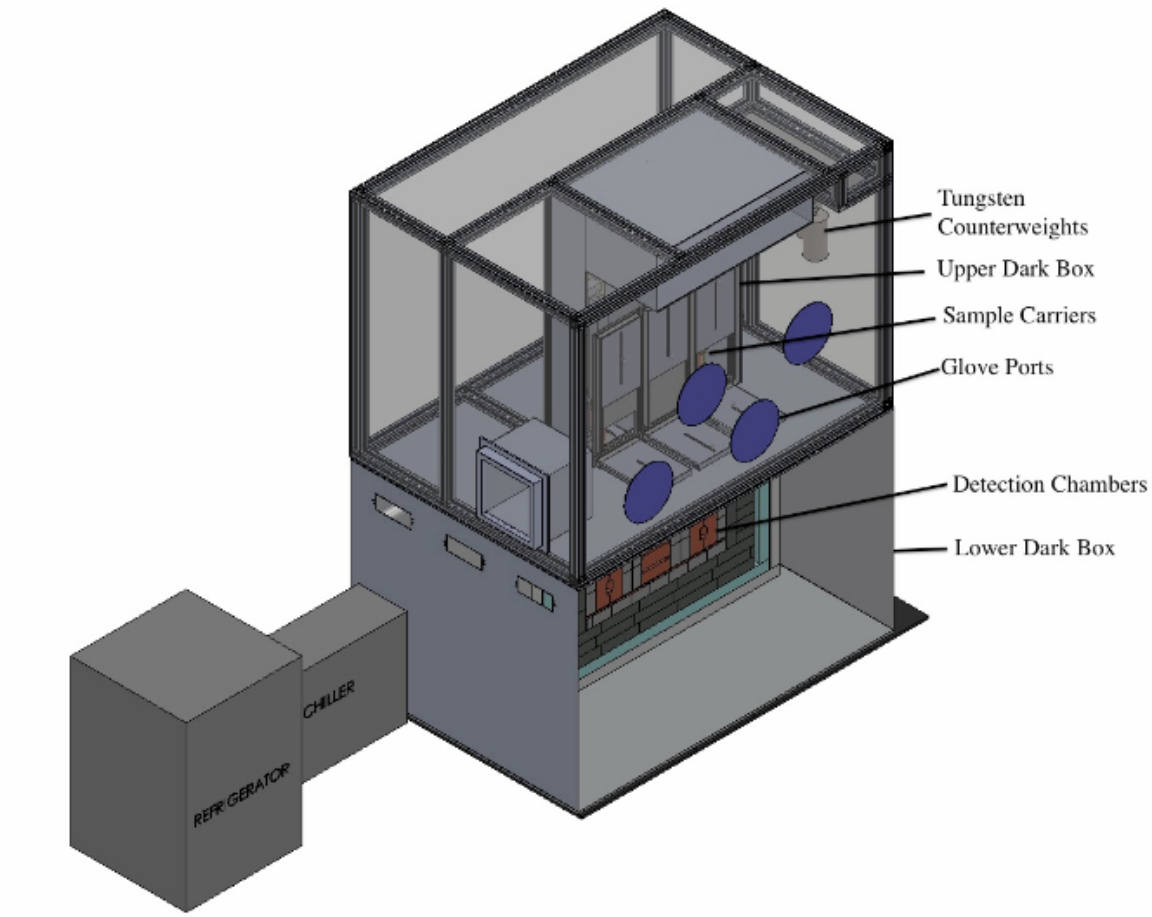

Figure 2.2: SolidWorks representation of the ULB LSC. From left to right, the components of the ULB LSC system include a refrigerator for sample storage,chiller (heat exchanger) for cooling the sample chambers, and the sample changer in a radon exclusion box on top of the dark box that houses the sample chambers.

The sample changer assembly relies on a system of pulleys and counterweights to lower the samples into the light guide chambers. The height of the assembly was limited by the room dimensions and the length of the sample plug. The pulley movement into the dark box included three right angle turns to mitigate the possibility of ambient light entering the detector chambers. The sample plug includes a copper

sample holder with room for a calibration point source on top of a 20 mL vial. A set pin holds the sample holder on the end of a solid copper plug, set below a lead-filled plug. The plugs fill the pathway through the copper light guide and lead layers above the sample to minimize the light path for external gammas to the sample chamber. The plugs are guided into the sample chamber by aluminum guide rails. There are small adjustments that can be made on the guide rails for fine-tuning the sample placement. The plugs are raised and lowered by raising or lowering the tungsten counterweights on the right side of the rails.

2.1.4 GEANT4 Simulation

Initial simulations were made for the estimated, intentionally conservative, source terms for each of the following: external gammas, PMT glass, copper shielding, reflective coating, lead shielding, and cross-talk between vials. A summary of the time and activities represented, events thrown, and hits recorded for each simulation is given in Table 2.1. The time indicates the number of days of decay that are simulated; the number of events thrown is the number of decays that happens within the listed time (the activity multiplied by the time). The source for the external gamma-ray simulation (UGroom) is a normalized gamma-ray spectrum collected in the shallow underground laboratory.

The external gamma simulations were based off measurements made of the background in the SUL with a NaI detector. The activities estimated for the two different lead volumes (60 Bq kg^{-1} and 3 Bq kg^{-1}) were estimated based off the literature value of 0.356 particles s^{-1} m^{-2}/(Bq kg^{-1}) (Vojtyla, 1996). The assumptions for the copper were order of magnitude concentrations of 10 ppt levels for ^{238}U and ^{232}Th and 100 ppb for ^{40}K (Leonard et al., 2008). The reflective coating was initially intended to be layers of Ta_2O_5 and SiO_2. Analysis of the precursor, tantalum(V) ethox-

Table 2.1: Source Terms and Recorded Hits for Medium Fidelity Simulations

Simulation	Source	Time (d)	Activity	Events	Hits
Ext. Gammas	UGroom	1.03		10^{10}	2
PMT	^{238}U	1000	0.4 mBq	34560	57
Glass	^{232}Th	1000	0.3 mBq	25920	35
	^{40}K	1000	8.3 mBq	717120	92
	^{60}Co	1000	2 mBq	172800	203
Total Hits					387
Refl. Coating	*Total Hits*				3460
Horizontal	^{238}U	1000	0.61 μBq cm^{-2}	32669	2316
Channel	^{232}Th	1000	0.20 μBq cm^{-2}	10890	807
	^{40}K	1000	1.31 mBq cm^{-2}	8154	113
Total Hits					3236
Vertical	^{238}U	1000	0.61 μBq cm^{-2}	14293	44
Channel	^{232}Th	1000	0.20 μBq cm^{-2}	4764	7
	^{40}K	1000	1.31 mBq cm^{-2}	3567	2
Total Hits					53
Outer	^{238}U	1000	0.61 μBq cm^{-2}	117745	98
Surface	^{232}Th	1000	0.20 μBq cm^{-2}	39248	19
	^{40}K	1000	1.31 mBq cm^{-2}	29389	1
Total Hits					118
Copper	^{238}U	100	125 μBq kg^{-1}	61090	305
Shielding	^{232}Th	100	40 μBq kg^{-1}	19549	60
	^{40}K	100	300 μBq kg^{-1}	146617	18
	^{60}Co	100	0.23 μBq cm^{-1}	12635	38
Total Hits					421
Lead	Outer-Middle	10	60 Bq kg^{-1}	21400000	14
Shielding	Outer-PMT	10	60 Bq kg^{-1}	1070000	0
^{210}Pb	Middle-Inner	10	3 Bq kg^{-1}	229000	10
	Middle-PMT	10	3 Bq kg^{-1}	25000	2
	Middle-Central	10	3 Bq kg^{-1}	129000	6
	Extra-Inner	10	3 Bq kg^{-1}	8330	3
Total Hits					34
Cross-Talk	2615 keV γs	1000	10 γ min^{-1}	14400000	29.5

ide, showed U/Th content of <0.04 ng/g (0.047 pg cm^{-2}) and <1 ppm (1.169 ng cm^{-2}) of natural potassium in the tantalum(V) ethoxide (Kozono et al., 2000) and

(McLean and Watterson, 2014), respectively). These values were used to estimate the impurity levels in the SiO_2 precursor, *d*-t-butoxydiacetoxysilane, as well. These precursor impurity values were carried over as assumptions for the coating materials. Surface source concentrations of 0.012 pg cm^{-2} of ^{238}U and ^{232}Th (with decay chains in secular equilibrium) and 0.3 ng cm^{-2} of natural potassium, were simulated for all of the surfaces on the copper light guide. The estimates for the PMT glass were conservative estimates taken from the analysis done in the high-energy physics community: 8.3 mBq PMT^{-1} of ^{40}K, 2 mBq PMT^{-1} of ^{60}Co, 0.4 mBq PMT^{-1} of ^{238}U, and 0.3 mBq PMT^{-1} of ^{232}Th (Akerib et al., 2013). Cross-talk was addressed with a 2615 keV gamma source (representing the highest-energy background gamma from ^{208}Tl), emitting at a rate of 10 γ-rays per minute. The activity estimates were calculated for the plastic vials and environmental neutrons as shown below in Eq. 2.1.

$$\begin{aligned}
&\text{Activity}\left(\frac{\text{decays}}{\text{day}}\right) \\
&= \begin{matrix}\text{Specific} \\ \text{Activity}\end{matrix}\left(\frac{\mu\text{Bq}}{\text{kg}}\right) \times \text{Mass}\left(\text{kg}\right) \times 86400\left(\frac{\text{s}}{\text{day}}\right) \\
&= 125\left(\frac{\mu\text{Bq}}{\text{kg}}\right) \times 0.01\left(\text{kg}\right) \times 86400\left(\frac{\text{s}}{\text{day}}\right) \\
&= 0.1\left(\frac{\text{decays}}{\text{day}}\right)
\end{aligned} \tag{2.1}$$

The background of the polyethylene LSC vials was estimated by calculation instead of simulation. The estimation is based on the mass of the vial, specific activity of ^{238}U, ^{232}Th, and ^{40}K and an assumed contamination level. Part per trillion levels of U/Th were assumed for a 10-g plastic vial, resulting in 12.5 μBq kg^{-1} of ^{238}U,

for a total of $\sim$125 μBq kg^{-1} including ^{238}U daughters. For a 10-g plastic vial, that is 1.25 μBq, or 0.1 decays per day. The combined activity of the ^{232}Th and ^{40}K is assumed to be half of the activity of the ^{238}U chain, resulting in a total estimated background count rate of $\sim$0.15 decays per day. This will be an overestimate of the background actually observed for these contributors because of the less than 100% detection efficiency for decays in the vial walls.

The estimated neutron background for the liquid scintillation cocktail is calculated from the 2.4 $\pm$ 0.4 $\times$ 10^{-6} neutrons cm^{-2} s^{-1} neutron background measured in the underground proportional counter ULBPC system at PNNL, described in Sec. 2.1.1. The cross-sections and reaction rates were calculated for 20 mL of the GEANT4 liquid scintillation cocktail consisting of ^{12}C, ^{13}C, ^{1}H, ^{2}H, ^{16}O, ^{17}O, ^{18}O, ^{14}N, ^{15}N. This resulted in a the total macroscopic neutron capture cross-section of 0.016 $\pm$ 0.003 cm^{-1}. By multiplying the macroscopic neutron capture cross-section by the neutron flux over the sample volume, a reaction rate of $(7.67 \pm 1.28) \times 10^{-7}$ neutron captures per second is calculated. Over a period of one day, the resulting background is estimated to be 0.066 ± 0.011 cpd. A background count rate of 0.016 $\pm$ 0.003 cpd from ^{64}Cu, produced by thermal neutron capture on ^{63}Cu, is calculated for the 76.7 kg of copper in the light guide and a 0.009% efficiency for resulting counts from the vial. Inelastic scattering of neutrons on lead produces a dominant 803 keV gamma-ray that may reach the liquid scintillation cocktail producing unwanted scintillation events. Two (extrema) situations were studied for the efficiency of energy deposition by the 803-keV gamma-rays: (1) All 803 keV gamma-rays are emitted isotropically from the inner surface of the inner-most 5.08 cm of lead and (2) All 803 keV gamma-rays are emitted isotropically from the outer surface of the inner-most 5.08 cm of lead. The efficiency of production of an energy deposition in the LSC cocktail was $(2.5 \pm 0.2) \times 10^{-4}$ and $(1.5 \pm 0.4) \times 10^{-5}$ for extrema situations 1

and 2, respectively. The background calculated with the higher of the two efficiencies results in 0.027 ± 0.005 cpd background rate, which is a small part of the overall background rate. Combined, neutron background estimate is 0.109 ± 0.012 cpd. More detail on these calculations is available in literature (Erchinger et al., 2015).

The estimated background count rate from these contributing factors is 13.9 ± 1.2 counts per day, referred to here-after as the physics or radiative emissions background. A breakdown of the contributing factors that were estimated is given in Table 2.2.[1] This is by no means an exhaustive list of factors that contribute to the overall background, but an estimate of the leading contributors of the physics background. Systematic background sources are not included in the 13.9 counts per day estimate.

Table 2.2: Background contributors to the sample vials in the left or right measurement chambers due to ubiquitous radionuclides in the environment and instrument construction materials. The background rate is estimated in counts per day (cpd) (Erchinger et al., 2015).

Background source (contributing radionuclides)	Rate (cpd)	Fraction (%)
External γ-rays (U/Th/K)	2 ± 1	14.4 %
Lead shield (^{210}Pb)	3.4 ±0.6	24.5 %
Copper shielding (U/Th/K/^{60}Co)	6.6 ±0.26	47.6 %
Light guide coating (U/Th/K)	0.008 ±0.001	<1 %
PMTs (U/Th/K/^{60}Co)	1.6 ±0.1	11.5 %
Vial plastic (U/Th/K)	0.15	1.1 %
Cross-talk (Presumed 2615 keV γ-ray)	0.03 ±0.004	<1 %
Neutrons	0.11 ±0.012	<1 %
Total estimated background rate	13.9 ±1.2	

[1]Reprinted from Applied Radiation and Isotopes, Volume 105, Erchinger, J.L., *et. al.*, Development of a low background liquid scintillation counter for a shallow underground laboratory, Page 216, Copyright (2015), with permission from Elsevier.

2.2 High-Fidelity Simulation

2.2.1 Improvements to GEANT4 Simulation

The medium-fidelity GEANT4 model was useful for initial estimations and showed how effective a background reduction method would be. As progress was made and the ULB LSC design was changed, the simulation and geometry were modified. The high-fidelity simulation geometry uses the final dimensions as represented in shop drawings for the physical materials. The polyvinyl toluene (PVT) veto panels were added with associated offset from the borated polyethylene panels. The dimensions for the lead shield and copper light guide were updated, with cavities inserted for the sample holder plugs. These cavities were made as cylinders in each layer in order for the material to be changed between the layer material and air for full and partial build simulations. The copper cooling plate was not added into the bottom of the lead layer in the simulation, but the amount of lead surrounding the light guide is consistent with the design and build.

2.2.2 GEANT4 Geometry

The dimensions and materials of the simulation geometry pieces are given in Table 2.3. Several parts have multiple copies or are separately defined in order to reflect the material definition. A visualization of the geometry is shown in Figure 2.3.

Table 2.3: GEANT4 Geometry Dimensions and Materials

Layer	Material	X (cm)	Y (cm)	Z (cm)
World	Air	150.0	150.0	150.0
Veto Panels	PVT	130.18	109.86	100.00
Borated Poly	BoratedPE	119.38	99.06	89.20
Outer Shield	Pb	104.14	83.82	60.96
LB Shield	Pb			
ULB Shield	Pb			
Inner Shield	Cu			
Extra Shield	Pb	7.62	2.54	2.54
Inner Cavity	Air	4.00	27.94	5.00
Inner Vertical Cavity	Air			
PMT Cavity	Air	7.62	7.62	25.40
PMT Endcap	Pb	17.78	17.78	11.64
Part	Material	OD (cm)	Thickness or Length (cm)	Inner Thickness (cm)
Port Hole	Cu	5.40	10.40	
Port Fill	Pb	4.83	10.40	
Port Hole LB	Pb	5.40	5.08	
Port Hole ULB	Pb	5.40	5.08	
Port Hole I	Cu	4.27	7.5	
Vial	PET	2.70	5.0	4.8
Liquid	LSC2	2.5	4.07	
PMT Glass	Glass	6.4	0.2	
PMT Tube	LightAl	6.6	18.6	
PMT Base	LightAl	6.6	3.0	

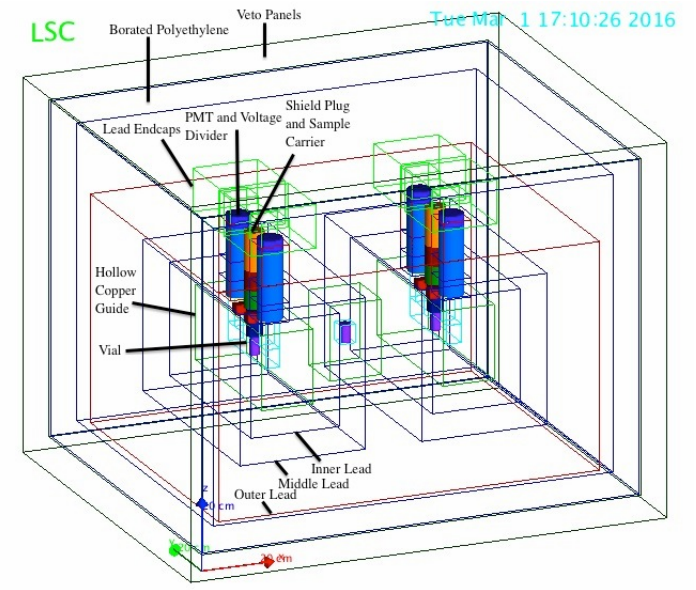

Figure 2.3: Visualization of the high-fidelity GEANT4 simulation geometry. The external housing is the cosmic veto assembly, which surrounds a layer of borated polyethylene. The lead cave was housed inside the polyethylene. The two chambers are visible inside the lead cave. Each chamber includes layers of low-background and ultra-low-background lead around the copper light guides. Each chamber has two PMTs one either end of the light guide with lead end caps above the PMTs. Sample vials with LSC cocktail are placed in the center of the chambers, and shield plugs have been inserted into the sample port of each chamber between the PMTs. A central chamber in the center of the lead cave houses a sample vial inside a copper block.

2.2.3 Validation

The GEANT4 model was updated in parallel with the the installation and operation of the partial build of the ULB LSC. Simulations were run that included the borated polyethylene and veto panels as well air-filled cavities for the sample plug. The dimensions and sectioning of the lead and copper shields were not included at this point. The simulation results for external gammas on this configuration were $\sim$2600 (2633 $\pm$ 77) cpd, within 10% of the $\sim$2500 (2586 $\pm$ 71and 2363 $\pm$ 68, respectively) cpd observed for the Ultima Gold AB and uLLT cocktail backgrounds.

2.2.4 Simulations Performed

Simulations were performed for the full build to estimate the final observed background from a variety environmental sources. The associated source reference file was included in the LSC executable file while the source placement, geometry, and intensity were defined in the LSC macro. Table 2.4 shows the simulation source, placement, time, histories run, and hits, and Table 2.5 gives the resulting counts per day.[2] A comparison of the expected background count rate from the high fidelity to medium fidelity models is given in Table 2.6. For the external gamma simulation, the source was a histogram file (UGroom.dat) of a gamma spectrum simulated to match a measured background in the underground laboratory. From the simulations, the expected environmental background is 9.8 $\pm$0.9 counts per day.

[2]Reprinted from Applied Radiation and Isotopes, In Press, Erchinger, J.L. *et. al.*, Background characterization of an ultra-low background liquid scintillation counter, Page 2, Copyright (2017), with permission from Elsevier.

Table 2.4: Source Terms and Hits Recorded for High Fidelity Simulations

Simulation	Source	Time (d)	Activity	Events	Hits
Ext. Gammas	UGroom	0.45		4320000000	1
PMT	^{238}U	1000	0.4 mBq	34560	0
Glass	^{232}Th	1000	0.3 mBq	25920	3
	^{40}K	1000	8.3 mBq	717120	13
	^{60}Co	1000	2 mBq	172800	0
Total Hits					16
Refl. Coating	*Total Hits*				3405
Horizontal	^{238}U	1000	0.61 μBq cm^{-2}	25475	2334
Channel	^{232}Th	1000	0.20 μBq cm^{-2}	8340	597
	^{40}K	1000	1.31 mBq cm^{-2}	6363	129
Total Hits					3060
Vertical	^{238}U	1000	0.61 μBq cm^{-2}	8163	67
Channel	^{232}Th	1000	0.20 μBq cm^{-2}	2673	20
	^{40}K	1000	1.31 mBq cm^{-2}	2039	1
Total Hits					88
Outer	^{238}U	1000	0.61 μBq cm^{-2}	187566	143
Surface	^{232}Th	1000	0.20 μBq cm^{-2}	61406	26
	^{40}K	1000	1.31 mBq cm^{-2}	46849	0
Total Hits					169
Copper	^{238}U	100	125 μBq kg^{-1}	21345	62
Shielding	^{232}Th	100	40 μBq kg^{-1}	8538	12
	^{40}K	100	1000 μBq kg^{-1}	85379	90
	^{60}Co	100	0.69 μBq cm^{-1}	21916	117
Total Hits					281
Lead	Outer-LB	10	60 Bq kg^{-1}	22600000	117
Shielding	Outer-PMT	10	60 Bq kg^{-1}	786000	0
^{210}Pb	LB-ULB	10	30 Bq kg^{-1}	6690000	1
	LB-PMT	10	30 Bq kg^{-1}	250000	0
	ULB-Inner	10	3 Bq kg^{-1}	322000	3
	ULB-PMT	10	3 Bq kg^{-1}	25000	0
	ULB-Central	10	3 Bq kg^{-1}	139000	11
	Extra-Inner	10	3 Bq kg^{-1}	8330	0
Total Hits					5
Cross-Talk	2615 keV γs	1000	10 γ min^{-1}	14400000	8
Neutrons	Thermal	1000000	$(2.4 \pm 0.4) \times 10^{-6}$ (cm^{-2} s^{-1})	11937650	14
	Fast	1000000	$(1.0 \pm 0.2) \times 10^{-5}$ (cm^{-2} s^{-1})	49740210	3430
Total Hits					3444
PMT Base	^{238}U	100	56.7 mBq	4896000	61
	^{232}Th	100	10.53 mBq	910080	7
	^{40}K	100	3.43 mBq	296640	0
	^{60}Co	100	0.5 mBq	43200	1
Total Hits					69

Table 2.5: High Fidelity background contributors to the sample vials in the left or right measurement chambers due to ubiquitous radionuclides in the environment and instrument construction materials. The background rate is estimated in counts per day (cpd) (Erchinger et al., 2017).

Background source (contributing radionuclides)	Rate (d^{-1})	Fraction (%)
External γ-rays (U/Th/K)	1.5 ±0.9	15.3
Lead shield (^{210}Pb)	0.50 ±0.22	5.1
Copper shielding (U/Th/K/^{60}Co)	2.81 ±0.17	28.7
Light guide coating (U/Th/K)	3.41 ±0.06	34.8
PMTs (U/Th/K/^{60}Co)	0.03 ±0.01	0.3
PMT Base	1.38 ±0.08	14.1
Vial plastic (U/Th/K) *(calculation)*	0.15	1.5
Cross-talk (Presumed 2615 keV γ)	0.008 ±0.003	0.1
Neutrons	0.0003444 ±0.0000059	0.1
Total estimated background rate	9.78 ±0.91	

Table 2.6: High Fidelity background contributors to the sample vials in the left or right measurement chambers due to ubiquitous radionuclides in the environment and instrument construction materials. The background rate is estimated in counts per day (cpd).

Background source (contributing radionuclides)	High Fidelity CR (cpd)	Medium Fidelity CR (cpd)
External γ-rays (U/Th/K)	1.5 ±0.9	2 ± 1
Lead shield (^{210}Pb)	0.50 ±0.22	3.4 ±0.6
Copper shielding (U/Th/K/^{60}Co)	2.81 ±0.17	6.6 ±0.26
Light guide coating (U/Th/K)	3.41 ±0.06	0.008 ±0.001
PMTs (U/Th/K/^{60}Co)	0.03 ±0.01	1.6 ±0.1
PMT Base	1.38 ±0.08	
Vial plastic (U/Th/K)	0.15	0.15
Cross-talk (Presumed 2615 keV γ)	0.008 ±0.003	0.03 ±0.004
Neutrons	0.0003444 ±0.0000059	0.11 ±0.012
Total estimated background rate	9.78 ±0.91	13.9 ±1.2

3. BUILDING UP TO AN UNDERGROUND SYSTEM

3.1 Above-Ground Testing

3.1.1 PMT and PXI Testing

Initial tests were performed with a Hamamatsu R11410-20 PMT with a Hamamatsu E2979 PMT base to look at energy spectra of point sources on a vial of cocktail, Single Photoelectron (SPE) data, and determining PXI settings for PMT and scintillation light. Initial PXI settings were selected based on the rise time and pulse time scales of the scintillation light pulses. An example of a typical pulse is shown in Figure 3.1. The PXI settings used for the direct PMT output (no preamplifier) are summarized in Table 3.1. The rise time is 10 ns and pulse time is ∼40 ns total, with one afterpulse feature 120 ns after the trigger. The minimum settings available on the PXI 500-Express are 8 ns for the trigger filter rise time and 0.040 ns for the energy filter rise time and flat top. The threshold was set just above the noise peak. The trace delay was set to center the pulse in the acquired trace data, and the waveform length long enough to include the entire waveform and after-effect. Integrator mode 1 was chosen to use the integrator for determining energy instead of trapezoidal filtering. The offset was set to 10% and the digital gain maxed at 3.190 to try and use as much of the ADC dynamic range as possible. Testing with the ^{3}H base showed pulses on the order of mV. Since the ADC range on the PXI is 2 V, increasing gain made use of more of the ADC range. This narrows the energy range to the region of interest for alpha/beta measurements, with a maximum around 3 MeV. Focusing on this energy range displays spectral features in more detail than a wider energy range.

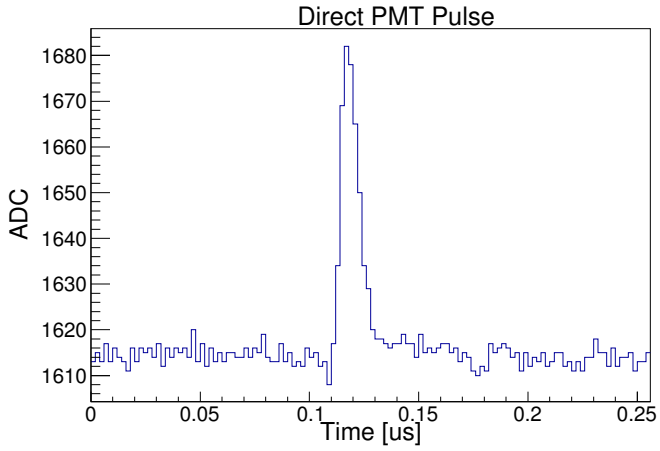

Figure 3.1: Example of pulse with direct output from the PMT.

Table 3.1: Initial PXI Settings in PixieViewer

Tab	Setting	Value
Trigger Filter	Rise Time (μs)	0.040
	Flat Top (μs)	0.040
	Threshold (ADC units)	1.6
Energy Filter	Rise Time (μs)	0.112
	Flat Top (μs)	0.112
	Tau (μs)	0.018
	Integrator	1
Waveform	Trace Length (μs)	0.256
	Delay (μs)	0.150
Oscilloscope	Time Bin (μs)	0.067
	% Offset	10%
	Gain	3.190

With these settings, the PMT response to a series of gamma point sources on the LSC cocktail was investigated. Four data sets were taken using the following radionuclides set on the cap of the 20 mL vial: ^{109}Cd, ^{57}Co, ^{133}Ba, ^{137}Cs, ^{22}Na, ^{60}Co. The vial with Ultima Gold A/B Cocktail was set between R11410 (test) and

R8778 (trigger) PMTs, ∼0.635 cm from each PMT face. Energy spectra for a 30-minute count time and threshold of 2 ADC units are shown in Figure 3.2 for this setup. Variable source activities resulted in variable intensities, but the Compton edges consistently increased with increasing energy. For all sources, the maximum channel was 32768. The scale is linear as opposed to the semilogarithmic scale used by most commercial liquid scintillation counters. Compton scattering is the primary interaction between the gammas from the external sources and the LSC cocktail for the energies of these decays. In the external standard spectra, the Compton edge is in the downturn of the energy spectrum towards the end of the spectrum, and the continuum extends down to the lower energy portion of the spectrum. For some radionuclides with gamma decays at multiple energies, such as ^{22}Na, the Compton spectra for the various gamma decays can be distinguished. The energies of the dominant gamma rays are used to calculate the Compton edge energies using Eq. 3.1, where E is the energy of the gamma ray and E_{max} is the maximum energy transferred to an electron (Compton Edge).

$$E_{max} = \frac{2E^2}{2E + m_e c^2} \tag{3.1}$$

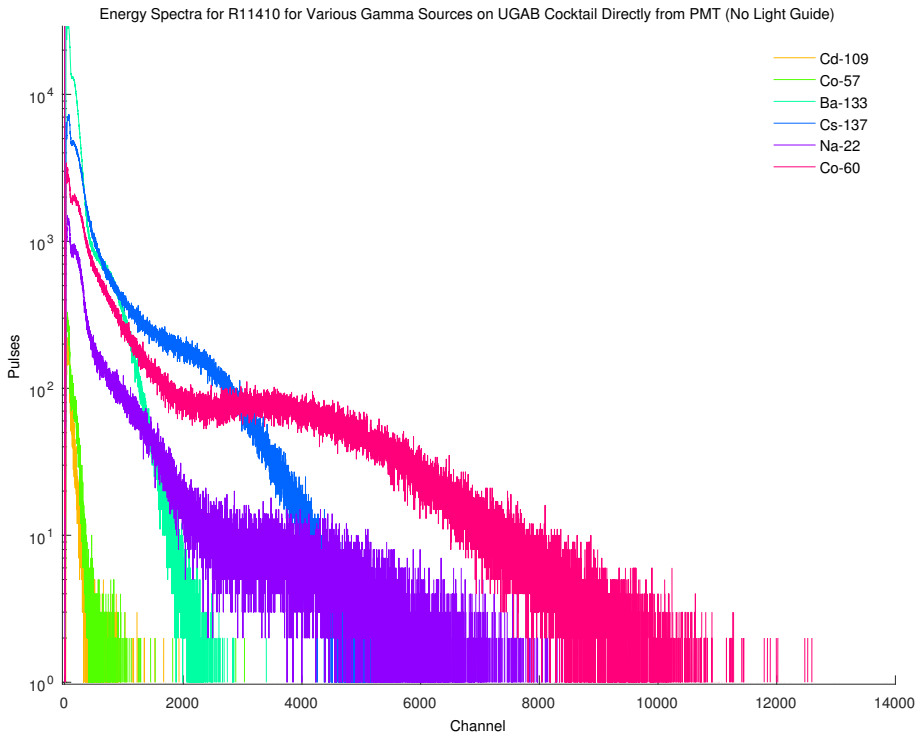

Figure 3.2: MCA spectra for various gamma sources on the UG-AB cocktail with PMTs 0.635 cm from the PMT faces.

The same tests were repeated with the curved (bent) light guide (BLG) optically coupled to the PMTs. The same spectral features were observed with the curved light guide installed as with the direct PMT trials, shown in Figure 3.3. Note that the endpoints are at higher channel numbers with the bent light guide. The number of counts per bin is higher than observed with the direct PMT setup and the spectral features are more pronounced. The higher channel endpoints indicated that more photons are impinging on the PMT face compared to the direct PMT measurements as a result of higher light collection efficiency with the light guide than without it. The higher count rates mean more events are propagated and detected, leading to

the conclusion of higher detection efficiency with the light guide than without despite the further distance between the PMTs and vial. The photon propagation is almost twice as high with the bent light guide than even having the PMTs close to the vial. Both data sets are plotted together in Figure 3.4, where this improvement in photon propagation and the effects on spectral range and features are visible.

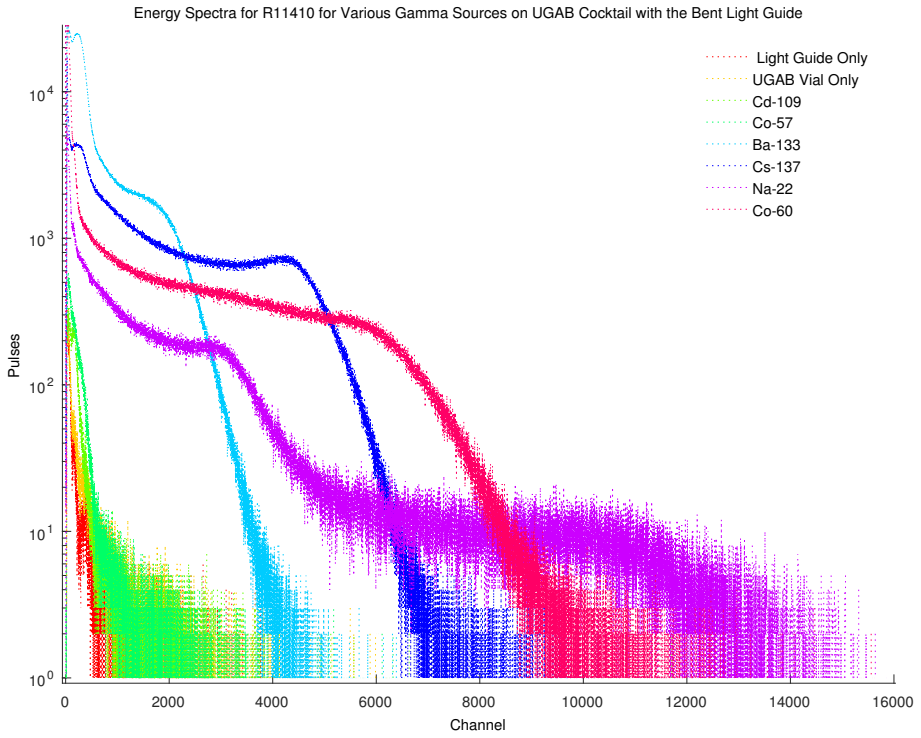

Figure 3.3: MCA spectra for various gamma sources on the UG-AB cocktail with PMTs coupled to the bent light guide.

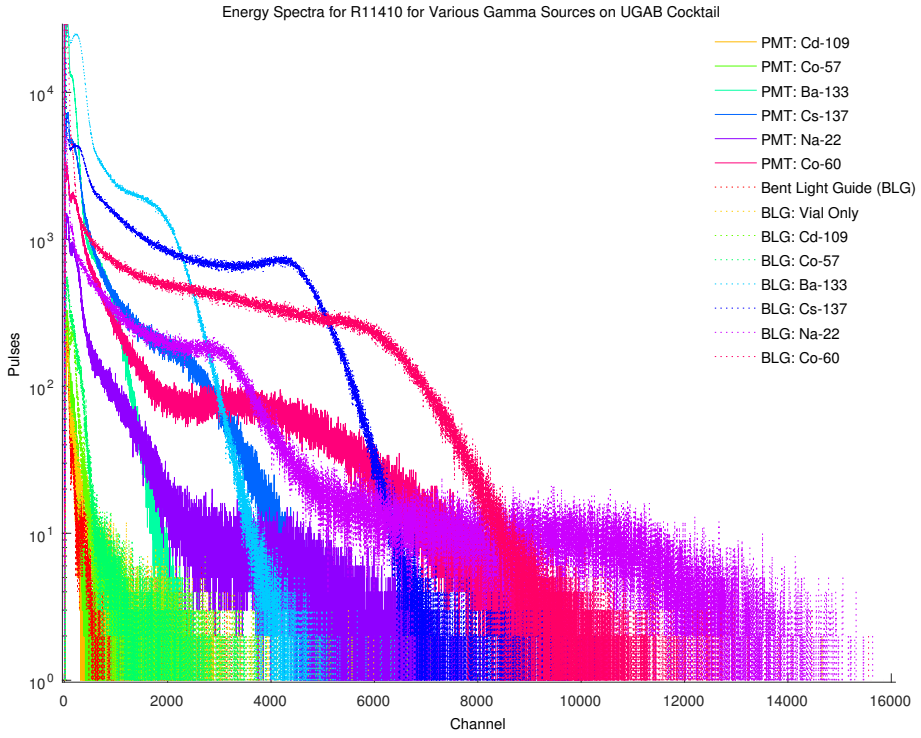

Figure 3.4: MCA spectra for various gamma sources on the UG-AB cocktail with and without the bent light guide.

Ideally a single photoelectron spectrum shows the PMT response to a single, double, and possibly higher multiples of photoelectrons. Knowing the single photoelectron value is important for gain calculations and calibrations. Back-calculating the number of photons that hit the PMT face from the number of photoelectrons for a given spectral response is useful in determining the light collection efficiency of a light guide. By using a 5.08 cm x 10.16 cm x 20.32 cm lead brick (thickness of 5.08 cm between vial and PMT) and increased distance to attenuate the photons from the vial, the photoelectron response in Figure 3.5 was obtained. The PMTs were moved incrementally further from the vial out to a distance of 30 cm for a series of

tests with ^{57}Co and ^{137}Cs. To further attenuate the photons incident on the PMT, a lead brick was placed between the vial and PMT, $\sim$2 cm in front of the PMT face. The resulting response from the ^{137}Cs trials shows peaks for single, double, and triple photoelectron events around MCA channels of 25, 45, and 55 in Figure 3.5 for the above-ground testing setup. The digital amplification was maximized to expand the spectrum as much as possible, but the low number of photoelectrons converted limited the spectral distribution within the low number of channels shown.

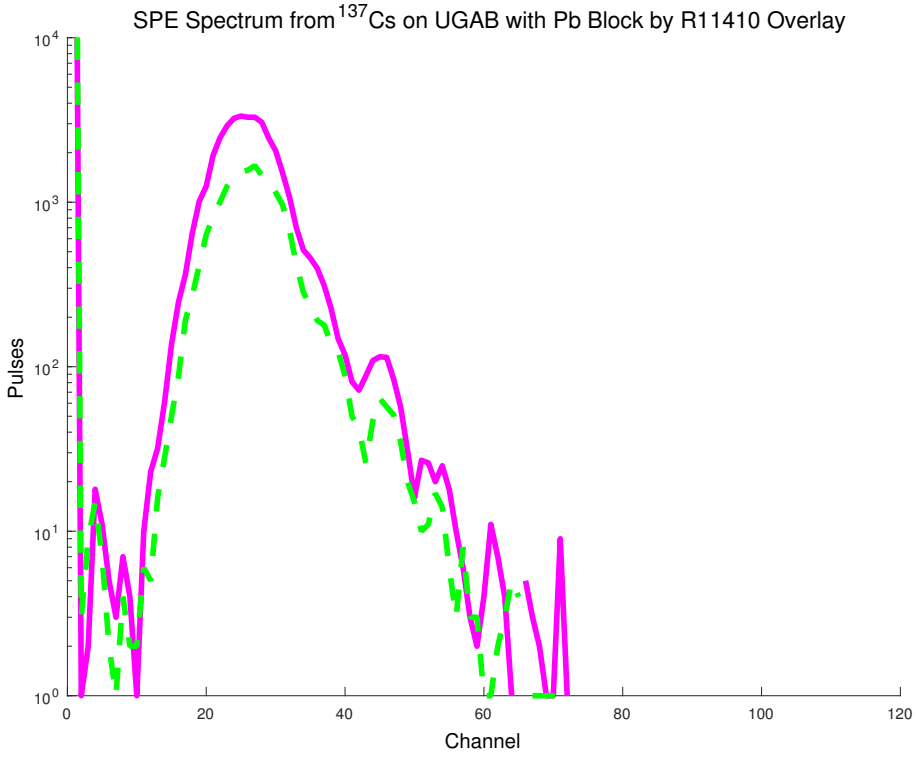

Figure 3.5: Single photoelectron spectrum for R11410 in above ground testing.

3.1.2 Veto Panel Calibration and Testing

Veto panels of BC-408 equivalent plastic were obtained from Eljen Technology (Sweetwater, TX). Specifications for each are given in Table 3.2. Panel 4 has three holes for sample ports centered along the length of the panel.

Table 3.2: Veto Panel Specifications

Panel	Placement	Model Number Serial #	Dimensions (mm)	PMT A/B	PMT Serial #
1	Back	550-20x354x513-1	20 x 354 x 513	A	206910
		6378-01-01		B	206916
2	Front	550-20x354x513-1	20 x 354 x 513	A	206917
		6378-01-02		B	206912
3	Bottom	550-20x433x513-1	20 x 433 x 513	A	206914
		6378-01-03		B	206909
4	Top	550-20x433x513-1	20 x 433 x 513	A	206915
		6378-01-04		B	206911
5	Right	550-20x354x393-1	20 x 354 x 393	A	206906
		6378-01-05		B	206913
6	Left	550-20x354x393-1	20 x 354 x 393	A	206908
		6378-01-06		B	206907

Voltages were set to first match with the PMTs on each panel, then the panels to each other. Adjustments were made after initial matching to adjust the placement of the valley between the high-energy gamma and muon events. A preamplifier was used in signal processing for the MCA spectra for the above-ground testing of voltage settings. With a preamplifier added into the signal processing path, the PixieViewer setting were adjusted accordingly for energy calculations through trapezoidal filtering. The charge integration and slight amplification provided by the preamplifier increased the voltage of the output signals, utilizing a larger portion of

the ADC range for diagnostic testing while still including the high-energy portion of the gamma spectrum.

The voltages in Table 3.3 show the high voltage settings for each PMT in the veto panel array determined from above-ground testing. The peak and valley channels from the above ground testing for each panel are given in Table 3.4. Adjustments were made once underground, and revised voltages are given in Section 5.2.

Table 3.3: HV Settings for Veto Panels

Panel	Channel	PMT A (V)	PMT B (V)	Threshold
1 (Back)	0	745	730	100
2 (Front)	1	660	655	100
3 (Bottom)	2	1150	980	150
4 (Top)	3	920	970	140
5 (Right)	4	810	810	100
6 (Left)	5	920	920	100

Table 3.4: Peak and Valley Channels from Initial Testing of the Veto Panels

Panel	Peak Channel	Trough Channel
1 (Back)	4600	2700
2 (Front)	4600	2700
3 (Bottom)	4500	2800
4 (Top)	5000	2900
5 (Right)	4600	2900
6 (Left)	4500	2900

3.2 Cleaning Processes

Before taking the equipment into the underground cleanroom laboratory, all the equipment and materials were cleaned and bagged. Most materials were wiped down with ethanol to remove dirt, grease, and oils. Smaller, machined pieces, such as screws or T-blocks, were sonicated in ethanol or 3% by volume micro-90 (soap reagent) solution. The copper pieces for the light guide were etched with a sulfuric acid/peroxide mixture and passivated with nitric acid, dried with N_2 and bagged before being sent for coating with silver. The coated light guides were cleaned with an ethanol wipe before going underground. The lead was divided into two cleaning groups. Most of the lead bricks were cleaned with an ethanol wipe, but the lead for the innermost layer surrounding the light guides was etched in sulfuric acid and nitric acid/peroxide solutions, rinsed, dried and bagged. Excess acid on the external surfaces of the copper quadrants and lead bricks was assumed to be removed with the ethanol wipe and nitrogen dry. The contributions to the background count rate of the uranium and thorium that leached into the materials from the acids were not calculated or simulated, but might have resulted a small increase in the background count rate above the expectation from simulation.

3.3 Shield Build and Lower Cave Build

The lower cave and dark box was built over the summer and fall of 2015. Snapshots of the progress are shown in Figure 3.6. The base plate, bottom veto panel, borated polyethylene, and lower lead layers were laid down first. One light guide and surrounding lead were laid in place and the inside of the light guides left under a nitrogen purge. The PMT mounts and PMTs were added with the Hamamatsu E2979 bases. Lead was stacked up around the PMTs, bases, and the full lead stack to the last layer with the bases. No endcaps were added around the PMT cavities

and the shield plug hole remained open during testing. The side borated polyethylene panels and veto panels were added and all edges taped to increase stability and close potential light leaks. The top panels were then set in place and taped to cover light gaps. The hole cut in the panels for cable feedthrough was covered with an L-shaped aluminum plate, with room for the cables to feed out the bottom. Copious amounts of tape were used to minimize the chances of light leakage into the system. The tape is assumed not to contribute to the background due since it is external to the shielding and was cleaned prior to use. The three sample port holes on the top panel were covered with 3"x3" aluminum plates taped in place.

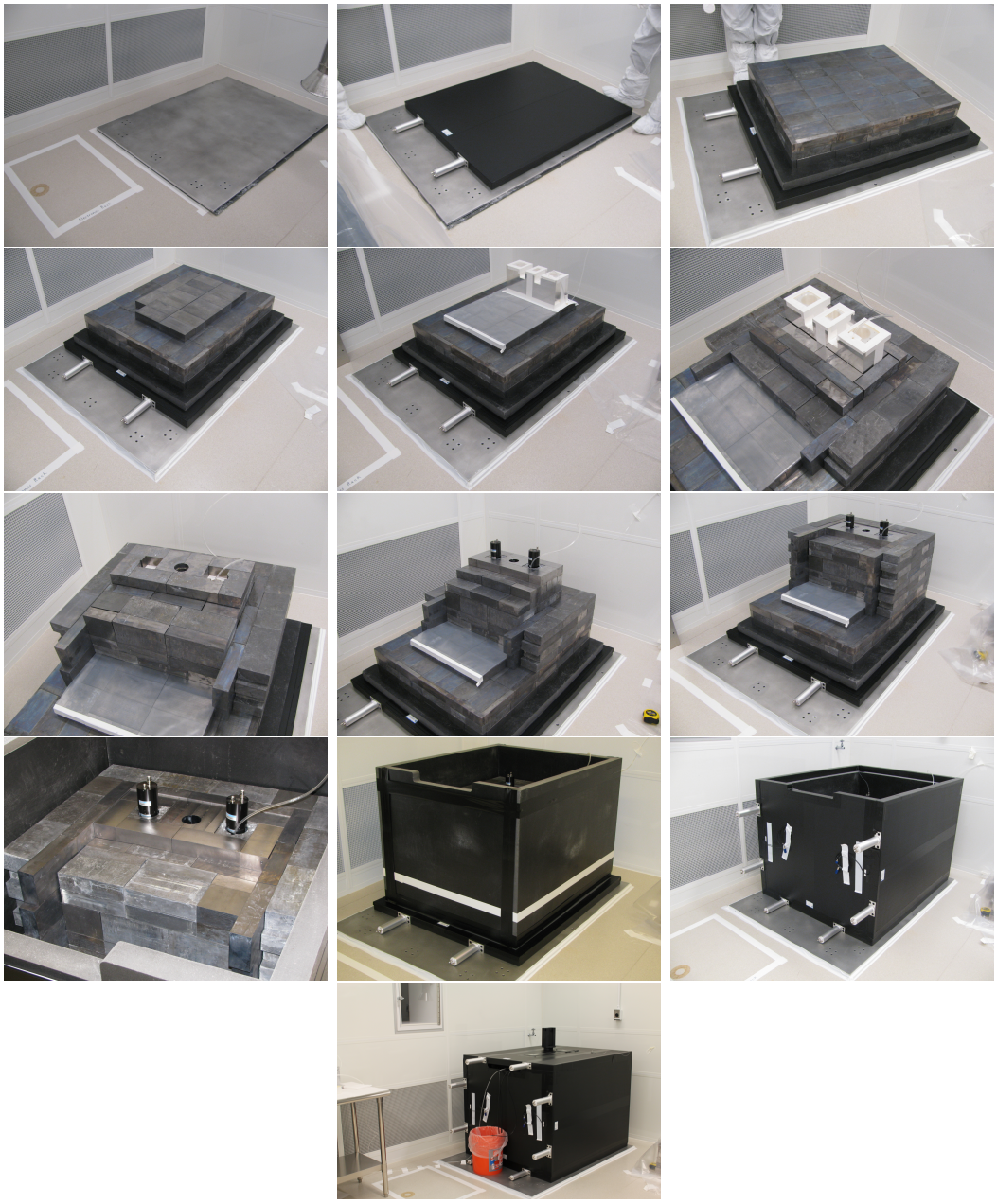

Figure 3.6: Progress of the partial build.

Simulations performed without the shield plug hole and endcaps as part of the shielding agreed within 10% with the number of coincidence counts observed between the PMTs, as stated in Section 2.2.3.

3.3.1 Electronics Rack Setup

The electronic equipment consists of the detectors internal to the lower cave assembly cabled to further electronics setup on the electronics rack (Figure 3.7). The signal from the PMTs fed directly into the Pixie 500 Express card in an NI 1082 Chassis. The PMTs are powered by iseg NHQ 222M HV modules in an Ortec 4001 NIM crate. Each module powers two PMTs, so each chamber has its own PMT power module. The veto panel PMTs are powered by iseg NHS 6020P modules. Each module powers six PMTs: PMT A for each of the six panels is powered on one module (left) and PMT B for each panel powered by a second (right). An Ortec 4003 preamplifier power NIM module is also mounted in the NIM crate. Two Ortec 2005 Charge-Integrating preamplifiers are available for characterizing energy spectra. The signal from each of the twelve veto panel PMTs is summed in a custom built summing box. The summed veto signal is shaped by a Canberra 2005 preamplifier and connected to the Pixie 500e card to use as an anti-coincidence trigger for LSC samples. Each detector chamber is instrumented to a dedicated Pixie 500 Express card. The Pixie 500 Express card has 4 input channels to utilize. Channels 0 and 1 are each dedicated to one detector PMT, channel 2 is the anti-coincidence veto panel signal, and channel 3 is dedicated to the fiber optic trigger input. The NI 1082 crate houses a NI PXIe-8135 embedded controller with a 64-bit Windows 7 operating system. This computer is used to operate the Pixie 500 Express modules. The NIM crate and PXI crate, monitor, and LED driver box are all powered by an APC Smart-UPS SMT2200RM2U universal power system (UPS). A shelf for the the LED calibration units is also reserved for the electronics rack. The LED driver box controls the signal to the LED in the fiber optic box. The fiber optic cables that run from the fiber optic box into the lower cave assembly transmit a fraction of the light

emitted by the LED into the light guides for gain and threshold calibrations.

Figure 3.7: Data acquisition system, including PXI crate, NIM electronics, and computer accessories.

3.4 Changes After Partial Build

3.4.1 Light Guide Recoating and Additions

The machined light guides were initially coated without any further polishing. As stated in Section 2.1.1, the reflectance after the initial silver coating was 74%. This reflectance value was too low to to achieve the goal of a 1 keV threshold. The initial predictions of 67.4% light collection at the PMT from an event in the vial had as-

sumed a 99% specularly reflective surface. With a 74% reflective surface, the fraction of light making it to the PMT dropped to 13.8%, as modeled in RayTracerPro. The light guides were sent back for refinishing with instruction to polish the guides before re-coating. The thin silver coating was again applied with Low Pressure Chemical Vapor Deposition (LPCVD). The reflectance of these polished and re-coated guides was 88%, which increases the modeled light transmission to 34.5%. The maximum reflectance for silver is 95% at 420 nm, with a light collection efficiency of 60.1%. Lead bricks that were machined to go into the light guide slots had to be machined further down by 0.16 cm to achieve a slip fit into the slots. The fiber optic cables for PMT calibration were not installed in the partial build, but were set into the appropriate channels in the light guide for later use with the full build. Thermocouples were also added to each of the light guides in the full build to compare the environment temperature to the target temperature of 5° C with the cooling plate running.

3.4.2 ABS to Full Pulley

In the partial build, a 3-D printed sample holder and sample pulley were used for inserting samples into the light guide chamber. While this accomplished getting the sample into the chamber, it left the holes (light paths) in the sample plug line open. The full build includes an upper assembly portion with a pulley system to lower a sample plug of copper and lead above the sample holder. This additional lead and copper not only blocks the light path down to the sample position, but replaces the air with shielding materials. Endcaps were also added around the top of the PMT cavities. In the partial build, with no shield plug or end caps, the average external photon background was $\sim$2500 $\pm$ 70 cpd (according to both experiment and simulation). With the shield plug and endcaps in place, that number

was expected to drop to $\sim 2 \pm 1$ cpd according to the external photon contribution in GEANT4 background simulations. A side-by-side comparison of the two sample changer mechanisms is shown in Figure 3.8.

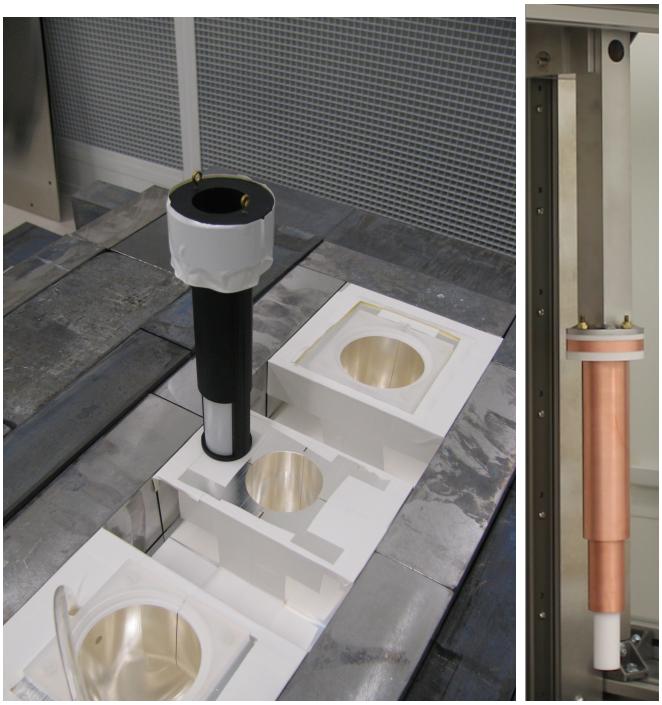

Figure 3.8: ABS sample changer from the partial build (left) and the shield plug from the full build (right).

3.5 Full Build

The full build was constructed in the spring of 2016 from the base third layer of lead up through the sample changer mechanism in the upper assembly. The partial build was first dismantled down to the first three layers of lead and central fourth low background brick section. Figure 3.9 shows the starting point for the full build and the build progress to final status. Several sheets of 0.0381 cm polytetrafluoroethylene (PTFE) were laid on top of the raised low background section as thermal insulation

between the lead and copper cooling plate. The sheeting layers were not doubled up to maintain a level surface. The copper cooling plate was assembled underground. The 0.635 cm copper tubing for each of the three lines was bent to shape and hammered into the tubing channel that was coated with vacuum grease. The plates were screwed together and the tubing was leak-tested with a vacuum to check for damage during bending or setting the lines. The tubing lines were bent up to run the height of the lead. The copper cooling plate was placed on top of the PTFE sheeting in line with the low background lead section. Tygon® tubing of 1.27 cm outer diameter (OD) and 0.635 cm inner diameter (ID) was cut to 45.72 cm lengths and slid onto each of the 6 external copper tubing lines. The Tygon®tubing will act as insulation for the tubing against any contact with lead bricks along the vertical length to the top of the cave.

The fiber optic cables were inset into the light guides as the light guides were mated and slid into their insets on the copper cooling plate. Initially, the coating on the light guides had increased the dimensions just enough so they would not fit into the slots on the copper plate. The silver plating had to be filed off around all the outer surfaces before the guides were mated and set in place. Teflon sheets were cut to cover the surface area of the light guides and exposed copper plate for better thermal insulation of the light guides.

With the insulated light guides in place, the lead was stacked around the guides, starting with the ultra-low background bricks and moving outward to the standard lead bricks. A 15.24 cm-wide stack of standard lead bricks was intended to fill the area to be later dedicated to the central chamber. Due to the additional thicknesses of the light guide coating and Teflon insulation, which were unaccounted for in the model, the space for the 15.24 cm for the central lead stack was actually only $\sim$14.73 cm wide. To fill the space, 5.08 cm x 10.16 cm x 20.32 cm lead bricks were stacked

in the center with every other layer offset toward alternating sides (see Figure 3.11). The final build is thus not an exact replica of the SolidWorks or GEANT4 models. Since cross-talk was not an issue in any of the GEANT4 simulations and the shielding around each of the light guides is still consistent, the experimental results are not expected to change drastically from the simulated predictions.

The lead was stacked up to the level of the light guides first, then the PMTs and bases added before the lead was stacked around them. The side borated polyethylene and veto panels were added around the lead cave. Endcaps were set up around the PMTs on the top layer of lead with the caves open toward the feedthrough for the cables to exit. Figure 3.12 shows the endcaps in progress to the final state. The cables were taped in place and run through the feedthrough slots in the aluminum plate before the top borated polyethylene and veto panel were added. A Bosch 80/20® frame for the upper assembly of sample carriers was constructed around the veto panels. Aluminum panels covered each of the four vertical sides to create the dark box. The edges of the dark box, feedthrough, and clamshells were taped up around the cables to minimize light leakage inside the cave. An aluminum plate was placed on top of the veto panel. The top Bosch 80/20® frame was constructed on the aluminum plate, without paneling for the dark box enclosure originally designed around the pulley and sample plug housing. The cave area is kept dark during operation by tape aprons around the sample plugs, which are to be inspected before the voltage is turned on for each run. One big take-away during this build process was that tolerances were not fully considered.

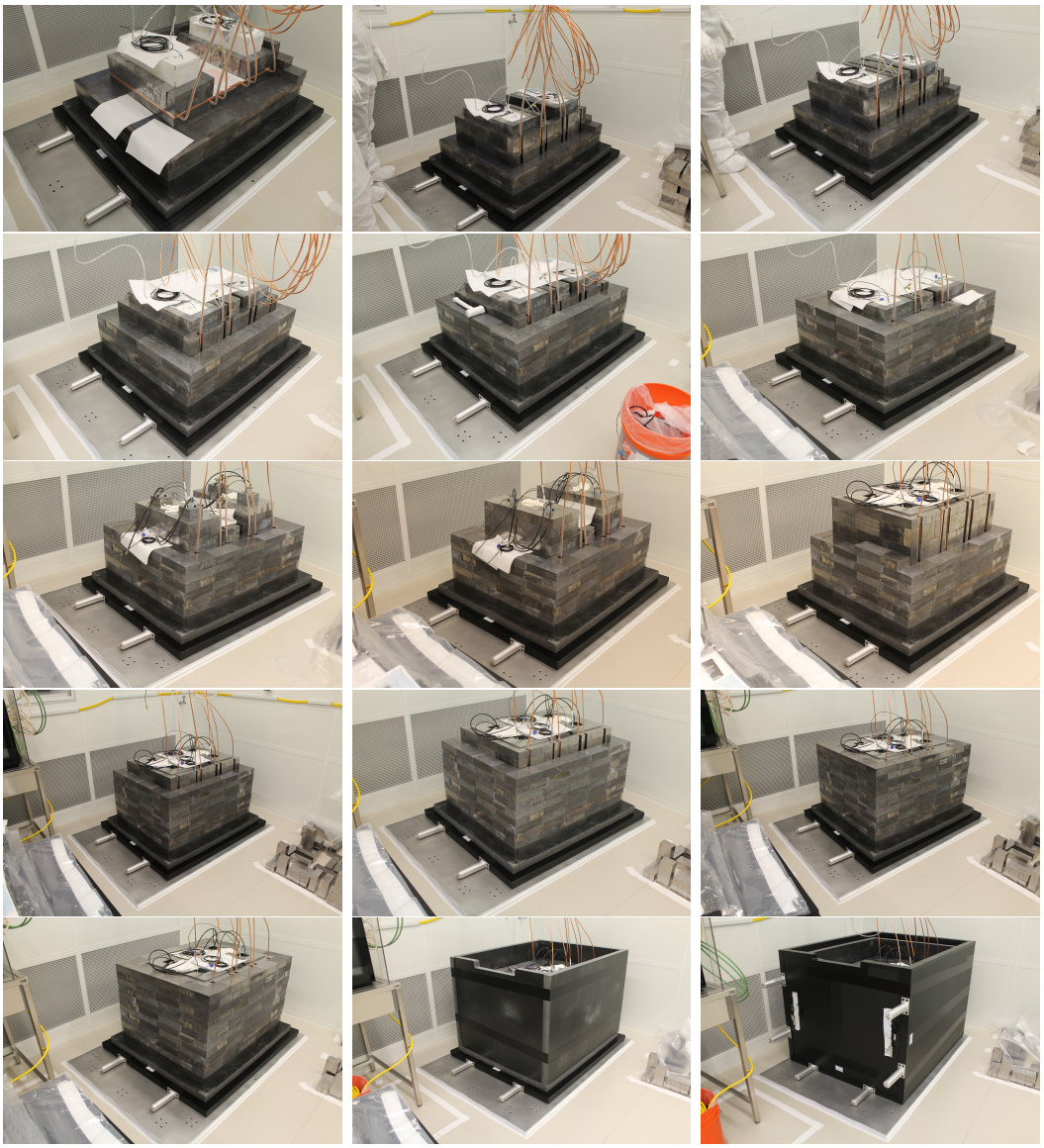

Figure 3.9: Progress of the full build.

Figure 3.10: Final assembly of the ULB LSC, showing the upper assembly of Bosch 80/20® frame and sample carriers above the lower dark box around the detector chambers (left) and a close-up of a sample carrier and shield plug assembly (right).

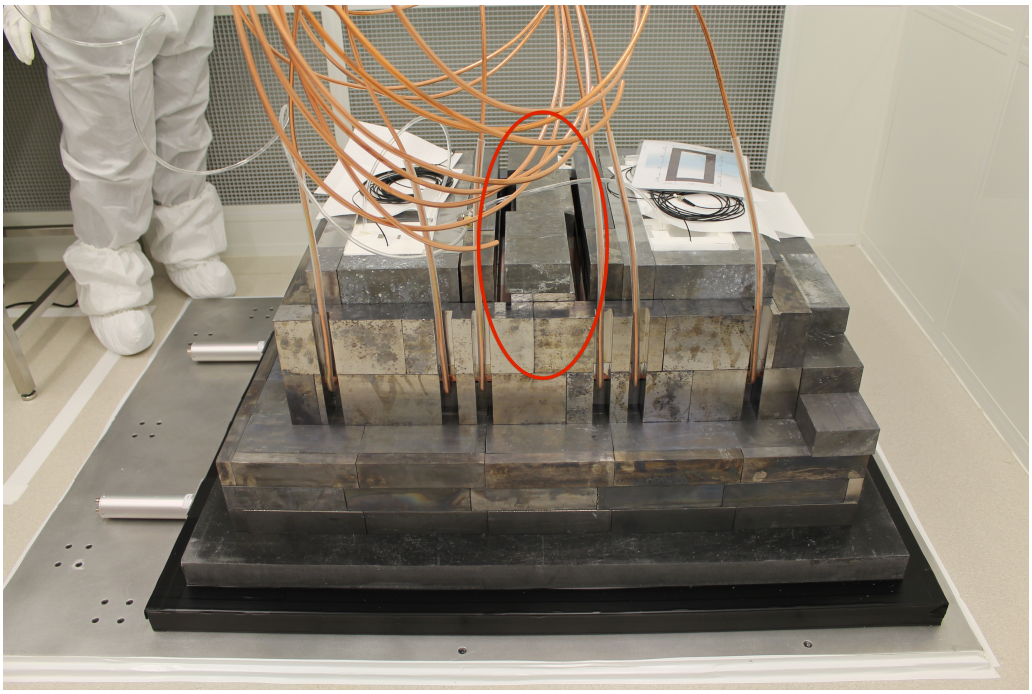

Figure 3.11: Offset of central bricks.

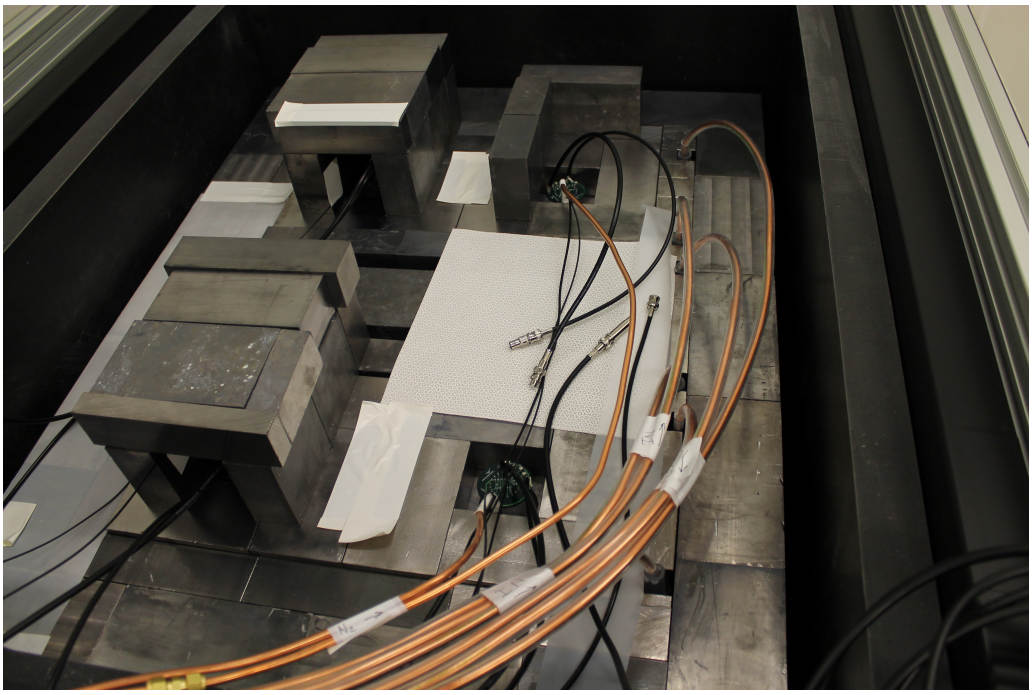

Figure 3.12: Endcaps over PMT ports in the ULB LSC full build.

4. PSD CODE DEVELOPMENT

In order to extract information from coincident events recorded through the XIA Pixie 500 Express cards and PixieViewer software, the recorded data must be converted to an appropriate format for off-line data analysis. The raw coincident data is stored in a binary format by the XIA system. For full data analysis and the ability to apply different selection criteria, the data was converted from a binary format, and initially filtered into coincident event pairs, to a format where event data can be analyzed with the ROOT framework developed by CERN (CERN, 1997). As a ROOT file, all the event parameters associated with each event and can be used to apply different filters on the data. For this research, the Pixie 500 Express module, channel information, and event waveform data acquired with the Pixie 500 Express was processed with the ROOT analysis framework for offline event acceptance/rejection, with potential pulse shape analysis for future data sets, as shown in the flowchart in Figure 4.1 (CERN, 1997).

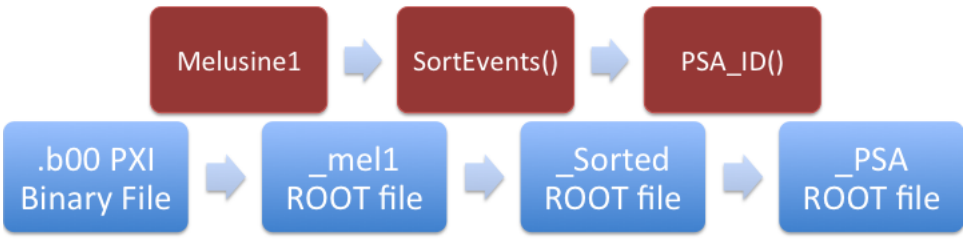

Figure 4.1: Flowchart showing the order of data processing routines and generated output files.

The "list mode" data from the Pixie-500 Express, with detailed waveform and

the associated timing and energy information for each event, is output into a binary file by the XIA modules. The binary file is converted to a ROOT file by melusine1, a custom PNNL software. A melusine1 processing file can impose a channel veto, energy threshold, and coincidence timing window on the list mode data during processing. The list mode data in the ROOT output file generated by melusine1 is then analyzed based on event pairing, a user-defined energy threshold, and energy equivalence between the two PMTS with SortEvents.cxx. Events that meet the pairing and energy criteria are accepted as "true" coincident events and are saved to a second ROOT file. Analysis of mixed radionuclide sample sets would include a third step for pulse shape analysis of the accepted events for categorization as alpha or beta events with PSA_ID.cxx. The PSA_ID code analyzes each event for the rise time, decay time, total integrated pulse charge, and rising and tailing integrated pulse charges, and saves the resulting analysis to a third ROOT file. The details of and parameters used in each of the codes are given in the relevant subsection below. The codes are attached in Appendix B for reference.

4.1 Pixie Binary File Processing

In "list mode" acquisition for the Pixie 500 Express, the event data that is received and processed online with the Pixie 500 Express module is stored as a binary file by the XIA system. This binary file has a 32-bit file header followed by channel-by-channel event data with a 16-bit channel header and waveform data for that channel's event. The file header contains information about the module and data acquisition parameters, such as the block size, module number, run format, length of the channel header, coincidence pattern, coincidence window, maximum length of traces plus headers, and the trace length (in blocks) of the traces from channels 0-3. After the file header, all the event data is stored in block units, with 16 bits of

channel and event information at the beginning, and waveform data stored after the the file header. The channel and event information recorded includes the hit pattern of the event, status flags, the number of blocks of trace data that follow the header, the number of blocks in the trace data of the previous record, the trigger time, energy, channel number, and pulse shape analysis values based on user and standard parameters. The number of bits of waveform data that are stored depend on the waveform length and the energy filter range selected in the PixieViewer software. The waveform length will determine the length of time that is represented, and the energy filter range will determine the binning factor (2 ns, 4 ns, 8 ns, etc.). In list mode, the events are recorded in chronological order based on the timestamps recorded for each event during online processing.

The binary output file from the PXI module containing all the list mode data, with the details of each event, is converted to a ROOT file with the melusine1 program developed at PNNL. The program selects and saves the events in the binary file that match given input parameters in a configuration file for melusine1. The event information for selected events is saved into a ROOT event in the ROOT output file. As a ROOT event, the information about that event is associated with that particular event, allowing the user to select, view, and filter based on parameters associated with the events. For example, the energy, channel, timing, or waveform data for any event can be accessed individually by using the identification number, or "Index", for a particular event. Conversely, such data can also be viewed for events within a given parameter range. For example, the event energy of events in specific channels can be displayed by using a specification for events in those specific channels.

The configuration file for melusine1, named ULBLSC.melusine1, looks like the Figure 4.2 below. The main section of the configuration file includes the following:

- input and output file paths - defined for user-specified directories
- TimeSort - Sort events based on time? Yes or No
- TimeWindow - Window of time in microseconds to look before and after current event for coincident events (equal to half of the coincidence window)
- prefix/suffix - addendum to filename
- fields - include energy (in 16-bit PXI energy units), time (timestamp of the event after the start of data acquisition), trigggerTime (the timestamp of when the event crossed the threshold to trigger the data collection), channel (the channel on the PXI card which registered the event), waveform data (the ADC response as a function of time for each event)

```
dataset
        inputPath               /Users/erch154/Desktop/PXI_testing
        outputPath              /Users/erch154/Desktop/PXI_testing/10nsOutput
        name                    pixie500e_test
        postfix                 _mel1
        maxWaveform             128
        #step                   10
        timeSort                true
        timeWindow              0.010           #microseconds

        fields
                channel
                time
                triggerTime
                energy
                waveform
        end
end
```

Figure 4.2: Configuration file for melusine1 processing

For processing ULB LSC events, the TimeSort is on and the TimeWindow is set to 10 nanoseconds (meaning a 20 ns coincidence window). This coincidence window is the initial filter condition for accepting coincidence events. The 20 ns coincidence

window used was determined from the expected pulse length and after looking at the accepted event rate for several time windows - 20 ns, 50 ns, and 100 ns. The number of accepted events for each of these coincidence windows did not change, and the 100 ns time window was more than enough to cover coincident events. Given that the number of accepted events did not change between 100 ns and 20 ns, the 20 ns window was determined to be long enough for true coincident events while minimizing the number of random coincidences that would be included if the time window were significantly lengthened (>100 ns).

All of the potential "field" options were retained for ULB LSC events, meaning that each event saved to the ROOT file will include the energy, time, triggerTime, channel, and waveform data associated with that event. The file can also contain minimum and maximum energy cutoffs for accepted events and a veto for events with a certain coincident channel (for example, the cosmic veto channel). Neither the energy thresholds nor the coincident channel veto were implemented for the data sets obtained here for the ULB LSC.

Binary output files from the Pixie 500 Express are processed interactively with the melusine1 program for this research, though the program also has the capability to be run in batch process from the command line. From the command line, the command "melusine1" opens the program as a Graphical User Interface (GUI). In the GUI, the configuration file is chosen and the input, selection, and processing criteria is loaded. The Pixie binary files to be processed are then selected individually. The program accepts binary files from Pixie 4, 500, and 500 Express cards, and the correct file type must be selected to process the intended files. Once all the files are selected, the program runs sequentially for each input, and the output is generated in the file path designated in the configuration file.

The event data is saved to the ROOT output file in a TTree structure with three

"Trees" and associated "leaves" as shown in the bulleted list below (Brun and Rademakers, 1997; Brun and *et al.*, 2014). The "Trees" represent categories of information, and the "leaves" are the parameters saved in that category. The "EventData" tree contains the event information, identified as the "leaves", for each event that has been saved. The "ChannelData" tree contains the information identified by the "leaves" for each channel on the connected Pixie 500 Express cards. The "Stats" tree contains the metadata for the file itself. The events retained in this file are coincident within the time window defined in the melusine1 configuration file. The energy, time, channel and waveform data from the "EventData" tree will be used in further event processing.

- EventData
  - Index - event number for coincident event
  - Subindex - event number in reference to events within coincidence window
  - Veto - tag if the event was a vetoed event
  - Channel - channel in which the event was recorded
  - Time - clock time of event
  - TriggerTime - time of event trigger
  - Energy - PXI 16-bit energy value of event
  - Waveform - trace data
  - WaveformLength - length of trace data (ns)
- ChannelData
  - channel - channel numbers of active channels
  - Real Time - real time of active channels
  - Live Time - live time of active channels
  - Total Events - total events in active channels
  - Vetoed Events - total vetoed events for active channels
  - Coincidence Events - total coincident events for active channels
  - Below Threshold Events - events below energy threshold for active channels
- Stats
  - name - filename
  - value - file statistics

4.2 Melusine1 ROOT File Processing

After processing through melusine1, the ROOT output files have all the event information for events within the selection conditions defined in the melusine1 configuration file. For the ULB LSC data, the selection condition is a 20 ns coincidence window defined as the TimeWindow in the configuration file. With this condition implemented in the binary to ROOT file conversion, all the events in the ROOT file should events within 20 ns of each other. A second processing step is required to select events based on paired channel events, an energy threshold, and an energy equivalence between coincident pulses. The events from the melusine1 output file are sorted into "true" coincident events and "rejected" events based on time and energy parameters, hence the "SortEvents" step in the process. The event parameters that the code uses to determine event selection include the selected and coincident event energies, channels, and subindexes. The first selection is on the channel. Only events from channels 0 and 1 (PMTs A and B of the left chamber) or 4 and 5 (PMTs A and B of the right chamber) are selected as coincident sample events. For events in channels 1 and 5, the previous event is checked to ensure it is in channel 0 or 4, respectively, before events in both channels are saved. If there is no paired event in the corresponding paired channel, the event is rejected. The second selection is based on an energy threshold defined by the user. Both the selected and coincident events must have energies above the energy threshold for both to pass to the next selection criteria. If either or both of the paired events is below the energy threshold, both events are rejected. For the data analysis in this research, events were not rejected based on this energy threshold selection criteria. For samples containing alpha-emitting radionuclides, this would allow filtering of background or noise events below the alpha peak(s). The third selection filter for coincident events is a

selection based on "energy equivalence" between the two coincident pulses. Essentially, this filters out random coincidences from background, PMT flashes, and dark current events. For such random events, it is typical for the pulse in one channel to be small while the other is large. For a true LSC energy deposition event, the light detected from a radioactive decay should be about equal, with $\sim 50\%$ variation, between the PMTs. This type of pulse comparison is typical of other commercial low background systems (Sciences, 2002).

The energy of the selected pulse must be within $\pm$ 50% of the energy of the coincident pulse to be categorized as a "true" sample light event. The 50% value is a slightly conservative estimate based on both the largest light emission differential from a sample event in a vial and the calculated light emission, propagation, and photoelectron conversion for the low-energy beta emitter tritium as shown in Equations 4.1 through 4.3. When performing analysis on low energy events, using tritium as an example, 50% will be a conservative estimate for keeping all true events while excluding most of the random coincidences. Using the 82% rate of photons escaping the vial, 34.5% propagation of light through the light guide, and 30% quantum efficiency of the photocathode on the PMTs, the 6 keV average beta energy of tritium would result in 7 photoelectrons. At the minimum transmission point, of those 7, 4 photoelectrons are generated in one of the PMTs and 3 in the other. Energy equivalence of 50% is the minimum acceptable level in order to have at least one photoelectron in each PMT to provide coincidence for tritium.

$$6 \text{ keV x } 14 \text{ photons/keV x } 0.82 \text{ x } 0.345 \text{ x } 0.3 = 7 \text{ photoelectrons} \tag{4.1}$$

$$3 \pm 1.5 = 1.5\text{-}4.5 \text{ photoelectrons} \tag{4.2}$$

$$4 \pm 2 = 2\text{-}6 \text{ photoelectrons} \tag{4.3}$$

No energy cuts were implemented for converting files, but an energy threshold of 25 keV was implemented during spectral integration for count rate and activity calculations. A threshold of 25 keV will be high enough to exclude any low energy or electronic noise present in the data, and coincides with the low end of bin 1 out of 100 used in generating spectra.

In the melusine1 event file conversion, the event timestamp is used to determine the order in which events occurred and if there were coincident events within a defined coincidence window (TimeWindow). Based on the time order in which events occur within the TimeWindow, each event registered as coincident within the Time Window is given a subindex number. The subindex indicates when the event took place relative to other events within the time window. The subindex also increments with the channel. For example, for a coincidence event between channels 0, 1, and 2, (a coincident event between the PMTs and veto assembly), the index would be the same for the data from all three channels, but the subindex values would be 0, 1, and 2 for the respective events. If other waveform data was recorded for a second trigger within that coincidence window, such as a pileup event or afterpulse, those events would have subindices of 3, 4, etc. For the data from coincident light events from a ULB LSC sample, only the initial trigger and coincident events and corresponding waveform data from channels 0 and 1 (PMTs) is of interest. Only the data from events with a subindex of 0 and 1 are included in the final data set of "true" sample light events.

The energy threshold and energy equivalence value (in percent) are user-defined variables from a command line prompt in the SortEvents code. The output file name reflects both of these values, so multiple analysis sets can be created from the same initial event input file if the user has a need to analyze a variety of data sets based on either of these selection criteria. The user is also prompted for the initial event

input file name and which chamber the data was collected in. (The calibration data for each of the chambers is used for calculating the event energy in keV at this stage and is selected based on which chamber is indicated by the user.) The SortEvents code was written to save data from coincident events in channels 0 and 1 for the left chamber Pixie 500 Express card and 4 and 5 from the right chamber Pixie 500 Express card, since these channels are the input channels for the PMTs in their respective chambers.

The SortEvents.cxx code is loaded and executed in ROOT. When prompted on the command line, the filename of the melusine1 output ROOT file to be analyzed should be typed in. The following prompts for energy threshold (in Pixie units), energy equivalence (in percentage), and chamber identification (right or left as 0 or 1) are entered by the user. The code loops over all events in the designated input file, reading in all the data for the current and coincident events during each loop. For an event in channel 0 or 1 (either of the PMTs in the right chamber) or channel 4 or 5 (either of the PMTs in the left chamber) above the user-defined energy threshold, the data from the current event is compared to the data from the matching event in the other channel (from the other PMT). For example, if the event is in channel 0 (on PMT A in the right chamber) and above the stated energy threshold, the next event is analyzed to see if it is a channel 1 event (on PMT B in the right chamber) above the energy threshold. If the channel 0 event is followed by a channel 1 event, the energies are both compared to see if the channel 1 event energy is within $\pm$ 50% of the channel 0 event energy. If the energies are within the defined uncertainty, the event moves to the subIndex check. If the subIndex is greater than 1, the event is an afterpulse feature or second trigger. Events with a subIndex less than 2 (0 or 1) are accepted and saved.

Paired events that are accepted through all the parameter tests are considered

true LSC events and are saved to a new ROOT file with the prefix "Sorted_#Percent_Energies_T#", where the "#Percent" shows as the energy equivalence value entered by the user ("50Percent" for this analysis) and the "T#" shows as the threshold value entered by the user (T0 for this analysis). Since these variables are a user input and generate unique output files, different data sets using different user input values for these variables can be created. For the events that pass all the selection criteria, the event parameters are saved for both of the coincident events. In addition, the energy for each of the coincident events is calculated based on an energy calibration of the PMTs. The energies of each event are saved, as is the sum of the coincident events for the total event energy. The output file includes the raw event data for all of the accepted PMT events, the event energies for the PMTs and the summed event energy in the initial Pixie units, and the event energies for the PMTs and the summed event energy in keV. The output structure is shown in the bulleted list below.

- sortedEvents
  - clone of EventData for accepted event
- acceptedEnergies (Energies of Accepted Events)
  - entry (entry number)
  - E_PMTA (PXI energy of PMT A)
  - E_PMTB (PXI energy of PMT B)
  - E_Total (Summed PXI event energy from both PMTs)
- EcalEnergies (Energy-Calibrated Specta of Accepted Events)
  - Energy_Ch0 (Calculated energy of PMT A)
  - Energy_Ch1 (Calculated energy of PMT B)
  - Energy_Event (Sum of calculated energies of PMT A and PMT B)
  - Energy_PXISum (Calculated total event energy from total event energy calibration)

4.3 Pulse Shape Analysis of Sorted Event ROOT Files

Depending on the signal processing for the data stream, there are different paths for performing pulse shape analysis on the LSC event data. A custom code was developed for analysis of signals directly from the PMT. For signals passed through a preamplifier, pulse shape analysis could be performed using an adaptation of a Pulse Shape Analysis (PSA) tool already developed at PNNL for the Ultra Low Background Proportional Counter system. Neither of the tools was used for data collected in this research since there were no mixed alpha/beta samples analyzed, but could be used for mixed samples in the future. The PNNL PSA tool for preamplifier

output still needs to be adapted to handle two sets of templates (one for alpha and one for beta), and both methods would need to be benchmarked against known samples.

4.3.1 ROOT File Processing for Direct PMT Output

The output file from the SortEvents step contains only accepted LSC events. For output directly from the PMTs, these LSC events can be analyzed with the PSA_Identify.cxx code (see Appendix B) to distinguish alpha and beta events. This code calculates an integrated pulse charge in ADC units for the total pulse and the falling edge of the pulse in addition to the rise time and decay time based on the waveform data of the event. The total pulse charge is calculated by summing all the waveform data and subtracting off an average baseline determined from the first quarter of the waveform data of each pulse.

A series of parameters and ratios are calculated to determine the most useful separation parameter for separating alpha and beta events. The output from the PSA analysis is saved in the two data structures below. The parameters in bold font are those indicative of alpha and beta characteristics: Peak to Charge Ratio and Fall Time (DT_ns).

The Peak to Charge ratio uses the ratio of integral of the prompt portion of the waveform (along the rising edge) to the total integral of the waveform as a distinguishing characteristic between alpha and beta decays. Pulses from beta decays are faster and have a shorter decay time than pulses from alpha decays. Alpha decays cause triplet-state excitation in the solvent and fluor molecules. These triplet states decay by fluorescence which increases the decay time of the pulse. These pulse characteristics result in lower peak to charge ratios for alpha pulses than for beta pulses. The decay time and this peak-to-charge ratio are both useful parameters for

separating and isolating alpha and beta events.

- PSAData
  - iEntry
  - waveformLength
  - BaselineAvg
  - BaselineAvg_Final
  - BaselineArea
  - TotalPulseSum
  - TotalPulseCharge
  - CalcMax
  - MaxBin
  - MaxAvg
  - PromptSum
  - PromptBaseline
  - PromptCharge
  - **PeakToChargeRatio**
- TimingData
  - iEntry
  - TotalPulseCharge
  - CalcMax
  - MaxBin
  - PromptCharge
  - **PeakToChargeRatio**
  - RTBIN_PERCENT_MAX_10
  - RT_ns
  - RT_LOW
  - RT_HIGH
  - **DT_ns**
  - DT_LOW
  - DT_HIGH

4.3.2 ROOT File Processing for Preamplifier Output

For data recorded with preamplifiers in the signal processing chain, an adaptation of a different Pulse Shape Analysis tool developed at PNNL will be used for alpha/beta discrimination on future data sets. This tool uses template matching to identify acceptable events and calculate a gross and net energy spectrum for the sample. The templates are created by the user manually selecting a series of good events to be averaged into a "good" event template. The template is scaled per unit energy in order to be applied across the all events. Once the templates are created, the events in raw data are matched against the template. If the match is within a certain user-specified margin of error, it is a good event; otherwise the event is discarded. Events are still tagged by channel, so events from the cosmic veto channel are separated from the detector spectra. A background file is fed into the program for background-subtraction from the "good" event detector spectrum. The activity of the sample is calculated from the net energy spectrum. By the end of processing, the user has a file that displays the cosmic, gross detector, and net detector spectra with the activity calculation stated on the display. For the ULB LSC, the program must be adapted to have two sets of templates - one for alpha events and one for beta events. The two spectra can be separated with the template matching and the separate calculated activities shown for each particle type.

4.4 Summary of Analysis Methods

Event data collected for ULB LSC samples must be converted to a useful file format, filtered through a series of selection parameters, and then differentiated into alpha and beta events. Several different programs are used in this series of analysis steps, some developed specifically for these data sets and some already developed at PNNL. The files are first converted from binary to ROOT files using the PNNL

program melusine1. The output from this conversion stage includes all the event data for events within the coincidence window specified for the conversion (20 ns for this data). This event data is then screened in the SortEvents code for events passing a set of selection criteria based on coincident event pairing and energies. Events that pass the selection criteria are saved to a new output file containing only the true sample events, their associated parameters, and the energy spectra calculated from energy calibration of the appropriate chamber. These events can be further analyzed using pulse shape analysis to identify alpha and beta events in the data. The selection conditions for true events are implemented between the file conversion and event processing stages. The coincident event timing is the first selection criteria the event data is tested against during file conversion with melusine1. Events are assessed for a paired event, energy equivalence between the two pulses, energy above a user-defined threshold, and initial trigger events during event processing with the SortEvents code. Events that pass all these selection criteria are considered true light events from the ULB LSC sample. The data taken for this research included both direct PMT output and preamplifier output signals. The data was all processed the same through melusine1 and the SortEvents code. Different settings were used in the data acquisition software to differentiate between the two signal types while the data was getting processed online during acquisition. Pulse shape analysis was not used in the data collected for this research, as none of the samples for which data was collected were mixed alpha/beta samples. However, the foundation for using such methods on future samples has been laid.

5. CHARACTERIZATION OF ULB LSC PARTIAL BUILD

Initial characterization of the ULB LSC with a partial build was intended to a) assess the impact of the low background measures implemented, b) determine if any design changes were necessary, and c) compare the experimentally observed backgrounds to simulation results. The partial build was a trial run for the electronics, veto assembly, data collection, and post-processing analysis. The background data from the partial build was consistent with the simulation results for a modified simulation geometry reflecting the partial build setup. Post-processing of the pulses captured in list mode data involved two codes - melusine1 and SortEvents - described in Chapter 4.

5.1 Electronics Setup

Pulses recorded with the partial build were from the direct PMT output. The low background Hamamatsu R11410 PMTs and E2979 socket assembly fed directly in a 50 ohm RG-58 BNC-SMA cable connected at the other end to the PXI 500e card. No signal processing or shaping elements such as a preamplifier or amplifier were added before digital processing. The direct PMT output was affected only by the digital gain amplifier and threshold setting within the PixieViewer software. The integrator mode was enabled for the direct PMT output. With the integrator mode enabled, the baseline values after the pulse were integrated into the energy value as well, effectively lowering the energy value by averaging these 0-energies in with the pulse. A separate, manual energy calculation was added in to the SortEvents processing using an average baseline subtraction from the pulse shape for the data collected with the partial build.

For data collection with the partial build, the settings used for data acquisition

with PixieViewer were adjusted for direct PMT output and are shown below in Table 5.1.

Table 5.1: Settings in PixieViewer for Data Acquisition with the ULB LSC Partial Build were optimized for signals directly off the PMT.

(a) Module Parameters

Module	0
Energy Filter	1
Coincidence Pattern	144

(b) Channel Parameters

Setting/Channel	0	1	2	3
Threshold (ADC units)	5	5	10	100
Trigger Rise Time (μs)	0.04	0.04	0.04	0.04
Trigger Flat Top (μs)	0.04	0.04	0.04	0.04
Energy Rise Time (μs)	0.112	0.112	0.112	0.112
Energy Flat Top (μs)	0.112	0.112	0.112	0.112
Tau (μs)	0.018	0.018	0.018	0.018
Trace Length (μs)	0.256	0.256	0.256	0.256
Trace Delay (μs)	0.15	0.15	0.15	0.1
Voltage Offset (%)	10	10	10	10
Gain	1	1	2.61	1
Pulse Inverted	Yes	Yes	Yes	Yes

5.2 Veto Panel Characterization

All six panels were cleaned above ground, moved underground, and characterized in conjunction with the partial build. The panels were gain matched before the panel signals were combined into the veto assembly signal. First, the PMT signals were matched for each panel. The PMT signals were combined for each of the 6 panels, and the panel responses were matched to each other. Adjustments to the PMT voltages were made during this stage to match the placement of the valley between

the high-energy gamma and muon events in the MCA spectrum. The PMTs were checked against one another after the voltage adjustments, and the panel signals were checked against each other after fine adjustment of voltages. Once the voltages were set for all the PMTs and the PMT and panel signals were matched, the panel signals were combined for a single veto assembly signal to feed into the Pixie module as the veto for cosmic-coincident events. The voltages in Table 5.2 show the high voltage settings for each PMT in the veto panel array. With a gain of 3, these voltages place the muon valley at channel 1500 (out of 32768) for the individual panel energy spectra, at channel 3000 for the panel MCA spectra, and at channel 4000 for the summed panel MCA spectrum.

Table 5.2: HV Settings for Veto Panels

Panel	Channel	PMT A (V)	PMT B (V)
1 (Back)	0	655	630
2 (Front)	1	720	705
3 (Bottom)	2	1250	1035
4 (Top)	3	1040	1010
5 (Right)	4	695	695
6 (Left)	5	795	800

The gain potentiometers on all the panels were set to maximum. The gain potentiometers on Panels 5 and 6 (the side panels) were inaccessible since the PMTs are sunk internally in the panel. Since these two gain potentiometers could not be adjusted, all the panels were left with the manual gain at maximum. Adjustments to gain were implemented through the digital gain amplifier in the PixieViewer software. Spectra were collected with the digital gain at 1.000, 3.000, and finally at 2.610. For the summed panel spectrum, gamma contribution was intended to end

close to 2.5×10^3 channels. With the gain set to 2.610 in Pixie Viewer Oscilloscope, the edge was approximately 3×10^3 channels. With this criteria, spectra were obtained for the cosmic veto assembly with the goal of seeing a broad muon spectrum while keeping high-energy gammas, as shown in Figure 5.1.

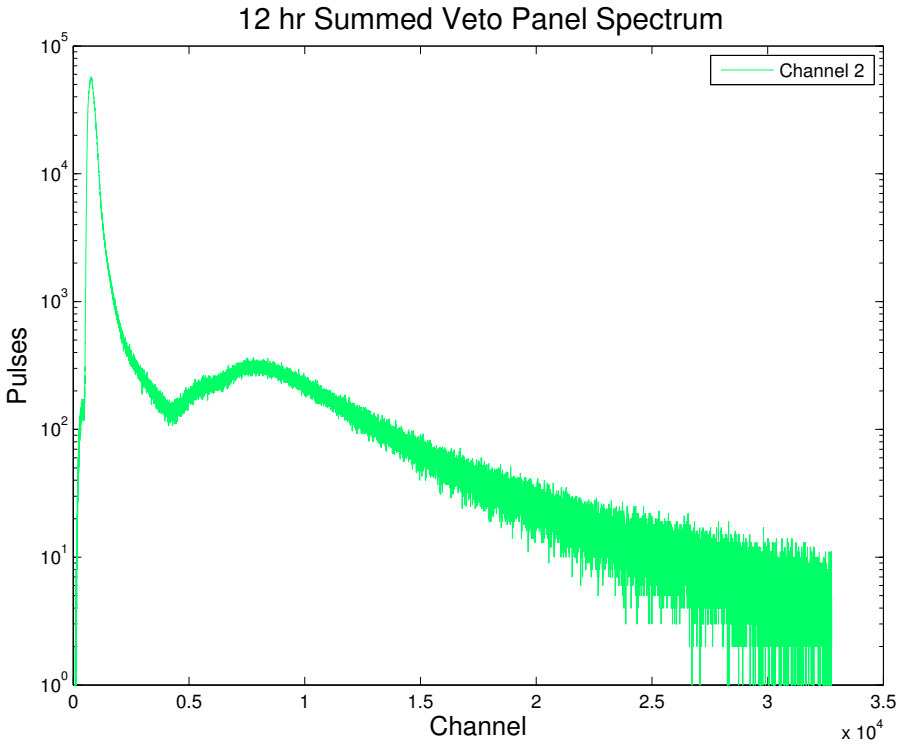

Figure 5.1: The cosmic veto spectrum includes the high energy gamma rays at the low end while the majority of the energy spectrum is dedicated to the muon through-peak. The spectrum displayed here was a 12 hour data acquisition.

The initial spectra was acquired with the direct PMT output from the veto panels summed through a series of BNC tees. The settings in the Pixie Viewer software were the same for the veto assembly as for the detector PMTs in the detection chamber, with exceptions on the gain setting, pile-up inspection (enabled for veto assembly),

and out of range (enabled for veto assembly) settings. However, the trace data from the summed PMTs from the veto assembly was broader and noisier than from the individual PMTs on the veto panels. As PMTs were added, the data became increasingly distorted. With all twelve PMTs summed together, the trace was longer than the specified trace length initially specified in the Pixie Viewer software. A charge-integrating preamplifier is used to rectify this in the full build. The trigger on the rising edge of the veto pulses remains the means of identifying an event in the veto assembly, which is used to reject chamber events coincident with an event in the veto assembly.

5.3 Background Characterization

The partial build of the system consisted of one of the light guide chambers constructed within the veto assembly, with manual sample changes while the chamber PMTs powered down. The PMTs were required to be powered down during sample changes due to the direct exposure to ambient light when removing/inserting the sample. Nevertheless, background data was collected for several configurations of the chamber: empty (no sample), light-blocking vial in sample carrier, empty vial in sample carrier, and 20 mL samples of DI water, UltimaGold AB LSC cocktail (UG AB), and UltimaGold uLLT LSC cocktail (UG uLLT). Backgrounds were collected for 12 hours and extrapolated to counts per day. These initial tests allowed for evaluation of electronic read-out system performance, the GEANT background model predictions, and provided an initial look at the systematic background not associated with radiation. Data was not collected for longer periods since the goals of the partial build were focused on logistics and electrical checks, initial background count rate estimates, and order of magnitude validation of the model. Longer measurements were reserved for full characterization of the final configuration with the full

build. The raw data from the PXI output was filtered first with melusine1, accepting coincident events within a 20 ns coincidence window that triggered both PMTs but not the cosmic veto array, then with the SortEvents program that accepts events with PMT energies matched within 50% energy equivalence. The raw PXI output and filtered data (by timing and energy) from SortEvents processing for each of the background configurations is given in Table 5.3. The filtered data is limited to paired events within the timing window and within the defined energy equivalence values; this filtered data is the final data set used for calculation and comparison.

Table 5.3: Count rates for 12-hour runs of various sample configurations.

Run Configuration	Run Time (s)	Raw CPD	Filtered CPD
Empty Chamber	44064	44 ± 9	10 ± 4
Light-Blocking Vial	44064	14 ± 5	4 ± 3
Empty Vial	44064	38 ± 9	14 ± 5
20 mL DI Water	44064.1	52 ± 10	31 ± 8
20 mL Ultima Gold uLLT	44064.1	5532 ± 104	2363 ± 68
20 mL Ultima Gold AB	44064.1	5488 ± 104	2586 ± 71

The filtered data show an overall background count rate for the system of 10 ± 4 counts per day for the empty chamber. These events may be attributable to light emission from the PMTs themselves and pose a potential limiting systematic background. The light-blocked data shows 4 ± 3 counts per day, which can be attributed to accidental coincidences between the two PMTs and provides circumstantial evidence to support the hypothesis of light emission from the PMTs. An empty vial as the sample registered a count rate of 14 ± 5 counts per day, and 20 mL DI water sample had an increased count rate of 31 ± 8 counts per day. These increased rates may be due to Cerenkov light production processes. Twelve-hour counts of 20 mL

samples of the Ultima Gold uLLT and AB cocktails yielded count rates of 2363 ± 68 and 2586 ± 71 counts per day, respectively, after offline processing. Simulations of the partial shield build in GEANT4 estimated the count rate due to external photon interactions with the scintillation cocktail to be 2633 ± 77 counts per day. The data for both the UG AB and UG uLLT cocktails were within 10% of the simulation results, validating the model on order of magnitude for background estimates. This background is similar to the background rates of commercial aboveground LSC systems, ∼1-2 counts per minute. From similar simulations of the full shield build, the expected background rate from radiation sources within the shield was ∼10 ± 1 counts per day. Adding the ∼15 ± 5 counts per day level of systematic background rates suggested by the above studies to the expected background rate of ∼10 ± 1 counts per day from simulation, then the system may achieve background rates of the order of ∼25 ± 5 counts per day.

5.4 Initial Sample Analysis

LSC samples of the following radionuclides were prepared in 6 mL vials with Ultima Gold AB cocktail: ^{3}H,^{90}Sr, ^{160}Tb, and ^{89}Sr. The 6 mL samples were placed in 20 mL LSC vials then vacuum-sealed in polyethylene tubing as described in the procedures in Appendix D. The vials were counted for 8-12 hours in the ULB LSC based on availability and access to the laboratory. These initial trials were again limited to shorter counting times because the effort was focused on developing a frame of reference for the detection capabilities (spectral response by radionuclide) rather than characterizing the samples or fully characterizing the system. Count rates and statistical errors for the samples with the respective activities are given in Tables 5.4, 5.5, and the efficiencies in Table 5.6. Backgrounds were subtracted on a bin-by-bin basis from sample spectra, with the errors on each bin propagated

through subtraction and scaling, as consistent with other low-background systems in the shallow underground laboratory. From the count rate data, ^{89}Sr cannot be distinguished from background. Note that the background count rates of the blank are different for the raw Pixie data and the filtered (energy-matched and paired) data. Since the respective backgrounds are subtracted from the raw and filtered sample data, the background-subtracted count rates for the filtered and raw data are independent (the background-subtracted filtered count rate can be higher than the background-subtracted raw count rate). The optics for photon transmission were less than optimal, since the reflectance on the light guide was 25% lower than ideal and the samples were double-packaged in plastic. The spectra obtained, shown in Figures 5.3 - 5.6, were inconclusive in assessing the energy range or spectral capabilities of the ULB LSC due to the low statistics above or indistinguishable from background. Background-subtracted spectra in Figures 5.7 - 5.10, normalized to counts per day, show little above background for ^{3}H, no statistically different signal from ^{89}Sr, and only slight spectral characteristics for the ^{90}Sr and ^{160}Tb spectra. The ^{89}Sr and ^{160}Tb spectra had fewer counts in the noise (first two) bins, resulting in negative count rates in those bins. This could be the result of lower chemiluminescence or electronic noise contributions during those trials and these bins have been excluded from analysis for all trials.

The background-subtracted sample count rates, stated in Table 5.5, are less than the activities of the samples with the exception of ^{90}Sr. The ^{89}Sr is not distinguishable above background, and the observed ^{3}H is less than 20% of the sample activity. The observed count rate of ^{160}Tb is slightly higher, but still less than 30% of the sample activity. The ^{90}Sr sample is the only sample within 50% of the sample activity. This sample had a total activity of 0.2 Bq, consisting of 0.1 Bq of the initial ^{90}Sr and 0.1 Bq of the in-grown ^{90}Y. The observed filtered count rate was $\sim$15% higher than the

Table 5.4: Count rates (s^{-1}) for the sample measurements collected with the partial build.

Radionuclide	Activity (Bq)	Run Time (s)	Raw Data (s^{-1})	Filtered Data (50%) (s^{-1})
None	0.0	263519	0.110 ± 0.001	0.069 ± 0.001
^{3}H	0.1	75600	0.124 ± 0.001	0.086 ± 0.001
^{89}Sr	0.1	14400	0.147 ± 0.003	0.068 ± 0.002
^{90}Sr	0.2	43200	0.405 ± 0.003	0.298 ± 0.003
^{160}Tb	0.1	43200	0.209 ± 0.002	0.097 ± 0.001

expected activity, which may be due to a combination of error in the stock solution activity, systematic errors in the sample preparations, and background of the LSC cocktail.

Table 5.5: Background-subtracted count rates (s^{-1}) for the sample measurements collected with the partial build.

Radionuclide	Activity (Bq)	Run Time (s)	Raw Data (s^{-1})	Filtered Data (50%) (s^{-1})
^{3}H	0.1	75600	0.014 ± 0.001	0.017 ± 0.001
^{89}Sr	0.1	14400	0.037 ± 0.003	0.000 ± 0.002
^{90}Sr	0.2	43200	0.295 ± 0.003	0.229 ± 0.003
^{160}Tb	0.1	43200	0.099 ± 0.002	0.028 ± 0.002

Table 5.6: Efficiencies for the sample measurements collected with the partial build.

Radionuclide	Activity (Bq)	Run Time (s)	Raw Data (%)	Filtered Data (50%) (%)
^{3}H	0.1	75600	14 ± 1	17 ± 1
^{89}Sr	0.1	14400	37 ± 3	0.0 ± 2
^{90}Sr	0.2	43200	148 ± 2	114 ± 1
^{160}Tb	0.1	43200	99 ± 2	28 ± 2

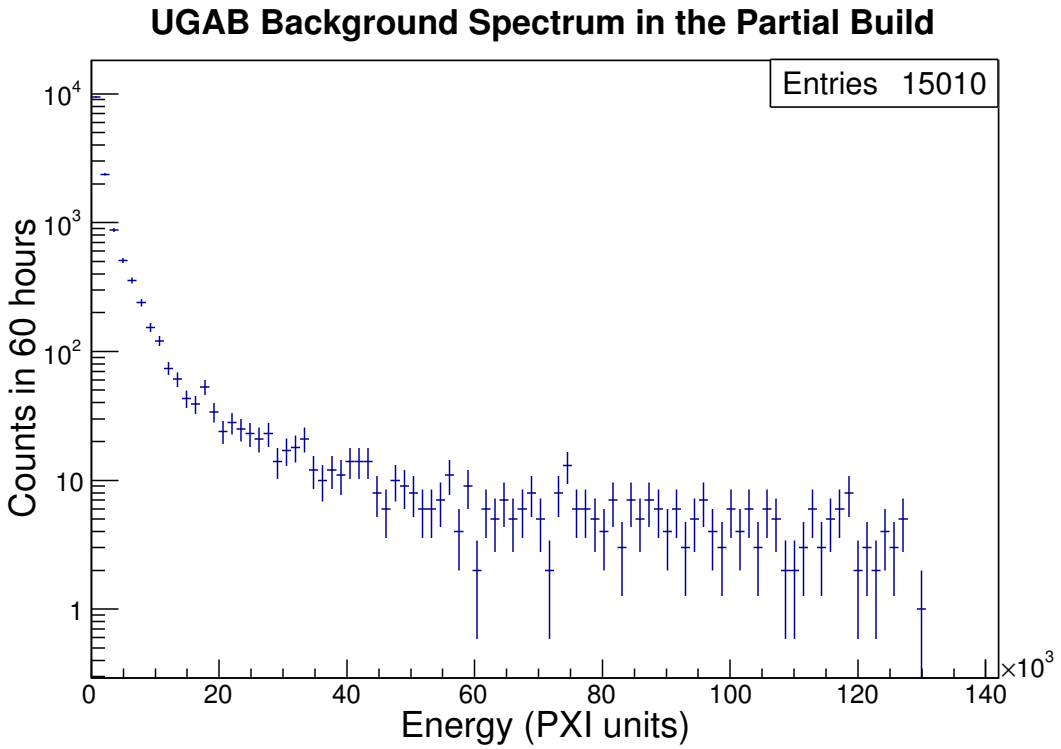

Figure 5.2: Background spectra in PXI energies for UGAB cocktail for the partial build with no energy cut and 50% energy equivalence.

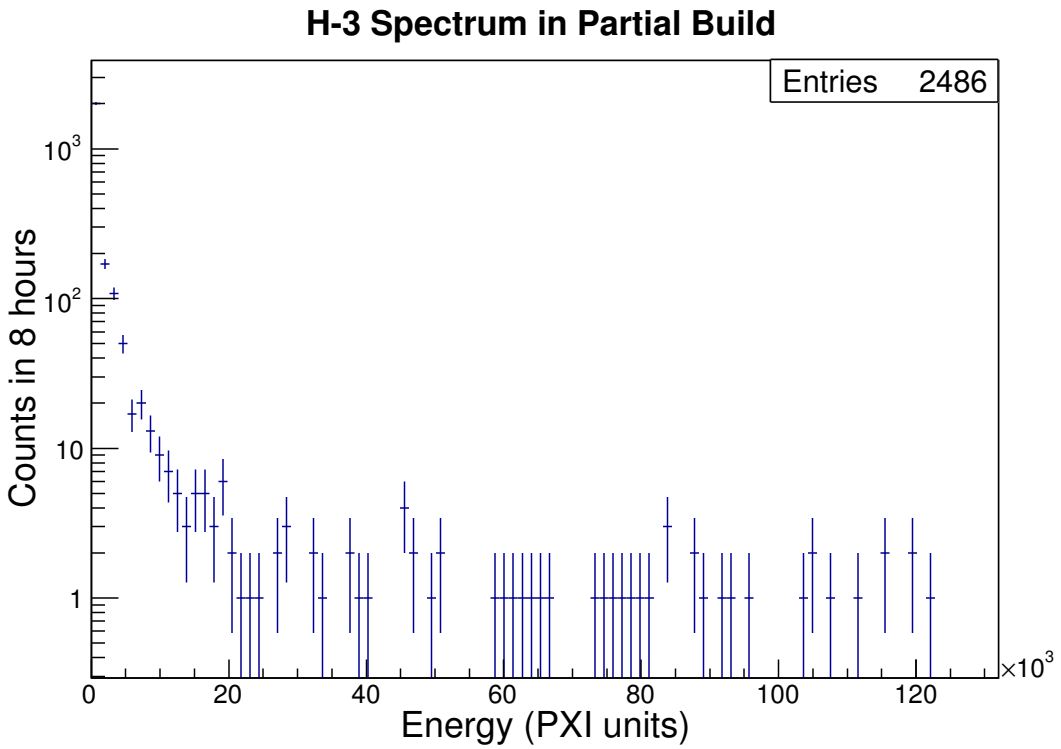

Figure 5.3: ^{3}H spectra with UGAB cocktail in PXI energies for the partial build with no energy cut and 50% energy equivalence.

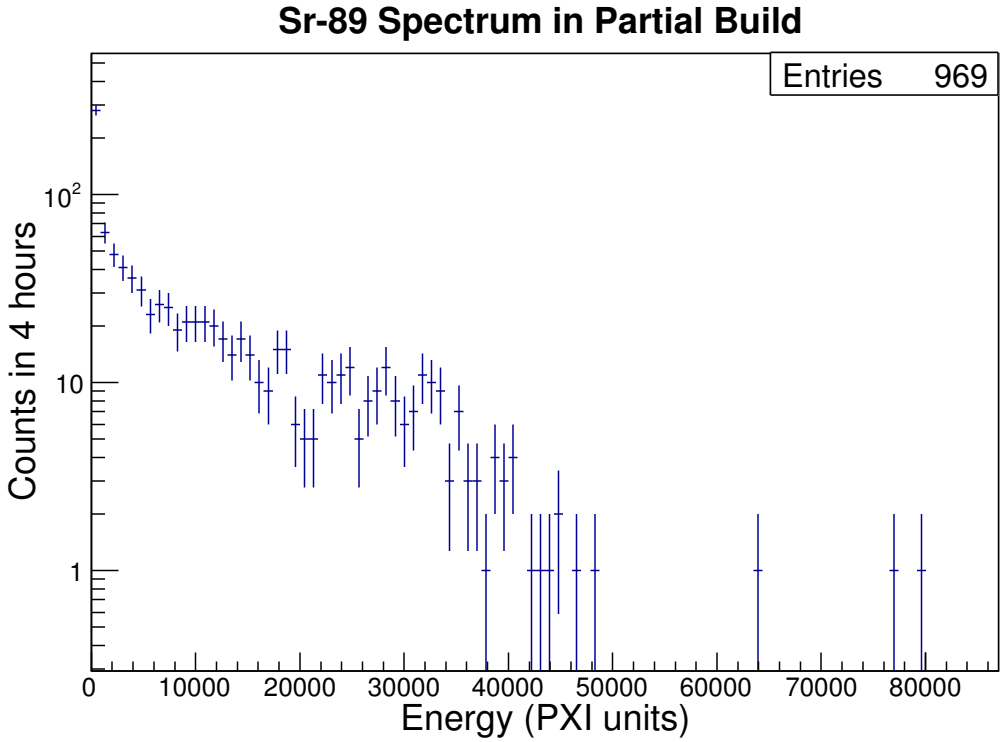

Figure 5.4: ^{89}Sr spectra with UGAB cocktail in PXI energies for the partial build with no energy cut and 50% energy equivalence.

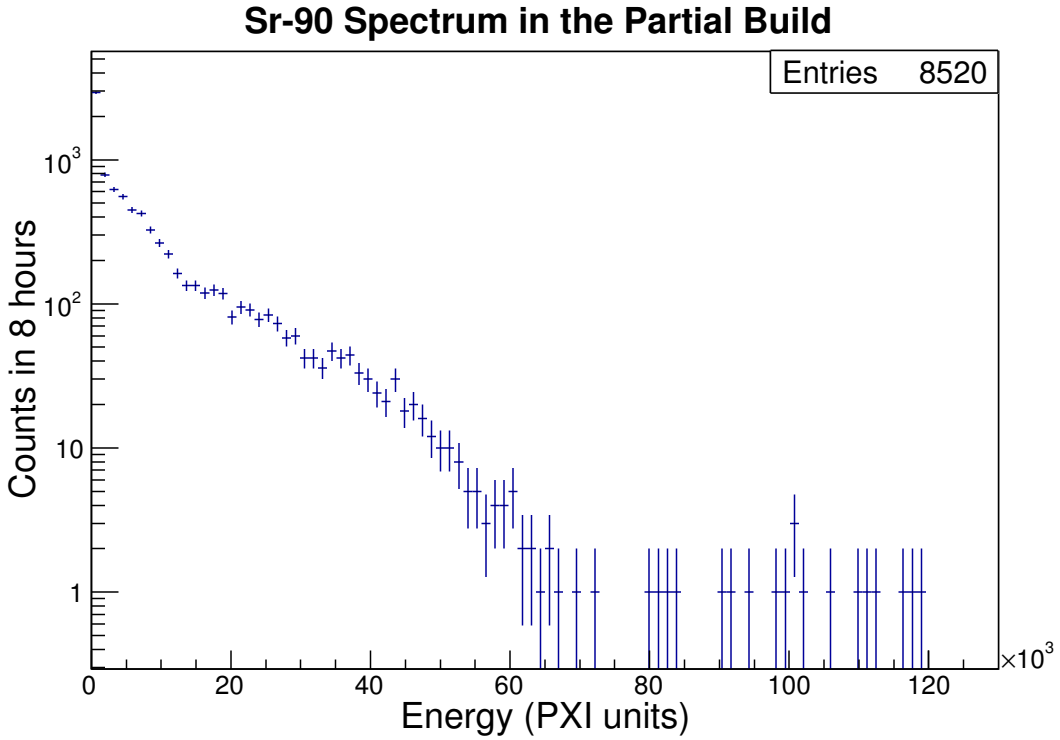

Figure 5.5: ^{90}Sr spectra with UGAB cocktail in PXI energies for the partial build with no energy cut and 50% energy equivalence.

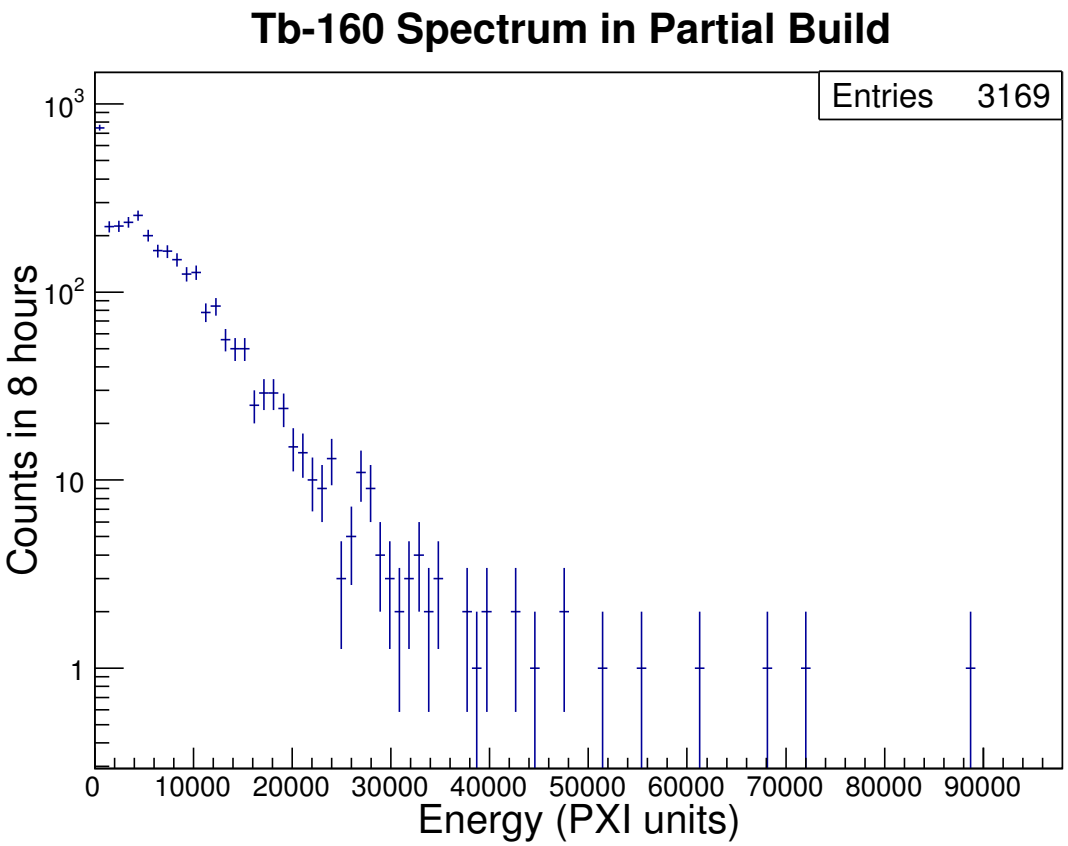

Figure 5.6: ^{160}Tb spectra with UGAB cocktail in PXI energies for the partial build with no energy cut and 50% energy equivalence.

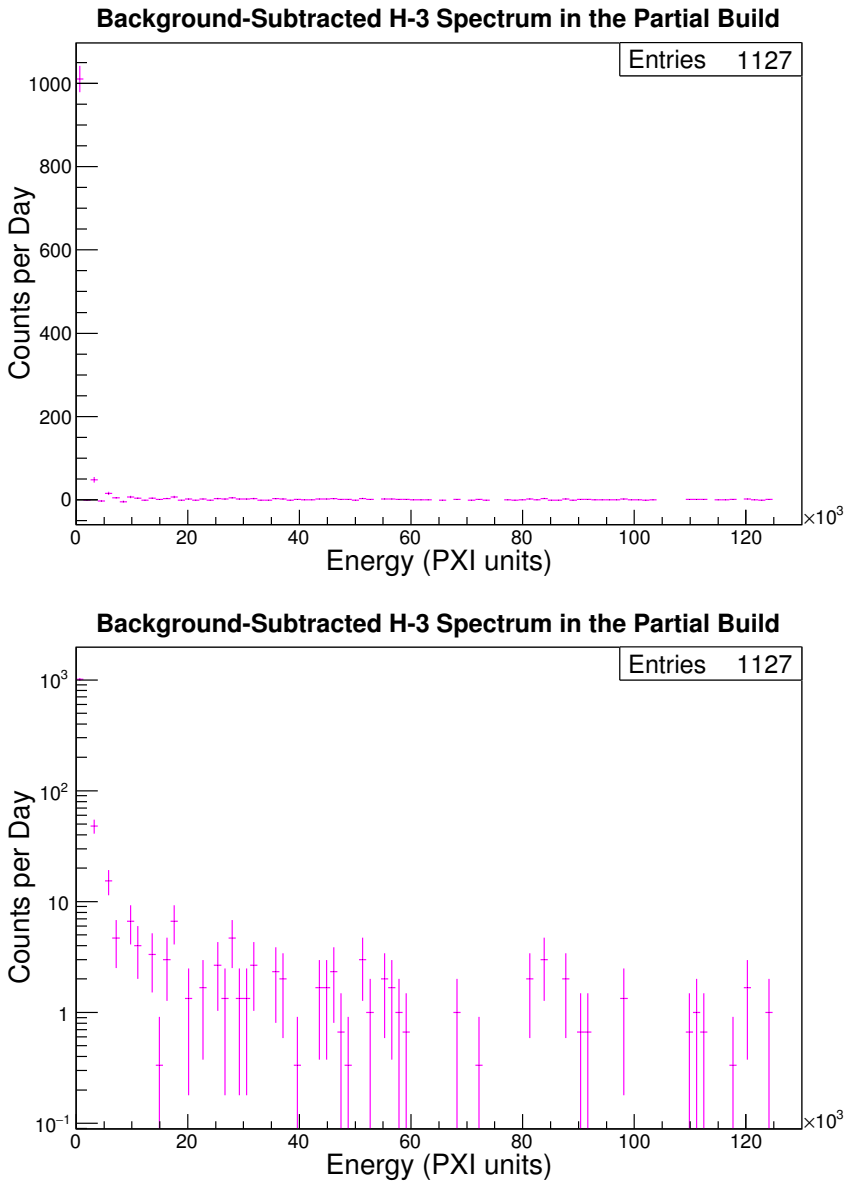

Figure 5.7: ^{3}H background-subtracted energy spectrum using PXI energy values for the partial build with no energy cut and 50% energy equivalence. Both plots represent the same data, the first on a linear scale and the second on a semilogarithmic scale.

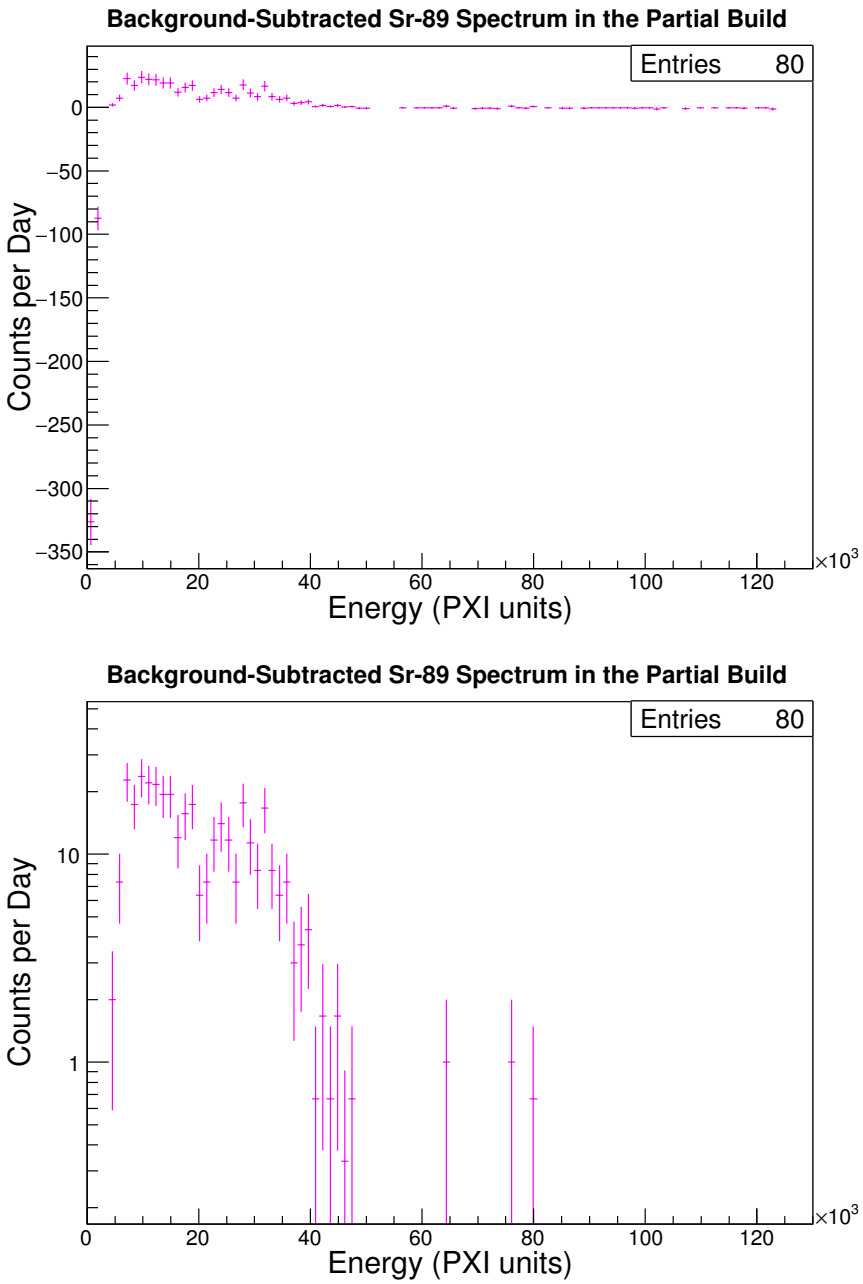

Figure 5.8: ^{89}Sr background-subtracted energy spectrum using PXI energy values for the partial build with no energy cut and 50% energy equivalence. Both plots represent the same data, the first on a linear scale and the second on a semilogarithmic scale.

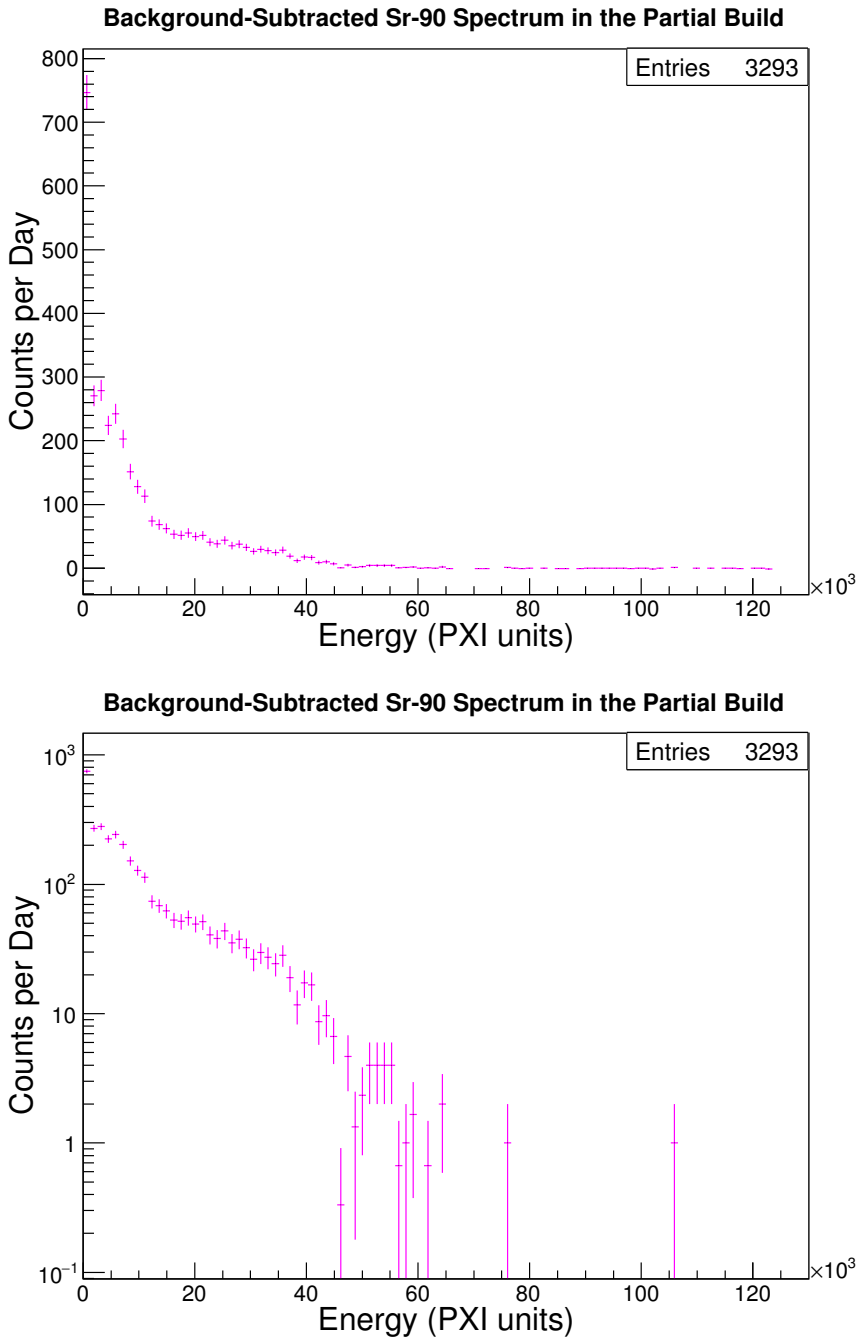

Figure 5.9: ^{90}Sr background-subtracted energy spectrum using PXI energy values for the partial build with no energy cut and 50% energy equivalence. Both plots represent the same data, the first on a linear scale and the second on a semilogarithmic scale.

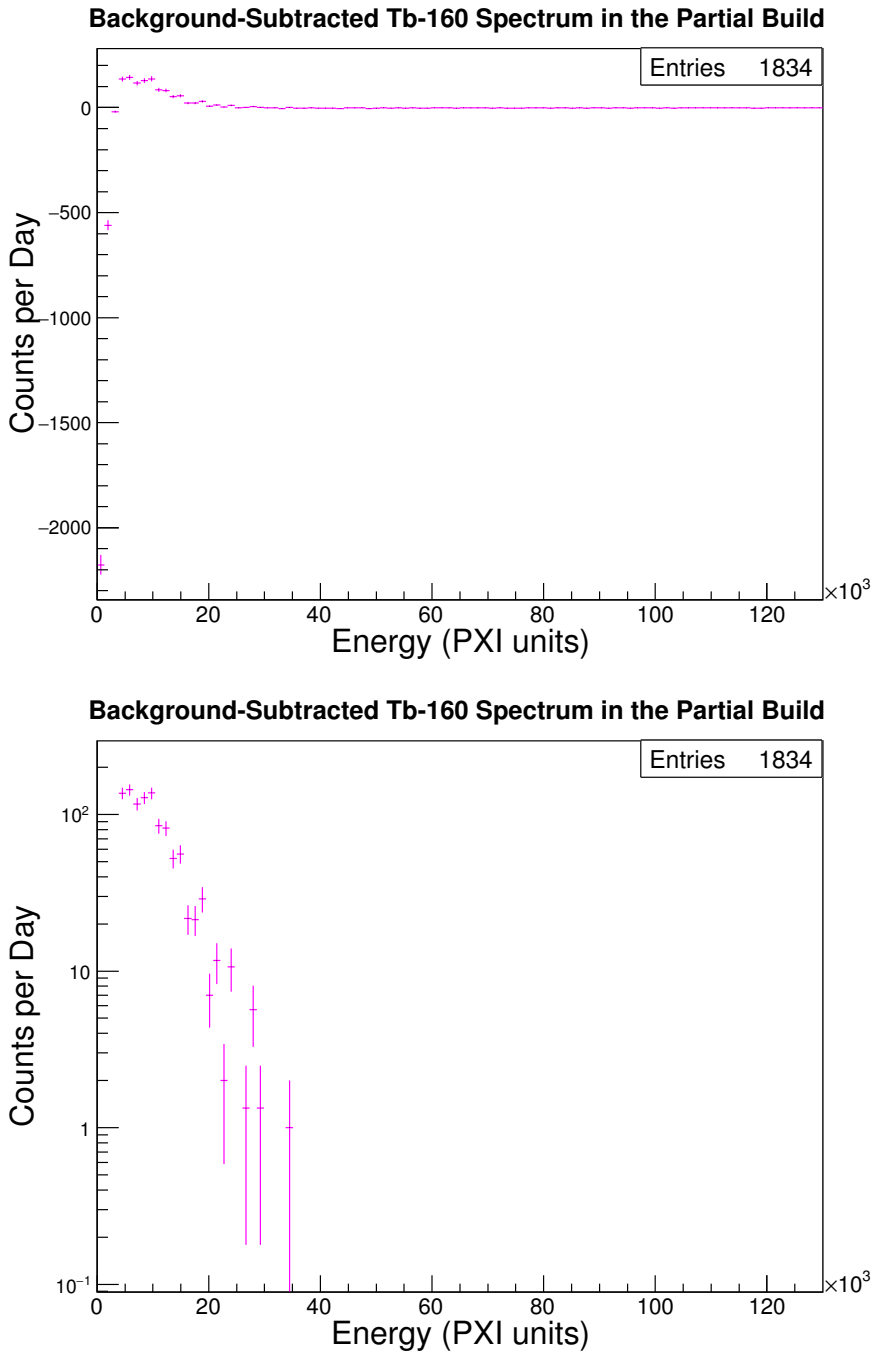

Figure 5.10: ^{160}Tb background-subtracted energy spectrum using PXI energy values for the partial build with no energy cut and 50% energy equivalence. Both plots represent the same data, the first on a linear scale and the second on a semilogarithmic scale.

5.5 Observations and Implications

The sample spectra for the different radionuclides do show some spectral characteristics unique to the radionuclide in the individual sample, such as differing endpoints relative to the beta energies and spectral shapes for both parent and daughter in the ^{90}Sr sample. This manifestation of decay characteristics in the spectrum showed promising initial results for the ability to perform spectral identification with the ULB LSC. Unfortunately, the efficiencies for the partial build are not as high as would be obtained with more conventional LSC analysis. The low efficiency values are likely due to the loss of photons during transmission between the sample and PMTs. The double-packaging around the samples and the 74% reflectance of the hollow copper light guide would contribute to this loss of photons and decreased efficiency. The issue of light collection was addressed prior to data collection with the full build. The light guides were polished and re-coated for a higher reflectance in order to improve photon propagation and total light collection. The samples were still packaged with a double layer of plastic bagging since two clean layers between the samples and detection chamber needed to be preserved. The improvements in light collection were imperative to improving sample detection (higher efficiencies and count rates), especially for samples such as ^{3}H and ^{89}Sr, as well as the distinction of spectral features (endpoints and parent/daughter overlap in spectra).

5.6 Changes Between the Partial and Full Builds

5.6.1 Light Guides

5.6.1.1 Light Collection Efficiency

Polishing the light guides improved reflectivity from 74% to 88%. The 88% reflectivity was simulated to have a total light collection efficiency of 34.5% for light

produced in the vial that makes it to either PMT. With the quantum efficiency of the PMTs of 30% at maximum, the maximum light collection efficiency is calculated to be 10.35%. Since the quantum efficiency of the PMTs cannot be greatly improved, either the light transmission efficiency of the light guide or the photon detection mechanism are the methods to improving the light collection efficiency.

$$\text{Light Collection Efficiency} = \epsilon_{LightGuide} \times \text{QE}_{PMT} \tag{5.1}$$

$$\text{Light Collection Efficiency} = 0.345 \times 0.3 \times 100\% \tag{5.2}$$

$$\text{Light Collection Efficiency} = 10.35\% \tag{5.3}$$

5.6.2 Build Geometry

Between the partial and full builds and characterization, the build geometry of the physical installation was upgraded. In the full build, two instrumented chambers were installed rather than the single chamber in the partial build. The chambers also included thermocouples and fiber optic cables in the full build for monitoring chamber temperature and the eventual fiber optic gain measurement system. Cooling lines and a cooling plate under the chambers were installed in the full build as well. When the pump and heat exchanger were running, chamber temperatures in the full build would be down to 8 °C compared to ambient temperature of 15 °C. Lead was stacked between the two chambers and the last external layers were added around the side and on the top of the cave in the full build, providing more shielding than was installed in the partial build. Lead end caps were built around the PMT ports and the dark box was built around the veto assembly to eliminate photon leakage from the room into the chamber.

5.6.3 Sample Changing Mechanism

The sample changing mechanism in the partial build was an ABS vial holder lowered into the chamber by hand using fishing line. In the full build, this vial holder was replaced by an OFHC vial holder with a lead and copper shield plug above it to fill the empty shield area in the sample port. The shield plug and vial holder were raised and lowered into the chamber by a pulley system with a tungsten counterweight. The pulley system was designed to be light-tight in order to be able to change samples without powering down the chamber PMTs. The light-tight panels and sample port shutters were not installed in the full build, so the system still needed to be powered down while samples were changed.

5.6.4 Electronics

Adjustments were made to the electronics between the partial and full builds as well. In the partial build, the chamber was instrumented with two Hamamatsu R11410 PMTs and E2979 sockets. The direct PMT output was input to the Pixie 500 Express module. The two chambers instrumented in the full build were outfitted differently. Each chamber had two Hamamatsu R11410 PMTs, but the E2979 socket assemblies were replaced with custom built voltage dividers. The voltage dividers were built out of low-background Cirlex® material and Mill-Max component sockets, which are not considered low-background due to beryllium content. The voltage divider was designed to follow the division scheme laid out according to the PMT specification sheet while running at positive instead of negative high voltage (K.K., 2011). The direct PMT signal was used as input for the Pixie 500 Express for the right channel. The PMT signals were fed through Canberra 2005 preamplifiers for the left chamber. The signals from the preamplifiers were the inputs into the Pixie 500 Express module dedicated to the left chamber. Since the tubes were under

different operation and the left chamber signals were shaped in the preamplifier, the parameters on the Pixie modules were optimized for the new conditions of the full build.

6. CHARACTERIZATION OF ULB LSC FULL BUILD

6.1 Electronics and Data Acquisition

In the full build of the ULB LSC, both of the outer chambers were built up and instrumented with low-background Hamamatsu R11410 PMTs with custom voltage dividers. The signal connections from the voltage dividers ran through the veto assembly and out of the dark box for input into signal processing or the Pixie 500 Express module. The outer chambers were designated as "left" and "right" based on orientation from the front of the system. The signals from the PMTs in the "left" chamber were run through charge-integrating Canberra 2005 preamplifiers before going into Pixie 500 Express module S/N 120. The signals from the "right" chamber PMTs were fed directly into Pixie 500 Express module 127 without any further signal processing. The differences in signal conditioning and associated settings in PixieViewer between the two chambers were to identify differences in detection capability and identify which method results in the highest detection efficiency. Since the signals going into the two Pixie 500 Express modules were inherently different, the digital processing settings in the PixieViewer software were also different for the two modules. Examples of the waveforms from the left (with preamp) and right (without preamp) chambers are shown in Figure 6.1. Only the first 704 ns of the waveforms are visible due to limitations within the PixieViewer settings, but the signal processing and calculations are performed using over 1.5 μs of the trace length. The preamplifier is charge-integrating, so the energy corresponds to the full height of the pulse above baseline and is calculated with trapezoidal filtering. The signal decays exponentially back to baseline based on the decay time constant of the RC circuit in the preamplifier (50 μs (Can, 2010)). For the direct PMT signal without

the preamplifier, the energy is equal to the integral of the pulse above baseline. Both signals exhibit ringing from contributions from the overcautious length of cable and the badge reader exterior to the room. The contribution from the badge reader has been mitigated in other systems with a faraday cage around the reader. The settings for the PMT channels on the left chamber (channels 0 and 1) were optimized for the preamplifier, basing energy calculations and triggering thresholds on the rising edge and flat top of the preamplifier pulse. This rising edge of the preamplifier output corresponds to the integrated charge of the pulse from the PMT that was collected, then discharged, from a capacitor in the preamplifier. The energy calculation is looks at the the average amplitude over the flat top, with decay time correction, after the first 1.9 μs for the calculation to exclude the ringing effects. The settings for the PMT channels on the right chamber (channels 4 and 5) were optimized to process direct PMT output pulses. These channels had the integrator mode in the PixieViewer software activated, so that energy calculations were based on integrating the pulse charge (of the initial pulse, above baseline) and trigger thresholds were based on the smaller pulse size relative to the preamplifier output. The pulse processing settings designated in the PixieViewer software are given in Table 6.1.

The veto panels were again matched based on PMT response and panel responses, with initial reference to the voltage settings from the partial build. Final values for the high voltage settings used for the veto assembly in the full build are shown in Table 6.2. The high voltages for the PMTs in the left and right chambers were initially set to the nominal voltage recommended by the vendor and with the positive polarity required by the custom voltage divider: +1500 V. The PMT responses for each chamber were then matched by adjusting the voltage for a series of trials using external gamma sources with Ultima Gold AB samples, prior to acquiring the data sets for energy calibrations. The voltage settings used for the initial trials were

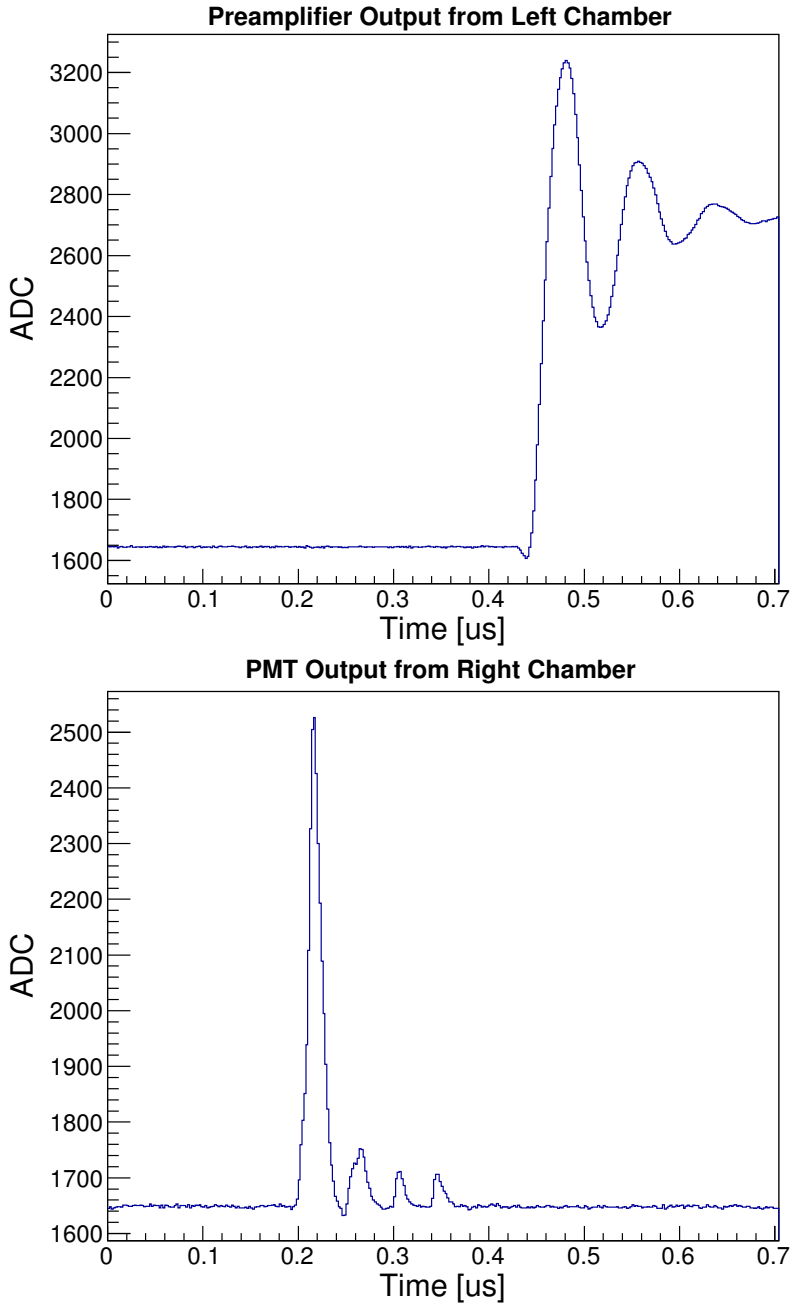

Figure 6.1: Waveforms from the left and right chambers, respectively, were processed differently based on signal conditioning.

Table 6.1: Settings in PixieViewer for the Full Build Data Acquisition

(a) Module Parameters

Module	120	127
Energy Filter	1	1
Coincidence Pattern	8	8

(b) Channel Parameters

Channel	0	1	2	4	5	6
Threshold (ADC units)	10	10	120	5	5	120
Trigger Rise Time (μs)	0.256	0.256	0.256	0.256	0.256	0.256
Trigger Flat Top (μs)	0.248	0.248	0.248	0.248	0.248	0.248
Energy Rise Time (μs)	1.968	1.968	0.752	1.536	1.536	0.72
Energy Flat Top (μs)	0.064	0.064	1.28	0.496	0.496	1.28
Tau (μs)	41.2	42.3	42.9	50	50	41
Trace Length (μs)	0.704	0.704	0	0.704	0.704	0
Trace Delay (μs)	0.5	0.5	0.5	0.25	0.25	0.25
Voltage Offset (%)	10	10	10	10	10	10
Gain	1	1	1	2.60998	2.60998	1
Pulse Inverted	No	No	No	Yes	Yes	No

observed to be too high to view the endpoint of the ^{90}Y beta spectrum during the initial sample trials. The voltages on the PMTs in the left chamber were decreased, with respect to a matched response, for data taken after the initial trials; the "tau" was decreased, corresponding to an increase of spectral range, for the right chamber after the initial trials, but the voltages of the PMTs remained constant. The voltage settings for the chamber PMTs are given in Table 6.3.

For the veto assembly, expected count rates for each of the six panels were calculated based on a 1 muon s^{-1} cm^{-2}. For all the panels combined, the expected count rate is 80.1 s^{-1} for the surface area normal to a directly incident cosmic muon. The observed count rate was 120.8 $\pm$ 1.4 s^{-1}, which includes contributions from high-energy gamma rays as well as any contributions from off-normal axes. This observed

Table 6.2: High Voltage Settings for the Veto Assembly in the Full Build.

Panel	PMT A HV (V)	PMT B HV (V)
0	630	630
1	1100	1100
2	705	690
3	1250	1050
4	665	665
5	760	770

Table 6.3: High Voltage Settings for the Left and Right Chamber PMTs for the Initial Trials and Long Trials.

Initial Trials		
	Left Chamber	Right Chamber
PMT A	1550 V	1750 V
PMT B	1650 V	1650 V
Long Trials		
	Left Chamber	Right Chamber
PMT A	1465 V	1750 V
PMT B	1550 V	1650 V

value is almost exactly 150% of the expected value. The higher count rate from observed data is due to the implemented threshold, interactions on surfaces off-normal from a direct muon trajectory, and contribution from gamma rays.

The dark count rate (dark CR) for the left and right chambers is calculated based on the accidental coincidence rates between the two PMTs in each chamber. The calculations follow Equation 6.1, with the count rates for the individual PMTs determined from data acquisition with only the sample chamber in place. With no Ultima Gold cocktail in place, there is no relation to cosmic events or decay events from impurities in the Ultima Gold cocktail. The dark count rates for the left and right chamber were calculated to be $(135 \pm 0.2) \times 10^{-7}$ s^{-1} and $(22.1 \pm 0.5) \times 10^{-12}$

s^{-1}, respectively. The differences between chambers are due to the addition of the preamplifier into the signal processing on the left chamber in addition to differences in efficiencies between the chambers and quantum efficiencies of the individual PMTs.

$$\text{Dark CR } (s^{-1}) = 2 \times \text{Coinc. Window (s)} \times \text{CR}_{PMTA} \ (s^{-1}) \times \text{CR}_{PMTB} \ (s^{-1}) \tag{6.1}$$

6.2 Energy Calibration

Energy calibrations were done for each PMT in both chambers using four point sources: ^{137}Cs, ^{22}Na, ^{60}Co, and ^{241}Am. The ^{137}Cs, ^{22}Na, and ^{60}Co sources were new sources from Eckert and Zeigler, purchased with activities of 1 μCi $\pm$ 3% each as of May 2016. The ^{241}Am source is a calibration source from the ULB PC system, with an activity of 39.5 μCi $\pm$ 3% as of November 2011. Data was collected for both chambers with each of the sources placed on a background sample vial with Ultima Gold AB cocktail, rotating each source through for a new data acquisition. The Ultima Gold sample in each chamber remained constant through this process. Each source was measured in MCA mode for one hour in each of the two chambers. After rotating through all four sources, MCA spectra were available for each of the four sources for both PMTs individually for both the left and right chambers. Resulting spectra for each PMT was used to determine the energy calibration scheme for each PMT using the Compton energies of the dominant gammas from the sources listed, shown in Table 6.4. The energy calibrations assumed isotropic photon emission from energy deposition (50% incident on each PMT at the maximum). Correlating the Compton Energy of the high-energy gamma emission from each of the radionuclides gave a four-point energy calibration with 1117.6 keV from ^{60}Co as the highest calibration

point and 48.3 keV from ^{241}Am as the lowest calibration point.

Table 6.4: The gamma energies and Compton energies used in the energy calibrations.

Source	Gamma Energy (keV)	Compton Energy (keV)
^{137}Cs	662	477.65
^{60}Co	1332	1117.62
^{22}Na	1274.5	1061.70
^{241}Am	59.5	48.26

Energy calibrations were done separately for the short 20-hour data acquisition times and long 9-day (216-hour) data acquisition times due to changes in the settings between the two sets of data acquisition. Energy calibrations for the short and long runs are shown in Figure 6.2. The linearity of the calibration using the Compton energies as the spectral endpoints was >99% in all cases. The equations of linear fits to each of the PMTs, shown in Table 6.5, were included in the post-processing to convert the PXI energy values to units of keV for accepted events. The calibration parameters were set in the post-processing codes to reflect whether the data was from an initial trial or long trial.

The energy ranges for both chambers, based on the calibrations, are given in Table 6.6. Note the limited range of the right chamber in the initial calibration, which corresponds to the cutoff in the sample spectra at ≈1600 keV. While the range for each of the PMTs will differ slightly, the range of the summed energy between both PMTs for the same event was limited to 0-2500 keV for analysis of this data set.

It is noted that these fits appear linear across a range of ∼50-1100 keV. It is expected, however, that the calibration would deviate at lower energies (∼5-30 keV)

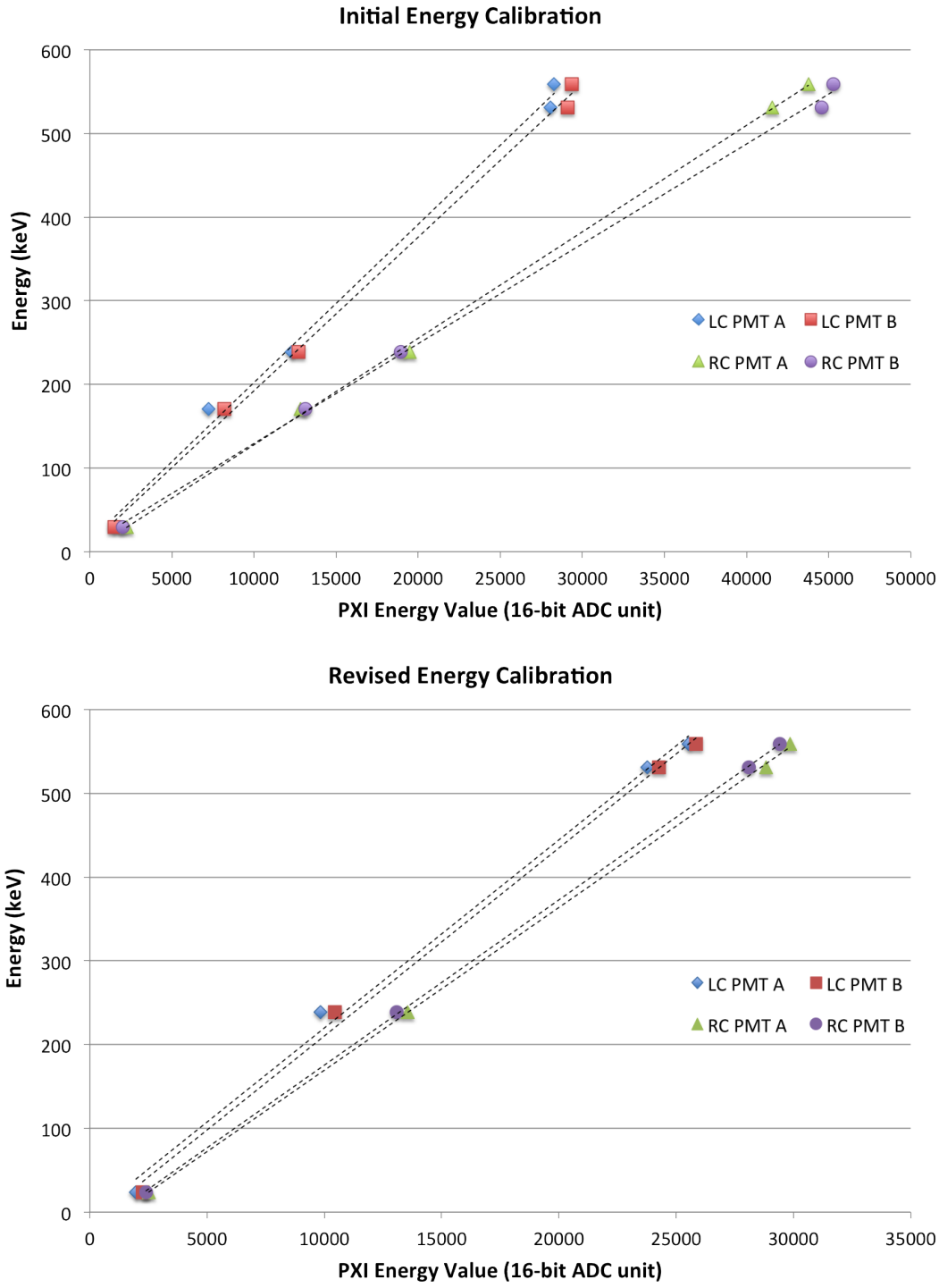

Figure 6.2: Initial and Revised Energy Calibration points. The associated equations are referenced in Table 6.5.

Initial Trial Calibration

Left Chamber	
PMT A	Energy (keV) = 0.0189*PXI value + 13.071 R^2 = 0.99581
PMT B	Energy (keV) = 0.0184*PXI value + 8.9047 R^2 = 0.9967
Right Chamber	
PMT A	Energy (keV) = 0.0127*PXI value + 0.5184 R^2 = 0.99934
PMT B	Energy (keV) = 0.0119*PXI value + 10.021 R^2 = 0.99889

Long Trial Calibration

Left Chamber	
PMT A	Energy (keV) = 0.0225*PXI value - 4.744 R^2 = 0.99562
PMT B	Energy (keV) = 0.0224*PXI value - 14.146 R^2 = 0.99719
Right Chamber	
PMT A	Energy (keV) = 0.0194*PXI value - 24.894 R^2 = 0.99983
PMT B	Energy (keV) = 0.0197*PXI value - 21.819 R^2 = 0.99994

Table 6.5: The energy calibrations for each PMT using the 4-point calibration from Compton energy endpoints of the four gamma sources. Calibrations were performed with the settings used in the initial short trials and the subsequent long trials.

Calibration	Left Chamber	Right Chamber
Initial Calibration	20 - 2400 keV	10 - 1600 keV
Revised Calibration	20 - 2900 keV	10 - 2500 keV

Table 6.6: The energy ranges for each PMT regarding the MCA spectrum available in the PixieViewer software.

due to the fewer (and very low) number of photons generated and propagated at these low energies. This would affect counting of tritium samples. The current setup was optimized for higher energy counting of ^{90}Sr/^{90}Y samples. Settings should be

revisited, and a calibration source of lower energy should be used to evaluate spectra from low-energy emitters such as tritium. A lower-energy calibration source could include an LSC vial filled with UG uLLT (tritium) cocktail with small copper discs in the bottom and lid of the vial. The 8 keV x-rays from the copper would provide a low-energy calibration point applicable for tritium counting.

6.3 Observed Background

6.3.1 Sample Preparation and Counting Conditions

Five clean vials were prepared by adding a mass of ∼20 mL of Ultima Gold AB cocktail by a clean 3 mL volumetric dropper. The vials were cleaned as per the procedures described in Appendix D and the dropper was rinsed with ethanol several times and left to dry before use. The clean vials were handled with gloves, but the mass of cocktail was added in a non-clean, but non-rad, laboratory. The vials were capped and taped closed after the cocktail was added. The exterior was wiped with ethanol twice, and the vials were transferred to a clean transfer bag for transfer to the clean hood for packaging according to the ULB LSC packaging procedures (see Appendix D). The vials were weighed before and after the addition of the cocktail in order to normalize the observed backgrounds by the mass of each sample. The vial number, mass of Ultima Gold AB, and normalization factor of the sample mass to a 20 mL sample (19.60 g, given the density of 0.98 g/mL) are shown in Table 6.7. The normalization factor will be used to normalize count rates from the actual sample mass to the expected count rate for a 20 mL (19.60 g) sample for comparison between samples.

The samples were rotated through both chambers with 20-hour counting times. These data acquisitions represent the short data collection sets. The counting order, counting time, and the reported output count rate from the PXI module are given in

Table 6.7: UGAB sample masses and normalization factors.

Vial	Mass of UGAB (g)	Normalization Factor
1	19.82	0.989
2	19.66	0.997
3	19.71	0.994
4	19.60	1.000
5	19.65	0.998

Tables 6.8 and 6.9. All five of UGAB samples were rotated through the left chamber; UGAB samples 1-4 were simultaneously rotated through the right chamber after measurement in the left chamber.

Table 6.8: Counting Live Time and output count rate (OCR) as reported by the PXI module for UGAB background samples counted in the Left Chamber.

Vial	Counting Time (s)	PMT A OCR (s^{-1})	PMTB OCR (s^{-1})
1	71999.6	0.0057	0.0052
2	71999.6	0.0065	0.0055
3	71999.6	0.0058	0.0052
4	71999.6	0.0056	0.0053
5	71999.6	0.0070	0.0064

Table 6.9: Counting Live Time and output count rate (OCR) as reported by the PXI module for UGAB background samples counted in the Right Chamber.

Vial	Counting Time (s)	PMT A OCR (s^{-1})	PMTB OCR (s^{-1})
1	71999.6	0.0086	0.0055
2	71999.6	0.0085	0.0056
3	71999.6	0.0081	0.0055
4	71999.6	0.0079	0.0053

Two of the background vials (one for each chamber) were counted for a long trial of 9 days in order to obtain data with higher statistical accuracy. The counting time and output count rates from the PXI modules are given in Table 6.10. Observed counts and spectral data for these trials will be normalized to a 20 mL background sample as a standardization for comparison and background subtraction.

Table 6.10: Counting Live Time and output count rate (OCR) as reported by the PXI module for UGAB background samples counted in the long trials.

Vial	Counting Time (s)	PMT A OCR (s^{-1})	PMTB OCR (s^{-1})
1 (LC)	777597	0.0049	0.0045
2 (RC)	777597	0.0080	0.0056

Background data collected with sample vials filled with Ultima Gold AB cocktail should be representative of the expected background within the demonstration samples since the same volume of the same batch of Ultima Gold AB is used in the demonstration samples. These data sets will be used for calculation of the expected background contributions in demonstration samples, which must then be subtracted from the sample spectra. In addition to the expected sample backgrounds, the chamber background was obtained with a series of two 16-day measurements. Counting times and observed count rates from the PXI modules for the sample carrier background measurements are shown in Table 6.11.

The chamber background is the background observed in the system with contributions only from the chamber environment. The sample carriers and plugs were lowered into place with no vial, cocktail, or sample included. Background contributions from the vial, packaging, and cocktail can be elucidated from differences between the observed chamber and cocktail backgrounds. The chamber backgrounds

Table 6.11: Counting Live Time and output count rate (OCR) as reported by the PXI module for measurements of the sample carrier backgrounds.

Vial	Counting Time (s)	PMT A OCR (s^{-1})	PMTB OCR (s^{-1})
LC	1.3824e+06	0.00087	0.00078
	1.3824e+06	0.00092	0.00082
RC	1.3824e+06	0.00012	0.00010
	1.3824e+06	0.00014	0.00013

and cocktail backgrounds will be compared to the background estimates obtained through simulation.

6.3.2 Observed Spectra and Count Rates

The data collected from the background trials described above was processed through file conversion and event selection using the methods described in Chapter 4. No pulse shape analysis was performed on the background data. Events were paired and selected on the same timing and energy parameters as set for the sample data, and the energies of the events were calculated from the equations derived from the external source calibrations. The appropriate parameters were applied to the corresponding chamber and PMT as identified by the user.

The resulting spectra from the event selection are shown in full in Appendix C, and a subset of key spectra are shown here in the text. The spectra are shown for the energy range associated with the demonstration samples discussed in Chapter 7, for which the background in the region between 0 and 2500 keV is of interest. The binning scheme of 100 bins for the energy range of 0-2500 keV is consistent with that of the demonstration samples for consistency in background subtraction.

The background spectra for the initial short trials of 20 hours were individually normalized to a 20 mL sample by scaling the spectra using the normalization factors derived from the cocktail mass for each of the vials. The normalized sample spectra

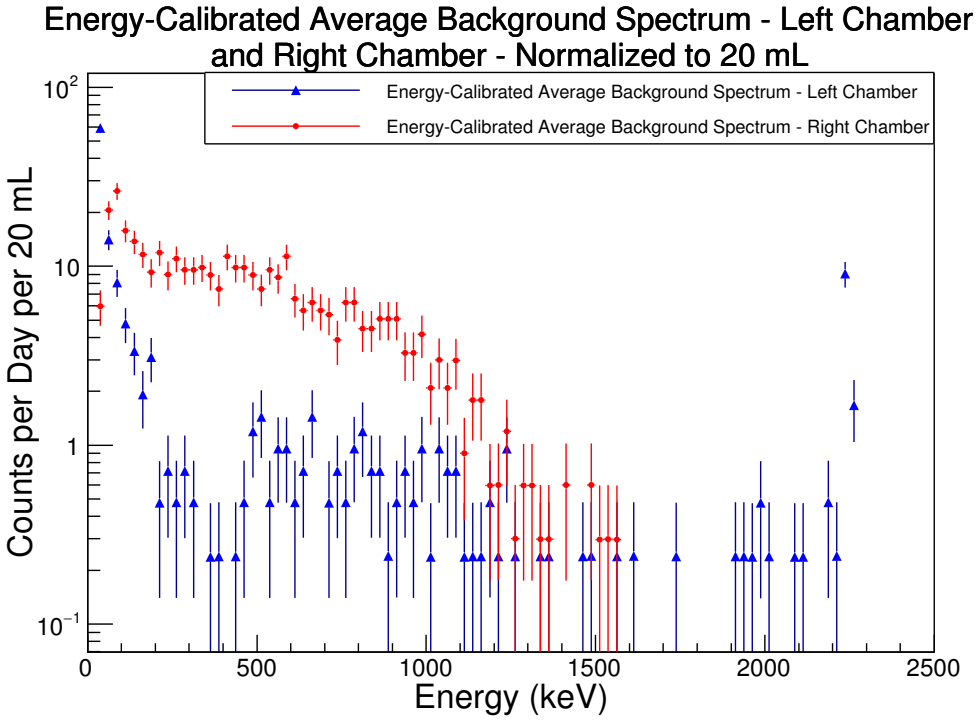

Figure 6.3: Average background for Ultima Gold cocktail in the left and right chambers.

for these trials were averaged to create an average background from the short trials. The average background of the Ultima Gold AB cocktail was derived for both the left and right chambers in this manner. Both are shown in Figure 6.3. The error for each bin was initially calculated using the sum-of-squares method for the measured spectra; this method is consistent with calculating uncertainty as the square root of the counts for a given counting time in counting statistics applied to radioactivity. This error was propagated through the scaling and averaging, and is shown graphically as vertical error bars in the spectra.

For the long trials of 9 days, the measured background spectra were normalized to a 20 mL volume using the normalization factors for the respective cocktail vials. The normalized spectra for the left and right chambers are shown in Figure 6.4. The

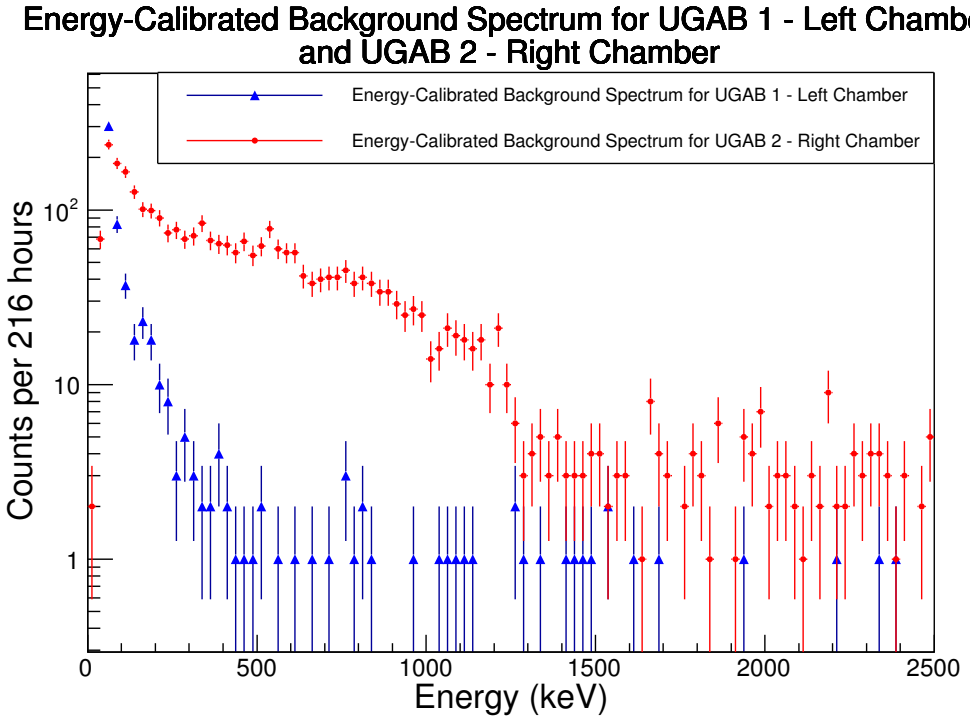

Figure 6.4: Long background for Ultima Gold cocktail in the left and right chambers.

normalized long spectra include the propagated error for each bin initially derived from the measured spectra. The error by bin is shown as vertical error bars on these spectra as well.

Background count rates were calculated for four regions of interest within this energy range. The regions of interest are identified with the full sample spectrum (25-2300 keV, or bins 1-92), the ^{90}Sr portion of the spectrum which includes contribution from ^{90}Y as well (25-550 keV, or bins 1-22), and the portion of the sample spectrum with only contribution from ^{90}Y (550-2300 keV, or bins 23-92). Note that the lowest energy bin is not included in the regions of interest for the sample spectra to remove any contribution from low energy noise. For further details on the definition of these regions of interest, please refer to Section 7.2. The counts in each region of interest were integrated to calculate the total number of background counts in each region.

The number of counts in the regions of interest for each of the trials is shown in Tables 6.12 and 6.13. The uncertainties in these numbers are propagated from the bin errors within the region of interest. The ratio of the uncertainties in the long trials to the short trials does trend nearly inversely with a factor of the square root of the ratio of counting time for the left chamber and directly inversely with the same factor for the right chamber, as would be expected.

Table 6.12: Raw background counts from Ultima Gold AB sample measurements in the left chamber.

Vial	Counting Time (s)	Counts in Energy Range 25-2300 keV	25-280 keV	280-2300 keV
Initial Short Trials				
1*	72000	91 ± 10	71 ± 8	20 ± 4
2	72000	104 ± 10	80 ± 9	24 ± 5
3	72000	81 ± 9	66 ± 8	15 ± 4
4	72000	98 ± 10	78 ± 9	20 ± 4
5	72000	190 ± 14	131 ± 11	59 ± 8
Long Trials				
1*	777600	556 ± 24	525 ± 23	31 ± 6

*Note that the count rate does not scale up linearly with time between the short and long trials of UGAB sample 1. The longer trial allows more counting time after the sample has stabilized at chamber temperature and the effect of light-induced chemiluminescence has faded. This effect is more pronounced in the left chamber (with preamplifier) than in the right chamber (direct, non-amplified signal).

The number of counts observed in each of the regions was scaled by the normalization factor for the vial, based on the mass of cocktail in the vial. With the number of counts observed for each vial normalized to 20 mL, the counts were then multiplied by a factor of (24/20) to calculate the number of counts per day, shown in Tables 6.14 and 6.15. The uncertainties calculated for these count rates (in counts

Table 6.13: Raw background counts from Ultima Gold AB sample measurements in the right chamber.

Vial	Counting Time (s)	Counts in Energy Range 25-2300 keV	25-280 keV	280-2300 keV
Initial Short Trials				
1	72000	310 ± 18	203 ± 14	107 ± 10
2+	72000	287 ± 17	193 ± 14	94 ± 10
3	72000	294 ± 17	193 ± 14	101 ± 10
4	72000	314 ± 18	207 ± 14	107 ± 10
Long Trials				
2+	777600	2971 ± 55	1960 ± 44	1011 ± 32

+Note that the count rate does scale up linearly with time between the short and long trials for UGAB sample 2. The effects of temperature stabilization and light-induced chemiluminescence are not as prominent in the right chamber.

per day) take into account the normalization factor and scaling to counts per day. The relative uncertainties in the count rates are given in Table 6.16. All are between 7-10% for the full sample spectrum in the left chamber and between 5-6% for the same in the right chamber. The long trials had smaller relative uncertainties, as expected, of <7% for the left chamber and <3% for the right chamber over the full sample range.

From the initial trials with all 5 background samples, an average UGAB background was calculated to be 135 counts per day with a standard deviation of 13 counts per day in the left chamber, and 360 counts per day with a standard deviation of 21 counts per day in the right chamber. This difference is due to the difference in detection efficiencies between the two chambers, which is discussed in Chapter 7.

For the purely environmental background estimate, the backgrounds were calculated from the measurement obtained with only the sample carrier inserted. The total counts from the two sets of 16-day measurements are summarized in Table 6.17

Table 6.14: Background count rates (d^{-1}) for each UGAB background sample in the left chamber.

Vial	Count Rate (d^{-1}) in Energy Range		
	25-2300 keV	25-280 keV	280-2300 keV
Initial Short Trials			
1	110 ± 10	90 ± 10	20 ± 5
2	125 ± 10	100 ± 10	30 ± 5
3	100 ± 10	80 ± 10	20 ± 5
4	120 ± 10	90 ± 10	20 ± 5
5	230 ± 20	160 ± 10	70 ± 10
Long Trials			
1	61 ± 4	58 ± 4	3 ± 1

Table 6.15: Background count rates (d^{-1}) for each UGAB background sample in the right chamber.

Vial	Count Rate (d^{-1}) in Energy Range		
	25-2300 keV	25-280 keV	280-2300 keV
Initial Short Trials			
1	370 ± 20	240 ± 20	130 ± 10
2	340 ± 20	230 ± 20	110 ± 10
3	350 ± 20	230 ± 20	120 ± 10
4	380 ± 20	250 ± 20	130 ± 10
Long Trials			
2	329 ± 10	217 ± 8	112 ± 6

and the count rate equivalents in Table 6.18. Summed spectra for the two measurements in left chamber and right chambers are shown in Figure 6.5. The average background for the left chamber was 11.0 ± 0.6 counts per day while that of the right chamber was 2.1 ± 0.1 counts per day, with a total of 32 days of counting time.

6.3.3 Contribution from Cosmics

The Ultima Gold cocktail samples (uLLT and UG AB) include contributions from the cocktail material, interacting environmental radioactivity, and leakage not

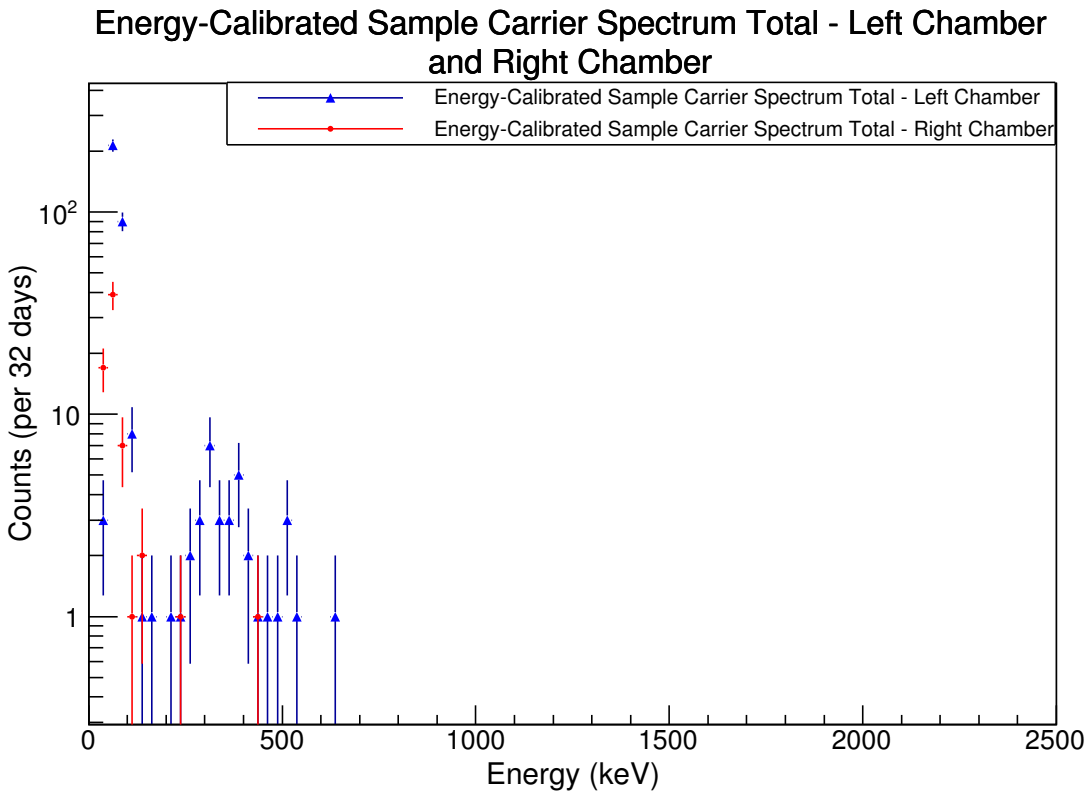

Figure 6.5: Average background for an empty chamber in the left and right chambers.

Table 6.16: Relative uncertainty in the background count rates for each sample.

Vial	Relative Uncertainty (%) in Energy Range		
	25-2300 keV	25-280 keV	280-2300 keV
Initial Short Trials			
1 (LC)	10.5	11.9	22.4
1 (RC)	5.7	7.0	9.7
2 (LC)	9.8	11.2	20.4
2 (RC)	5.9	7.2	10.3
3 (LC)	11.1	12.3	25.8
3 (RC)	5.8	7.2	10.0
4 (LC)	10.1	11.3	22.4
4 (RC)	5.6	7.0	9.7
5 (LC)	7.3	8.7	13.0
Long Trials			
1 (LC)	6.8	7.0	29.0
2 (RC)	3.0	3.6	5.1

Table 6.17: Raw background counts from the long trials.

Trial	Counts in Energy Range		
	25-2300 keV	25-280 keV	280-2300 keV
LC-1	163 ± 13	163 ± 13	0 ± 0
RC-1	26 ± 5	26 ± 5	0 ± 0
LC-2	189 ± 14	188 ± 14	1 ± 1
RC-2	42 ± 6	42 ± 6	0 ± 0

Table 6.18: Background count rates (d^{-1}) from the long trials.

Trial	Count Rate (d^{-1}) in Energy Range		
	25-2300 keV	25-280 keV	280-2300 keV
LC-1	10 ± 1	10 ± 1	0 ± 0
RC-1	2 ± 0	2 ± 0	0 ± 0
LC-2	12 ± 1	12 ± 1	0 ± 0
RC-2	3 ± 0	3 ± 0	0 ± 0

negated by the cosmic veto (<1% of cosmic muon rate). The leakage rate for the cosmic muons was conservatively calculated by taking the dividing the counts in the cosmic region of the UGAB spectrum (0.0011 ± 0.0001 s^{-1} for the left chamber and 0.0039 ± 0.0001 s^{-1} for the right chamber) into the calculated cosmic muon flux for the ULB LSC (80.1 s^{-1}). This results in leakage rates of 0.0014 ± 0.0001% and 0.0049 ± 0.0001% for the left and right chambers, respectively. Knowing the leakage rate to be <0.1%, the 0.1% unaccounted for corresponds to 1153 counts per day that could interact with the LSC cocktail and produce background in either chamber. Using the calculated leakage rates and uncertainties, background contributions from cosmic interactions could be ∼95 ± 3 counts per day for the left chamber and ∼336 ± 6 counts per day for the right chamber. Both chambers would be expected to experience the same leakage rate, assuming the chambers have the same efficiency and the calculated leakage rates are purely due to cosmic interactions. Such a difference in the leakage rates as observed between the two chambers in the ULB LSC suggests different efficiencies between the left and right chambers. This point if further discussed in Chapter 7.

6.3.4 Comparison of Simulation to Experimental Results

From simulations, the expected background was 25 s^{-1} with a radioactive emissions background of 9.8 counts per day as laid out in Table 6.19 and the 15 counts per day systematic background observed in the partial build.[1] The expected background did not take into account the electronics added into the signal processing (custom bases, preamplifiers), the extended low energy range with preamplifiers not previously observed with the direct PMT output in the partial build, or any effects

[1]Reprinted from Applied Radiation and Isotopes, In Press, Erchinger, J.L. *et. al.*, Background characterization of an ultra-low background liquid scintillation counter, Page 2, Copyright (2017), with permission from Elsevier.

from the differences between the GEANT4 model and the actual build geometry. The observed environmental background was 11.0 ± 0.6 counts per day for the left chamber and 2.1 ± 0.3 counts per day for the left chamber with the revised setup. Backgrounds with the Ultima Gold AB cocktail in the sample chamber were 61 ± 4 counts per day for the left chamber and 329 ± 10 for the right chamber. The background is below the targeted 100 counts per day for both chambers for the environmental background, and for both the empty chamber and cocktail backgrounds in the left chamber. The cocktail background in the right chamber is an order of magnitude higher than that of the left chamber.

Table 6.19: Background estimates for radioactive emissions using a high fidelity model for the ULB LSC (Erchinger et al., 2017).

Background source (contributing isotopes)	Rate (d^{-1})	Fraction (%)
External γ-rays (U/Th/K)	1.5 ±0.9	15.3
Lead shield (^{210}Pb)	0.50 ±0.22	5.1
Copper shielding (U/Th/K/^{60}Co)	2.81 ±0.17	28.7
Light guide coating (U/Th/K)	3.41 ±0.06	34.8
PMTs (U/Th/K/^{60}Co)	0.03 ±0.01	0.3
PMT Base	1.38 ±0.08	14.1
Vial plastic (U/Th/K) *(calculation)*	0.15	1.5
Cross-talk (Presumed 2615 keV γ)	0.008 ±0.003	0.1
Neutrons	0.0003444 ±0.0000059	0.1
Total estimated background rate	9.78 ±0.91	

7. SAMPLE ANALYSIS WITH ULB LSC

7.1 Sample Preparation

Five replicates of ∼1 Bq samples of ^{90}Sr/^{90}Y were created with Ultima Gold AB cocktail. The initial solutions had an activity concentration of 372.6 kBq ± 3% in 1.0054 g of solution. The dilution scheme is shown in Table 7.1. For all ULB LSC samples made during testing, the cocktail used was Ultima Gold AB cocktail. The loading fraction of the Ultima Gold cocktails for these samples was never more than 50%, which is consistent with Perkin Elmer's recommendations for the Ultima Gold cocktail (PerkinElmer, 2007). All the samples were prepared and packaged according to the procedure described in Appendix D. The clean vials and clean cocktail were supplied for the sample preparation in the radiological area. All were packaged with the 20 mL sample vial in a two layers of polyethylene tubing.

Table 7.1: Dilution Scheme from Stock solution to ULB LSC fraction for ^{90}Sr/^{90}Y.

Solution	Activity (Bq g^{-1})
Stock	371000 ± 11000
Dilution 1	3640 ± 110
Dilution 2	36.5 ± 1.1
Dilution 3	3.66 ± 0.11

The total sample set for ULB LSC is shown in Table 7.2. The sample activity is calculated from the mass of the solution added to the vial from Dilution 3. The small amount of solution was added to ∼ 20 mL of Ultima Gold AB solution for each of the samples.

Table 7.2: Set of $^{90}Sr/^{90}Y$ samples available for ULB LSC

Sample	Volume (mL)	Mass (g)	Activity (Bq)
90445	20	0.1362	0.998 ± 0.030
90446	20	0.1367	1.002 ± 0.030
90447	20	0.1365	1.000 ± 0.030
90448	20	0.1365	1.000 ± 0.030
90449	20	0.1369	1.003 ± 0.030

The samples composed for the demonstration set were created to be $\sim$ 1 Bq of activity each. For an activity of 1 Bq, a 100% efficient system would expect 86400 counts per day, with an uncertainty of $\sqrt{86400}$ or 294 counts per day. The 294 counts per day is a 0.3% relative uncertainty for the 86400 counts per day expected. Liquid scintillation counting is a high efficiency method, typically between 80-100% for high energy beta and alpha particles (L'Annunziata and Kessler, 2012), so counting for one day was expected to yield a relative uncertainty of $\sim$1% or less. Due to the time required to power down the system, change samples manually, and bring the system back online, the samples in the demonstration set were counted for 23 hours each during the "short" acquisition time data set, leaving one hour to change out the samples. The samples for the "long" acquisition time data set were counted for 3.5 days. For a 100% efficient system, the relative error for the long acquisition time would be expected to be 0.2% (550 counts out of 302400).

Compared to the 0.3% and 0.2% relative uncertainties in the short and long measurements, respectively, the 3% uncertainty of the activity of the stock solution dominates the uncertainty budget for the sample measurements. Other elements of the systematic uncertainty, though not as significant as error in stock solution activity, include the uncertainty in mass of LSC cocktail and stock solution during sample preparation (0.0005 g each), the background contributed by the LSC cocktail

(discussed in Chapter 6), and error in calibration (<1% in all cases).

7.2 Sample Analysis

Each of the samples in the demonstration set was counted for 23 hours in both the left and right chambers. Samples 90445 and 90449 were counted for 3.5 days in the left and right chambers, respectively. The event data for these files was converted and events selected using the process outlined in Chapter 4. For each of these data sets, a background normalized to 20 mL of Ultima Gold AB cocktail was subtracted. For the 23-hour data set, an average based on the five 20-hour background collections was used for the background subtraction. For the 3.5-day data collection, the long 9-day background normalized to 20 mL of Ultima Gold AB cocktail for the background subtraction. For all cases, the background subtraction included a live time normalization of the background spectrum to sample spectrum live time.

Between all the data sets collected for the demonstration samples, there were four data sets broken down in the list below. For the background-subtracted short acquisition set, the background subtracted from the sample spectra was the average background from the UGAB samples, normalized to 20 mL and to the sample counting time. The background subtraction for the long acquisition data set was done with the data from the long UGAB background trials, normalized to 20 mL of UGAB cocktail and the sample counting time.

- Short acquisition data sets
  - Individual sample trials - 10 total; 5 for each chamber
  - Background-subtracted sample data - 10 total; 5 for each chamber
- Long acquisition data sets

– Single sample trials - 2 in total; 1 for each chamber

– Background-subtracted sample data - 2 in total; 1 for each chamber

For each data set, the spectrum for the region from 0 keV to 2500 keV was selected and saved to 100 bins of 25 keV. The limits on the ^{90}Sr and ^{90}Y ranges were determined from the beta endpoints - 546 keV and 2280 keV, respectively. No energy cuts were implemented for converting files, but an energy threshold of 25 keV was implemented during spectral integration for count rate and activity calculations. A threshold of 25 keV will be high enough to exclude any low energy or electronic noise present in the data, and coincides with the low end of bin 1 out of 100 used in generating spectra. The integral of the counts in the defined regions of interest was recorded for each of the data sets, then normalized to counts per day according to the live time for each data set. The four regions of interest defined for integrating counts in the spectra are given in Table 7.3. The total sample count rate is determined from the full sample range (25-2300 keV).

Table 7.3: Regions of Interest Defined for Count Rate Calculations of the ^{90}Sr/^{90}Y data sets.

	Bins	Energy (keV)
Full Sample Range	(1,92)	25-2300
^{90}Sr Range	(1,22)	25-550
^{90}Y-only Range	(23,92)	550-2300

Based on GEANT4 predictions of energy deposition in a vial of LSC cocktail, an ideal spectrum of ^{90}Sr and ^{90}Y in secular equilibrium would have 128.4% of the total activity (100% of the ^{90}Sr and 28.4% of the ^{90}Y spectra) in the range from 0-546 keV, and 72.6% of the total activity in the ^{90}Y-only portion from 547-2280

keV. The total activity is 200% due to 100% ^{90}Sr and in-growth of the ^{90}Y daughter for an additional 100%. Using a threshold of 25 keV, ∼192% of the activity will be in Full Sample Range of 25-2300 keV. The ^{90}Sr range from 25-550 keV will include ∼93% of the ^{90}Sr activity and ∼27% of the ^{90}Y spectrum, for a total of ∼120% of the sample activity. The remaining portion of the ^{90}Y spectrum from 550-2300 keV will be ∼72% of ^{90}Y activity.

7.2.1 Spectra and Observations

The spectra from the samples showed differentiation between the ^{90}Y endpoint and ^{90}Sr endpoint for both chambers. The spectral shapes for the spectra differ between the chambers, however, due to the difference in pulse processing. The preamplifier in the signal processing from the left chamber amplifies the difference between the higher energy (on average) pulses from the ^{90}Y and the lower energy (on average) pulses from the ^{90}Sr.

Spectra of the samples from the "long" data acquisition sets are presented for each chamber in Figure 7.1, as are the background-subtracted spectra for the samples in Figure 7.2. This subset of the spectra generated from the data sets described above are shown here in the text; the full set of sample spectra and background-subtracted spectra are given in Appendix C.

7.2.2 Count Rate Data

The counts were integrated in each of the four regions of interest and used to calculate the count rates observed for each of the samples. The counts in each region for the raw sample data are given in Table 7.4 and 7.5. The total counts in the long trial are greater than those of the shorter trials due to the longer counting time.

The counts observed during measurement were divided by the live time to calculate the counts per day for the samples. No normalization to sample volume or

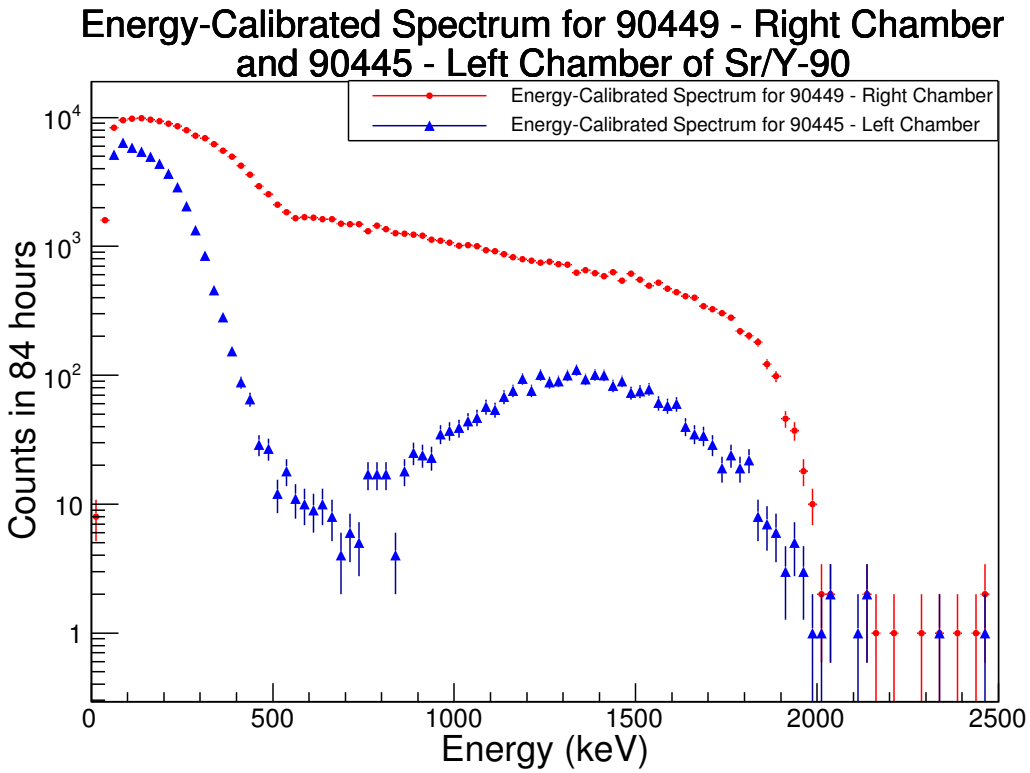

Figure 7.1: ^{90}Sr/^{90}Y spectra for the long acquisition, 3.5-day data sets. Sample 90445 was in the left chamber (blue) and Sample 90449 was in the right chamber (red).

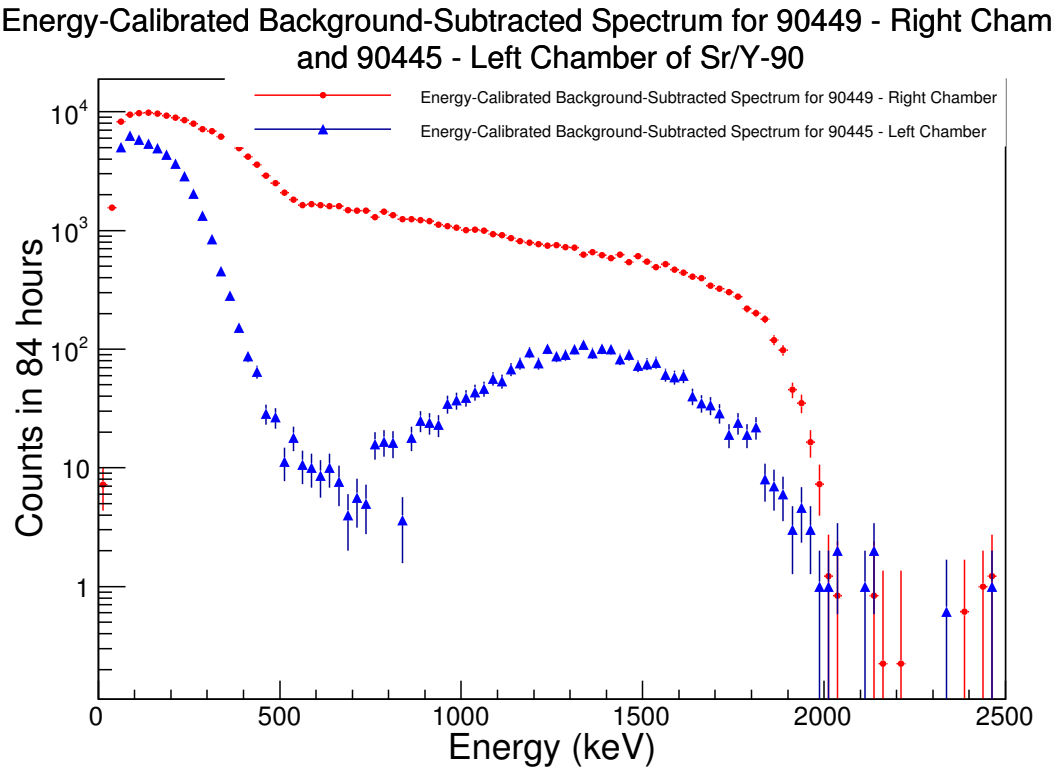

Figure 7.2: Background-subtracted spectra of the long 3.5-day SrY data sets. The backgrounds obtained from the long, 9-day background trials were normalized to the live time of the ^{90}Sr/^{90}Y data sets and normalized to 20 mL of UGAB cocktail, then subtracted from the SrY sample of the respective chamber.

Table 7.4: Counts from the regions of interest for sample measurements in the left chamber with the full build.

Sample	Counting Time (s)	Counts in Energy Range		
		25-2300 keV	25-280 keV	280-2300 keV
Initial Short Trials				
90445*	82800	15510 ± 125	10922 ± 105	4588 ± 68
90446	82800	13841 ± 118	10411 ± 102	3430 ± 59
90447	82800	13860 ± 118	10350 ± 102	3510 ± 59
90448	82800	15840 ± 126	11255 ± 106	4585 ± 68
90449	82800	9778 ± 99	7773 ± 88	2005 ± 45
Long Trials				
90445*	302400	46480 ± 216	44023 ± 210	2457 ± 50

*Note that the count rate does not scale up linearly with time between the short and long trials of sample 90445. The same effects of temperature stabilization and light-induced chemiluminescence as noted in Chapter 6 are present.

Table 7.5: Counts from the regions of interest for sample measurements in the right chamber with the full build.

Sample	Counting Time (s)	Counts in Energy Range		
		25-2300 keV	25-280 keV	280-2300 keV
Initial Short Trials				
90445	82800	55031 ± 235	42005 ± 205	13026 ± 114
90446	82800	52632 ± 229	40139 ± 200	12493 ± 112
90447	82800	49782 ± 223	37887 ± 195	11895 ± 109
90448	82800	49055 ± 221	37259 ± 193	11796 ± 109
90449	82800	48459 ± 220	36747 ± 192	11712 ± 108
Long Trials				
90449	302400	177634 ± 421	131663 ± 363	45971 ± 214

calculated sample activity was included in the count rate calculation. The observed count rates are compared to the expected count rates from the calculated sample activities later in this section. The count rates observed for the samples are shown in Table 7.6 for the left chamber and Table 7.7 for the right chamber.

Background contributions to each of these regions were calculated in the previ-

Table 7.6: Count rates (d^{-1}) from the regions of interest for sample measurements in the left chamber with the full build.

Sample	Count Rate (d^{-1}) in Energy Range		
	25-2300 keV	25-280 keV	280-2300 keV
Initial Short Trials			
90445	16180 ± 130	11400 ± 110	4790 ± 70
90446	14440 ± 120	10860 ± 110	3580 ± 60
90447	14460 ± 120	10800 ± 110	3660 ± 60
90448	16530 ± 130	11740 ± 110	4780 ± 70
90449	10200 ± 100	8110 ± 90	2090 ± 50
Long Trials			
90445	13280 ± 62	12578 ± 60	702 ± 14

Table 7.7: Count rates (d^{-1}) from the regions of interest for sample measurements in the right chamber with the full build.

Sample	Count Rate (d^{-1}) in Energy Range		
	25-2300 keV	25-280 keV	280-2300 keV
Initial Short Trials			
90445	57420 ± 250	43830 ± 210	13590 ± 120
90446	54920 ± 240	41880 ± 210	13040 ± 120
90447	51950 ± 230	39530 ± 200	12410 ± 110
90448	51190 ± 230	38880 ± 200	12310 ± 110
90449	50570 ± 230	38350 ± 200	12220 ± 110
Long Trials			
90449	50753 ± 120	37618 ± 104	13135 ± 61

ous chapter, shown in Tables 6.14 and 6.15. The average background was subtracted from the short sample trials, and the normalized long background was subtracted from the long sample trials. The background from each region of interest was subtracted from the sample count rate in the same region of interest. Errors with the background and sample measurements were propagated throughout the calculations. The background-subtracted count rates are shown in Tables 7.8 and 7.9 for the left

and right chambers, respectively.

Table 7.8: Background-subtracted count rates in counts per day (d^{-1}) from the regions of interest for sample measurements in the left chamber with the full build.

Sample	Count Rate (d^{-1}) in Energy Range		
	25-2300 keV	25-280 keV	280-2300 keV
Initial Short Trials			
90445	16050 ± 130	11300 ± 110	4750 ± 70
90446	14310 ± 120	10760 ± 110	3550 ± 60
90447	14330 ± 120	10700 ± 110	3630 ± 60
90448	16390 ± 130	11640 ± 110	4750 ± 70
90449	10070 ± 100	8010 ± 90	2060 ± 50
Long Trials			
90445	13219 ± 61	12520 ± 60	699 ± 14

Table 7.9: Background-subtracted count rates in counts per day (d^{-1}) from the regions of interest for sample measurements in the right chamber with the full build.

Sample	Count Rate (d^{-1}) in Energy Range		
	25-2300 keV	25-280 keV	280-2300 keV
Initial Short Trials			
90445	57060 ± 240	43590 ± 210	13470 ± 120
90446	54560 ± 240	41650 ± 210	12910 ± 120
90447	51590 ± 230	39300 ± 200	12290 ± 110
90448	50830 ± 230	38640 ± 200	12190 ± 110
90449	50210 ± 230	38110 ± 200	12100 ± 110
Long Trials			
90445	50423 ± 120	37401 ± 10	13023 ± 61

The observed split between the percentages of counts in ^{90}Sr and ^{90}Y sections to the full sample range is ∼74% to ∼26% compared to the ideal ∼64% to 36% and

$\sim$62% to $\sim$38% expected for a threshold of 25 keV. With the loss of photons in the light guide, a shift toward the lower energy portion of the spectrum is expected. Observations show this shift to be 10% over what was expected. From the energy deposition GEANT4 simulations in an LSC vial, 99.1% of the ^{90}Y activity should be present in the full sample range (25-2300 keV) and 93.0% of the ^{90}Sr activity should be present in the same range. Using these assumptions for the percentage of activity present in the spectrum, the count rates for ^{90}Sr and ^{90}Y for the left and right chambers are 0.08 ± 0.01 s^{-1} and 0.09 ± 0.01 s^{-1} for ^{90}Sr and ^{90}Y (0.17 ± 0.01 s^{-1} total) in the left chamber, and 0.30 ± 0.01 s^{-1} and 0.32 ± 0.01 s^{-1} for ^{90}Sr and ^{90}Y (0.62 ± 0.01 s^{-1} total) in the right chamber. The total activity in the samples was 1.00 Bq, with ^{90}Sr and ^{90}Y in secular equilibrium at 0.50 Bq each. With the observed shift in the spectra to lower energies, a higher percentage of each of the observed spectra and count rates for ^{90}Sr and ^{90}Y falls below the 25 keV threshold. Lower observed count rates would result from a higher portion of the spectrum falling below the threshold.

7.2.3 Efficiency Calculations

The count rates observed from the total of the ^{90}Sr/^{90}Y samples in the left and right chambers are those in the 25-2300 keV region of interest of Tables 7.8 and 7.9, respectively. The activity based on the mass of sample dilution added to each of the samples is shown in Table 7.2. The counting efficiency of the ULB LSC was calculated for each of the samples based on the short sample trials, as well as the long sample trials, using the observed count rates against the activity for each sample. The counting efficiency for each of the sample trials is shown in Table 7.10 for the left chamber and Table 7.11 for the right chamber. The average counting efficiency from the series of short trials was 16.5 ± 0.2% for the left chamber and 61.1 ± 0.8% for the

right chamber, while the counting efficiencies from the longer trials were 15.3 ± 0.5% and 58.2 ± 1.7% for the left and right chambers respectively. The efficiencies of the longer trials are statistically lower than the shorter trial, which could be attributed to the longer counting time of the samples after the chemiluminescence effect and sample temperature had stabilized.

Table 7.10: Efficiencies of the regions of interest for sample measurements in the left chamber in the full build.

Sample	Observed Count Rate (s^{-1})	Activity (Bq)	Efficiency (%)
Initial Short Trials			
90445	0.186 ± 0.001	0.998 ± 0.030	18.6 ± 0.6
90446	0.166 ± 0.001	1.002 ± 0.030	16.5 ± 0.5
90447	0.166 ± 0.001	1.000 ± 0.030	16.6 ± 0.5
90448	0.190 ± 0.002	1.000 ± 0.030	19.0 ± 0.6
90449	0.117 ± 0.001	1.003 ± 0.030	11.6 ± 0.4
Long Trials			
90445	0.153 ± 0.001	0.998 ± 0.030	15.3 ± 0.5

Table 7.11: Efficiencies of the regions of interest for sample measurements in the right chamber in the full build.

Sample	Observed Count Rate (s^{-1})	Activity (Bq)	Efficiency (%)
Initial Short Trials			
90445	0.660 ± 0.003	0.998 ± 0.030	66.2 ± 2.0
90446	0.631 ± 0.003	1.002 ± 0.030	63.0 ± 1.9
90447	0.597 ± 0.003	1.000 ± 0.030	59.7 ± 1.8
90448	0.588 ± 0.003	1.000 ± 0.030	58.8 ± 1.8
90449	0.581 ± 0.003	1.003 ± 0.030	57.9 ± 1.8
Long Trials			
90449	0.584 ± 0.001	1.003 ± 0.030	58.2 ± 1.7

7.3 Comparison Between Chambers

Differences between the left and right chamber responses span from electronics to spectral characteristics to counting efficiency. The right chamber (direct PMT output to PXI) has a higher efficiency at around 60% compared to the left chamber (preamplifier output to PXI) at around 15%. The lower counting efficiency of the left chamber for the same samples could be due to a combination of several factors. Pulse-pile up with the preamplifier output could cause a higher number of events to be rejected. In addition, analysis of the energy comparisons between paired events of the left chamber showed groupings of events with low energy on one PMT and high energy on the other. These events were cut during event selection based on the energy equivalence parameter. Some of these events are probable noise contributions, but some may be real events with inaccurate energy calculation, pile-up, or trigger conditions.

In the spectra from the left chamber, a more distinctive separation between the higher energy beta response and lower energy beta response is apparent. The difference in spectral characteristics is due to the pulse shaping introduced by the preamplifier and energy values assigned by the Pixie 500 Express modules. The methods of assessing energy and assigning energy values differ between the two chambers because of the difference in the input signals. The direct PMT input requires the integrator mode to be enabled for analysis of these pulses. This mode looks to integrate charge within the pulse above baseline. Implementation for fast pulses can cause some baseline to be included in the integration, effectively decreasing the energy value. This effect of implementation is consistent across the pulses from the same input, though, so calibration can take this into account. The energy values achieved with this method cannot be compared to those with assigned to the same

event processed through a preamplifier. The pulses from the preamplifier output do not have integrator mode enabled and are processed using trapezoidal filtering as described in the Pixie 500 Express Users Manual (LLC, 2016). The energy values for these pulses are based on the height of the rising edge above baseline, with corrections for signal decay time constant. Since the energy values are calculated with different methods, it is not surprising that the resulting energy spectra have different characteristics as well.

In the data collected for this research, the tau value for the right chamber was reduced between the initial and revised settings (short and long runs). In integrator mode, the tau value is essential a scaling factor for the incoming data that adjusts the dynamic range of the ADC and MCA spectrum. In further studies with this system, decreasing the voltages on the PMTs in the right chamber would assure that the full spectrum is being collected and that no events were out of range of the spectrum. If there are out-of-range events, decreasing the voltages to include their contributions would increase the count rates and better reflect the true activity of the sample. If further studies consistently reveal efficiencies <95%, despite adjustments to signal processing and analysis for both chambers, the loss of photons in the light guide may simply cause a loss of too many photons on the low energy edge of the spectrum and essentially eliminate their contribution to count rate and spectral assessments.

7.4 Comparison with Quantulus^{TM} Results

Three of the $^{90}Sr/^{90}Y$ samples were counted on the Quantulus^{TM} in PNNL's Radiochemical Analysis Laboratories, as was one blank. The count rates from the full spectrum (1024 channels) are shown in Table 7.12. The count rates shown for the $^{90}Sr/^{90}Y$ samples are already background-subtracted count rates. Each of the samples and blank were counted once for three hours.

Table 7.12: Count rate and efficiency data from measurements of a subset of samples on the Quantulus^{TM}.

Sample	Count Rate (s^{-1})	Activity (Bq)	Efficiency (%)
BLANK	0.07 ± 0.01	–	–
90448	1.06 ± 0.01	1.000 ± 0.001	106.0 ± 1.0
90447	1.07 ± 0.01	1.000 ± 0.001	107.0 ± 1.0
90446	1.04 ± 0.01	1.002 ± 0.001	103.8 ± 1.0

Based on the observed count rates and the calculated efficiencies for the ULB LSC and the Quantulus^{TM}, the Quantulus has the superior counting efficiency at ∼100%. The efficiency of the right chamber is higher than the left chamber in the ULB LSC, but both are well below that of the Quantulus. The efficiencies of the left and right chambers of the ULB LSC are presented alongside those of the Quantulus in Table 7.13.

Table 7.13: Count rates (s^{-1}) for the sample set from measurements in the left chamber, right chamber, and Quantulus^{TM}compared to the calculated activities.

		Count Rate (s^{-1})		
Sample	Activity (Bq)	Quantulus	Left Chamber	Right Chamber
90449	1.003 ± 0.001		0.117 ± 0.001	0.581 ± 0.117
90448	1.000 ± 0.001	1.06 ± 0.01	0.191 ± 0.002	0.589 ± 0.191
90447	1.000 ± 0.001	1.07 ± 0.01	0.167 ± 0.001	0.597 ± 0.167
90446	1.002± 0.001	1.04 ± 0.01	0.166 ± 0.001	0.632 ± 0.166
90445	0.998 ± 0.001		0.187 ± 0.002	0.661 ± 0.187
Blank	0.001 ± 0.000	0.001± 0.000	0.004 ± 0.001	0.07 ± 0.01

Adjustments to the analog and digital components of the signal processing may be able to increase the efficiency of the ULB LSC to where at least one of the two methods of data collection is competitive with the counting efficiency of the

Quantulus^{TM}. The goal of reducing the background count rate to less than 100 counts per day was accomplished; with an increased efficiency, the detection limits for the ULB LSC would be an order of magnitude than achievable with current commercial systems.

8. CONCLUSIONS

A new, state-of-the art measurement system has been built to improve detection sensitivities for liquid scintillation techniques. The background reduction methods implemented successfully reduced the background environment in both chambers below the targeted background level of 100 counts per day. These backgrounds were two orders of magnitude below the ∼1 count per minute background in commercially-available systems. Initial testing and characterization of the system show a wide energy range with opportunity for expansion of the lower energy portion of the spectrum, detection of ^{90}Sr and ^{90}Y, and a low environmental background below the targeted 100 counts per day level.

8.1 Performance of ULB LSC

8.1.1 Background Evaluation

The empty chamber backgrounds achieved with the ULB SLC are on the order of 11.0 ± 0.6 counts per day and 2.1 ± 0.1 counts per day for left and right chamber backgrounds, respectively. Background count rates including the vial, packaging, and Ultima Gold AB cocktail were 135 ± 13 counts per day and 360 ± 21 counts per day for the left and right chambers. These higher rates include interactions within the cocktail, contributions from the vial, as well as cosmic interactions not rejected by the veto assembly. The LSC cocktail used in this research may not be as clean as desired for an ultra-low background system. The levels of radioactivity in the cocktail are low enough to not be readily apparent on the Quantulus$^{\text{TM}}$, but may be high enough to be a limiting factor for the ULB LSC. Further tests with a demonstrated high-purity liquid scintillator, such as from one of the scintillator-based neutrino experiments, would illuminate the impact of the cocktail impurities on the

background count rates. The target range for the ULB LSC was 10 - 100 counts per day. Simulation of radioactive emissions backgrounds and systematic backgrounds observed with initial experimentation in the partial build gave estimates of ∼10 counts per day and ∼15 counts per day, respectively. The total expected background count rate for the same electronics setup and online processing as used in the partial build was been 25 counts per day. Between the partial build and full build data acquisition, changes to the electronics included exchanging Hamamatsu PMT bases for custom built PMT bases, differences in tube operation and signal processing, and build geometry. To account for the difference in tube operation, the settings in PixieViewer were adjusted accordingly for appropriate processing and evaluation. With these changes implemented, the observed backgrounds were expected to vary from the initially estimated 25 counts per day. The empty chamber backgrounds are well within the target range of <100 counts per day as the result of successful implementation of shielding methods and low background detection principles.

8.1.2 Demonstration Measurements

Sample measurements were made with both the partial build and full build configurations. The demonstration sample set for the full build consisted of five replicates of 1 Bq ^{90}Sr/^{90}Y samples. Each of the samples was measured for 23 hours to assess variance between samples, and one sample was measured for 84 hours to obtain sample count rates with low relative uncertainty and calculating detection efficiency. These sets of initial and long trials were performed in both the right and left chambers. Both chambers exhibited detection of the beta decay events and resulting spectra with the characteristic beta shapes of both ^{90}Sr and ^{90}Y.

8.1.2.1 Energy Range

For the configuration in which the demonstration samples were measured, the energy range spanned from ∼25 to ∼2500 keV. Calibrations were performed with a set of external standards using the Compton energies as calibration points. These tests showed a linear energy calibration from 50 - 1100 keV. Calibration for the low-energy portion of the spectrum would require a lower energy calibration point, such as the ^{64}Cu x-ray at 8 keV, and should be performed before a full measurement suite of low-energy beta samples is attempted.

For samples with energies on the higher end of the spectrum (1 MeV or greater), parameters can be set can be set to expand the energy spectrum beyond 2.5 MeV. Reducing the high voltage and/or digital gain should expand the spectrum enough for measuring high-energy (>3 MeV) decays. If necessary, the jumpers in the charge-integrating preamplifiers could be changed from the high gain (A-B) to low gain (A-C) setting to further expand the energy range. Both of these methods would effectively raise the low energy threshold in the process of extending the energy range. Conversely, parameters can also be adjusted to magnify on the lower energy portion of the spectrum by such means as increasing the digital gain, adjusting high voltage if necessary, or increasing the tau value for the right chamber.

8.1.2.2 Efficiency Calculations

While the ULB LSC did detect the beta emissions in the LSC cocktail, the detection efficiency was low for both chambers. The average detection efficiency for the left chamber was 16.5 ± 0.2% and that of the right chamber was 61.1 ± 0.8%. The detection efficiencies were lower for the longer data acquisitions, at 15.3 ± 0.5%for the left chamber and 58.2 ± 1.7% for the right chamber. Lower efficiencies for longer measurements could result from settling of the radioactive portion of the sample

against the bottom or side of the vial, separation of the radioactive sample fraction from the cocktail, and/or reduction of the chemiluminescence of the sample after enclosure in the dark environment for a period of days.

8.1.3 Comparison with Quantulus^{TM} Results

Three of demonstration samples were measured with both the ULB LSC and Quantulus$^{\text{TM}}$. The measurements on the Quantulus$^{\text{TM}}$ had detection efficiencies just over 100%. The small amount (<0.06 s^{-1}) over the 100% could be due to background events over the measured blank background or impurities in the sample solution or cocktail. With reference to the efficiency of the systems, the ULB LSC needs much improvement to close the gap from ∼18% and ∼61% to the 100% demonstrated with the Quantulus$^{\text{TM}}$. In terms of background environment, the ULB LSC has the advantage over the Quantulus$^{\text{TM}}$. The background with the blank for the Quantulus$^{\text{TM}}$was ∼0.07 s^{-1} compared to the ∼0.001 s^{-1} for the left chamber and ∼0.004 s^{-1} for the right chamber of the ULB LSC. The high background count rate in the Quantulus$^{\text{TM}}$is consistent with literature reports and is due to a less comprehensive cosmic veto, high cosmic ray interaction rate above ground, and less passive shielding compared to the ULB LSC.

8.2 Future Improvements

Improvements to the systematic background rates and the low energy threshold should come with implementation of changes to the electronics (such as removing the remaining cosmic background and eliminating noise contributions on the low energy range). The pulse shaping and processing needs to be optimized and tested on a mixed alpha/beta sample.

Improving on light collection efficiency would be the most significant improvement to a ULB LSC 2.0 installment. Different coating material, a finer polish in the

channels, different mating mechanism for the cut sections may offer options to achieve higher light collection efficiency. Finding a way to have clean samples that involved different packaging or containment would be another way to reduce photon loss.

Several physical additions to the ULB LSC were left to finish the design basis. The dark box sliders on the pulley system will allow for simultaneous operation of the two instrumented chambers without having to power down between samples. The fiber optic calibration system was not tested in the underground installation before these measurements. Calibration parameters for low and high intensity flux on the PMTs in the underground system would need to be identified from testing with the instrumented chambers. This system would also be used for gain stabilization and adjustments during or between measurements.

In terms of sample measurements, improvements could first be made in preparing new sets of standards after the lessons learned in the first rounds of testing. Samples would be in the 20 mL in a vacuum-sealed bag configuration. Ideally, two more sets of multiple standards would be prepared for ^{3}H and ^{90}Sr/^{241}Am. Testing with replicates of decade activities with count rates on the order of 10, 100, and 1000 counts per day would assess the efficiencies and spectral abilities at low to high count rates with associated signal over background.

8.3 Further Studies

A new PSA code was discussed for use with the preamplifier data output. This code is an adaptation of an analysis system already in place with other low-background systems in the SUL. This method uses template matching to define the shape of a good event. The event data is separated into the observed, cosmic, and background-subtracted sample spectra, and the activity of the sample is calculated based on the background-subtracted spectrum.

For adaptation for the ULB LSC, two sets of templates would need to be considered for alpha and beta events. The shapes are differentiated based on fast and slow components of the rising edge of the preamplifier signal. This method would need to be tested with known, prepared mixed alpha/beta standards to evaluate the effectiveness of this method and make any necessary adjustments.

Further testing will better characterize the absolute low energy threshold, detection efficiency for low-energy beta emitters, and response to mixed alpha/beta sources. Benchmark testing with other known standards would establish a low-energy threshold, further investigate response by decay energy, and verify the counting efficiencies of the ULB LSC should be performed. Testing with alpha emitting sources would elucidate the energy calculations and spectral response to alpha particles, as well as test the alpha/beta discrimination capabilities in post-processing. The fiber optic system could be used to experimentally determine the light collection efficiency of the light guides and PMTs, based on the known number of photons exiting the fiber compared to the number of photoelectrons generated by the PMTs. This test will provide more information on the spectral capabilities achievable with ULB LSC. Testing the observed count rates against known activities of the standards will give the counting efficiencies across‘ different decay energies.

REFERENCES

(2010). *Scintillation Detector Preamplifier Model 2005: Operator's Manual*. Canberra Industries, Inc., Canberra Industries, Inc., One State Street, Meriden, CT 06450.

Aalseth, C., Day, A., and *et al.*, E. H. (2009). Design and construction of a low-background, internal-source proportional counter. *J. Radioanal. Nucl. Ch.*, 282:233–237.

Aalseth, C. *et al.*. (2012). A shallow underground laboratory for low-background radiation measurements and materials development. *Rev. Sci. Instrum.*, 83:113503.

Agostinelli, S., Allison, J., and *et al.*, K. A. (2003). Geant4—a simulation toolkit. *Nucl. Instrum. Meth. A.*, 506(3):250 – 303.

Akerib, D., Bai, X., and *et al.*, E. B. (2013). An ultra-low background {PMT} for liquid xenon detectors. *Nucl. Instrum. Meth. A.*, 703:1 – 6.

Allison, J., Amako, K., and *et al.*, J. A. (2006). Geant4 developments and applications. *IEEE T. Nucl. Sci.*, 53(1):270–278.

Bagan, H., Tarancon, A., and *et al.*, G. R. (2008). Classical vs. evolved quenching parameters and procedures in scintillation measurements: The importance of ionization quenching. *Nucl. Instrum. Meth. A.*, 592:361–368.

Barnett, J. M. and McKlveen, J. (1992). The measurement of ^{222}rn in drinking water by low-level liquid scintillation counting. *J. Radioanal. Nucl. Chem.*, 16L(2):357–364.

Bernacki, B. E., Douglas, M., and *et al.*t, J. L. E. (2015). Optical design considerations for efficient light collection from liquid scintillation counters. *Appl. Opt.*, 54(9):2413–2423.

Brun, R. and *et al.*, F. R. (2014). *User's Guide*. CERN, 6 edition. URL https://root.cern.ch/root/htmldoc/guides/users-guide/ROOTUsersGuide.html.

Brun, R. and Rademakers, F. (1997). Root - an object oriented data analysis framework. volume 389 of *Proceedings AIHENP'96 Workshop*, pages 81–86, Lausanne. CERN.

Carles, G., Gunther, E., and *et al.*, G. G. (2004). Ionization quenching inlsc. *Appl. Radiat. Isotopes*, 60:447–451.

Courti, A., Bouisset, P., and Chevallier, P. (2001). Beta spectrometry for environmental radioactivity measurements.

Currie, L. A. (1968). Limits for qualitative detection and quantitative determination. application to radiochemistry. *Anal. Chem.*, 40(3):586–593.

Douglas, M. *et al.*. (2016). Liquid scintillation counting of environmental radionuclides: a review of the impact of background reduction. *J. Radioanal. Nucl. Chem.*, 307:2495–2504.

Eikenberg, J., Jggi, M., Beer, H., and Baehrle, H., editors (2009). *Application of liquid scintillation counting technique to the determination of* ^{90}*Sr in milk samples*, Advances in Liquid Scintillation Spectrometry 2008.

E.P. Hardy, J. (1977). Final tabulation of monthly 90sr fallout data: 1954-1976. Technical Report HASL-329, Health and Safety Laboratory Report, U.S. Energy Research and Development Administration, New York.

Erchinger, J., Aalseth, C., and *et al.*, B. B. (2015). Development of a low background liquid scintillation counter for a shallow underground laboratory. *Appl. Radiat. Isotopes*, 105:209 – 218.

Erchinger, J., Orrell, J., Aalseth, C., Bernacki, B., Douglas, M., Fuller, E., Keillor, M., Marianno, C., Morley, S., Mullen, C., Panisko, M., and Warren, G. (2017). Background characterization of an ultra-low background liquid scintil-

lation counter. *Applied Radiation and Isotopes*, pages –.

Finch, Z., Seiner, B., and *et al.*, L. A. (2016). Toward sufficient reduction of radio-impurities for ^{32}si sediment age dating. *J. Radioanal. Nucl. Chem.*, 307(3):24512458.

Geibert, W., van der Loeff, M. R., and *et al.*, C. H. (2002). Actinium-227 as a deep-sea tracer: sources, distribution and applications. *Earth Planet. Sc. Lett.*, 198(1–2):147 – 165.

Geibert, W. and Voge, I. (2008). Progress in the determination of 227ac in sea water. *Mar. Chem.*, 109(3–4):238 – 249. Measurement of Radium and Actinium Isotopes in the marine environment.

Heilgeist, M. (2000). Use of extraction chromatography, ion chromatography and liquid scintillation spectrometry for rapid determination of strontium-89 and strontium-90 in food in cases of increased release of radionuclides. *J. Radioanal. Nucl. Ch.*, 245(2):249–254.

Janovics, R., Bihari, Á., and *et al.*, L. P. (2014). Monitoring of tritium, 60co and 137cs in the vicinity of the warm water outlet of the paks nuclear power plant, hungary. *J. Environ. Radioactiv.*, 128:20 – 26.

Kaihola, L. (1994). Ultra-sensitive alpha particle detection in the presence of high beta activity by low-level liquid scintillation spectrometry. *Radiocarbon*.

Keillor, M., Aalseth, C., and *et al.*, A. D. (2011). Cascades: an ultra-low background germanium crystal array at pacific northwest national laboratory. *AIP Conf. Proc.*, 1412:208–215.

Keillor, M. E., Aalseth, C. E., and Day, A. R. *et al.*. (2009). Design and construction of an ultra-low-background 14-crystal germanium array for high efficiency and coincidence measurements. *J. Radioanal. Nucl. Ch.*, 282(3):703–708.

Kern, Z., Molnr, M., and *et al.*, E. S. (2009). High resolution, well-preserved tritium

record in the ice of bortig ice cave, bihor mountains, romania. *Holocene*, 19(5):729–736.

Kim, C., Al-Hamwi, A., and *et al.*, A. T. (2009). Validation of rapid methods for the determination of radiostrontium in milk. *Appl. Radiat. Isotopes*, 67:786–793.

K.K., H. P. (2011). R11410-10 tentative data sheet. Online. URL http://www-eng.lbl.gov/s̃human/NEXT/MATERIALS&COMPONENTS/PMT/PMT_R11410-10%20data%20sheet%20110404%28F%29-3.pdf.

Koarashi, J., Mikami, S., and Nakada, A. (2008). Monitoring methodologies and chronology of radioactive airborne releases from tokai reprocessing plant. *J. Nucl. Sci. Technol.*, 5:462–465.

Kozono, S., Takashi, R., and Haraguchi, H. (2000). Determination of ultratrace impurities in high purity tantalum materials by on-line anion exchange matrix separation and inductively coupled plasma mass spectrometry. *Anal. Sci.*, 16(1):69–74.

L'Annunziata, M. F. and Kessler, M. J. (2012). Chapter 7 - liquid scintillation analysis: Principles and practice. In L'Annunziata, M. F., editor, *Handbook of Radioactivity Analysis (Third Edition)*, pages 423 – 573. Academic Press, Amsterdam, third edition edition.

Leonard, D., Grinberg, P., and *et al.*, P. W. (2008). Systematic study of trace radioactive impurities in candidate construction materials for exo-200. *Nucl. Instrum. Meth. A.*, 591(3):490 – 509.

LLC, X. (2016). *Pixie-4 Express User Manual*. XIA LLC, Hayward, CA, 4.21 edition.

Lopez, M., Sanchez, A., and Esocbar, V. (2004). Application of ultra-low level liquid scintillation to the determination of ^{222}rn in groundwater. *J. Radioanal. Nucl. Chem.*, 261(3):631–636.

Matsuura, K., Sasa, Y., and *et al.*, C. N. (1995). Levels of tritium concentration in the environmental samples around jaeri tokai. *J. Radioanal. Nucl. Chem.*, 197(2):295–

307.

Maxwell, S. and Culligan, B. (2009). Rapid method for determination of radiostrontium in emergency milk samples. *J. Radioanal. Nucl. Ch.*, 279(3):757760.

McLean, D. and Watterson, J. (2014). Coating impurities. Private Communication.

Morgenstern, U. and Taylor, C. (2009). Ultra low-level tritium measurement using electrolytic enrichment and lsc. *Isot. Environ. Healt. S.*, 45(2):96–117.

Nikolov, J., Todorovic, N., and *et al.*, M. J. (2013). Different methods for tritium determination in surface water by lsc. *Appl. Radiat. Isotopes*, 71:51–56.

Noakes JE, Schnhofer F, P. H., editor (1992). *A rapid method for the determining ^{89}Sr and ^{90}Sr from nuclear accidents*, Liquid Scintillation Spectrometry 1992 Conference.

Oikawa, S., Takata, H., and *et al.*, T. W. (2013). Distribution of the fukushima-derived radionuclides in seawater in the pacific off the coast of miyagi, fukushima, and ibaraki prefectures, japan. *Biogeosciences*, 10(50315047).

Percival, D. and Martin, D. (1974). Sequential determination of radium-226, radium-228, actinium-227, and thorium isotopes in environmental and process waste samples. *Anal. Chem.*, 46(12):1742–1749.

PerkinElmer, I. (2007). Perkinelmer scintillation cocktails & consumables. Application note, PerkinElmer, Inc.

Plastino, W., Chereji, I., and *et al.*, S. C. (2007). Tritium in water electrolytic enrichment and liquid scintillation counting. *Radiat. Meas.*, 42:68–73.

Plastino, W. and Kaihola, L. (2004). Surface and underground ultra low-level liquid scintillation spectrometry. *Radiocarbon*, 46(1).

Rapkin, E. (1971). A history of the development of the modern liquid scintillation counter. *Liquid scintillation counting*, 2:61–100.

Runkle, R., Aalseth, C., and *et al.*, V. B. (2012). Opportunities for decay count-

ing of environmental radioisotopes using ultralow- background detection systems. Technical Report PNNL-21709, Pacific Northwest National Laboratory, Richland, WA.

Salonen, L. (1993). A rapid method for monitoring of uranium and radium in drinking water. *The Science of the Total Environment*, 130/131:23–35.

Salonen, L. and Hukkanen, H. (1997). Advantages of low-background liquid scintillation alpha-spectrometry and pulse shape analysis in measuring turn, uranium and 22'ra in groundwater samples. *J. Radioanal. Nucl. Chem*, 226(1-2):67–74.

Salonen, L., Kaihola, L., and *et al.*, B. C. (2012). Chapter 9 - environmental liquid scintillation analysis. In L'Annunziata, M. F., editor, *Handbook of Radioactivity Analysis (Third Edition)*, pages 625 – 693. Academic Press, Amsterdam, third edition edition.

Sanchez-Cabeza, J. and Pujol, L. (1998). Simultaneous determination of radium and uranium activities in natural water samples using liquid scintillation counting. *Analyst.*, 123:399–403.

Sciences, P. L. (2002). *Wallac 1220 Quantulus^{TM}Instrument Manual*. PerkinElmer Life Sciences, Turku, Finland. pages 27-28.

Seifert, A., Aalseth, C. E., and Day, A. R. *et al.*. (2013). The design, construction, and initial characterization of an ultra-low-background gas-proportional counting system. *J. Radioanal. Nucl. Ch.*, 296(2):915–921.

Suzuki, A., Sakurai, H., and *et al.*, K. E. (1999). Pulse height distributions of beta rays in 14c measurement.with liquid scintillation counting system quantulus. *IEEE T. Nucl. Sci.*, 46(3):302–305.

Takagai, Y., Furukawa, M., and *et al.*, Y. K. (2014). Sequential inductively coupled plasma quadrupole mass-spectrometric quantification of radioactive strontium-90 incorporating cascade separation steps for radioactive contamination rapid survey.

Anal Methods-UK, 6:355–362.

Torres, J., Llaurad, M., and *et al.*, G. R. (2000). Determination of 90sr in aquatic organisms by extraction chromatography: method validation. *Anal. Chim. Acta.*, 414:101111.

Vaupotic, J., Ogrinc, N., and *et al.*, M. B. (2011). Tritium mapping in spring waters in slovenia. *Geochem. J.*, 45(6):505–512.

Vojtyla, P. (1996). Fast computer simulations of background of low-level ge - spectrometers induced by 210pb210bi in shielding lead. *Nucl. Instrum. Meth. A.*, 117(1–2):189 – 198.

APPENDIX A

GEANT4 GEOMETRY FILES

A.1 Initial Iterative Geometry File

```
GEOMETRY_VERSION:
4A
WORLD_SIZE(x,y,z)(cm):
100     100     100 cm
WORLD_MATERIAL:
Air
OUTER_SHIELD_SIZE(x,y,z)(cm):
99.06   73.66   55.88 cm
OUTER_SHIELD_MATERIAL:
Pb
MIDDLE_SHIELD_SIZE(x,y,z)(cm):
68.58 43.18 25.40
MIDDLE_SHIELD_MATERIAL:
Pb
INNER_SHIELD_SIZE(x,y,z)(cm):
15.24   33.02   15.24 cm
INNER_SHIELD_MATERIAL:
Cu
EXTRA_SHIELD_SIZE(x,y,z)(cm):
7.62    2.54    2.54 cm
EXTRA_SHIELD_POSITION(x,y,z)(cm):
0       3.81    0 cm
EXTRA_SHIELD_MATERIAL:
Pb
INNER_CAVITY_SIZE(x,y,z)(cm):
5.08    27.94   5.08 cm
INNER_CAVITY_MATERIAL:
Air
PMT_CAVITY_SIZE(x,y,z)(cm):
7.62    7.62    25.40 cm
PMT_CAVITY_MATERIAL:
Air
VIAL_OD(cm):
2.7
VIAL_THICKNESS(cm):
6.08
VIAL_INNER_THICKNESS(cm):
5.78
VIAL_MATERIAL:
PET
LIQUID_OD(cm):
2.5
LIQUID_THICKNESS(cm):
4.07
LIQUID_MATERIAL:
LSC2
PMT_GLASS_OD(cm):
6.4
PMT_GLASS_LENGTH(cm):
```

```
0.2
PMT_GLASS_MATERIAL:
Glass
PMT_TUBE_OD(cm):
6.6
PMT_TUBE_LENGTH(cm):
18.6
PMT_TUBE_MATERIAL:
LightAl
PMT_BASE_OD(cm):
6.6
PMT_BASE_LENGTH(cm):
3
PMT_BASE_MATERIAL:
LightAl
NUMBER_OF_PMTS:
4
PMT_0_POSITION(x,y,z)(cm):_z_ignored
228.6   101.6   0
PMT_1_POSITION(x,y,z)(cm):_z_ignored
228.6   -101.6  0
PMT_2_POSITION(x,y,z)(cm):_z_ignored
-228.6  101.6   0
PMT_3_POSITION(x,y,z)(cm):_z_ignored
-228.6  -101.6  0
```

A.2 Medium Fidelity Geometry File

```
GEOMETRY_VERSION:
4A
WORLD_SIZE(x,y,z)(cm):
150    150    150 cm
WORLD_MATERIAL:
Air
OUTER_SHIELD_SIZE(x,y,z)(cm):
99.06  73.66  55.88 cm
OUTER_SHIELD_MATERIAL:
Pb
MIDDLE_SHIELD_SIZE(x,y,z)(cm):
68.58 43.18 25.40
MIDDLE_SHIELD_MATERIAL:
Pb
INNER_SHIELD_SIZE(x,y,z)(cm):
15.24  33.02  15.24 cm
INNER_SHIELD_MATERIAL:
Cu
EXTRA_SHIELD_SIZE(x,y,z)(cm):
7.62   2.54   2.54 cm
EXTRA_SHIELD_POSITION(x,y,z)(cm):
0      3.81   0 cm
EXTRA_SHIELD_MATERIAL:
Pb
INNER_CAVITY_SIZE(x,y,z)(cm):
5.08   27.94  5.08 cm
INNER_CAVITY_MATERIAL:
Air
PMT_CAVITY_SIZE(x,y,z)(cm):
7.62   7.62   25.40 cm
PMT_CAVITY_MATERIAL:
Air
VIAL_OD(cm):
2.7
VIAL_THICKNESS(cm):
5
VIAL_INNER_THICKNESS(cm):
```

```
4.8
VIAL_MATERIAL:
PET
LIQUID_OD(cm):
2.5
LIQUID_THICKNESS(cm):
4.07
LIQUID_MATERIAL:
LSC2
PMT_GLASS_OD(cm):
6.4
PMT_GLASS_LENGTH(cm):
0.2
PMT_GLASS_MATERIAL:
Glass
PMT_TUBE_OD(cm):
6.6
PMT_TUBE_LENGTH(cm):
18.6
PMT_TUBE_MATERIAL:
LightAl
PMT_BASE_OD(cm):
6.6
PMT_BASE_LENGTH(cm):
3
PMT_BASE_MATERIAL:
LightAl
PMT_ENDCAP_SIZE(x,y,z)(cm):
27.94 27.94 16.72
#10.16 10.16 7.83
PMT_ENDCAP_MATERIAL:
Pb
PMT_ENDCAPHOLE_SIZE(x,y,z)(cm):
7.62   7.62   6.56 cm
PMT_ENDCAPHOLE_MATERIAL_ignored:
Air
NUMBER_OF_PMTS:
```

```
4
PMT_0_POSITION(x,y,z)(cm):_z_ignored
228.6  101.6  0
PMT_1_POSITION(x,y,z)(cm):_z_ignored
228.6  -101.6 0
PMT_2_POSITION(x,y,z)(cm):_z_ignored
-228.6 101.6  0
PMT_3_POSITION(x,y,z)(cm):_z_ignored
-228.6 -101.6 0
```

A.3 High Fidelity Geometry File

```
GEOMETRY_VERSION:
4A
WORLD_SIZE(x,y,z)(cm):
150    150    150 cm
WORLD_MATERIAL:
Air
VETO_SIZE(x,y,z)(cm):
130.18         109.86         100 cm
VETO_MATERIAL:
PVT
VETO_HOLE_SIZE(x,y,z)(cm):
120.02         99.7    89.84 cm
VETO_HOLE_MATERIAL:
Air
BORATED_POLY_SIZE(x,y,z)(cm):
119.38         99.06  89.2 cm
BORATED_POLY_MATERIAL:
BoratedPE
POLY_HOLE_SIZE(x,y,z)(cm):
109.22         88.9    79.38 cm
POLY_HOLE_MATERIAL:
Air
OUTER_SHIELD_SIZE(x,y,z)(cm):
104.14         83.82  60.96 cm
OUTER_SHIELD_MATERIAL:
Pb
#MIDDLE_SHIELD_SIZE(x,y,z)(cm):
#68.58 43.18 25.40
#MIDDLE_SHIELD_MATERIAL:
#Pb
LB_SHIELD_SIZE(x,y,z)(cm):
34.29  63.5    40.32 cm
LB_SHIELD_MATERIAL:
Pb
ULB_SHIELD_SIZE(x,y,z)(cm):
24.13  53.34  30.16 cm
ULB_SHIELD_MATERIAL:
Pb
INNER_SHIELD_SIZE(x,y,z)(cm):
13.97  43.18  20 cm
INNER_SHIELD_MATERIAL:
Cu
EXTRA_SHIELD_SIZE(x,y,z)(cm):
7.62    2.54    2.54 cm
EXTRA_SHIELD_POSITION(x,y,z)(cm):
0       3.81    0 cm
EXTRA_SHIELD_MATERIAL:
Pb
INNER_CAVITY_SIZE(x,y,z)(cm):
4       24.13  5 cm
```

INNER_CAVITY_MATERIAL:
Air
INNER_VERTCAVITY_SIZE(x,y,z)(cm):
4 4 7.5 cm
INNER_VERTCAVITY_POSITION(x,y,z)(cm):
0 10.16 0 cm
INNER_VERTCAVITY_MATERIAL:
Air
PMT_CAVITY_SIZE(x,y,z)(cm):
7.62 7.62 20.48 cm
PMT_CAVITY_MATERIAL:
Air
PORT_HOLE_OD(cm):
5.4
PORT_HOLE_THICKNESS(cm):
10.32
PORT_HOLE_POSITION(x,y,z)(cm):
247.65 0 253.2
PORT_HOLE_MATERIAL:
Cu
PORT_FILL_OD(cm):
4.83
PORT_FILL_THICKNESS(cm):
10.32
PORT_FILL_POSITION(x,y,z)(cm):
0 0 0
PORT_HOLE_MATERIAL:
Pb
#Air
PORT_HOLE_LB_OD(cm):
5.4
PORT_HOLE_LB_THICKNESS(cm):
5.08
PORT_HOLE_LB_POSITION(x,y,z)(cm):
0 0 0
PORT_HOLE_LB_MATERIAL:
Pb
PORT_HOLE_ULB_OD(cm):
5.4
PORT_HOLE_ULB_THICKNESS(cm):
5.08
PORT_HOLE_ULB_POSITION(x,y,z)(cm):
0 0 0
PORT_HOLE_ULB_MATERIAL:
Pb
PORT_HOLE_I_OD(cm):
4.27
PORT_HOLE_I_LENGTH(cm):
7.5
PORT_HOLE_I_POSITION(x,y,z)(cm):
0 0 0

PORT_HOLE_I_MATERIAL:
Cu
VIAL_OD(cm):
2.7
VIAL_THICKNESS(cm):
5
VIAL_INNER_THICKNESS(cm):
4.8
VIAL_MATERIAL:
PET
LIQUID_OD(cm):
2.5
LIQUID_THICKNESS(cm):
4.07
LIQUID_MATERIAL:
LSC2
PMT_GLASS_OD(cm):
6.4
PMT_GLASS_LENGTH(cm):
0.2
PMT_GLASS_MATERIAL:
Glass
PMT_TUBE_OD(cm):
6.6
PMT_TUBE_LENGTH(cm):
18.6
PMT_TUBE_MATERIAL:
LightAl
PMT_BASE_OD(cm):
6.6
PMT_BASE_LENGTH(cm):
3
PMT_BASE_MATERIAL:
LightAl
PMT_ENDCAP_SIZE(x,y,z)(cm):
17.78 17.78 11.64 cm
#27.94 27.94 16.72
#10.16 10.16 7.83
PMT_ENDCAP_MATERIAL:
Pb
PMT_ENDCAPHOLE_SIZE(x,y,z)(cm):
7.62 7.62 6.56 cm
PMT_ENDCAPHOLE_MATERIAL_ignored:
Air
NUMBER_OF_PMTS:
4
PMT_0_POSITION(x,y,z)(cm):_z_ignored
247.65 101.6 0
PMT_1_POSITION(x,y,z)(cm):_z_ignored
247.65 -101.60
PMT_2_POSITION(x,y,z)(cm):_z_ignored
-247.65 101.6 0
PMT_3_POSITION(x,y,z)(cm):_z_ignored
-247.65 -101.60

APPENDIX B

OFFLINE PULSE ANALYSIS CODES

B.1 SortEvents Code: Identifies and Selects True Coincident Events

B.1.1 Event Selection Using Initial Calibration

```
//
//  SortEvents.cxx
//
//
//  Created by Erchinger, Jennifer L on 11/23/15.
//
//
//#include "SortEvents_CalcE.h"
#include <iostream>
#include "stdio.h"
#include "stdlib.h"
#include <string>
#include "TFile.h"
#include "TTree.h"
#include "TObject.h"

using namespace std;



void SortEvents_Preamp(){
    gROOT->Reset();

    int channel_val = 0;
    double energy_val = 0;
    int subIndex_val = 0;
    int pEE = 50;


    //Import ROOT file from melusine1
    string melFile;
    cout << "Melusine File: ";
    cin >> melFile;

    TFile *melFileIn = new TFile(melFile.c_str());
    TTree *eventData = (TTree*)melFileIn->Get("eventData");

    eventData->SetBranchAddress("channel",&channel_val);
    eventData->SetBranchAddress("energy",&energy_val);
    eventData->SetBranchAddress("subIndex",&subIndex_val);

    int channelThresh = 0;
    cout << "Enter energy threshold (Ch 0,1): ";
    cin >> channelThresh;
    cout << "Percent Energy Equivalence (int in %): ";
    cin >> pEE;

    char prefix[30];
    sprintf(prefix,"Sorted_%dPercent_Energies_T%d_",pEE,channelThresh);
    string sortedFileName = prefix + melFile;
    TFile *sortedFile = new TFile(sortedFileName.c_str(),"RECREATE");
    TTree *sortedEvents = eventData->CloneTree(0);
    TNtuple *acceptedEnergies;
    acceptedEnergies= new TNtuple("acceptedEnergies","Energies of Accepted
        Events","entry:E_PMTA:E_PMTB:E_Total");
    EcalEnergies = new TNtuple("EcalEnergies","Energy-Calibrated Specta of
```

```
        Accepted Events","Energy_Ch0:Energy_Ch1:Energy_Event:Energy_PXISum")
        ;
    acceptedEnergies->SetDirectory(sortedFile);
    EcalEnergies->SetDirectory(sortedFile);


    int numEntries = eventData->GetEntries();
    cout << "Number of Entries to Sort: " << numEntries << endl;


    int numRejected = 0;
    int numAccepted = 0;
    int numWritten = 0;
    int channel_val = 0;
    double energy_val = 0;
    int subIndex_val = 0;
    double sigma = 0;
    double range_high = 0;
    double range_low = 0;
    int Ch0_Threshold = channelThresh;
    int Ch1_Threshold = channelThresh;
    int Ch2_Threshold = 0;
    double nextEnergy = 0;
    double prevEnergy = 0;
    int nextChannel = 0;
    int prevChannel = 0;
    int prev2Channel = 0;
    int ch2=0;
    int En0 = 0;
    int unmatched = 0;
    int afterpulse = 0;
    int other = 0;
    int matchedChbadE = 0;
    double energy_total = 0;

    int waveformLength;
    int BaselineSum=0;
    double baselineLength_init = 0;
    double baselineLength_end = 0;
    double BaselineAvg =0;
    int BaselineSum_Final=0;
    double BaselineAvg_Final=0;
    double BaselineComp=0;
    double BaselineArea=0;
    double TotalPulseSum = 0;
    double TotalPulseCharge=0;
    double eventCharge = 0;
    double prevCharge = 0;
    double nextCharge = 0;
    double charge_total = 0;

    double multHigh = 1.0+(double(pEE)/100.0);
    double multLow = 1.0-(double(pEE)/100.0);
    //Energy Calibration
    double Ch0slope = 0;
    double Ch0intercept = 0;
```

```
double Ch1slope = 0;
double Ch1intercept = 0;
double Energy_Ch0 = 0;
double Energy_Ch1 = 0;
double Energy_Event = 0;
double SumSlope = 0;
double SumIntercept = 0;
double Energy_PXISum = 0;

int chamber = 0;
cout<<"Left (0) or right (1) chamber?";
cin>>chamber;

if (chamber == 0) {
    Ch0slope = 0.0189;
    Ch0intercept = 13.071;
    Ch1slope = 0.0184;
    Ch1intercept = 8.9047;
    SumSlope = 0;
    SumIntercept = 0;
}
if (chamber == 1) {
    Ch0slope = 0.0127;
    Ch0intercept = 0.5184;
    Ch1slope = 0.0119;
    Ch1intercept = 10.021;
    SumSlope = 0;
    SumIntercept = 0;
}

/*Sort events based on energy, channel, and subindex.
  Coincident Events for Channels 0 and 1 are saved if
  BOTH energies are above threshold for the first
  instance of the trigger and within 50% of first energy.*/

for (int ev =0; ev<numEntries; ev++) {
    eventData->GetEntry(ev);
    //Get waveform values
    energy_val = eventData->GetLeaf("energy")->GetValue();

    eventCharge = energy_val;

    //switch based on channel
    switch (channel_val) {
        case 0:
            if (eventCharge > Ch0_Threshold) {
                eventData->GetEntry(ev+1);
                nextChannel = eventData->GetLeaf("channel")->GetValue();
                nextEnergy = eventData->GetLeaf("energy")->GetValue();
                range_high = energy_val*multHigh;
                range_low = energy_val*multLow;

                nextCharge=nextEnergy;

                if (nextChannel == 1 && nextCharge > Ch1_Threshold &&
                    (range_high > nextCharge && nextCharge > range_low))
```

```
                    {
                    if (subIndex_val < 2) {
                        numAccepted++;
                        break;
                    }
                    else {
                            afterpulse++;
                        numRejected++;
                        break;
                    }
                }
                else {
                    if (nextChannel==1) {
                        matchedChbadE++;
                    }
                    unmatched++;
                    numRejected++;
                    break;
                }
            }
            else {
                if (energy_val == 0) {
                    En0++;
                }
                numRejected++;
                break;
            }



        case 1:
            if (eventCharge > Ch1_Threshold) {
                eventData->GetEntry(ev-1);
                prevChannel = eventData->GetLeaf("channel")->GetValue();
                prevEnergy = eventData->GetLeaf("energy")->GetValue();
                range_high = prevEnergy*multHigh;
                range_low = prevEnergy*multLow;

                prevCharge=prevEnergy;

                if (prevChannel == 0 && prevCharge > Ch0_Threshold &&
                    (range_high > eventCharge && eventCharge > range_low
                    )) {
                    if (subIndex_val < 2) {
                        sortedEvents->Fill();
                        eventData->GetEntry(ev);
                        sortedEvents->Fill();
                        energy_total = energy_val+prevEnergy;
                        acceptedEnergies->Fill(ev,prevEnergy,energy_val,
                            energy_total);


                        //Energy calculation for Ch0, Ch1, and Event
                        Energy_Ch0 = Ch0slope * prevEnergy +
                            Ch0intercept;
                        Energy_Ch1 = Ch1slope * energy_val +
```

```
                            Ch1intercept;
                        Energy_Event = Energy_Ch0 + Energy_Ch1;
                        Energy_PXISum = SumSlope * energy_total +
                            SumIntercept;
                        EcalEnergies->Fill(Energy_Ch0,Energy_Ch1,
                            Energy_Event,Energy_PXISum);

                        numWritten++;

                        numAccepted++;
                        break;
                    }
                    else {
                            afterpulse++;
                        numRejected++;
                        break;
                    }
                }
                else {
                    if (prevChannel==0) {
                        matchedChbadE++;
                    }
                    unmatched++;
                    numRejected++;
                    break;
                }
            }
            else {
                if (energy_val == 0) {
                    En0++;
                }
                numRejected++; break;

            }

        case 2:
            ch2++;
            break;


        case 4:
            if (eventCharge > Ch0_Threshold) {
                eventData->GetEntry(ev+1);
                nextChannel = eventData->GetLeaf("channel")->GetValue();
                nextEnergy = eventData->GetLeaf("energy")->GetValue();
                range_high = energy_val*multHigh;
                range_low = energy_val*multLow;

                nextCharge=nextEnergy;

                if (nextChannel == 5 && nextCharge > Ch1_Threshold &&
                    (range_high > nextCharge && nextCharge > range_low))
                    {
                    if (subIndex_val < 2) {
                        numAccepted++;
                        break;
```

```
                    }
                    else {
                        afterpulse++;
                        numRejected++;
                        break;
                    }
                }
                else {
                    if (nextChannel==5) {
                        matchedChbadE++;
                    }
                    unmatched++;
                    numRejected++;
                    break;
                }
            }
            else {
                if (energy_val == 0) {
                    En0++;
                }
                numRejected++;
                break;
            }



        case 5:
            if (eventCharge > Ch1_Threshold) {
                eventData->GetEntry(ev-1);
                prevChannel = eventData->GetLeaf("channel")->GetValue();
                prevEnergy = eventData->GetLeaf("energy")->GetValue();
                range_high = prevEnergy*multHigh;
                range_low = prevEnergy*multLow;

                prevCharge=prevEnergy;

                if (prevChannel == 4 && prevCharge > Ch0_Threshold &&
                    (range_high > eventCharge && eventCharge > range_low
                    )) {
                    if (subIndex_val < 2) {
                        sortedEvents->Fill();
                        eventData->GetEntry(ev);
                        sortedEvents->Fill();
                        energy_total = energy_val+prevEnergy;
                        acceptedEnergies->Fill(ev,prevEnergy,energy_val,
                            energy_total);


                        //Energy calculation for Ch0, Ch1, and Event
                        Energy_Ch0 = Ch0slope * prevEnergy +
                            Ch0intercept;
                        Energy_Ch1 = Ch1slope * energy_val +
                            Ch1intercept;
                        Energy_Event = Energy_Ch0 + Energy_Ch1;
                        Energy_PXISum = SumSlope * energy_total +
                            SumIntercept;
```

```
                                EcalEnergies->Fill(Energy_Ch0,Energy_Ch1,
                                    Energy_Event,Energy_PXISum);

                                numWritten++;

                                numAccepted++;
                                break;
                            }
                            else {
                                afterpulse++;
                                numRejected++;
                                break;
                            }
                        }
                        else {
                            if (prevChannel==4) {
                                matchedChbadE++;
                            }
                            unmatched++;
                            numRejected++;
                            break;
                        }
                    }
                    else {
                        if (energy_val == 0) {
                            En0++;
                        }
                        numRejected++; break;

                    }

                default:
                    cout<< "Not a Valid Channel." << endl;
                    break;
            }
        }

        //Save Good Events to New ROOT File
        sortedEvents->Write();
        acceptedEnergies->Write();
        EcalEnergies->Write();
        cout<<"Done! Accepted: " << numAccepted << " Rejected: " << numRejected
            << endl;
        cout<<"Channel 2 events: "<<ch2<< " and 0 energy events: "<<En0<<endl;
        cout<<"Total unmatched events: "<<unmatched<<" Match Ch, Unmatched E
            events: "<<matchedChbadE<<" Afterpulse events: "<<afterpulse<<endl;
        cout<<"Good Events: " << numAccepted/2 << endl;
        cout<<"numWritten : "<<numWritten<<endl;

        melFileIn->Close();
        sortedFile->Close();
    }
```

B.1.2 Event Selection Using Revised Calibration

```
//
//  SortEvents.cxx
//
//
//  Created by Erchinger, Jennifer L on 11/23/15.
//
//
//#include "SortEvents_CalcE.h"
#include <iostream>
#include "stdio.h"
#include "stdlib.h"
#include <string>
#include "TFile.h"
#include "TTree.h"
#include "TObject.h"

using namespace std;

void SortEvents_Preamp(){
    gROOT->Reset();

    int channel_val = 0;
    double energy_val = 0;
    int subIndex_val = 0;
    int pEE = 50.0;


    //Import ROOT file from melusine1
    string melFile;
    cout << "Melusine File: ";
    cin >> melFile;

    TFile *melFileIn = new TFile(melFile.c_str());
    TTree *eventData = (TTree*)melFileIn->Get("eventData");

    eventData->SetBranchAddress("channel",&channel_val);
    eventData->SetBranchAddress("energy",&energy_val);
    eventData->SetBranchAddress("subIndex",&subIndex_val);

    int channelThresh = 0;
    cout << "Enter energy threshold (Ch 0,1): ";
    cin >> channelThresh;
    cout << "Percent Energy Equivalence (int in %): ";
    cin >> pEE;

    char prefix[30];
    sprintf(prefix,"Sorted_%dPercent_Energies_T%d_",pEE,channelThresh);
    string sortedFileName = prefix + melFile;
    TFile *sortedFile = new TFile(sortedFileName.c_str(),"RECREATE");
    TTree *sortedEvents = eventData->CloneTree(0);
    TNtuple *acceptedEnergies;
    acceptedEnergies= new TNtuple("acceptedEnergies","Energies of Accepted
        Events","entry:E_PMTA:E_PMTB:E_Total");
    EcalEnergies = new TNtuple("EcalEnergies","Energy-Calibrated Specta of
        Accepted Events","Energy_Ch0:Energy_Ch1:Energy_Event:Energy_PXISum")
        ;
```

```
acceptedEnergies->SetDirectory(sortedFile);
EcalEnergies->SetDirectory(sortedFile);


int numEntries = eventData->GetEntries();
cout << "Number of Entries to Sort: " << numEntries << endl;


int numRejected = 0;
int numAccepted = 0;
int numWritten = 0;
int channel_val = 0;
double energy_val = 0;
int subIndex_val = 0;
double sigma = 0;
double range_high = 0;
double range_low = 0;
int Ch0_Threshold = channelThresh;
int Ch1_Threshold = channelThresh;
int Ch2_Threshold = 0;
double nextEnergy = 0;
double prevEnergy = 0;
int nextChannel = 0;
int prevChannel = 0;
int prev2Channel = 0;
int ch2=0;
int En0 = 0;
int unmatched = 0;
int afterpulse = 0;
int other = 0;
int matchedChbadE = 0;
double energy_total = 0;

int waveformLength;
//long waveData[wLength];
int BaselineSum=0;
double baselineLength_init = 0;//waveformLength/4;
double baselineLength_end = 0;//3*waveformLength/4;
double BaselineAvg =0;
int BaselineSum_Final=0;
double BaselineAvg_Final=0;
double BaselineComp=0;
double BaselineArea=0;
double TotalPulseSum = 0;
double TotalPulseCharge=0;
double eventCharge = 0;
double prevCharge = 0;
double nextCharge = 0;
double charge_total = 0;

double multHigh = 1.0+(double(pEE)/100.0);
double multLow = 1.0-(double(pEE)/100.0);
//Energy Calibration
double Ch0slope = 0;
double Ch0intercept = 0;
double Ch1slope = 0;
```

```
double Ch1intercept = 0;
double Energy_Ch0 = 0;
double Energy_Ch1 = 0;
double Energy_Event = 0;
double SumSlope = 0;
double SumIntercept = 0;
double Energy_PXISum = 0;

int chamber = 0;
cout<<"Left (0) or right (1) chamber?"<<endl;
cin>>chamber;

if (chamber == 0) {
    Ch0slope = 0.0256;
    Ch0intercept = 20.85;
    Ch1slope = 0.0255;
    Ch1intercept = 22.124;
    SumSlope = 0;
    SumIntercept = 0;
}
if (chamber == 1) {
    Ch0slope = 0.0243;
    Ch0intercept = 5.4131;
    Ch1slope = 0.0247;
    Ch1intercept = 7.1029;
    SumSlope = 0;
    SumIntercept = 0;
}

/*Sort events based on energy, channel, and subindex.
  Coincident Events for Channels 0 and 1 are saved if
  BOTH energies are above threshold for the first
  instance of the trigger and within 50% of first energy.*/

for (int ev =0; ev<numEntries; ev++) {
    eventData->GetEntry(ev);
    //Get waveform values
    energy_val = eventData->GetLeaf("energy")->GetValue();

    eventCharge = energy_val;

    //switch based on channel
    switch (channel_val) {
        case 0:
            if (eventCharge > Ch0_Threshold) {
                eventData->GetEntry(ev+1);
                nextChannel = eventData->GetLeaf("channel")->GetValue();
                nextEnergy = eventData->GetLeaf("energy")->GetValue();
                range_high = energy_val*multHigh;
                range_low = energy_val*multLow;

                nextCharge=nextEnergy;

                if (nextChannel == 1 && nextEnergy > Ch1_Threshold &&
                    (range_high > nextCharge && nextCharge > range_low))
                    {
```

```
                    if (subIndex_val < 2) {
                        numAccepted++;
                        break;
                    }
                    else {
                        afterpulse++;
                        numRejected++;
                        break;
                    }
                }
                else {
                    if (nextChannel==1) {
                        matchedChbadE++;
                    }
                        unmatched++;
                    numRejected++;
                    break;
                }
            }
            else {
                if (energy_val == 0) {
                    En0++;
                }
                numRejected++;
                break;
            }


        case 1:
            if (eventCharge > Ch1_Threshold) {
                eventData->GetEntry(ev-1);
                prevChannel = eventData->GetLeaf("channel")->GetValue();
                prevEnergy = eventData->GetLeaf("energy")->GetValue();
                range_high = prevEnergy*multHigh;
                range_low = prevEnergy*multLow;

                prevCharge=prevEnergy;

                if (prevChannel == 0 && prevEnergy > Ch0_Threshold &&
                    (range_high > eventCharge && eventCharge > range_low
                    )) {
                    if (subIndex_val < 2) {
                        sortedEvents->Fill();
                        eventData->GetEntry(ev);
                        sortedEvents->Fill();
                        energy_total = energy_val+prevEnergy;
                        acceptedEnergies->Fill(ev,prevEnergy,energy_val,
                            energy_total);


                        //Energy calculation for Ch0, Ch1, and Event
                        Energy_Ch0 = Ch0slope * prevEnergy +
                            Ch0intercept;
                        Energy_Ch1 = Ch1slope * energy_val +
                            Ch1intercept;
```

```
                        Energy_Event = Energy_Ch0 + Energy_Ch1;
                        Energy_PXISum = SumSlope * energy_total +
                            SumIntercept;
                        EcalEnergies->Fill(Energy_Ch0,Energy_Ch1,
                            Energy_Event,Energy_PXISum);

                        numWritten++;

                        numAccepted++;
                        break;
                    }
                    else {
                            afterpulse++;
                        numRejected++;
                        break;
                    }
                }
                else {
                    if (prevChannel==0) {
                        matchedChbadE++;
                    }
                        unmatched++;
                    numRejected++;
                    break;
                }
            }
            else {
                if (energy_val == 0) {
                    En0++;
                }
                numRejected++; break;

            }

        case 2:
            ch2++;
            break;

        case 4:
            if (eventCharge > Ch0_Threshold) {
                eventData->GetEntry(ev+1);
                nextChannel = eventData->GetLeaf("channel")->GetValue();
                nextEnergy = eventData->GetLeaf("energy")->GetValue();
                range_high = energy_val*multHigh;
                range_low = energy_val*multLow;

                nextCharge=nextEnergy;

                if (nextChannel == 5 && nextCharge > Ch1_Threshold &&
                    (range_high > nextCharge && nextCharge > range_low))
                    {
                    if (subIndex_val < 2) {
                        numAccepted++;
                        break;
                    }
                    else {
```

```
                        afterpulse++;
                        numRejected++;
                        break;
                    }
                }
                else {
                    if (nextChannel==5) {
                        matchedChbadE++;
                    }
                    unmatched++;
                    numRejected++;
                    break;
                }
            }
            else {
                if (energy_val == 0) {
                    En0++;
                }
                numRejected++;
                break;
            }



        case 5:
            if (eventCharge > Ch1_Threshold) {
                eventData->GetEntry(ev-1);
                prevChannel = eventData->GetLeaf("channel")->GetValue();
                prevEnergy = eventData->GetLeaf("energy")->GetValue();
                range_high = prevEnergy*multHigh;
                range_low = prevEnergy*multLow;

                prevCharge=prevEnergy;

                if (prevChannel == 4 && prevCharge > Ch0_Threshold &&
                    (range_high > eventCharge && eventCharge > range_low
                    )) {
                    if (subIndex_val < 2) {
                        sortedEvents->Fill();
                        eventData->GetEntry(ev);
                        sortedEvents->Fill();
                        energy_total = energy_val+prevEnergy;
                        acceptedEnergies->Fill(ev,prevEnergy,energy_val,
                            energy_total);


                        //Energy calculation for Ch0, Ch1, and Event
                        Energy_Ch0 = Ch0slope * prevEnergy +
                            Ch0intercept;
                        Energy_Ch1 = Ch1slope * energy_val +
                            Ch1intercept;
                        Energy_Event = Energy_Ch0 + Energy_Ch1;
                        Energy_PXISum = SumSlope * energy_total +
                            SumIntercept;
                        EcalEnergies->Fill(Energy_Ch0,Energy_Ch1,
                            Energy_Event,Energy_PXISum);
```

```
                                numWritten++;

                                numAccepted++;
                                break;
                            }
                            else {
                                afterpulse++;
                                numRejected++;
                                break;
                            }
                        }
                        else {
                            if (prevChannel==4) {
                                matchedChbadE++;
                            }
                            unmatched++;
                            numRejected++;
                            break;
                        }
                    }
                    else {
                        if (energy_val == 0) {
                            En0++;
                        }
                        numRejected++; break;

                    }

                default:
                    cout<< "Not a Valid Channel." << endl;
                    break;
            }
        }

        //Save Good Events to New ROOT File
        sortedEvents->Write();
        acceptedEnergies->Write();
        EcalEnergies->Write();
        cout<<"Done! Accepted: " << numAccepted << " Rejected: " << numRejected
            << endl;
        cout<<"Channel 2 events: "<<ch2<< " and 0 energy events: "<<En0<<endl;
        cout<<"Total unmatched events: "<<unmatched<<" Match Ch, Unmatched E
            events: "<<matchedChbadE<<" Afterpulse events: "<<afterpulse<<endl;
        cout<<"Good Events: " << numAccepted/2 << endl;
        cout<<"numWritten : "<<numWritten<<endl;

        melFileIn->Close();
        sortedFile->Close();

    //        return 0;
    }
```

B.2 PSA Identify Code: Performs Pulse Shape Analysis on Direct PMT Output

```
//
//  PSA_Identify.cxx
//
//
//  Created by Erchinger, Jennifer L on 5/29/15.
//
//

#include <iostream>
#include <stdio.h>
#include <stdlib.h>
#include <string>
#include <sstream>
#include <algorithm>
#include <TFile.h>
#include <TTree.h>
#include <TNtuple.h>

using namespace std;

int PSA_Identify(){
    //Import ROOT file
    string rootFile;
    cout<<"Enter the filename of the file containing waveform data:";
    cin>>rootFile;

    TFile *inpFile = new TFile(rootFile.c_str());
    TTree *eventData;
    inpFile->GetObject("eventData",eventData);

    string prefix = "PSA_ID_";
    string outfileName = prefix + rootFile;
    TFile *outfile = new TFile(outfileName.c_str(),"RECREATE");

    TNtuple *fData;
    fData = new TNtuple("PSAData","Data from PSA
        Calculations","iEntry:waveformLength:BaselineAvg:BaselineAvg_Final:B
        aselineArea:TotalPulseSum:TotalPulseCharge:CalcMax:MaxBin:MaxAvg:Pro
        mptSum:PromptBaseline:PromptCharge:PeakToChargeRatio");
    TNtuple *fTimingData;
    fTimingData = new TNtuple("TimingData","Data from Timing
        Calculations","iEntry:channel:TotalPulseCharge:CalcMax:MaxBin:Prompt
        Charge:PeakToChargeRatio:RT_LOW:RT_ns:RT_LOW:RT_HIGH:DT_ns:DT_LOW:DT
        _HIGH");

    int nEntries = 0;
    nEntries = eventData->GetEntries();
    cout << "Number of Entries: " << nEntries << endl;
    const int numEntries = nEntries;

    int waveformLength;
    int eventNum;
    int channel;
    double energy;
    double triggerTime;
```

```
        for(int iEntry=0;iEntry<numEntries;iEntry++){
            //Get data for iEntry
            eventData->GetEntry(iEntry);
            //Get # of waveform values
            waveformLength = eventData->GetLeaf("waveformLength")->GetValue();
            cout << "WaveformLength = " << waveformLength << endl;
            const int wLength = waveformLength;
            cout<< "wLength = " << wLength <<endl;
            //Get waveform values
            long waveData[wLength];
            for (int i=0; i<waveformLength; i++) {
                waveData[i] = eventData->GetLeaf("waveform")->GetValue(i);
            }

            //Find baseline and calculate baseline sum
            int BaselineSum=0;
            double baselineLength_init = waveformLength/4;
            double baselineLength_end = 3*waveformLength/4;
            double BaselineAvg =0;
            for(int j=0;j<baselineLength_init;j++){
                BaselineSum+=waveData[j];
            }
            BaselineAvg = BaselineSum/baselineLength_init;

            int BaselineSum_Final=0;
            double BaselineAvg_Final=0;
            for (int k=baselineLength_end; k<waveformLength; k++) {
                BaselineSum_Final+=waveData[k];
            }
            BaselineAvg_Final = BaselineSum_Final/(waveformLength-
                baselineLength_end);

            double BaselineComp=0;
            BaselineComp = BaselineAvg_Final-BaselineAvg;

            double BaselineArea=0;
            BaselineArea = BaselineAvg*waveformLength;

            //Find Total Pulse Integral
            double TotalPulseSum = 0;
            for (int l=0; l<waveformLength; l++) {
                TotalPulseSum+=waveData[l];
            }

            //Subtract Baseline integral from Pulse Integral to get Pulse Charge
            double TotalPulseCharge=0;
            TotalPulseCharge=TotalPulseSum-BaselineArea;

            //Find Peak with 3-point average
            double ThreePointAvg[wLength];
            double CalcMax = 0;
            int MaxBin = 0;
            for (int m=1; m<waveformLength-1; m++) {
                ThreePointAvg[m] = (waveData[m-1] + waveData[m] + waveData[m+1])
                    /3;
                if (ThreePointAvg[m]>CalcMax) {
```

```
            CalcMax = ThreePointAvg[m];
            MaxBin = m;
            cout << "Comparison Maximum is: " << CalcMax <<" at bin: "<<
                MaxBin << endl;
        }
    }

    double MaxAvg = *std::max_element(ThreePointAvg,ThreePointAvg+
        waveformLength);
    cout << "Maximum from Three-Point Average is: " << MaxAvg <<endl;


    //Integrate pulse up to peak
    double PromptSum =0;
    double PromptBaseline =0;
    for (int n=baselineLength_init; n<=MaxBin; n++) {
        PromptSum += waveData[n];
        PromptBaseline += BaselineAvg;
    }

    double PromptCharge=0;
    PromptCharge = PromptSum - PromptBaseline;

    //Calculate Peak/Total Charge Ratio
    double PeakToChargeRatio = PromptCharge/TotalPulseCharge;

    //Calculate Rise Time JLE 11/3/2015
    double PERCENT_MAX_10 = (0.2*(CalcMax-BaselineAvg))+BaselineAvg;
    double PERCENT_MAX_90 = (0.9*(CalcMax-BaselineAvg))+BaselineAvg;
    double RT_ThreePointAvg[wLength];
    double DT_ThreePointAvg[wLength];

    int RTBIN_PERCENT_MAX_10 = 0;
    int RTBIN_PERCENT_MAX_90 = 0;
    int RT_LOW = MaxBin;
    int RT_HIGH = MaxBin;

    for (int wave_bin=baselineLength_init+1; wave_bin<MaxBin; wave_bin++
        ) {
        RT_ThreePointAvg[wave_bin] = (waveData[wave_bin-1] + waveData
            [wave_bin] + waveData[wave_bin+1])/3;
        if (RT_ThreePointAvg[wave_bin-1]<PERCENT_MAX_10 &&
            RT_ThreePointAvg[wave_bin]>=PERCENT_MAX_10) {
            RTBIN_PERCENT_MAX_10 = wave_bin;
            if (RTBIN_PERCENT_MAX_10<RT_LOW) {
                RT_LOW = RTBIN_PERCENT_MAX_10;
            }
        }
        if (RT_ThreePointAvg[wave_bin-1]<PERCENT_MAX_90 &&
            RT_ThreePointAvg[wave_bin]>=PERCENT_MAX_90) {
            RTBIN_PERCENT_MAX_90 = wave_bin;
            if (RTBIN_PERCENT_MAX_90<RT_LOW) {
                RT_HIGH = RTBIN_PERCENT_MAX_90;
            }
        }
```

```
            int RT_BINS = RT_HIGH-RT_LOW;

            int RT_ns = RT_BINS*2;

            //Calculate Decay Time JLE 11/3/2015
            int DTBIN_PERCENT_MAX_10 = 0;
            int DTBIN_PERCENT_MAX_90 = 0;
            int DT_LOW = waveformLength;
            int DT_HIGH = waveformLength;

            for (int wave_bin_dt=MaxBin;wave_bin_dt<waveformLength-1;wave_bin_dt
                ++) {
                DT_ThreePointAvg[wave_bin_dt] = (waveData[wave_bin_dt-1] +
                    waveData[wave_bin_dt] + waveData[wave_bin_dt+1])/3;
                if (DT_ThreePointAvg[wave_bin_dt-1]>PERCENT_MAX_10 &&
                    DT_ThreePointAvg[wave_bin_dt]<=PERCENT_MAX_10) {
                    DTBIN_PERCENT_MAX_10 = wave_bin_dt;
                    if (DTBIN_PERCENT_MAX_10<DT_LOW) {
                        DT_LOW = DTBIN_PERCENT_MAX_10;
                    }
                }
                if (DT_ThreePointAvg[wave_bin_dt-1]>PERCENT_MAX_90 &&
                    DT_ThreePointAvg[wave_bin_dt]<=PERCENT_MAX_90) {
                    DTBIN_PERCENT_MAX_90 = wave_bin_dt;
                    if (DTBIN_PERCENT_MAX_90<DT_HIGH) {
                        DT_HIGH = DTBIN_PERCENT_MAX_90;
                    }
                }


            int DT_BINS = DT_LOW-DT_HIGH;

            int DT_ns = DT_BINS*2;

        //        //Separate E based on channel
            channel = eventData->GetLeaf("channel")->GetValue();


            //Fill nTuples
            fData->Fill(iEntry,waveformLength,BaselineAvg,BaselineAvg_Final,
                BaselineArea,TotalPulseSum,TotalPulseCharge,CalcMax,MaxBin,
                MaxAvg,PromptSum,PromptBaseline,PromptCharge,PeakToChargeRatio);
            fTimingData->Fill(iEntry,channel,TotalPulseCharge,CalcMax,MaxBin,
                PromptCharge,PeakToChargeRatio,RT_LOW,RT_ns,RT_LOW,RT_HIGH,DT_ns
                ,DT_LOW,DT_HIGH);
            //Print Values
            cout << "WaveformLength\tBaselineAvg_Init\tBaselineAvg_End
                \tPulseIntegral\tPeakIntegral\tPeakHeight(Avg)\tPeakBin\tRatio
                \tRT_ns\tDT_ns"<<endl;
            cout << waveformLength << "\t" << BaselineAvg << "\t" <<
                BaselineAvg_Final << "\t" << TotalPulseCharge << "\t" <<
                PromptCharge << "\t" << CalcMax << "\t" << MaxBin << "\t" <<
                PeakToChargeRatio << "\t" << RT_ns << "\t" << DT_ns << endl;
```

```
        }

        //Plot Ratio for all events
        fData->Draw("PeakToChargeRatio >> hRatio");
        fData->Draw("PeakToChargeRatio:TotalPulseCharge >> hRatio2Total");
        fData->Draw("PeakToChargeRatio:PromptCharge >> hRatio2Prompt");
        fData->Draw("PromptCharge:TotalPulseCharge >> hPrompt2Total");
        fTimingData->Draw("RT_ns:TotalPulseCharge >> hRT2Total");
        fTimingData->Draw("DT_ns:TotalPulseCharge >> hDT2Total");

        outfile->Write();
        outfile->Close();
        inpFile->Close();

        return numEntries;
    }
```

APPENDIX C

SPECTRA FROM FULL BUILD

C.1 Left Chamber Spectra

C.1.1 Background Spectra

C.1.1.1 Individual Background Sample Spectra

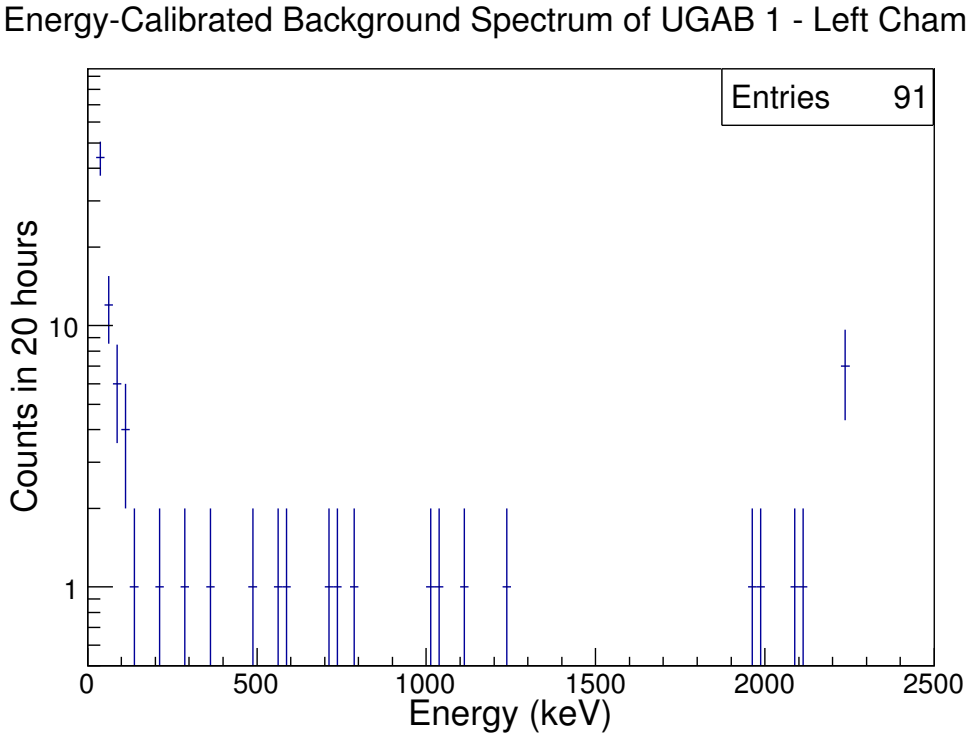

Figure C.1: Spectrum of UGAB 1 Sample from 20-hour acquisition in the left chamber.

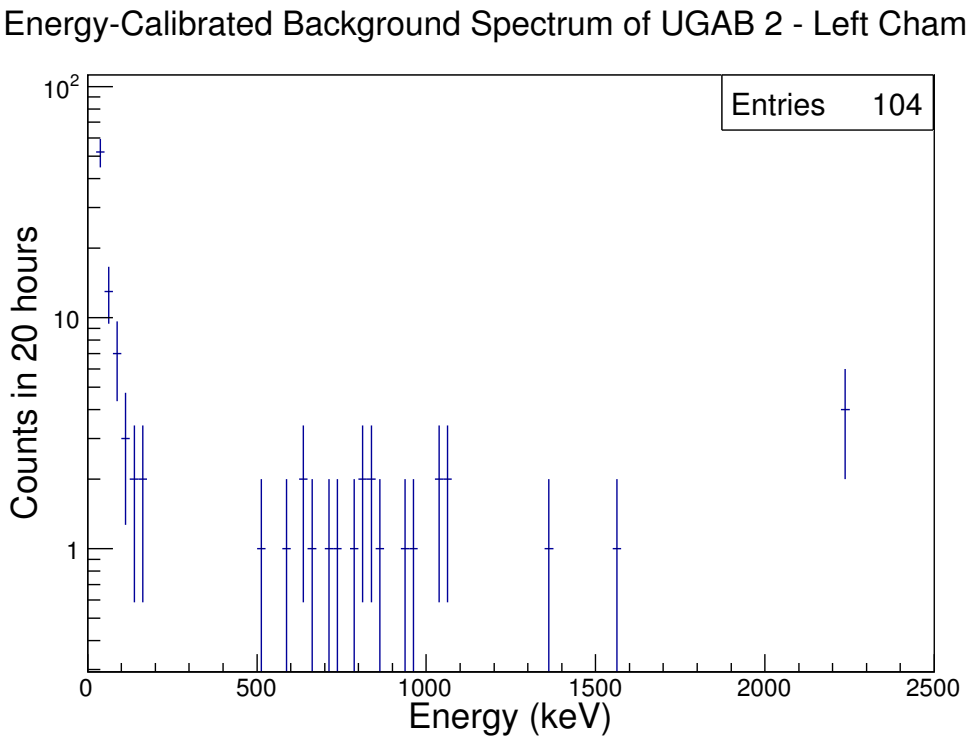

Figure C.2: Spectrum of UGAB 2 Sample from 20-hour acquisition in the left chamber.

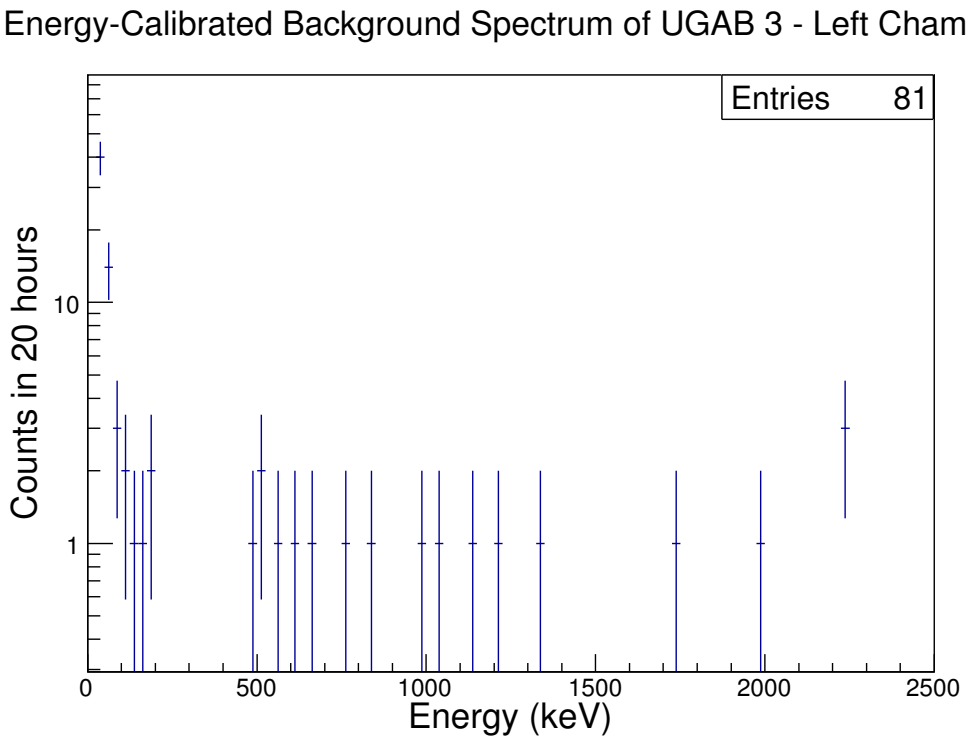

Figure C.3: Spectrum of UGAB 3 Sample from 20-hour acquisition in the left chamber.

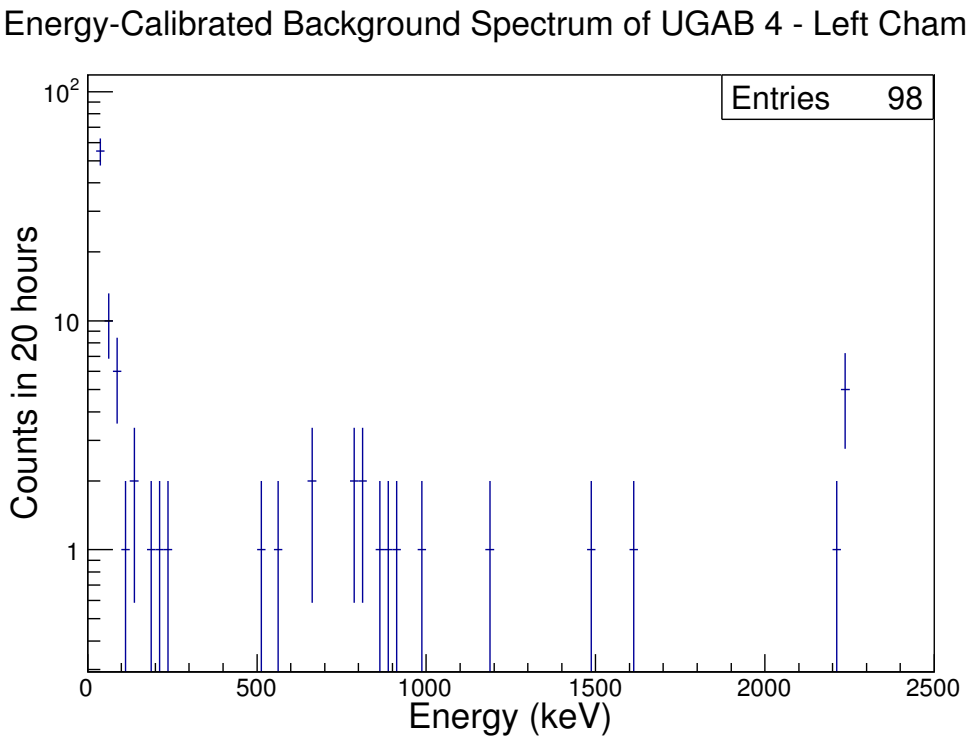

Figure C.4: Spectrum of UGAB 4 Sample from 20-hour acquisition in the left chamber.

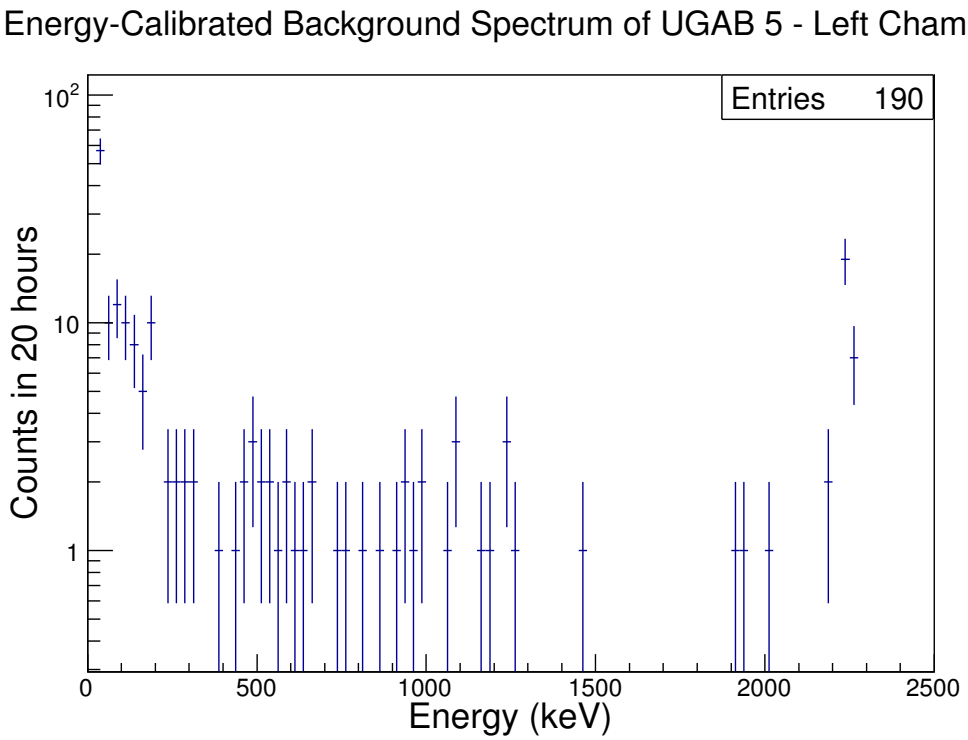

Figure C.5: Spectrum of UGAB 5 Sample from 20-hour acquisition in the left chamber.

C.1.1.2 Average of Individual Background Spectra

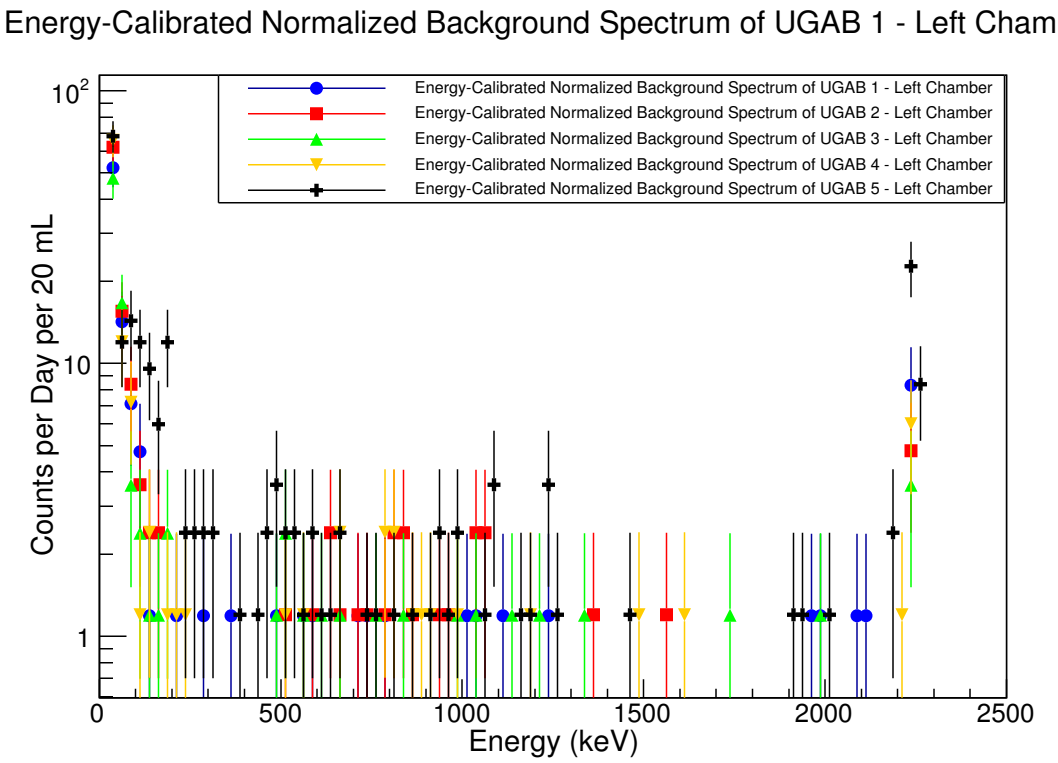

Figure C.6: Mass-normalized spectra of the UGAB background samples for the left chamber in counts per day.

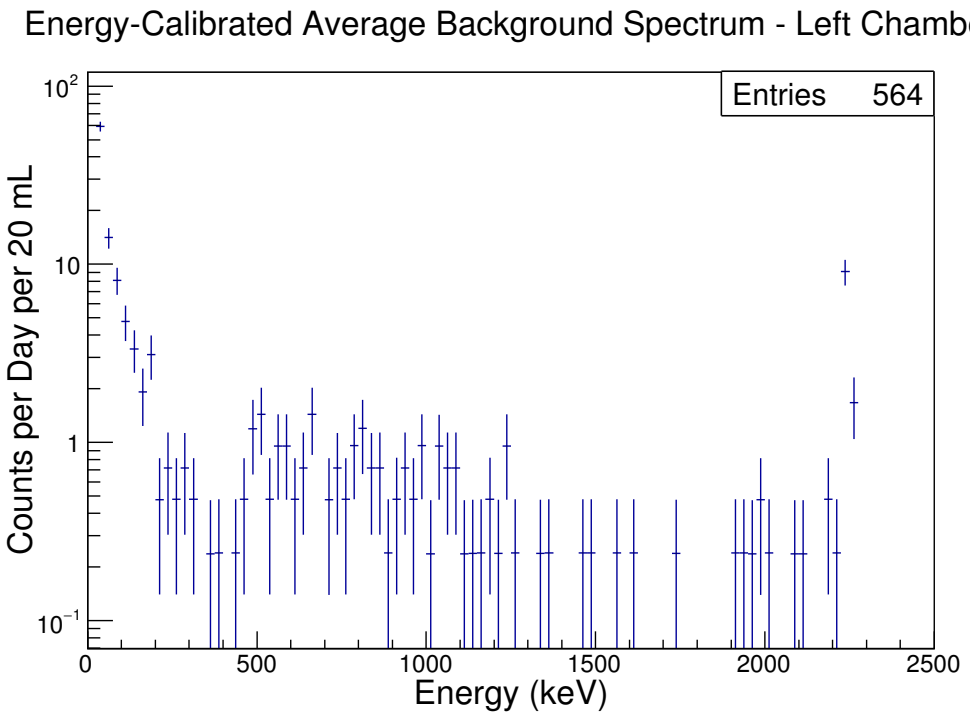

Figure C.7: Average UGAB background spectrum for 20 mL of cocktail for the left chamber in counts per day.

C.1.1.3 Long Background Spectra

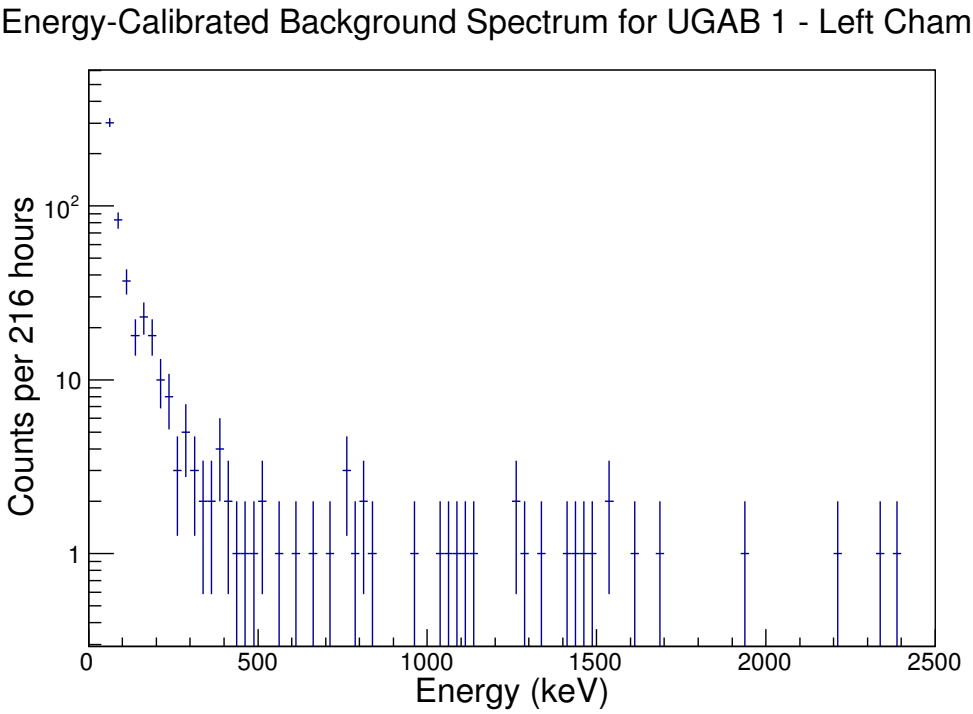

Figure C.8: Spectrum of UGAB 1 Sample from 216-hour acquisition in the left chamber.

C.1.2 Sample Spectra

C.1.2.1 Individual Sample Spectra

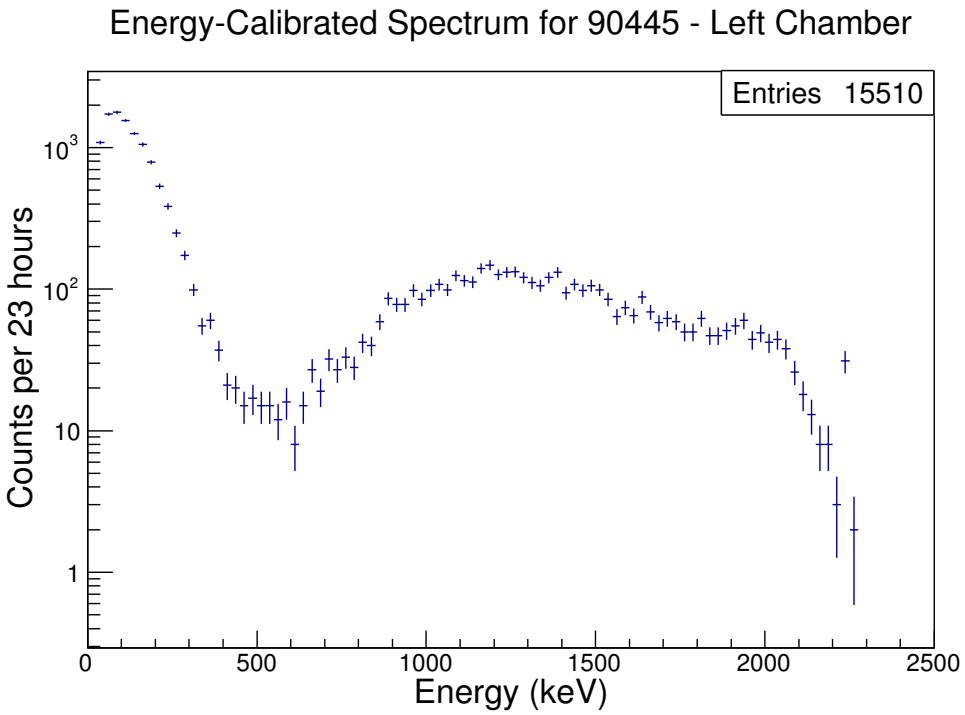

Figure C.9: Spectrum of sample 90445 from 23-hour acquisition in the left chamber.

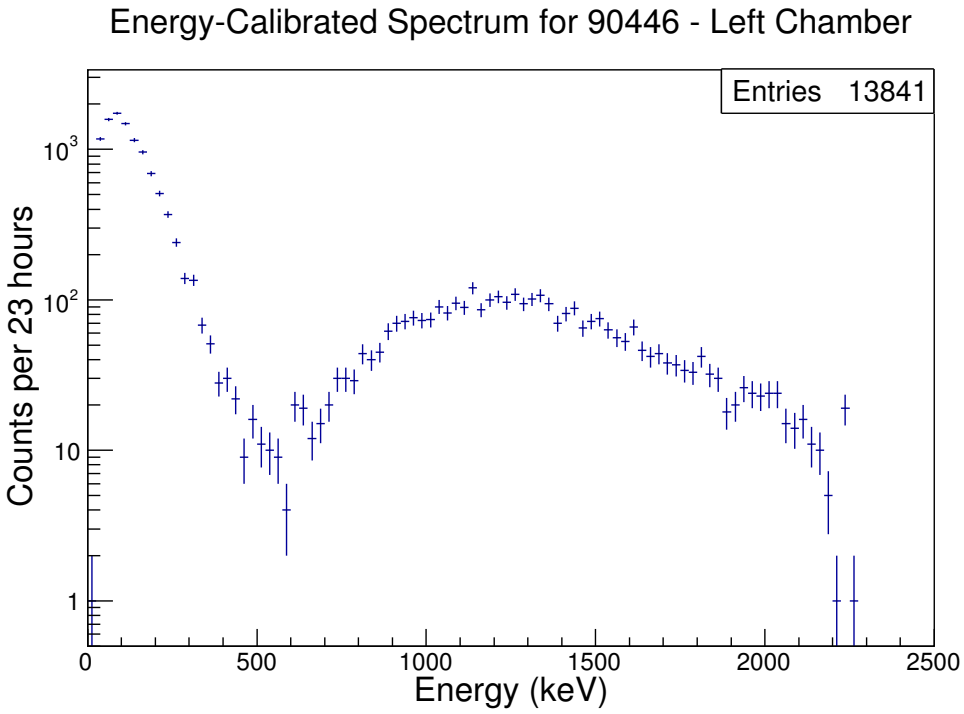

Figure C.10: Spectrum of sample 90446 from 23-hour acquisition in the left chamber.

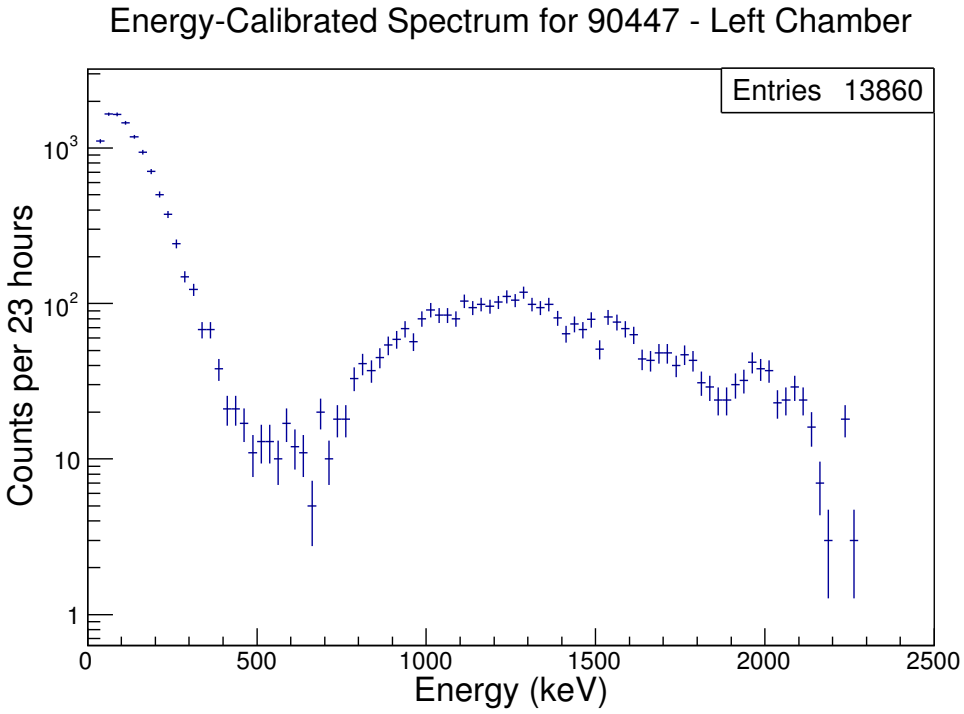

Figure C.11: Spectrum of sample 90447 from 23-hour acquisition in the left chamber.

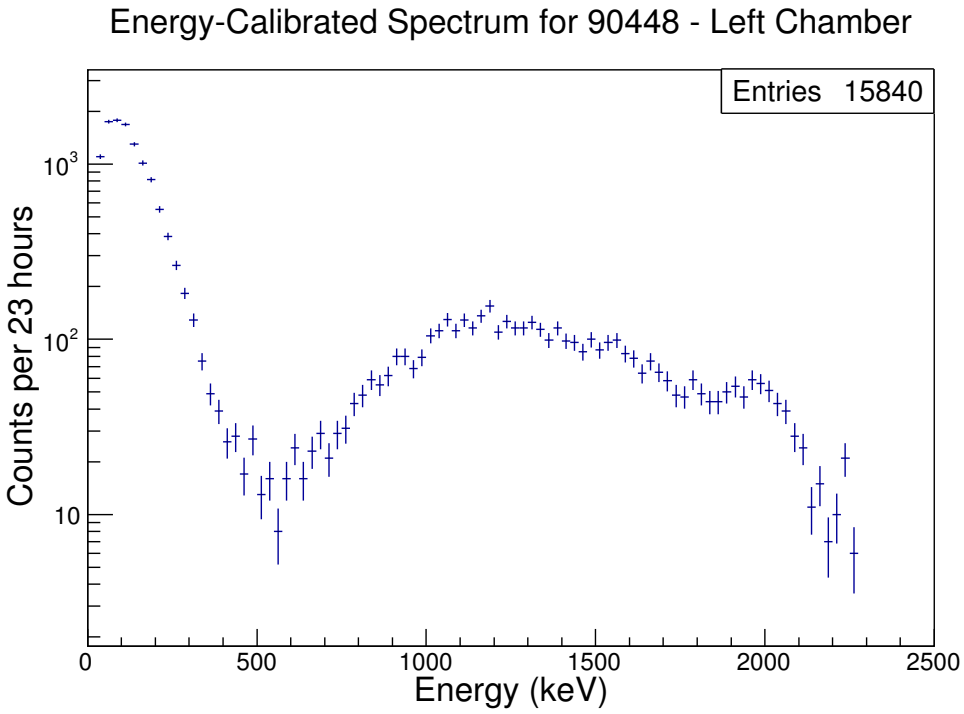

Figure C.12: Spectrum of sample 90448 from 23-hour acquisition in the left chamber.

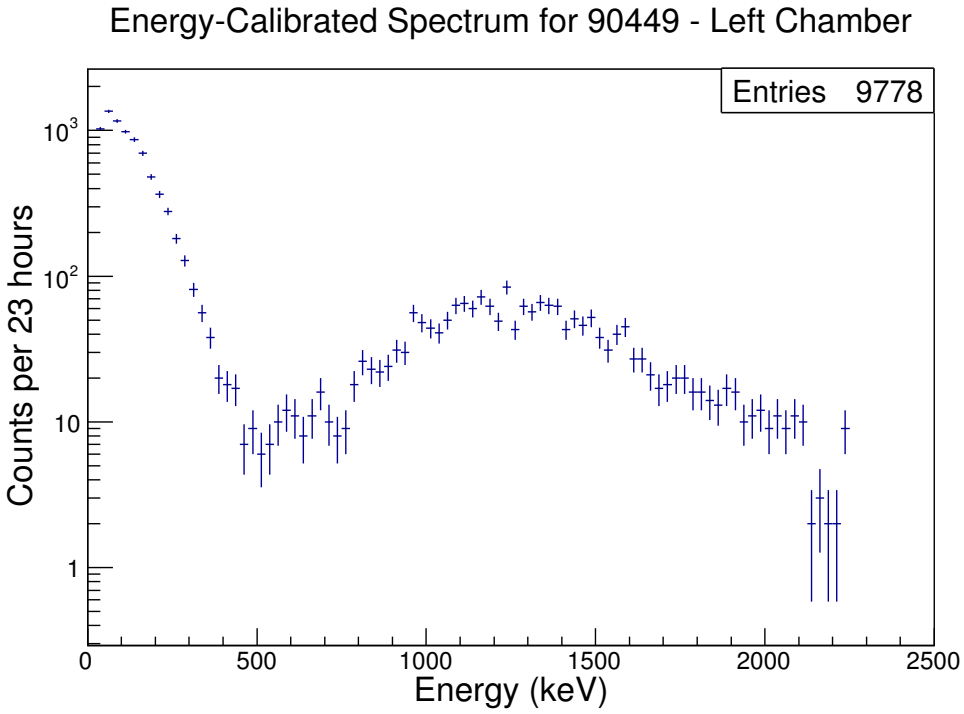

Figure C.13: Spectrum of sample 90449 from 23-hour acquisition in the left chamber.

C.1.2.2 Long Sample Spectra

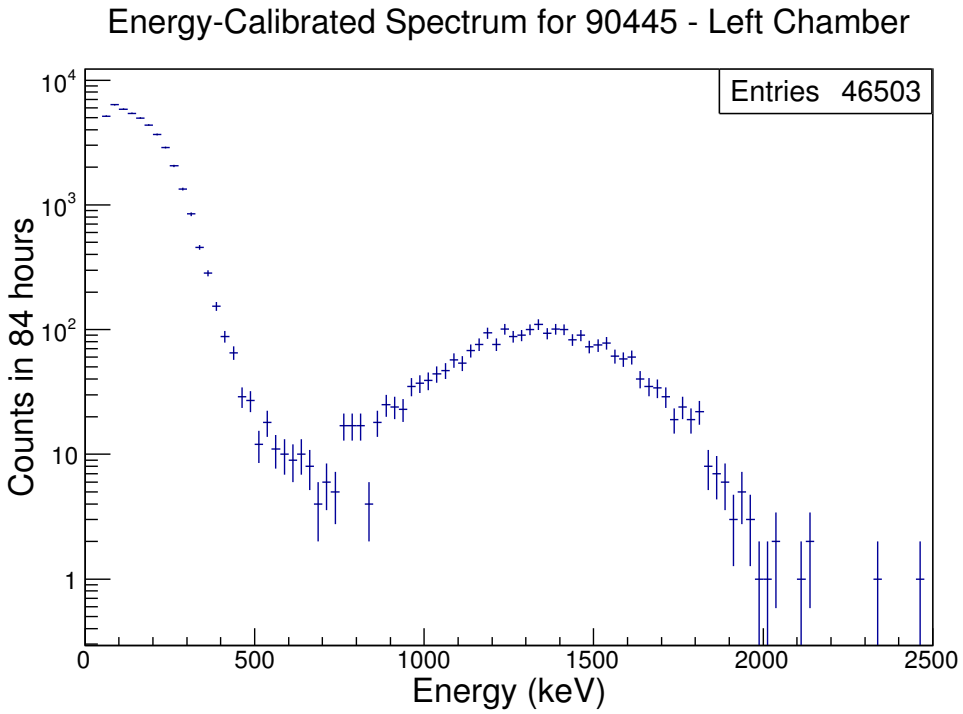

Figure C.14: Spectrum of sample 90445 from 84-hour acquisition in the left chamber.

C.1.3 Background-Subtracted Sample Spectra

C.1.3.1 Individual Sample Spectra

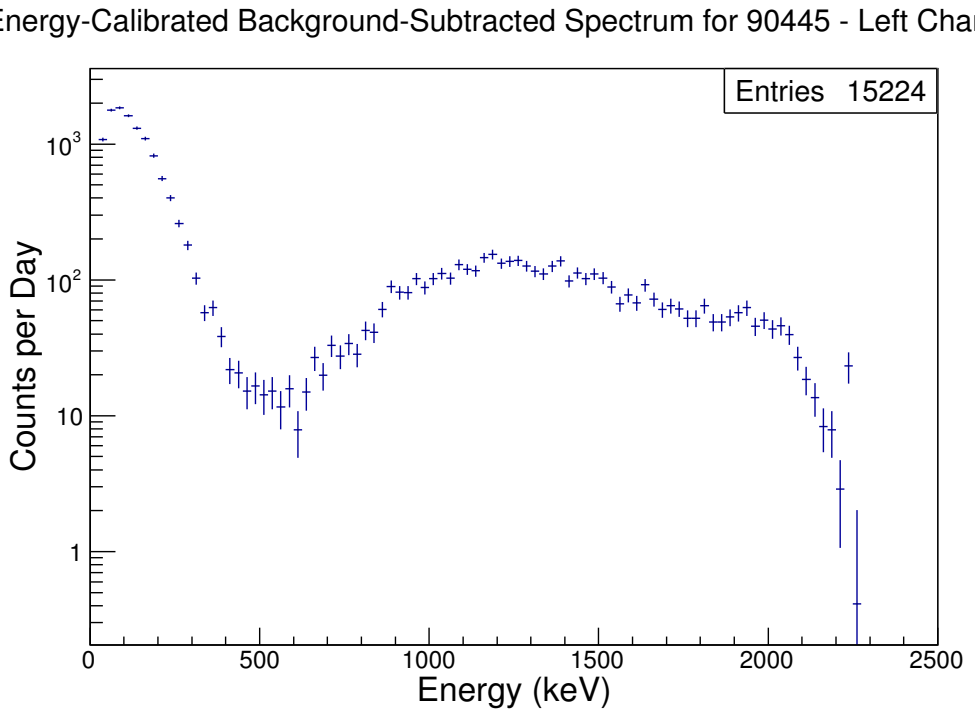

Figure C.15: Background-subtracted spectrum of sample 90445 from 23-hour acquisition in the left chamber.

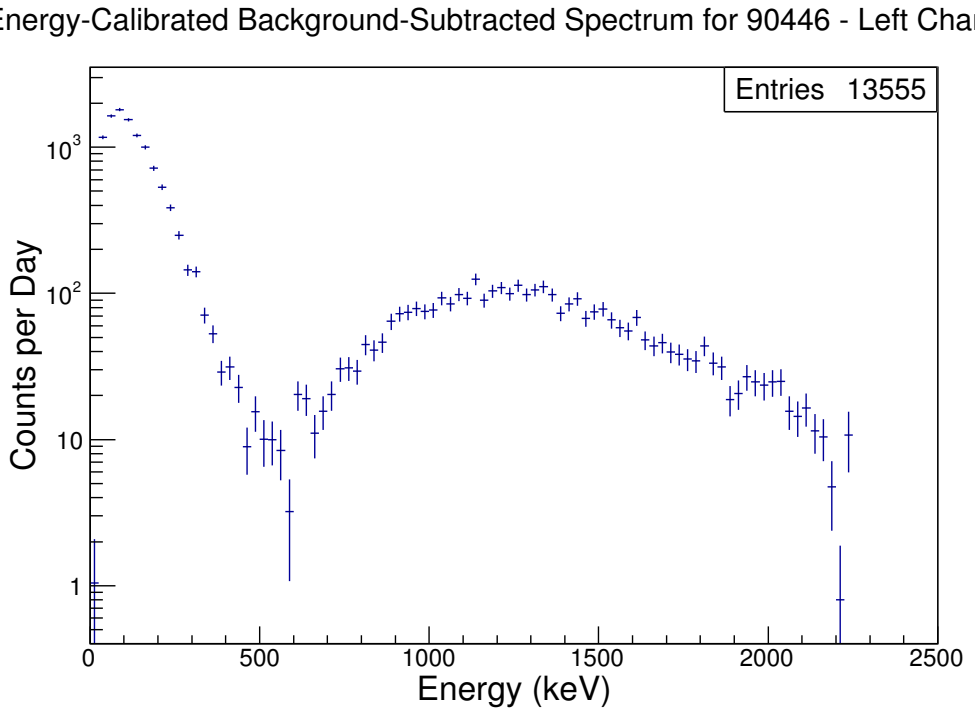

Figure C.16: Background-subtracted spectrum of sample 90446 from 23-hour acquisition in the left chamber.

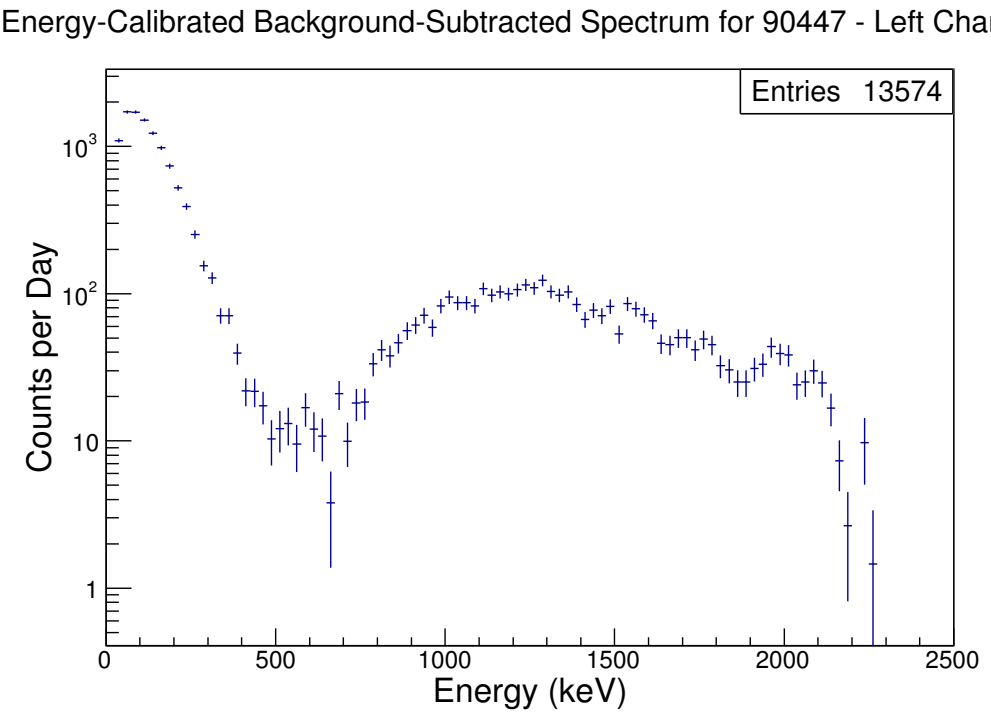

Figure C.17: Background-subtracted spectrum of sample 90447 from 23-hour acquisition in the left chamber.

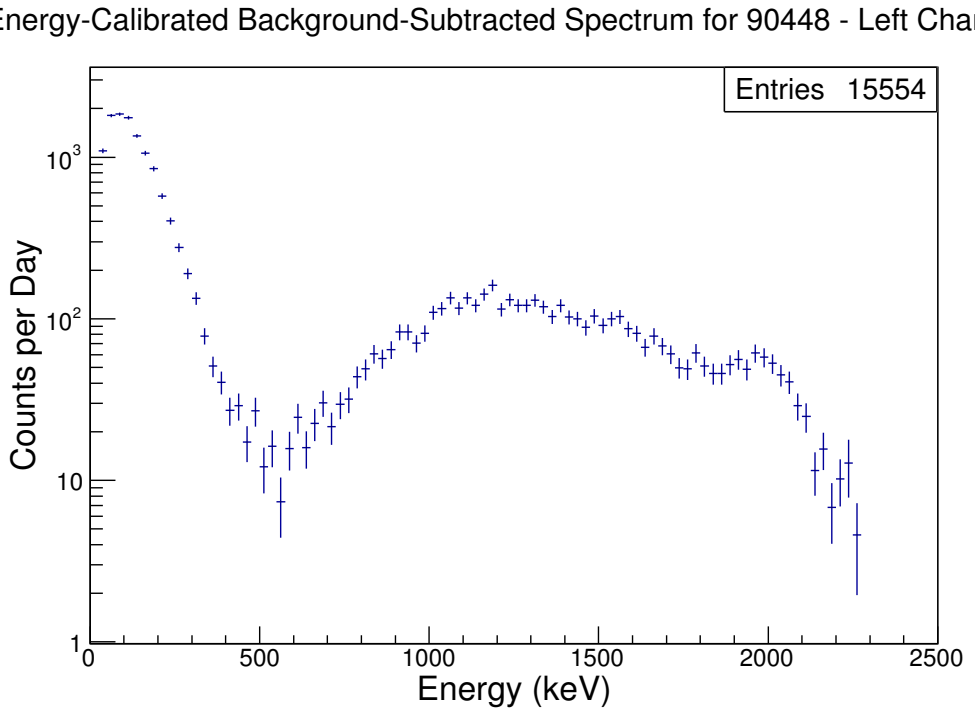

Figure C.18: Background-subtracted spectrum of sample 90448 from 23-hour acquisition in the left chamber.

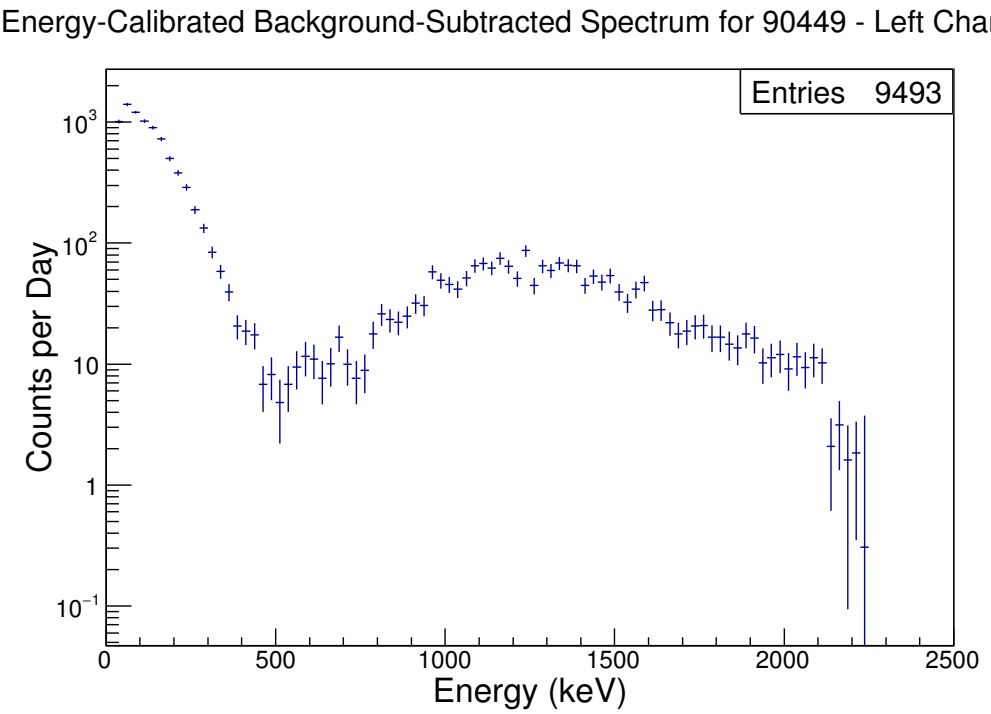

Figure C.19: Background-subtracted spectrum of sample 90449 from 23-hour acquisition in the left chamber.

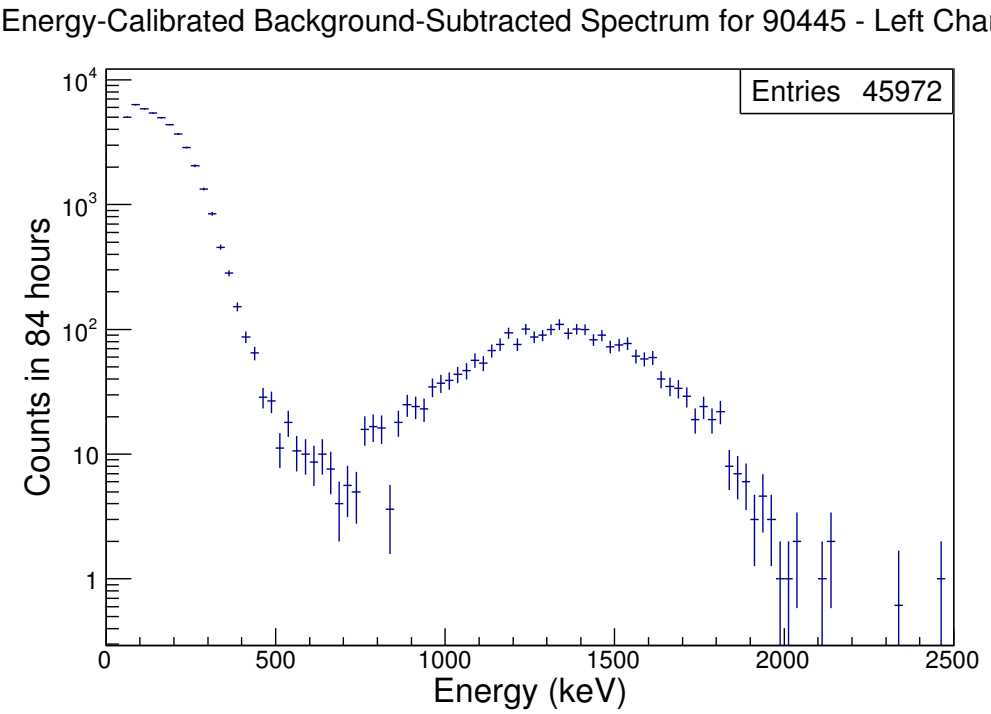

Figure C.20: Background-subtracted spectrum of sample 90445 from 84-hour acquisition in the left chamber.

C.2 Right Chamber Spectra

C.2.1 Background Spectra

C.2.1.1 Individual Background Sample Spectra

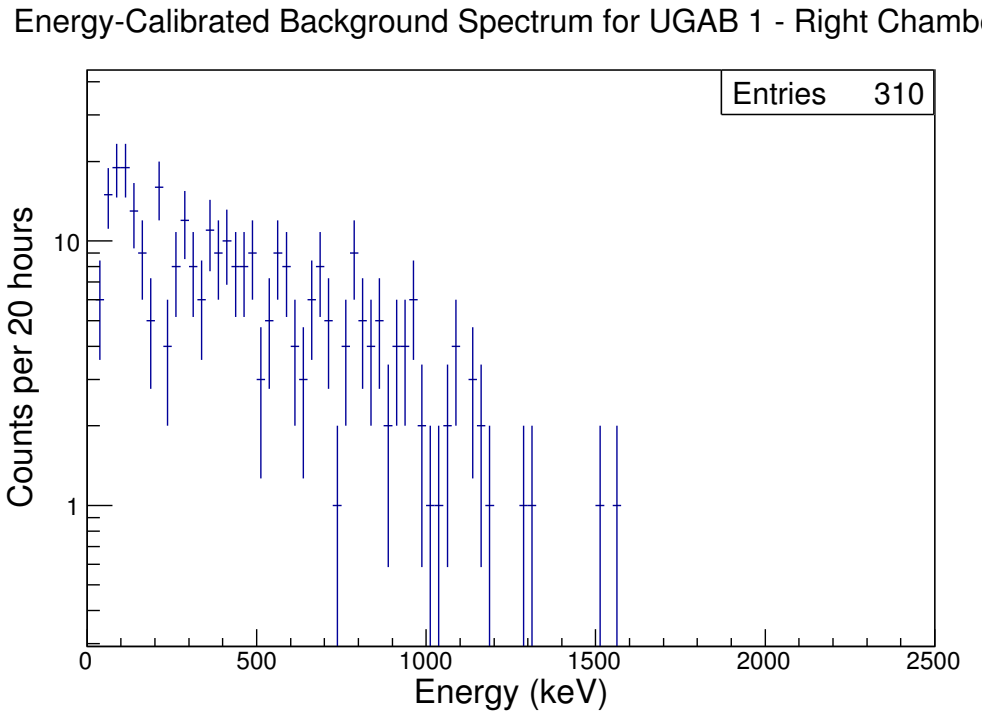

Figure C.21: Spectrum of UGAB 1 Sample from 20-hour acquisition in the right chamber.

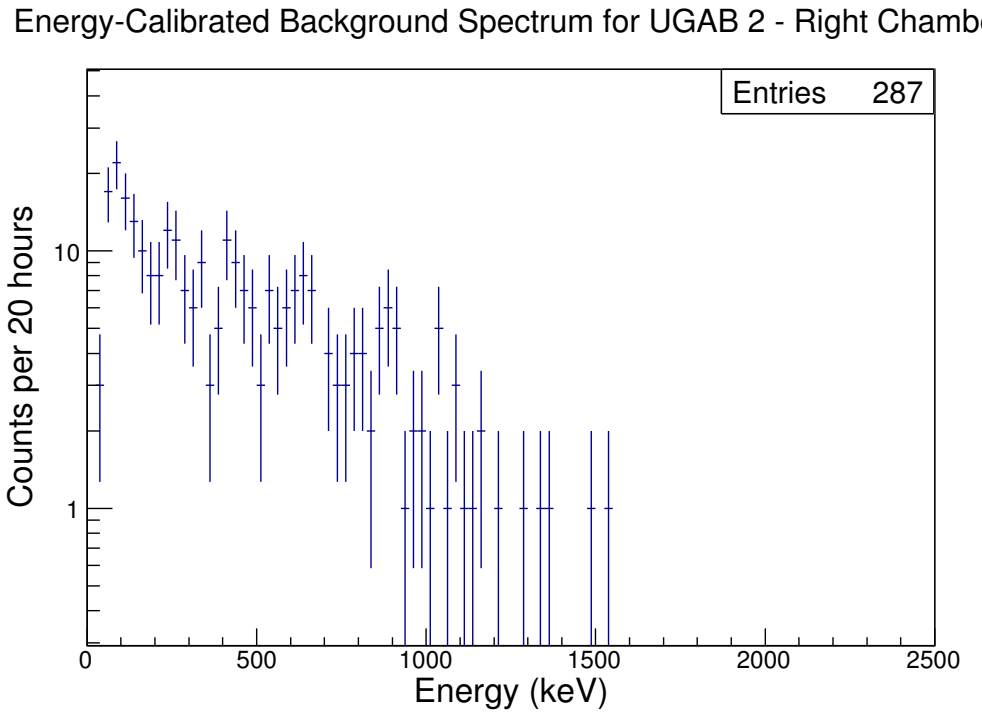

Figure C.22: Spectrum of UGAB 2 Sample from 20-hour acquisition in the right chamber.

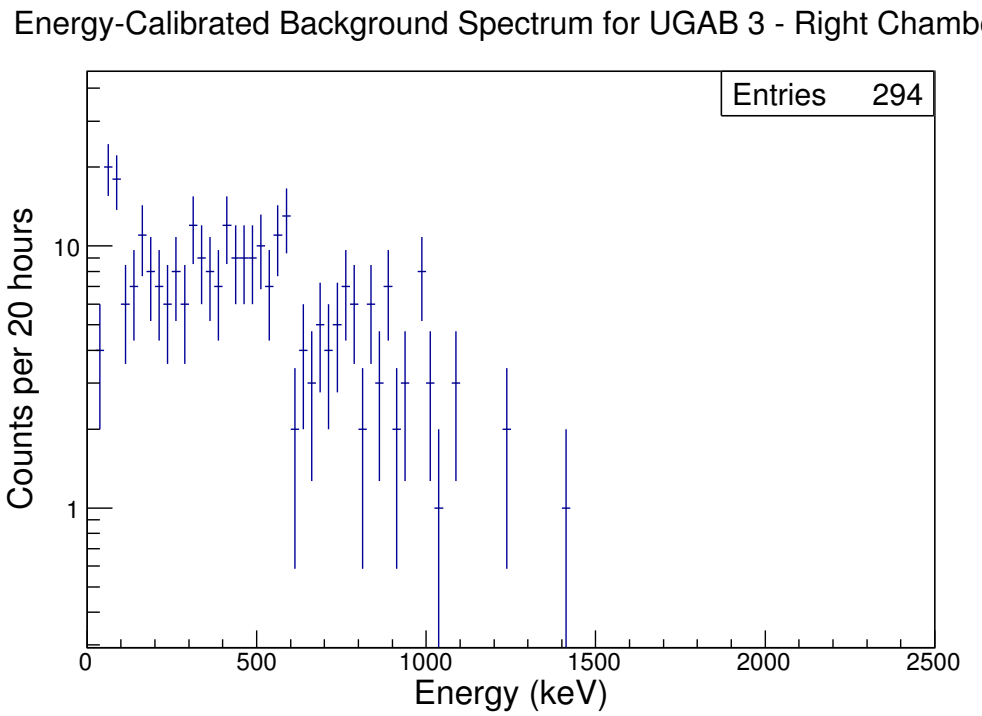

Figure C.23: Spectrum of UGAB 3 Sample from 20-hour acquisition in the right chamber.

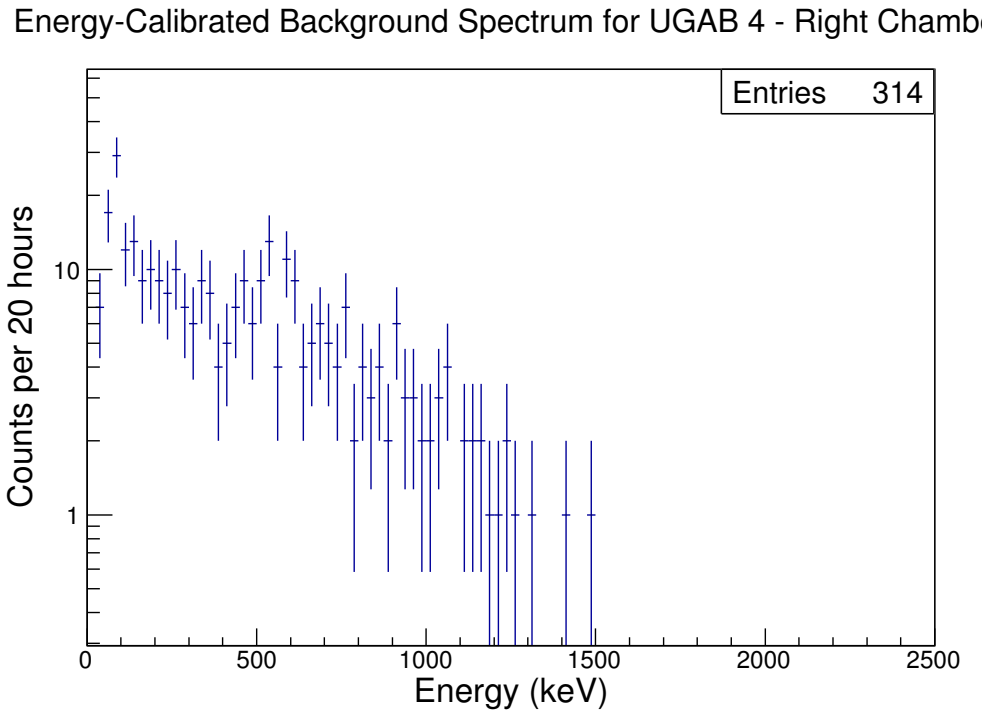

Figure C.24: Spectrum of UGAB 4 Sample from 20-hour acquisition in the right chamber.

C.2.1.2 Average of Individual Background Spectra

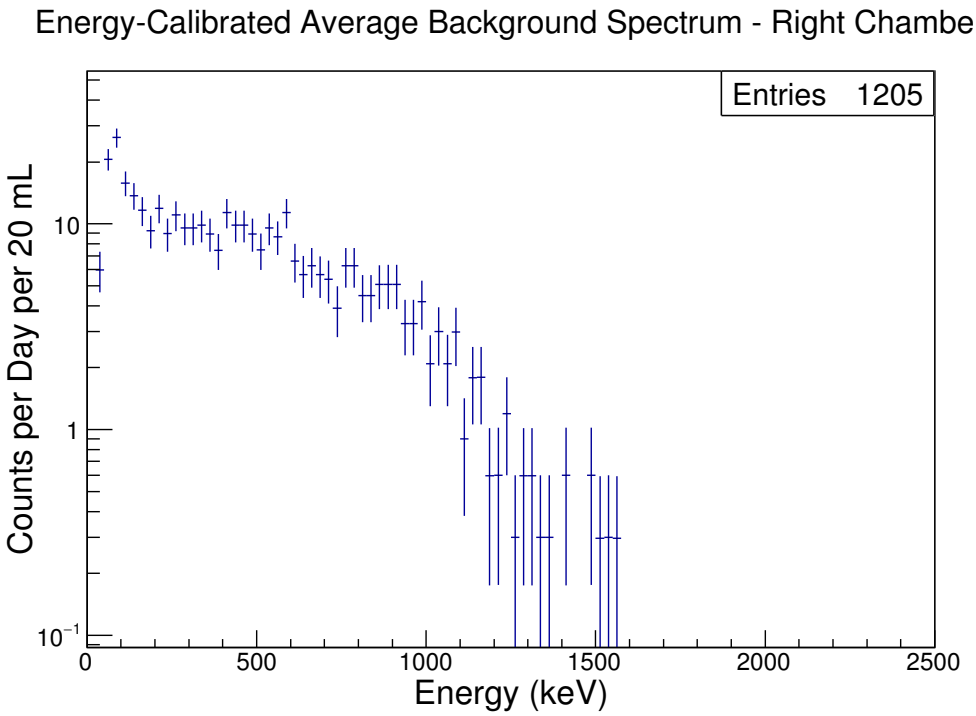

Figure C.25: Mass-normalized spectra of the UGAB background samples for the right chamber in counts per day.

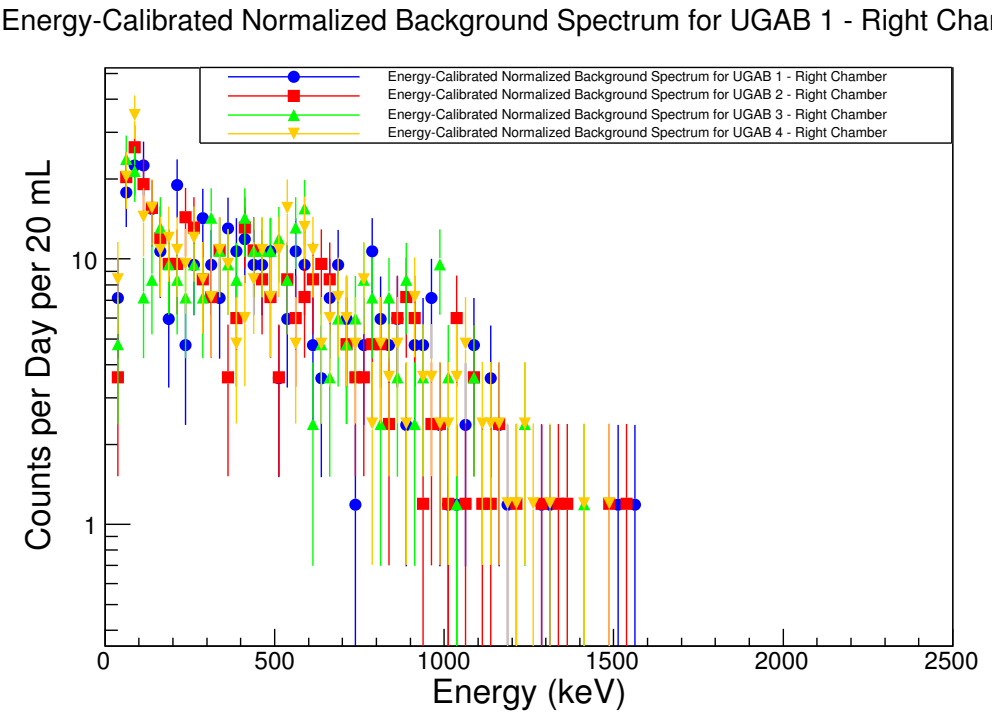

Figure C.26: Average UGAB background spectrum for 20 mL of cocktail for the right chamber in counts per day.

C.2.1.3 Long Background Spectra

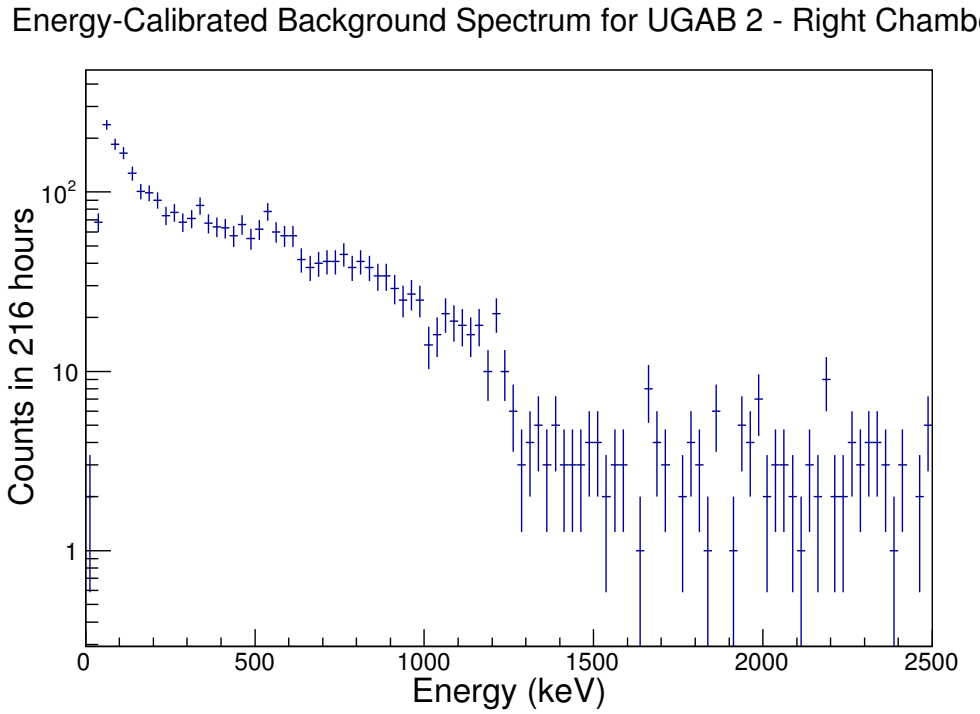

Figure C.27: Spectrum of UGAB 2 Sample from 216-hour acquisition in the left chamber.

C.2.2 Sample Spectra

C.2.2.1 Individual Sample Spectra

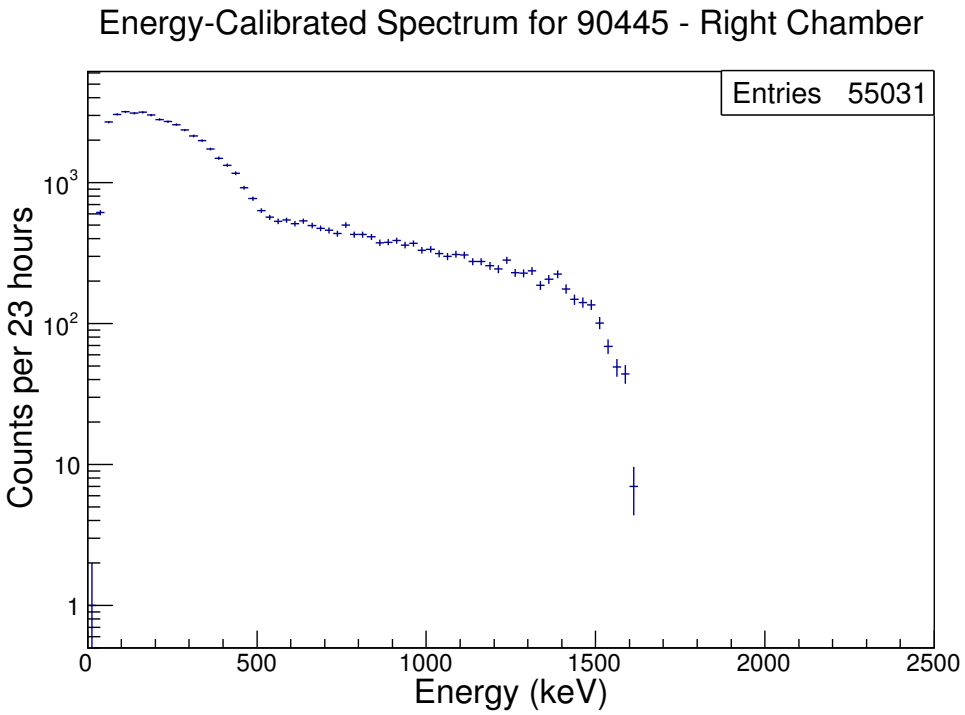

Figure C.28: Spectrum of sample 90445 from 23-hour acquisition in the right chamber.

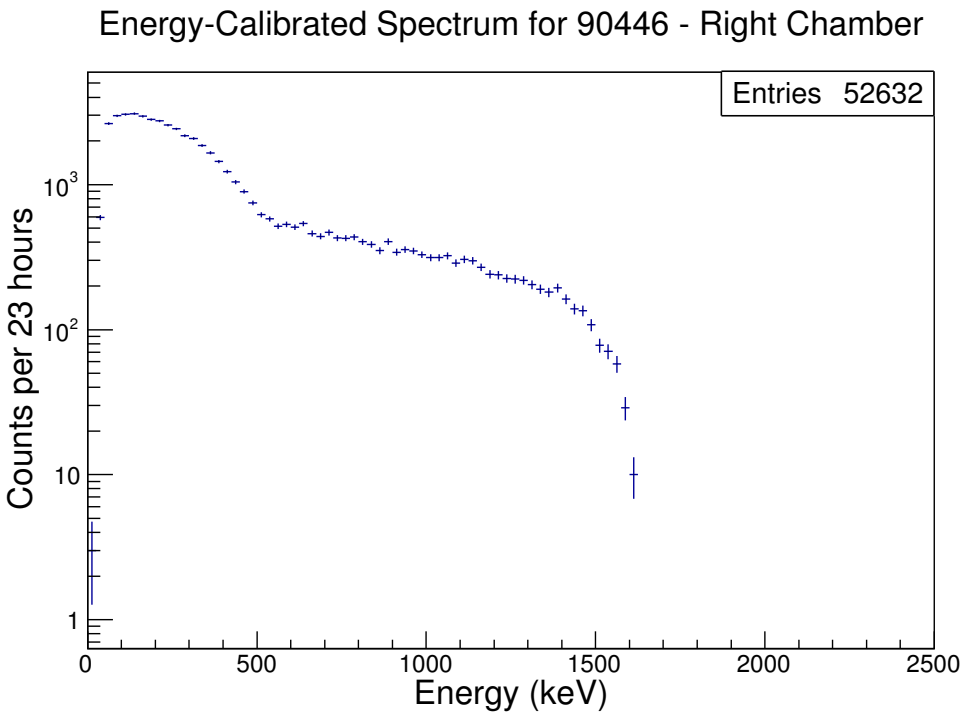

Figure C.29: Spectrum of sample 90446 from 23-hour acquisition in the right chamber.

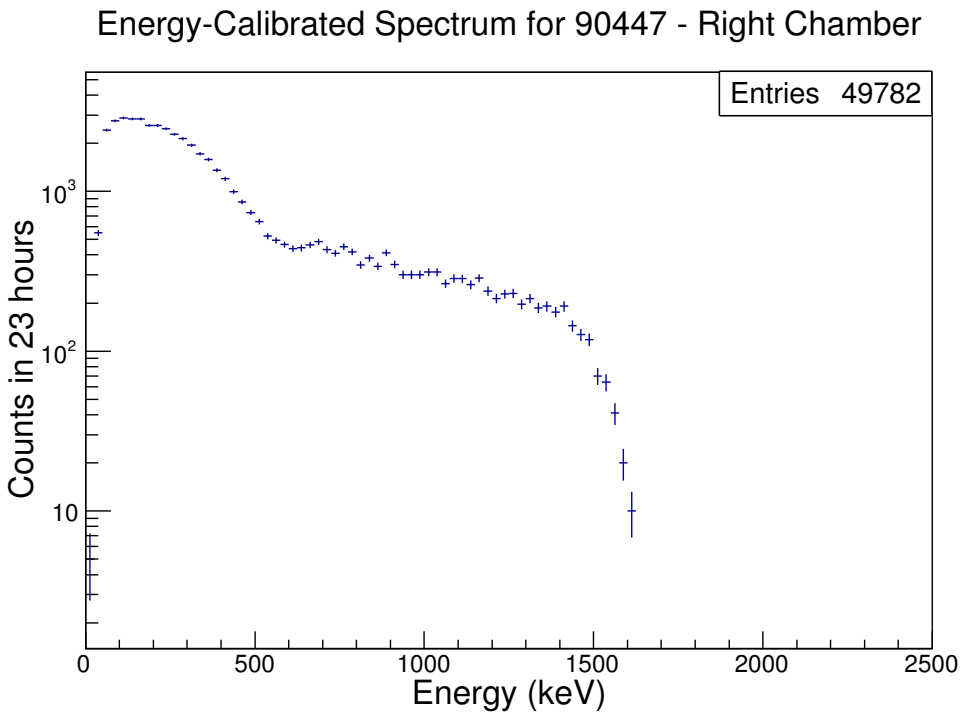

Figure C.30: Spectrum of sample 90447 from 23-hour acquisition in the right chamber.

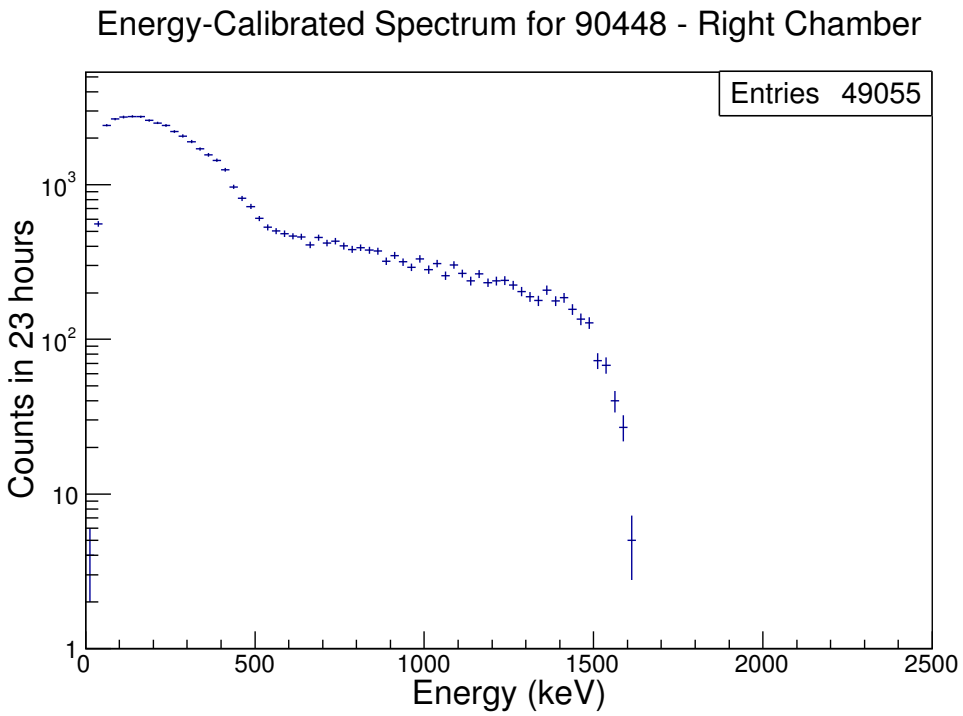

Figure C.31: Spectrum of sample 90448 from 23-hour acquisition in the right chamber.

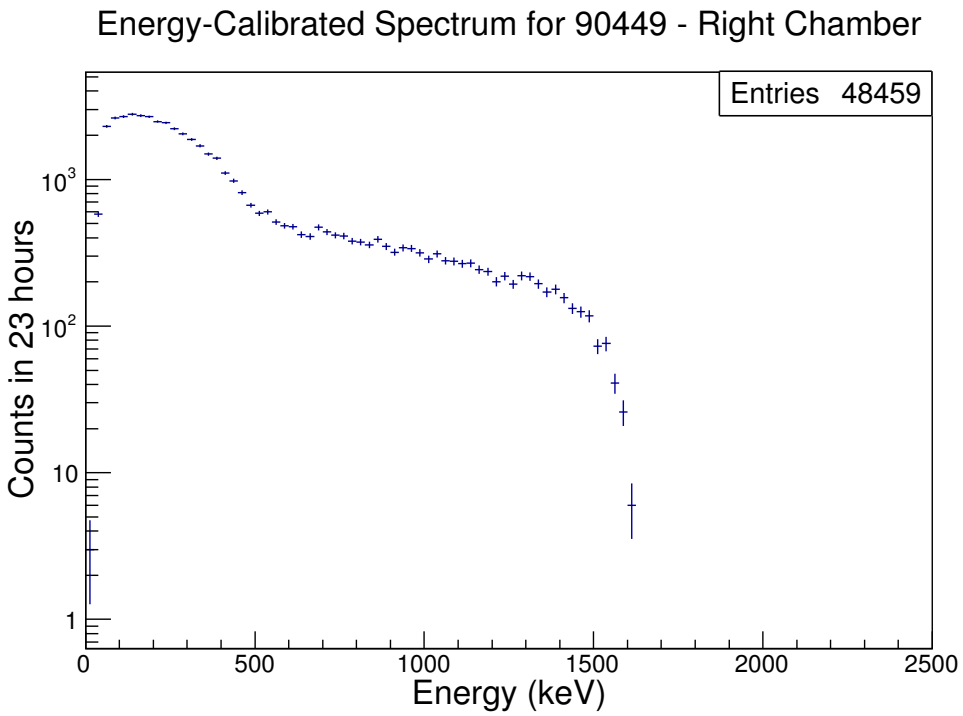

Figure C.32: Spectrum of sample 90449 from 23-hour acquisition in the right chamber.

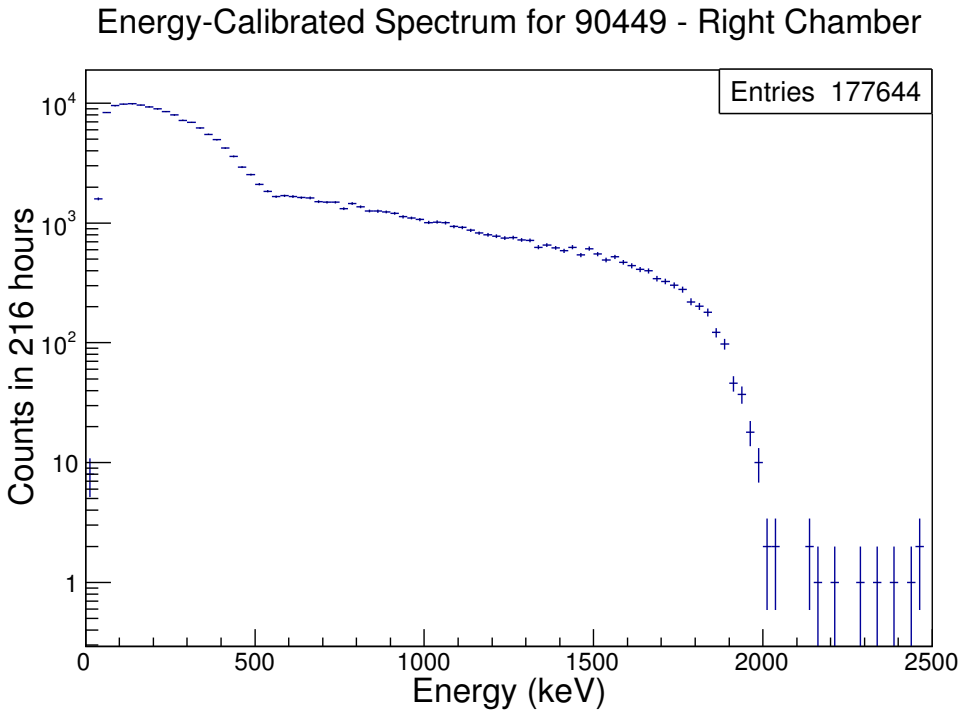

Figure C.33: Spectrum of sample 90449 from 84-hour acquisition in the right chamber.

C.2.3 Background-Subtracted Sample Spectra

C.2.3.1 Individual Sample Spectra

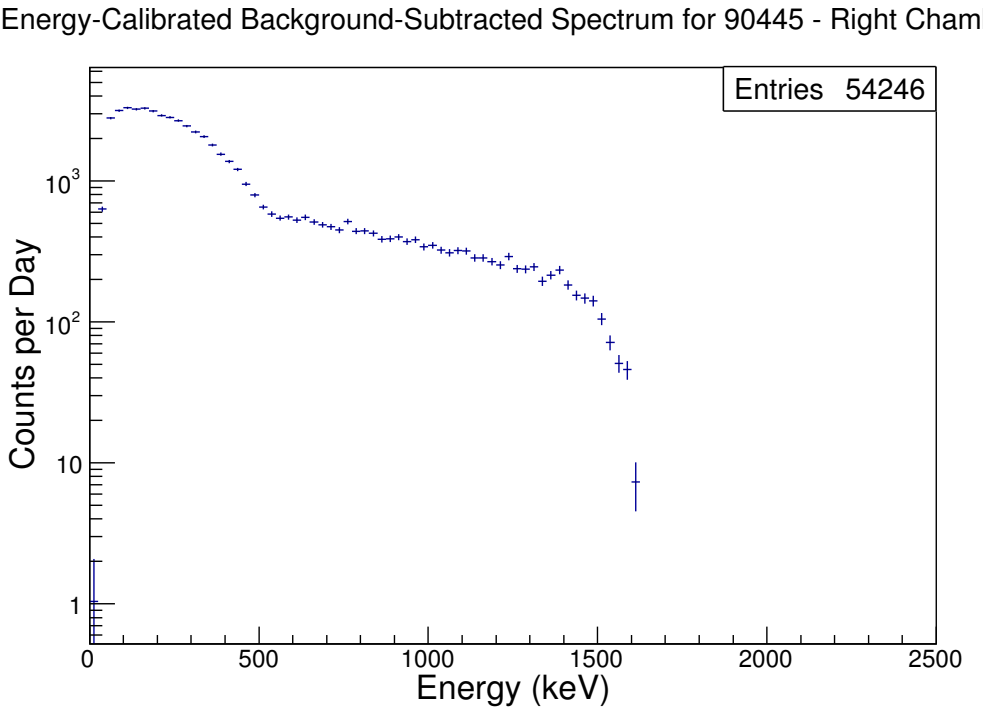

Figure C.34: Background-subtracted spectrum of sample 90445 from 23-hour acquisition in the right chamber.

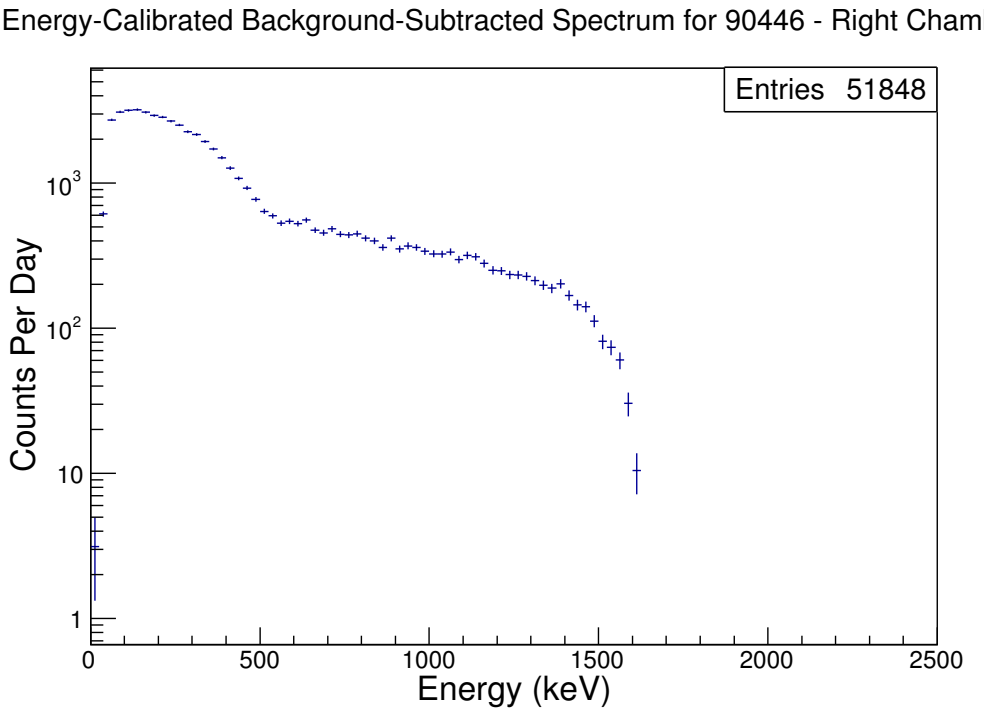

Figure C.35: Background-subtracted spectrum of sample 90446 from 23-hour acquisition in the right chamber.

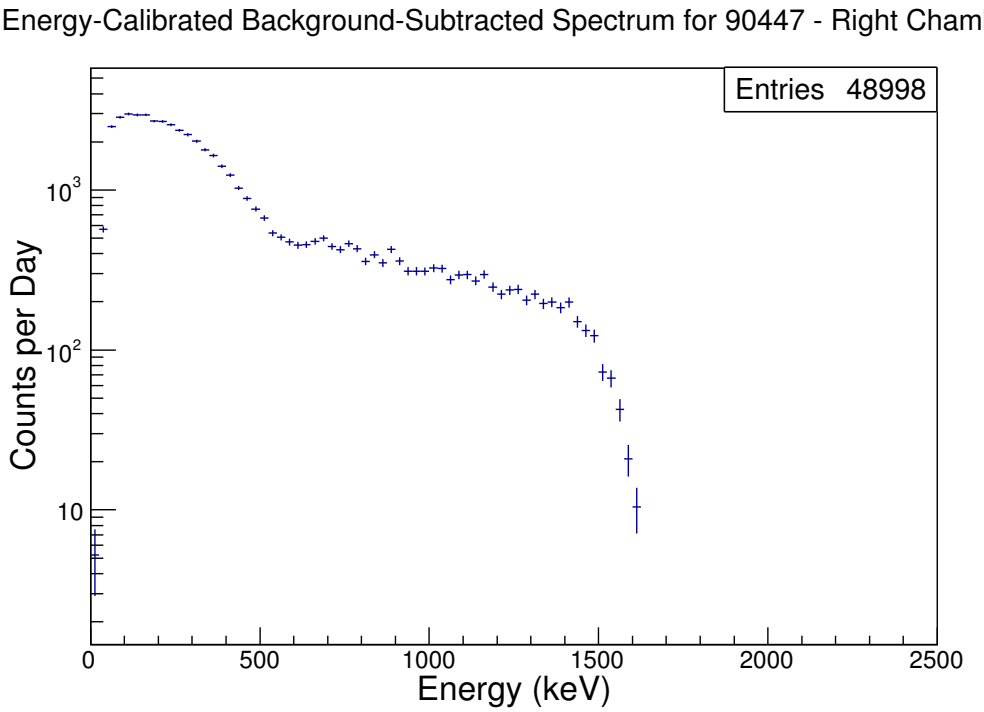

Figure C.36: Background-subtracted spectrum of sample 90447 from 23-hour acquisition in the right chamber.

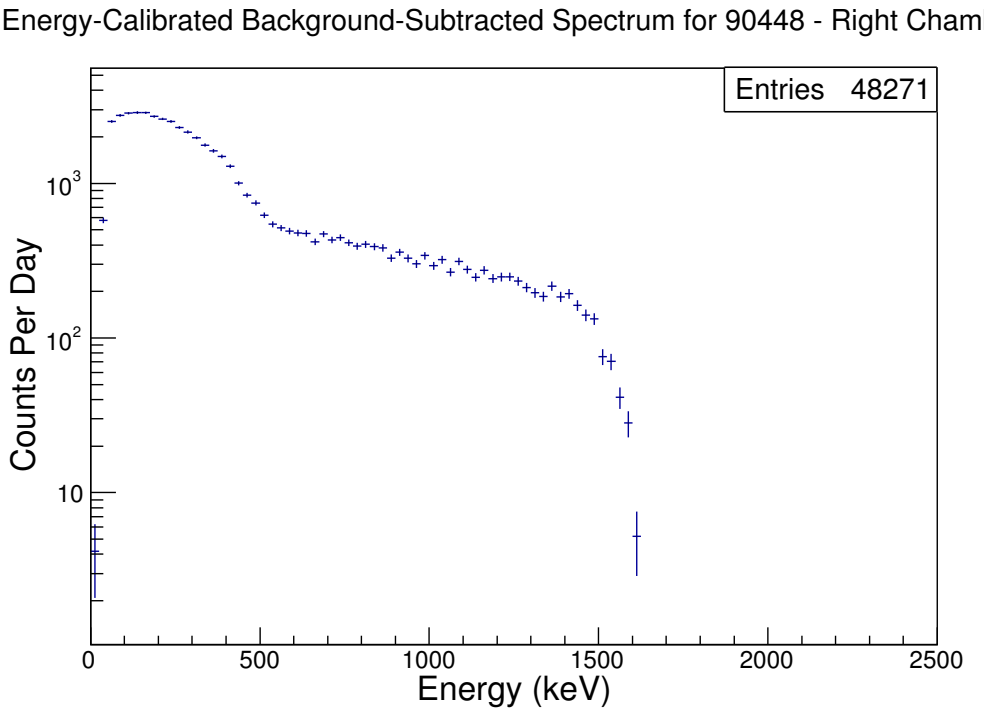

Figure C.37: Background-subtracted spectrum of sample 90448 from 23-hour acquisition in the right chamber.

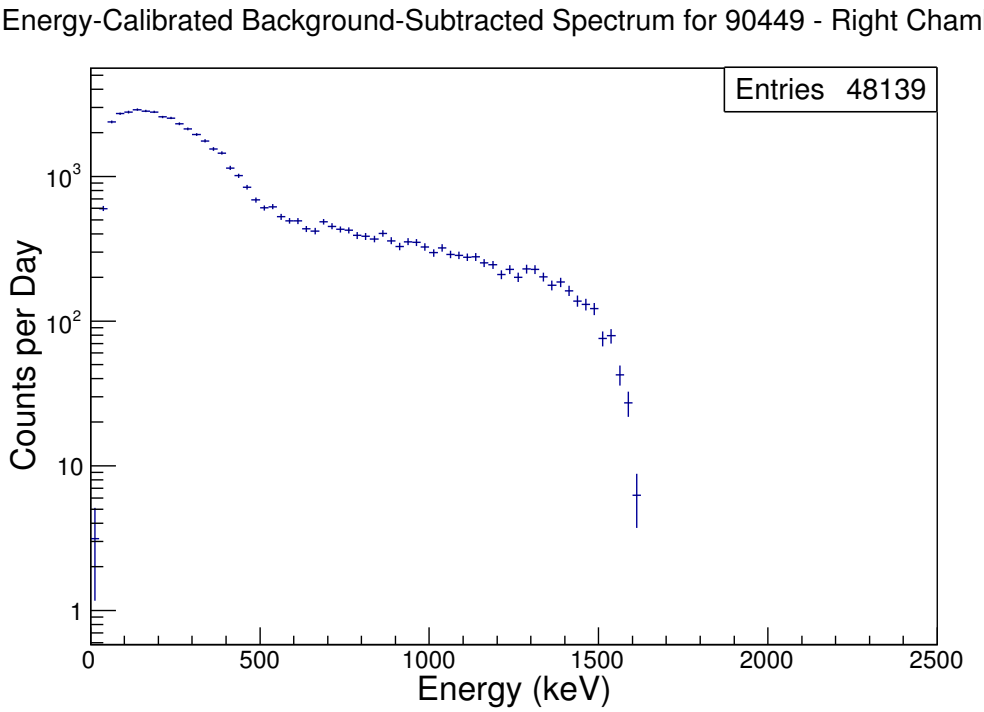

Figure C.38: Background-subtracted spectrum of sample 90449 from 23-hour acquisition in the right chamber.

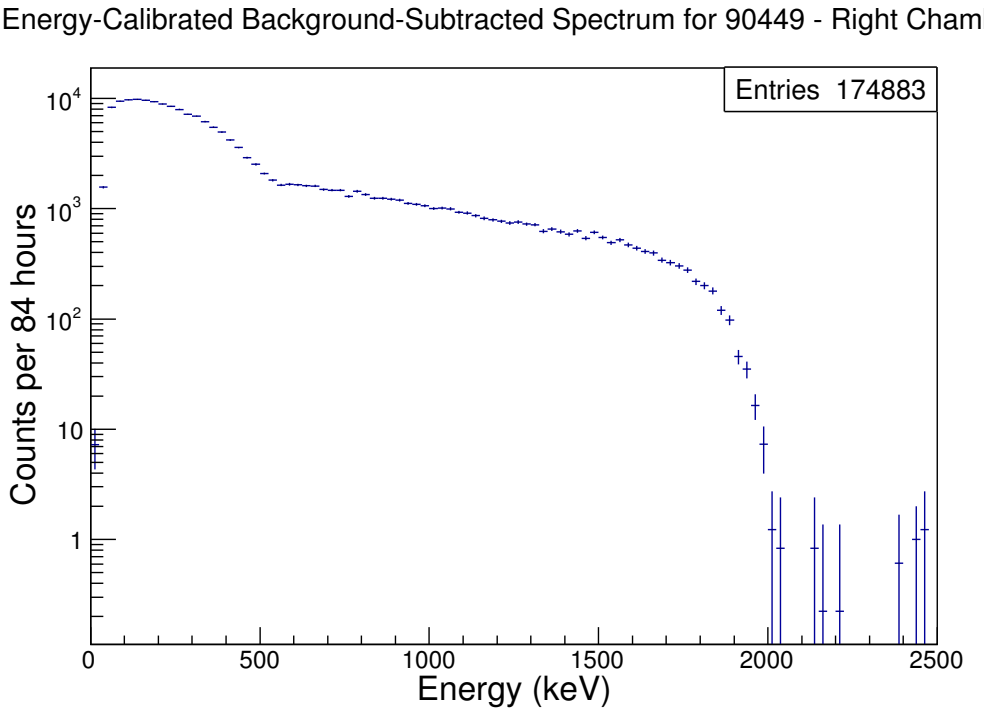

Figure C.39: Background-subtracted spectrum of sample 90449 from 84-hour acquisition in the right chamber.

APPENDIX D

SAMPLE PREPARATION PROCEDURES

Scope

This procedure is only for the preparation and transfer of liquid scintillation counting (LSC) samples and standards intended for measurement in the ultra-low-background liquid scintillation counting (ULB LSC) system located in the 3425 shallow underground laboratory.

Purpose

The 3425 shallow underground laboratory will be used to perform very low background radiometric sample counting. Samples (both radiologically controlled samples and uncontrolled environmental samples) and calibration standards will be used in cleanroom areas of the 3425 building. These "samples and standards" will initially be prepared in the 3420 radiation detection laboratories. The purpose of this procedure is to address two distinct concerns associated with these preparation and measurement activities:

1. Satisfying radiological control requirements for PNNL laboratories.
2. Maintaining cleanliness within the 3425 shallow underground laboratory building.

For the first item, radioactive material must be packaged as "Non-dispersible radioactive material" and will be removed from 3425 at not greater than six-month intervals for RCT swipe testing as part of the unique procedures that 3425 staff and RadCon have developed to minimize contamination risk. As part of these procedures, routine radiological surveys are not performed in the clean areas of 3425. During the 6-month swipe test the tape around the vial lids will be inspected to determine if there is any degradation of the quality of the seal. If there is any question about the tape seal quality, then the sample/source will be removed from service.

For the second item, in order to maintain cleanliness, a controlled process is needed to prepare and transfer samples and standards to the clean areas of the 3425 shallow underground laboratory building.

This procedure presents the methods for preparing and transferring samples and standards that comply with the regulatory requirements as well as maintaining cleanliness. In particular, this procedure addresses the preparation of LSC samples and standards. LSC samples and standards must be packaged first as sealed containers and second as cleanroom compliant items; both packaging stages are specified by this procedure.

Applicability (required)

This procedure describes the process for packaging and transferring sealed radioactive LSC samples and standards from radiological laboratories to the 3425 cleanrooms. Clean transfer and final packaging will be performed in a laminar flow hood in 3420/1508, after which the samples and standards may be transferred to 3425 for counting, calibration, and/or QC checks.

This procedure applies to research staff and radioactive material custodians who package and handle liquids and solids for measurement in the ULB LSC system in the 3425 shallow underground laboratory. There are several cases in which this procedure is required, as described below:

1. Radioactive samples (i.e., liquid or solid samples that are received as radioactive material or determined to be radioactive material after receipt) must be packaged in accordance with this procedure for counting in 3425.

2. Environmental samples (i.e., samples that are not identified as radioactive material by the client) are not subject to the RBA exit survey portion of this procedure. However, the same packaging and transfer methods are required to ensure cleanliness in the 3425 building and consistent counting geometry in the ULB LSC system.
3. Calibration standards (i.e., liquids or solids spiked with known amounts of radioactive material) must be packaged in accordance with this procedure for use in 3425.

Definitions (optional)

The term "sample/standard" will refer collectively to samples (both radiologically controlled samples and uncontrolled environmental samples) and/or calibration standards (i.e., liquids or solids spiked with known amounts of radioactive material).

The term "clean LSC vial" will refer to a standardized LSC vial with a screw cap that has been approved for use by the Radiological Engineer (for example a PerkinElmer Super Polyethylene vial) and prepared as "clean" through an ethanol sonication process described in this procedure.

The following terms will be used in this procedure to describe the four layers of cleanliness control used in the transfer of radioactive samples/standards to the 3425 cleanrooms. Presented in order from the innermost to the outermost containment, the terminology used is as follows:

Primary layer. The primary layer refers to the clean LSC vial used as the primary sealed package encapsulating a solid or liquid LSC sample/standard. The vial screw cap must be taped closed. This is the innermost layer of plastic around the sample/standard.

Clean layer. The clean layer refers to *either* the clean LSC 20 mL vial *or* clean vacuum bag into which the primary layer is placed for transfer within the 3425 cleanrooms. If used as the clean layer, the clean LSC 20 mL vial screw cap must be taped closed. If used as the clean layer, the clean vacuum bag must be heat-sealed. This is the innermost layer that may be exposed within the 3425 cleanroom laboratories.

Holder layer. Often, multiple LSC samples/standards will be prepared in a measurement activity. For example, a set of three might contain an environmental sample, a process blank, and a known calibration standard. The holder layer is an additional clean bag or container that can hold multiple LSC sample/standard vials for ease of transference within the 3425 cleanroom laboratories. This layer is clean and allowed to be exposed within the 3425 cleanroom laboratories.

Transfer layer. A transfer layer is the outermost plastic bag or container placed over or around the holder layer to prevent environmental contamination as the samples/standards are transferred from one laboratory location to another during the preparation and transfer stages and steps.

Building-to-building layer. This closeable container layer is only used to transport all the samples/standards between buildings in the PSF complex.

Responsible Staff

Custodian (radioactive material custodian)
- Responsible for control of the radioactive material packaged under this procedure.
- Returns packaged samples/standards to the originating laboratory by their expiration date.
- Maintains correct information in the RMT database.

Materials Services Representative (MSR)
- Assists with RMT database entries and evaluation of radioactive material inventories against building limits.

Radiological Engineer

- Reviews and approves new sample containment configurations as "non-dispersible radioactive material" as well as maintains records of testing of approved containment configurations.

Radiation Protection Technologist (RPT)

- Performs contamination surveys of packaged radioactive material initially, and at the six-month intervals required for work in 3425. Surveys are performed outside the 3425 building.

Research Staff

- Coordinates with CSM of a laboratory where packaging will be performed.
- Prepares samples/standards for packaging under this procedure.
- Transfers samples/standards within the PSF complex and 3425 building under this procedure.

Procedure Staff Roles

There are three staff roles described in this procedure, each relating to the level of cleanliness for transfer of samples/standards. The following terms will be used to describe these roles, in order of increasing cleanliness:

- Sample prep staff. The sample prep staff refers to the staff member who prepares the LSC samples/standards and packages them into the primary layer, typically in a contamination area (CA) or radiological buffer area (RBA).
- Sample transferor. The sample transferor is a staff member wearing clean gloves and lab coat who is responsible for transferring samples between laboratories.
- Cleanroom worker. A cleanroom worker is a staff member who has donned appropriate cleanroom garments in order to handle the clean bag without introducing contamination. The cleanroom worker may work in a laminar flow hood or in the 3425 cleanroom areas.

Hazard Analysis

No hazards identified for this procedure.

Emergency Response

In the event of an emergency, call 375-2400. State the problem to the operator, request any needed emergency assistance, and request notice of the appropriate personnel. If you need further instructions, be sure the operator has the telephone number where you can be reached. This applies 24 hours a day.

Prerequisites

Prior to transfer to the 3425 building, all LSC samples/standards must be prepared and sealed according to this procedure (or one of the procedures listed in the References section).

Research staff prerequisites:

- Read and follow procedure RDNS-1, *PSF Building 3425 and 3420 General Cleanroom Procedure.*
- Qualified Radiological Workers will perform the work described in this procedure.
- Staff who package radioactive LSC samples/standards under this procedure must complete PSF on-the-job mentoring (or equivalent briefing or OJT) to demonstrate knowledge and competence in this process. This evaluation is performed by both 3425 Cognizant Space Managers (CSMs) and research staff having prior 3425 building, sample-handling experience.

Precautions and Limitations

This procedure is intended for radioactive samples/standards that are less than 50% of the radioactive material limits of 10 CFR 835 Appendix E. It is understood that samples may have only limited radiological information. In this case, use the best available information and obtain help from your MSR

as needed to verify that the samples are within the radioactive material limits.

- Note: The 10 CFR 835 Appendix E limits are provided in HDI subject area Controlling Sealed Radioactive Sources and Licensed Radioactive Material, Exhibit: Values for Individual DOE Sealed Radioactive Sources Requiring Both Inventory and Leak Tests.
- Note: Radioactive material that contains less than 1 µCi alpha activity and 5 µCi beta/gamma activity will always meet these inventory limits.

Always practice good clean techniques as described in RDNS-1, *PSF Building 3425 and 3420 General Cleanroom Procedure*.

NEVER open a LSC vial or vacuum-sealed bag (i.e., the clean layer) in the 3425 building!

Packaging Material

The following packaging materials must be used for this procedure.

- The containers must be standard polyethylene screw-cap LSC vials with a capacity of 6 mL and/or 20 mL.
  - PerkinElmer Super Polyethylene vials are approved for packaging under this procedure.
  - Other types of vials may be qualified for use under this procedure by leak testing an initial lot of vials using a statistically-based sampling plan. The MSR will develop and maintain documentation of this testing.
  - Tape used to seal vials may be standard 1⁄4" or 1⁄2" vinyl laboratory tape (e.g., 3M 471).
- Cleanroom bagging, if used as a clean layer, holder layer, or transfer layer, will be of thickness 2 mil or greater and will be able to be heat sealed.

Work Instructions

Introduction – Containment configurations

This procedure describes the process for packaging and transferring LSC samples/standards in two distinct, but similar containment configurations. The two containment configurations are named and defined as follows:

- **6mL-in-20mL**: In this containment configuration, the prepared liquid or solid LSC sample/standard is contained within a 6 mL clean LSC vial (primary layer). The 6 mL vial cap is taped-closed. This 6 mL vial is then contained within a 20 mL clean LSC vial (clean layer). The 20 mL clean LSC vial is taped-closed.
- **20mL-in-vacuum-bag**: In this containment configuration, the prepared liquid or solid LSC sample/standard is contained within a 20 mL clean LSC vial (primary layer). The 20 mL vial cap is taped-closed. This 20 mL vial is then contained within a vacuum-assisted, heat-sealable bag (clean layer).

In the 6mL-in-20mL containment configuration, it is a discretionary choice whether or not to use the vacuum-assisted, heat-sealable bag as an additional layer of protection around the 20 mL clean LSC vial.

The table below outlines the cleanliness layers for the two containment configurations described above.

Containment configuration	Primary layer (RBA)	Clean layer (3425/B121 lab)	Holder layer (3425 labs)	Transfer layer (Non-clean labs)	Building-to-building layer (Outside of buildings)
6mL-in-20mL	6 mL LSC vial *taped closed*	20 mL LSC vial *taped closed*	Cleanroom bin or bag *click-shut or sealed*	Closeable bag *heat sealed*	Closeable bucket or box
20mL-in-vacuum-bag	20 mL LSC vial *taped closed*	Vacuum bag *heat sealed*	Cleanroom bin or bag *click-shut or sealed*	Closeable bag *heat sealed*	Closeable bucket or box

The stages below provide the sequential process for packaging and transfer of samples and/or radioactive standards from the radiological laboratory in which they were prepared to a clean laboratory for processing, followed by transfer to the 3425 building. The procedures are very similar for the two distinct

containment configurations and the differences are noted throughout the detailed procedure.

Pre-packaging activities

1. Based on the best available information, verify that the quantity of radioactive material in the sample/standard will be less than 50% of the 10 CFR 835 Appendix E limits by the following steps.
- If the sample/standard is known to contain less than 1 μCi alpha activity and 5 μCi beta/gamma activity, it meets these limits.
- If the quantity of radioactive material is unknown or is above 1 μCi alpha activity or 5 μCi beta/gamma activity, contact your MSR for assistance.
- Note: It is understood that there may be only limited radionuclide information for samples. Use shipping papers, direct survey readings, preliminary counting data and other available information to make a good faith determination about meeting these limits.

2. Complete or verify the Radioactive Material Tracking (RMT) database entry for the samples/standards by one of the methods described below.
- For samples/standards that will be individually tracked, create a new RMT entry for the item. In the RMT Physical Form field, select "Nondispersible Radioactive material." Note the RMT ID number for use later in this procedure.
- For samples/standards that are part of an RMT consolidated inventory that has been set up previously, review the RMT entry and verify that the expected radioactive material content is consistent with the RMT entry.

LSC vial preparation

1. Inspect 6 mL and 20 mL LSC vials for obvious damage or manufacturing flaws that could prevent effective sealing of the screw cap.
2. Sonicate the 6 mL and 20 mL vials in a 3% by volume solution of Micro90/DI water. Rinse the vials thoroughly with DI water. Sonicate the vials for 60 minutes in DI water. Rinse thoroughly with DI water. Rinse with ethanol. Allow vials and caps to dry in a clean area, for example a HEPA-filtered, laminar flow hood. If a clean nitrogen line is available, the vials can be dried with nitrogen to eliminate excess ethanol and decrease drying time.
3. Once dry, match caps to vials and screw them on. Store vials and caps in clean bags in "Sets of 3"; if more vials are cleaned at once, multiple "Sets of 3" together in their clean bags can be stored in a larger clean bag and kept in a clean location for ease of access prior to the next stage. This creates a ready supply of clean LSC vials. Only extract vials and caps in their "Sets of 3" from this clean supply using fresh, clean gloves.

Packaging the LSC sample/standard in sealed vial

Note: Packaging is performed in the radiological laboratory where the sample/standard is initially processed. The vial may not be transferred to the 3425 laboratory until all packaging stages and steps in this procedure have been followed.

1. Select the containment configuration for the sample/standard to be prepared and obtain the correct volume LSC vials from the supply of clean vials and caps:
    a. **6mL-in-20mL**: Obtain one or more 6 mL LSC vials with caps.
    b. **20mL-in-vacuum-bag**: Obtain one or more 20 mL LSC vials with caps.
2. Take the clean vials and caps obtained in the previous step for the selected containment configuration to the radiological laboratory (e.g., RBA) for sample/standard preparation. Maintain the vials and caps in a clean condition as far as possible by using fresh, clean gloves to handle the vials and place the vials and caps on clean surfaces (e.g., fresh, clean polypropylene Kimtech Clean Room Wipes, such as Kimtech 33330, etc.).
3. Label the following information on the LSC vial caps.
    a. Unique RMT ID number.

    b. Expiration date for the packaged sample/standard, which is one year from the current date, in the following format: “Exp 5/20/12”.
    c. Prepare sticker labels in advance to accompany the clean LSC vials and caps to the RBA.
4. In an RBA, fill each LSC vial with the sample/standard material and LSC cocktail, avoiding any spillage on the threads or outside of the LSC vial.
    a. Note: It is assumed that a specific project or activity is defining and dictating the nature of the sample/standard preparation in this step. This will include things like the chemistry process, the target isotopes, the volume of the sample/standard, and the selected type and ratio of LSC cocktail mixture.
5. Change to fresh, clean gloves. Securely tighten the cap on the LSC vial.
6. Change to fresh, clean gloves. Wipe the closed vial with ethanol.
7. Change to fresh, clean gloves. Wipe the closed vial with ethanol. This repeats the previous step.
8. Change to fresh, clean gloves. Tape around the LSC vial lid as follows:
    a. To seal with vinyl laboratory tape, wrap the tape in a clockwise direction (when viewed from the top of the vial), stretching the tape enough to securely adhere to both the vial and lid. Wrap 1.5 to 2.5 wraps of tape, firmly sealing the end of the tape. Do not tab the end of the tape.
9. Have the RPT perform a contamination survey on the closed and taped LSC vial.
10. Request that the RPT complete a Radioactive Material Tag. Write the RMT ID number on the Radioactive Material Tag.

Transfer from radiological laboratory (e.g., RBA) to clean prep lab (e.g., 3420/1508)

These steps describe the process after initial packaging of a sample/standard is complete and the LSC vial is ready for subsequent transfer to a laboratory where the LSC vial/sample will be prepared for cleanroom work (e.g., 3420/1508). This procedure presumes the sample prep staff member has just completed a LSC sample preparation in one of the 3420 radiological laboratories (e.g., RBA) (see prior stage). As such, the LSC sample has been filled into a clean LSC vial and the screw cap has been closed to seal the container and the cap has been taped closed with vinyl laboratory tape. The specific LSC vial volume size is dictated by the containment configuration being used:

- **6mL-in-20mL**: The prepared LSC vial will be a 6 mL vial with the cap taped closed.
- **20mL-in-vacuum-bag**: The prepared LSC vial will be a 20 mL vial with the cap taped-closed.

The following transfer process requires three staff roles: one sample prep staff handling the samples/standards in the radiological laboratory (e.g., RBA), a sample transferor to move the samples/standards from the edge of the radiological laboratory (e.g., RBA) to the cleanroom preparation laboratory (e.g., 3420/1508), and a cleanroom worker ready to receive the samples in the cleanroom preparation laboratory (e.g., 3420/1508). For this part of the process it is permissible for one staff member to fulfill both the transferor and cleanroom worker roles, following the additional instructions noted. Note: During this stage the holder layer of cleanliness is not used.

1. Sample prep staff: Change to fresh, clean gloves. Wipe the exterior of the closed, taped LSC vial with ethanol. Bring the LSC vial to the edge of the radiological laboratory (e.g., RBA boundary). Note: In this step only one vial should be handled and transferred at a time, even if multiple LSC samples/standards were prepared in the prior stage. This restriction is to ensure all participating staff members have full dexterity available to adequately control the cleanliness of the transfer hand-off from the radiological laboratory to the cleanroom preparation.
2. Cleanroom worker: Working in a clean location (i.e., 3420/1508 laminar flow hood) and wearing clean gloves, prepare the clean layer and transfer layer to receive a single LSC vial from the radiological laboratory (e.g., RBA). Depending on the containment configuration being used, this preparation will be:
    a. **6mL-in-20mL**: The clean layer will be a clean 20 mL vial without the cap and the transfer layer will be a cleanroom bag. The clean 20 mL LSC vial will be placed in the cleanroom bag.
    b. **20mL-in-vacuum-bag**: The clean layer will be a close-fitting heat-sealable cleanroom

bag, twice heat-sealed on the bottom, that will be vacuumed closed at a later stage and the transfer layer will be a cleanroom bag. The clean vacuum bag will be placed in the cleanroom bag.

Note: The clean layer (*either* clean 20 mL LSC vial *or* clean vacuum bag) will be exposed to the 3425 cleanroom laboratory spaces. It is essential to maintain the cleanliness of this layer. The outer cleanroom bag is the transfer layer, used to maintain the cleanliness of the clean layer (*either* clean 20 mL LSC vial *or* clean vacuum bag) as it is moved from one location to another.

3. Cleanroom worker: Provide the transfer-bagged clean layer (*either* clean 20 mL LSC vial *or* clean vacuum bag) to the sample transferor. If one staff member is fulfilling both cleanroom worker and transferor roles, the cleanroom worker exits the clean zone with the transfer-bagged clean layer (*either* clean 20 mL LSC vial *or* clean vacuum bag) and becomes the transferor at that point.
4. Sample transferor and sample prep staff: Meet at the radiological laboratory (e.g., RBA) boundary to transfer a single prepared LSC vial sample/standard.
5. Sample transferor and sample prep staff: Standing on the clean side of the RBA boundary, the sample transferor will hold the transfer bag layer and the clean layer open to be accessible to the sample prep staff. The sample prep staff will carefully place the primary layer into the clean layer, taking care to prevent the LSC sample/standard or gloved hands from touching the upper portion of the clean layer and/or the transfer bag layer. Specifically, for the two containment configurations this entails the following identifications for what each staff member is holding:
    a. **6mL-in-20mL**:
    Sample transferor:
        - Transfer layer ➔ Cleanroom bag with open top.
        - Clean layer ➔ Clean 20 mL LSC vial without a cap.

    Sample prep staff:
        - Primary layer ➔ Prepared 6 mL LSC vial with cap taped closed.

    b. **20mL-in-vacuum-bag**:
    Sample transferor:
        - Transfer layer ➔ Cleanroom bag with open top.
        - Clean layer ➔ Close-fitting heat-sealable cleanroom bag to be vacuumed closed.

    Sample prep staff:
        - Primary layer ➔ Prepared 20 mL LSC vial with cap taped closed.
6. Sample transferor: Fold the clean transfer bag over to maintain the cleanliness of the clean layer (*either* clean 20 mL LSC vial *or* clean vacuum bag). A tape tab may be used to hold the transfer bag closed.
7. Sample transferor: Transfer the bagged LSC sample/standard to a cleanroom preparation laboratory (e.g., 3420/1508).

Processing in cleanroom preparation laboratory (e.g., 3420/1508)

1. Sample transferor: Standing in front of the laminar flow hood in the cleanroom preparation laboratory (e.g., 3420/1508), unfold the top of the outer plastic transfer bag. If one staff member is fulfilling transferor and cleanroom worker roles, the transferor arranges the unfolded plastic bag on a portable table located in front of the laminar flow hood and in the clean airflow. This is done so the clean layer (*either* clean 20 mL LSC vial *or* clean vacuum bag) can be accessed by the cleanroom worker without handling the transfer bag. The transferor can then take necessary actions to become the cleanroom worker for the next step.
2. Cleanroom worker: Starting with fresh, clean gloves, remove the clean layer (*either* clean 20 mL LSC vial *or* clean vacuum bag) from the clean transfer bag, taking care to touch only the outer surface of the clean layer (*either* clean 20 mL LSC vial *or* clean vacuum bag).
3. Cleanroom worker: Close and seal the clean layer. This requires seven steps. The containment configuration being used dictates the exact process of each of these seven steps, described here:
    a. **6mL-in-20mL**:
        1. Cap the clean 20 mL LSC vial.
        2. Change to fresh, clean gloves.
        3. Wipe the clean 20 mL LSC vial with ethanol.

4. Change to fresh, clean gloves.
5. Tape around cap seal with laboratory tape (as described above in step 7 of the *Packaging the LSC sample/standard in sealed vial* stage). Inspect the tape to verify that it is securely sealed and the end of the tape is not peeling back. Repeat taping if necessary to ensure a good tape seal.
6. Change to fresh, clean gloves.
7. Wipe the closed and taped LSC vial with ethanol.

Note: Optionally, additional cleanliness control may be added to the 6mL-in-20mL containment configuration by additionally following the vacuum-bagging steps for the 20mL-in-vacuum-bag containment configuration. To do so, add a close-fitting heat-sealable cleanroom bag around the clean 20 mL LSC vial just prepared and then follow the next seven steps for the 20mL-in-vacuum-bag containment configuration.

b. **20mL-in-vacuum-bag**:
   1. Make an initial heat seal near the top of the clean bag.
   2. Use a capillary needle connected to a vacuum hose to evacuate the air from the inside of the close-fitting heat-sealable cleanroom bag. Heat-seal the bag closed **twice** beneath the needle insertion point.
   3. Change to fresh, clean gloves.
   4. Wipe the vacuum bag with ethanol.
   5. Change to fresh, clean gloves.
   6. Trim excess vacuum bag material from edges without breaking the vacuum seal.
   7. Change to fresh, clean gloves.
   8. Wipe the vacuum bag containing the 20 mL LSC vial with ethanol.

4. Cleanroom worker: Place the clean layer (*either* clean 20 mL LSC vial *or* clean vacuum bag) LSC sample/standard into a new clean holder layer bag. Note: This is the first use of the holder layer (refer to the definitions and containment configuration table above). Several LSC samples/standards may be packaged into a single clean holder layer bag. Use a clean holder layer bag approximately matched to fit the intended number of LSC samples/standards that are being prepared for cleanroom use. Heat seal the holder layer bag when all LSC samples/standards are have been added.
   - Note: In future iterations of the development of this procedure, it is anticipated that a clean LSC tray holder or plastic bin that can be closed around multiple LSC vials will be used as the holder layer.
5. Cleanroom worker: Place the clean holder layer bag into a clean transfer layer bag. Use a sufficiently large clean transfer bag so that it may be cut open later without cutting the holder layer bag or LSC samples/standards.
6. Cleanroom worker: Heat seal the transfer bag. Remove the packaged LSC samples/standards from the laminar flow hood in their transfer bag.
   - Note: LSC samples/standards may be stored for a period of time in the general room area of a cleanroom preparation laboratory (e.g., 3420/1508) prior to completing the next series of stages. However, LSC samples/standards should be limited from exposure to light as this degrades the LSC cocktail mixture.

Transfer to and Receipt in 3425

1. Sample transferor: Place the transfer bag containing the LSC samples/standards in an appropriate building-to-building container (e.g. a tub with a lid or additional bag) and transport the samples to the 3425 building, meeting a cleanroom worker at the door to the gowning room (room B101).
2. Cleanroom worker: In the gowning room but before final cleanroom dress-in (wearing clean gloves), receive the LSC samples/standards in the transfer bag from the sample transferor (i.e., take the transfer bag out of the tub or additional bag).
3. Cleanroom worker: Using clean scissors cut the top off of the transfer bag and set the bag down in an orientation that allows the holder layer bag to be accessed and retrieved from the clean area of the gowning room.
4. Cleanroom worker: Dress into full cleanroom garb.

5. Cleanroom worker: Remove the clean holder layer bag full of LSC samples/standards from the transfer bag, taking care not to touch the outside of the transfer bag.
6. Cleanroom worker: Wipe the exterior of the clean holder layer bag containing the LSC samples/standards as needed and transfer into the cleanroom for further handling, storage, or counting.
7. Cleanroom worker: Once the samples are transferred into the laboratory, update the appropriate laboratory source/sample log to record the addition of the source/sample in 3425. The log is used to track the storage location, counting location, and 6-month swipe test of the source/sample.

Counting LSC samples/standards in 3425 counting laboratories

1. Generally, LSC samples/standards are expected to be stored as sets, together in a clean holder layer bag that will be stored within a refrigerated area. Move the LSC vial(s) to the counting laboratory and instrument in the holder layer bag.
2. From outside the holder layer bag, inspect the quality of the tape seal before opening the holder layer bag to retrieve a LSC sample/standard for counting. Ensure there are no apparent signs of loss of containment of the LSC sample/standard material from the containment configuration.
3. Prior to placing a LSC sample/standard into the ULB LSC instrument, re-inspect the clean layer of the LSC sample/standard to ensure there are no apparent signs of loss of containment of the LSC sample/standard material from the containment configuration.
4. When sample/standard counting is complete, create a new "post-measurement" clean holder layer bag to store the used sample/standard. If a set of samples/standards were in the same holder bag brought into the 3425 building, then after each measurement the samples/standards should be added to the new "post-measurement" clean holder layer bag. This segregation will assist in mitigating contamination transfer due to sample/standard handling.
5. If a sample/standard is no longer needed, transfer it back to the laboratory in which it was prepared. See the next stage.

Removing sealed vials from service

1. Transfer the sample or standard back to the originating laboratory prior to its expiration date.
2. For items entered as individual RMT items, modify the RMT entry as follows.
    a. If the packaged sample has been placed into a waste container, use the RMT Ship Out function to remove it as an active item. Note the RWDR number in the appropriate RMT field.
    b. If the packaged sample will be retained in a radiological laboratory, change the Physical Form in RMT to "Liquid" or "Particulate solid" as appropriate.

References

- Procedure RDNS-1, *PSF Building 3425 and 3420 General Cleanroom Procedure*.
- Procedure PSF-SAMPLE-01, *Packaging Radioactive Filters as Sealed Containers.*
- Procedure PSF-SAMPLE-02, *Packaging Radioactive Material in Vials as Sealed Containers.*

Exhibits/Attachments

The next two pages shows diagrams of the packing procedures for the **6mL-in-20mL** and **20mL-in-vacuum-bag** containment configurations.

6mL-in-20mL

Clean LSC vial supply

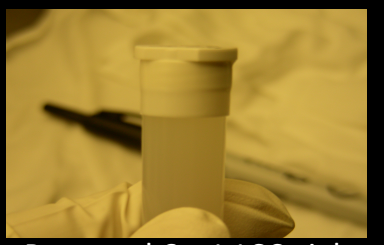

Prepared 6 mL LSC vial

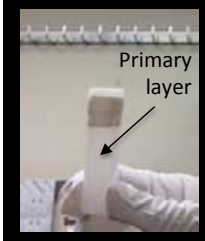

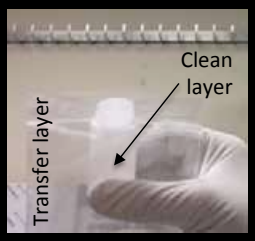

Transfer of 6 mL primary layer into a 20 mL clean layer at RBA boundary

Preparation of clean layer seal in 3420/1508

Placing clean layer (clean 20 mL LSC vial) into a holder layer, then into a transfer layer, and finally into a building-to-building layer.

20mL-in-vacuum-bag

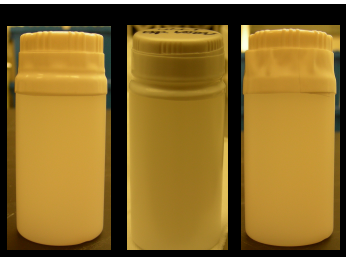

Clean LSC vial supply

Good, Mediocre, and Bad Seals

Prepared 20 mL LSC vial

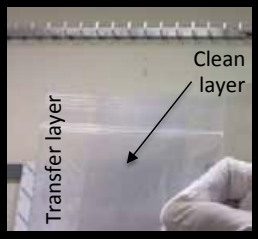

Transfer of 20 mL primary layer into vacuum-bag clean layer at RBA

Preparation of clean layer vacuum-seal in 3420/1508

Placing clean layer (clean vacuum-bag sealed 20 mL LSC vial) into holder layer, then into a transfer layer, and into a building-to-building layer.